Experimental and field studies of basalt-carbon dioxide interaction

Iwona Gałeczka

Faculty of Earth Sciences
University of Iceland
2013

Experimental and field studies of basalt-carbon dioxide interaction

Iwona Gałeczka

Dissertation submitted in partial fulfillment of a
Philosophiae Doctor degree in Geology

Advisors:

Dr. Sigurður Reynir Gíslason
Institute of Earth Sciences, University of Iceland

Dr. Domenik Wolff-Boenisch
Department of Applied Geology, Curtin University, Australia

Prof. Eric H. Oelkers
CNRS, Université Paul Sabatier, France

PhD Committee

Dr. Sigurður Reynir Gíslason
Institute of Earth Sciences, University of Iceland

Dr. Domenik Wolff-Boenisch
Department of Applied Geology, Curtin University, Australia

Prof. Eric H. Oelkers
CNRS, Université Paul Sabatier, France

Dr. Bergur Sigfússon
Reykjavik Energy, Iceland

Prof. Andri Stefánsson
Institute of Earth Sciences, University of Iceland

Opponents

Prof. Per Aagaard
Department of Geosciences, University of Oslo

Prof. Alessandro Aiuppa
Dipartimento di Scienze della Terra e del Mare, Palermo University

Faculty of Earth Sciences
School of Engineering and Natural Sciences
University of Iceland
Reykjavik, September 2013

Experimental and field studies of basalt-carbon dioxide interaction

Dissertation submitted in partial fulfillment of a *Philosophiae Doctor* degree in 2013

Copyright © 2013 Iwona Gałeczka
All rights reserved

Faculty of Earth Sciences
School of Engineering and Natural Sciences
University of Iceland
Sturlugata 7
101 Reykjavik
Iceland

Telephone: 525 4000

Bibliographic information:
Iwona Gałeczka, 2013, *Experimental and field studies of basalt-carbon dioxide interaction*, PhD dissertation, Faculty of Earth Sciences, University of Iceland, 189 pp.

ISBN 978-9935-9146-2-0

Printing: Háskólaprent
Reykjavik, Iceland, September 2013

Abstract

The main aim of this study was to design, build, and test a large scale laboratory high pressure column flow reactor (HPCFR) enabling experimental work on water-rock interaction in the presence of dissolved gases, demonstrated here by CO_2. The HPCFR allows sampling of a pressurized gas charged fluid along the flow path within a 2.3 m long titanium column filled with mineral, and/or glass particles. In this study, series of experiments were carried out using a carbonated aqueous solution (0.3-1.2 M $CO_{2(aq)}$) and basaltic glass grains. The scale of the HPCFR, the possibility to sample a reactive fluid at discrete spatial intervals under pressure, and the possibility to monitor the evolution of the dissolved inorganic carbon and pH *in-situ* all render the HPCFR unique in comparison with other columns constructed for studies of water-rock interactions. Experimental results at ambient temperature showed that the pH of injected pure water evolved from 6.7 to 9-9.5 and most of the dissolved iron was consumed by secondary minerals, similar to natural meteoric water-basalt systems. As CO_2-charged water replaced the alkaline fluid within the column, the fluid became supersaturated with respect to carbonates for a short time, but once the entire column was filled with the CO_2-charged water and the pH decreased to 4.5, the fluid remained undersaturated with respect to all carbonates. The mobility and concentration of several metals increased significantly in the CO_2-fluid phase and some of the metals, including Mn, Fe, Cr, Al, and As exceeded allowable drinking water limits. Iron became mobile and the aqueous Fe^{2+}/Fe^{3+} ratio increased along the flow path. Basaltic glass dissolution in the CO_2-charged water did not overcome the pH buffer capacity of the reactive fluid. The pH rose from an initial pH of 3.4 to 4.5 during the first 40 minutes of CO_2-charged water-basaltic glass interaction along the first 18.5 cm of the column but remained constant during the remaining 2.1 meters of the flow path.

In volcanic terrains at high latitude and/or altitude, sub-glacial reservoirs are formed within glaciers by geothermal activity and perhaps small eruptions at the base of ice caps. The reservoirs are periodically drained in glacial floods, called jökulhlaups. Some of these floods, especially those associated with large volcanic eruptions can be disastrous because of their size which is comparable to that of the Amazon River (>200,000 m^3/s). In July 2011 two floods about 2,000 m^3/s emerged from Icelandic glaciers (Mýrdalsjökull, Vatnajökull). Sub-glacial reservoirs and the geological basement can be looked upon as a laboratory column flow reactor filled up with rocks of a given chemical composition and surface area, where percolating fluid and external gas source react with each other and with the solid material. The fluid represents melt water and external gas source can represent magmatic gases such as CO_2, SO_2, HCl and HF.

Water samples collected during both floods had neutral to alkaline pH and conductivity up to 900 µS/cm. Alkalinity present mostly as HCO_3^- was ~9 meq/kg during the flood peak but stabilized at around 1 meq/kg. Small amount of H_2S (up to 1.5 µmol/kg) was detected. Concentrations of most of dissolved constituents including magmatic volatiles Cl^-, F^- and SO_4^{2-} in flood water were comparable to the annual concentrations variation of these elements in considered rivers. Comparison of the flood water with Icelandic groundwaters and simple reaction path modelling of fluid chemical evolution suggest that the dissolved element composition of the flood waters developed due to long-time (at least two years) water-rock interaction in presence of limited amount of gases without direct contact of water with magma. This suggests that the origin of the heat source for glacier melting and causing these floods to emerge, was geothermal rather than volcanic.

Útdráttur

Megintilgangur rannsóknarinnar var að hanna, byggja og prófa stóran háþrýstihvarfastokk *(e. high pressure column flow reactor)* til notkunar við tilraunir á rannsóknarstofu á efnaskiptum bergs og gasríks vökva, í þessu tilviki koltvíoxíðs (CO_2). Hvarfastokkurinn er 2.3 m langur og gerður úr títani. Stokkinn er hægt að fylla með steindum og/eða gleri og hönnun hans gerir kleift að taka sýni af gasríkum vökva í snertingu við steindirnar/glerið undir þrýstingi. Framkvæmd var röð tilrauna með hreinu vatni og kolsýrðum vatnslausnum (0.3-1.2 M $CO_{2(aq)}$) og basaltglerkornum. Stærð hvarfastokksins, möguleikinn á að taka vökvasýni á mismunandi lengdarbilum undir þrýstingi og að fylgjast með þróun uppleysts ólífræns kolefnis (DIC) og pH *in-situ* gerir hvarfastokkinn einstakan í samanburði við aðra slíka stokka sem hannaðir eru fyrir rannsóknir á efnahvörfum vatns og bergs. Niðurstöður tilrauna við 22 °C og án teljandi íblöndunar koltvíoxíðs sýndu að pH-gildi hreins vatns breyttist frá 6.7 í 9-9.5 við það að flæða í gegnum stokkinn og stærstur hluti uppleysts járns féll út í síðsteindum, líkt og í náttúrulegum kerfum basalts, regnvatns og grunnvatns *(e. meteoric waters).* Við það að skipta út alkalíska vökvanum í stokknum fyrir kolsýrt vatn varð vökvinn í fyrstu yfirmettaður með tilliti til karbónatsteinda en um leið og kolsýrða vatnið fyllti stokkinn og pH-gildið lækkaði í 4.5 hélst vökvinn undirmettaður með tilliti til allra karbónata. Hreyfanleiki og styrkur nokkurra málma jókst umtalsvert í CO_2-vökvafasanum og sumir málmanna, m.a. Mn, Fe, Cr, Al og As, fóru yfir leyfileg mörk í drykkjarvatni. Járn leystist og hlutfallslegur styrkur Fe^{2+}/Fe^{3+} í vatnslausn jókst við gegnumflæðið. Leysing basaltglersins náði ekki að brjóta niður búffereiginleika kolsýrða vatnsins. Á fyrstu 40 mínútunum, á meðan vatnið flæddi um fyrstu 18.5 cm stokksins, urðu efnaskipti kolsýrða vatnsins við basaltglerið til þess að pH-gildið hækkaði úr 3.4 í 4.5 en hélst svo stöðugt í gegnum seinni 2.1 metra stokksins.

Þar sem eldvirk svæði eru hulin jöklum myndast vatnsfylltir katlar undir jöklunum vegna jarðhita og jafnvel eldgosa. Katlarnir tæmast reglulega í jökulhlaupum. Sum þessara hlaupa, sér í lagi hlaup vegna eldvirkni, geta valdið miklum skaða og getur stærð þeirra verið á við Amazonfljótið (>200,000 m^3/s). Í júlí 2011 brutust tvö lítil jökulhlaup (um 2,000 m^3/s) undan Mýrdalsjökli í Múlakvísl og undan Vatnajökli í Köldukvísl. Það má líta á efnaskipti vatns, bergs og gastegunda í jökulkötlum, sem efnaskipti í háþrýstihvarfastokk. Stokkurinn er þá fylltur með bergi með ákveðinni efnasamsetningu og þekktu yfirborðsflatarmáli og vökvi og gas látið leika um bergið svo vökvi, gas og berg geti hvarfast. Vökvinn er lýsandi fyrir jökulbráð og gasið kvikugastegundir á borð við CO_2, SO_2, HCl og HF. Gildi pH vatnssýna sem safnað var á meðan flóðunum tveimur stóð voru hlutlaus eða basísk og leiðni allt að 900 µS/cm. Basavirkni (*e. alkalinity*), aðallega vegna bíkarbónats (HCO_3^-), mældist hæst ~9 meq/kg við hámark flóðsins úr Mýrdalsjökli en náði jafnvægi við um 1 meq/kg er líða tók á flóðin. Styrkur H_2S var lítill í vatninu (minni en 1.5 µmol/kg).

Styrkur flestra uppleystra efna í flóðvatninu, m.a. styrkur jónanna Cl^-, F^- og SO_4^{2-}, sem geta rakið uppruna sinn til kvikugass, var sambærilegur árssveiflu þessara efna í umræddum ám. Samanburður á flóðvatninu við íslenskt grunnvatn og einfaldir líkanareikningar á þróun vökvans benda til þess að efnasamsetning leystra efna í leysingarvatninu þróaðist við efnaskipti vatns og bergs á löngum tíma (a.m.k. tveimur árum) þar sem gas var í takmörkuðu magni og án beinnar snertingar vökvans við kviku. Þetta bendir til þess að hitagjafinn sem olli bráðnuninni, og þar með jökulhlaupunum, hafi verið jarðhiti fremur en eldsumbrot.

Contents

PREFACE

The work presented in this doctoral thesis is a result of study carried out at the Institute of Earth Sciences, University of Iceland during the period of August 2009-Septemper 2013. The study was part of the European Union Initial Training Network DELTA-MIN and the CarbFix project. The research resulted in four publications in international peer-reviewed journals:

1. Galeczka I., Wolff-Boenisch D., Jonsson T., Sigfusson B., Stefansson A., Gislason S.R. (2013) A novel high pressure column flow reactor for experimental studies of CO_2 mineral storage. *Applied Geochemistry* **30**, 91-104.
2. Galeczka I., Wolff-Boenisch D., Oelkers E.H., Gislason S.R. (2013) An experimental study of basaltic glass-H_2O-CO_2 interaction at 22 and 50 °C: Implications for subsurface storage of CO_2. *Geochimica and Cosmochimica Acta*, in review.
3. Galeczka I., Wolff-Boenisch D., Gislason S.R (2013) Experimental studies of basalt-H_2O-CO_2 interaction with a high pressure column flow reactor: The mobility of metals. *Energy Procedia* **37**, 5823-5833.
4. Galeczka I., Oelkers E.H., Gislason S.R. (2013) The chemistry and element fluxes of the July 2011 Múlakvísl and Kaldakvísl glacial floods, Iceland. Submitted to *Journal of Volcanology and Geothermal Research, August 26, 2013*.

The work done during the study has also been presented at local and international conferences and meetings resulting in published abstracts and reports:

1. Galeczka I., Wolff-Boenisch D., Gislason S.R. (2012) Experimental studies of basalt-H_2O-CO_2 interaction with a high pressure column flow reactor: the mobility of metals. VoN Research Symposium 2012, Reykjavik, Iceland.
2. Galeczka I., Wolff-Boenisch D., Gislason S.R., (2012) Experimental studies on in-situ CO_2 mineral storage: Presentation of a novel plug flow reactor. International Conference on Greenhouse Gas Technologies (GHGT) 2012, Kyoto, Japan.
3. Wolff-Boenisch D., Galeczka I., Gislason S.R., Oelkers E.H. (2012) Geochemical aspects of in-situ mineralization in seafloor basalts in presence of seawater. International Conference on Greenhouse Gas Technologies (GHGT) 2012, Kyoto, Japan.
4. Galeczka I., Eiriksdottir E.S., Gislason S.R. (2012) CO_2 sequestration before and during volcanic eruption - field and laboratory studies. Goldschmidt conference 2012, Montreal, Canada.

5. Galeczka I., Wolff-Boenisch D., Gislason S.R. (2012) Experimental studies on CO_2 mineral storage: A plug flow reactor study. Conference 'Mechanisms of Mineral Replacement Reactions' 2012, Oviedo, Spain.
6. Galeczka I., Wolff-Boenisch, D., Gislason S.R. (2012) Experimental studies on CO_2 sequestration: A plug flow reactor study. 30th Nordic Geological Winter Meeting, 2012, Reykjavik, Iceland.
7. Galeczka I., Gislason S.R. (2011) Hlaup í Sveðju og Köldukvísl 13. júlí 2011. Report in Icelandic.
8. Galeczka I., Eiriksdottir E.S., Gislason S.R. (2011) Hlaup í Múlakvísl 9. júlí 2011. Report in Icelandic.
9. Gislason S.R., Olsson J., Galeczka I., 2011. Volcanic ash from the first 24 hours of the 2011 Grimsvötn eruption: Cumulative grain size distribution and surface properties. Report.
10. Galeczka I., Wolff-Boenisch D., Gislason S.R. (2011) Experimental studies on CO_2 sequestration with a plug flow reactor. Goldschmidt conference 2011, Prague, Czech Republic.
11. Galeczka I., Wolff-Boenisch D., Gislason S.R. (2011) Modeling CO_2 sequestration in basaltic rocks with a plug flow reactor. The 2nd European Geothermal PhD day 2011, Reykjavik, Iceland.
12. Galeczka I., Wolff-Boenisch D., Gislason S.R. (2010) Experimental studies on CO_2 sequestration with a plug flow reactor. A Symposium on Current Research in Engineering and Natural Sciences at University of Iceland 2010, Reykjavik, Iceland.

Acknowledgements

This study was funded, the European Union through the European Marie Curie network Delta-Min, SP1-Cooperation CarbFix, the Environmental Fund of Reykjavík Energy, University of Iceland, RANNÍS, Hitaveita Suðurnesja, and Norðurál.

There are many people who I would like to thank regarding my PhD project. First of all I would like to thank my main supervisor Sigurður Gíslason for his support, smile and positive attitude which was necessary for me to believe in what I do. He gave me the opportunity to conduct fantastic PhD project which combined laboratory and field studies making me a better geochemists. Being a part of DELTA-MIN network and CarbFix group gave me the possibility to interact with highly skilled and very clever people.

My second supervisor Domenik Wolff-Boenisch spent with me most of the time in the laboratory teaching how to conduct experiments and how to fix all kind of problems by systematic and logical thinking. His office door was always open for me whenever I needed long or short answer for my questions. Even being on the

other side of the globe, he was still with me helping in writing and discussing continuously appearing problems in the laboratory. I am very grateful for that.

At the latest stage during my PhD project – the most stressful time for me – Eric Oelkers participated in finalizing my last manuscripts. He significantly contributed to the scientific discussion about the study. He helped me with writing and he guided me how to select results to make them publishable. He also helped me to understand what I have learned from my field and experimental studies.

Þortsteinn Jonsson taught me how to fix equipment, he encouraged me to disassemble the pumps/regulators/magnetic drivers/valves etc. when they did not work properly. I do not know how many hours we spent together forcing the CO_2 pump to work. He convinced me that equipment is just a thing and I cannot be afraid of taking it apart even if I might not be able to put it together again.

The first day I started working at the Institute, Domenik left me with Helgi Alfredsson who was assembling and testing the bailer. Due to lack of basic knowledge of CO_2-H_2O interaction and difficulties in understanding icelandic English, I barely caught what Helgi was telling when describing the principles of the bailer operation. Fortunately, with time I understood more and I became more interested. It was a fantastic preparation for what was waiting for me later with my experimental work. He was a great teacher who really enjoyed talking and showing how to perform laboratory work.

Eydís Salóme Eiríksdóttir was with me in the beginning of working in the lab, supporting when I was tired of my work and scared of Domenik. I could always count on her. She was fantastic teacher in the lab and in life, reminding me what is the most important in life and how essential is the contact with the nature.

My second Master studies supervisor, Jarek Majka sent me the advertisement about the PhD project conducted in Iceland when I was working at the Polish Geological Institute. He encouraged me to leave the job and try something exciting. I applied because I thought I will never get the position but luckily I was accepted so I owe big thanks to Jarek.

I would like to thank: Níels Óskarsson, Bergur Sifgússon, Andri Stefánsson and Ingvi Gunnarson for scientific discussions and help in the laboratory.

I would like to also acknowledge the DELTA-MIN and CarbFix members for scientific and social network meeting.

There are many colleagues who I want to thank for help, support, discussion and lot of fun time, especially: Kiflom Mesfin, Snorri Guðbrandsson, Nicole Keller, Hanna Kaasalainen, Utra Mankasingh, Sandra Snæbjörnsdóttir, Karolinka Michalczewska, Christian Grimm, Jonas Olsson, Alexander Gysi, Gabrielle Stockmann, Ari Hultqvist, Kevin Padilla, Alejandro Rodriguez, Ásgerdur Sigurðardóttir, Morgan Jones, Rebecca Neelay, Sylviane Lebon, Julia Björke, Gro Birkefeldt Pedersen, Stephane Beaussier.

Finally, I would like to thank my parents and the rest of my family and friends who were always supporting me and were waiting for me to come for a short vacation to Poland. I am extremely grateful to my husband Lukasz, who was the buffer with enormous capacity to take all my frustration, anger and sadness when things were not working. He never complained that the work was in the first place.

Chapter 1

Introduction

1.1. CARBON CYCLE

The carbon cycle is a short-term and/or long term transfer of carbon between atmosphere, lithosphere, hydrosphere and biosphere. The short-term and long-term expressions refer to the duration of the carbon transfer between reservoirs. The short-term carbon cycle lasts from days to tens of thousands of years, short time on a geological time scale. The duration of the long-term cycle varies from tens of thousands to millions of years (Berner, 2004). In the short-term carbon cycle, atmospheric carbon dioxide (CO_2) is converted into organic carbon by photosynthesis – the so called primary production – when chemical reaction between CO_2 and water with the presence of solar energy produces organic matter and oxygen. Organisms able to photosynthesize are consumed by other organisms – the so called consumers – which cannot utilize the solar energy directly and they convert the chemical energy stored in plants into metabolic energy and respire. During the respiration organic tissues react with oxygen producing CO_2 and water. In anaerobic conditions the organic matter is decomposed by fermentation during which CH_4 and CO_2 is produced. In marine environments phytoplankton consumes CO_2 and produces organic matter and O_2 in the same way as plants do on land with the exception that the gases are dissolved in seawater; nevertheless there is continues exchange of these gases between seawater and atmosphere. The decomposition of marine organic matter releases CO_2 and nutrients to the oceans. Some part of organic matter during short term cycle is also buried in marine sediments. In the long-term carbon cycle, in addition to the short-term carbon cycle, transport from and into the rocks is included. During the organic long term carbon cycle, the sediments, mostly muds, undergo a lithification process, and if they are exposed to the atmosphere, organic matter is oxidized and CO_2 is released as a product of its weathering. In the inorganic carbon cycle CO_2 interacts with the rainwater creating an acidic solution which dissolves minerals resulting in release of cations and anions into percolating fluids. Also organic acids produced by plants act in the same way. These elements are transferred into rivers and further into the sea where carbonates precipitate, mainly biogenically. Afterwards, carbonates may dissolve or may become a part of marine sediments and enter the geologic record. Continental drift

will eventually bring some of the marine carbonates into subduction zones where they break down and form magmatic CO_2. This magmatic CO_2 finds its way to the atmosphere through volcanoes and geothermal systems. Similarly, carbon dioxide derived from the mantle enters the atmosphere at oceanic ridges. A simplified reaction describing the long-term carbon cycle is as follow:

$$\mathbf{CaSiO_3} + 2CO_2 + 3H_2O = Ca^{2+} + 2HCO_3^- + H_4SiO_4 = \mathbf{CaCO_3} + \mathbf{SiO_2} + CO_2 + 3H_2O \quad (1)$$

This reaction indicates that atmospheric CO_2 reacts with silicate minerals (here wollastonite, $CaSiO_3$ as an example) producing solid carbonates and silica (for example calcite, aragonite and chert). In natural systems weathering involves Ca-Mg-aluminosilicates with aluminium precipitating as clay minerals.

The long-term carbon cycle consists of subsequent subcycles:

1. Chemical weathering of silicates.
2. Organic matter and carbonate burial and weathering.
3. Degassing of CO_2 and methane.

Chemical weathering of silicates. Silicate weathering plays an important role in the carbon cycle. Rates of weathering depend on the temperature, rainfall and runoff, lithology and relief, and land vegetation. The raise in temperature increases the rates of weathering and eventually leads to a negative feedback for the stabilization of the Earth's climate at geological time scale (Berner, 2004; Gislason et al, 2009; Walker et al., 1981; White and Blum, 1995). As presented by many studies, minerals dissolve faster at higher temperatures (Gislason and Oelkers, 2003; Gudbrandsson et al., 2011; Wolff-Boenisch et al., 2004; Wolff-Boenisch et al., 2011). In addition, higher temperature intensifies rainfall and runoff and therefore increases the weathering rate. The other factors such as sun radiation, greenhouse gasses and the continental drift will influence the local climate and the temperature and therefore the weathering rates. If the primary minerals are exposed to the atmosphere and there is no secondary minerals cover – the weathering rates increase.
Plants generally increase the weathering rates by secreting organic acids with the aim of uptaking nutrients released from the dissolution of minerals. When plants are decomposed, the supply of acids enhances the dissolution of minerals. In the presence of secondary clay cover, roots of the plants adsorb the moisture on clays enabling further dissolution of primary minerals. If the contact of water with the mineral surface is short – chemical weathering rates decrease, e.g. in absence of vegetation on high slopes (Berner, 2004).

Organic matter and carbonate burial and weathering. The organic carbon subcycle is represented by photosynthesis and burial of organic matter in sediments. Buried organic matter undergoes the oxidative weathering when exposed to

atmosphere or microbial and thermal decomposition to gasses containing reduced carbon, followed by oxidation of gases upon emission to the atmosphere. Both processes affect the level of atmospheric O_2 and CO_2. Burning the fossil fuels by humans is an accelerated process of weathering and thermal degassing of hydrocarbons but at a speed about 100 times faster than it would occur naturally (Berner, 2004).

In the long-term cycle, chemical weathering of carbonates has little direct effect on atmospheric CO_2. The dissolution of $CaCO_3$ followed by transport of Ca^{2+} and HCO_3^- to the oceans and precipitation of new $CaCO_3$ results in no net change in atmospheric CO_2. Even though there is no direct effect of carbonates weathering on the atmospheric CO_2, the CO_2 derived from carbonate weathering must be taken into account when calculating the total carbonate burial from weathering of silicates. Carbonate decomposition will lead to CO_2 degassing.

Degassing of CO_2 and methane. The degassing of CO_2 and CH_4 occurs in seismically active areas characterized by processes such as: spreading of tectonic plates, volcanic eruptions, orogenesis, hot spots, mid-plate regional metamorphism, diagenesis, and subduction. Degassing can be sudden and violent like during eruptions but also slow and continuous like from hot springs and fumaroles.

Volcanic emission of CO_2 from magma and from degassing of magma beneath volcanoes ranges between 0.15 and 0.26 Gt per year, whereas anthropogenic CO_2 emission is estimated to be 35 Gt in 2010 (Gerlach, 2011). It is significantly less than land use changes (3.4 Gt/year), light duty cars (3.0 Gt/year), and cement production (1.4 Gt/year) (Gerlach, 2011). The CO_2 release from volcanic systems is comparable to the CO_2 emission from 24 full-capacity 1000 MW coal-fired power plants (0.22 Gt/year) – which is 2% of the world's coal-fired electricity generating capacity. For comparison, Poland released about 0.31 Gt/year of CO_2 into the atmosphere in 2010 which is more than the world annual volcanic CO_2 emission (IEA, 2012). It has to be mentioned that the total rate of CO_2 emission of two of the biggest eruptions in the 20th century was estimated to be 0.007 Gt/hour (Eruption of Mount St. Helen on 18th May, 1980 and Mount Pinatubo on 15th June, 1991) and it exceeded anthropogenic rate of CO_2 emission which was 0.004 Gt/hour in 2010 (Gerlach, 2011). However, the overall contribution of both eruptions to the annual volcanic CO_2 emission was only 14%, which means that there would have to be at least seven eruptions of that size during one year to exceed the total amount of volcanic CO_2 released to the atmosphere and about 580 eruptions to exceed annual 2010 anthropogenic CO_2 emission.

1.2. THE CO_2 IN THE ATMOSPHERE

Many studies confirm rising global temperature and link it to the increased atmospheric CO_2 concentration caused by human activity, mainly by burning fossil

fuels (Crowley, 2000; IPCC, 2005; Johns et al., 2003; Karl and Trenberth, 2003; Manabe and Stouffer, 1994). Even though water vapour is the most abundant greenhouse gas, its amount is not related directly to the human activity but it is controlled by evaporation. However, increased temperature caused by increased atmospheric CO_2 content will affect the evaporation rate creating a positive feedback between CO_2, temperature and vapour. Figure 1 presents historical CO_2 concentration and temperature measured from the Vostock Antarctic ice cores. There is clearly a strong correlation between both parameters during the past 400,000 years indicating a positive feedback between CO_2 concentration and temperature. There are two scenarios regarding this correlation, one suggests that the increased CO_2 content and thus greenhouse gas effect increased the global temperature, and second one posits that increased temperature accelerated the CO_2 degassing from the oceans since CO_2 solubility decreases with increasing temperature. Nevertheless, clarification of this issue requires more data and analysis of the past sun radiation, Earth orbit and processes influencing the hydrosphere development. In addition, a model carried out by Stott et al. (2003) reveals that during the first half of the 20th century solar activity played an important role in the global temperature in contrast with the second half, when the climate was mostly affected by greenhouse gas increase. As can be seen in Fig. 1, and more recent references (Jouzel et al., 2007; Lüthi et al., 2008) the concentration of CO_2 in the past 400,000 years has never exceeded the amount of CO_2 measured at present day, indicating that fossil fuels used by human is a main source of increased CO_2 concentration since the industrial revolution.

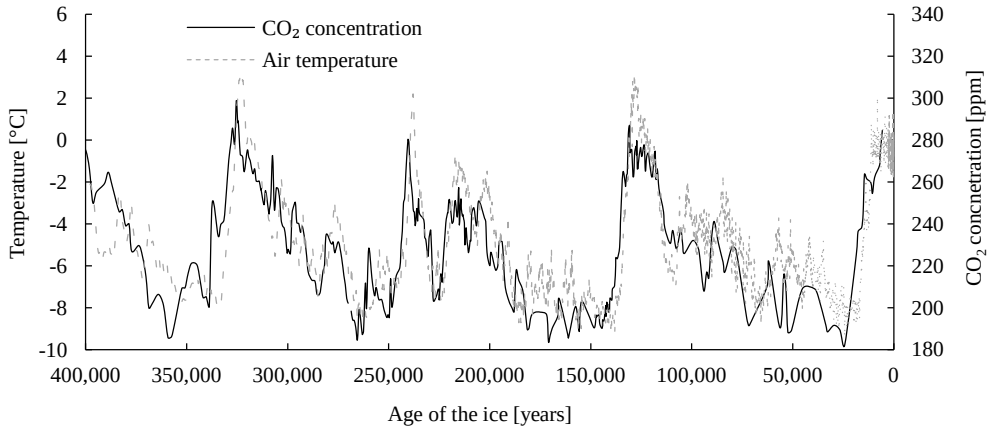

Figure 1. Global air temperature (grey dotted line) and CO_2 concentration (black line) over the past 400,000 years derived from Antarctic ice-core data (from Barnola et al. (2003) and Petit et al. (1999)).

The continuous measurement of atmospheric CO_2 concentration at the Mauna Loa Observatory reveals that the CO_2 concentration increased from about 315 ppm (by volume) in 1960 up to 398 ppm in the beginning of 2013 as depicted on Fig. 2a.

Annual variations in the CO_2 concentration stem from changes in seasonal biological activity. Rise in atmospheric CO_2 content is attributed primarily to the CO_2 emission from burning of fossil fuels. As presented in Fig. 2b, in 2010 the main source of human CO_2 emission was 1) burning of coal (41.7%), 2) burning of oil (34.1%), 3) burning of gas (18.5%), 4) cement production (4.9%) and 5) gas flaring (0.8%).
Even though the atmosphere is the smallest global CO_2 reservoir – it contains only 0.001% of the total carbon present in the atmosphere, oceans and upper crust – the increased CO_2 concentration has far-reaching effects including raising atmospheric temperature, intensification of the precipitation and hurricanes (Groisman et al., 2005), decrease of the ocean thermohaline circulation (Broecker, 1997), melting of glaciers and therefore increase in the sea water level, ocean acidification (Mackenzie and Anderson, 2013), and extinction of species in polar environments (Parmesan, 2006).

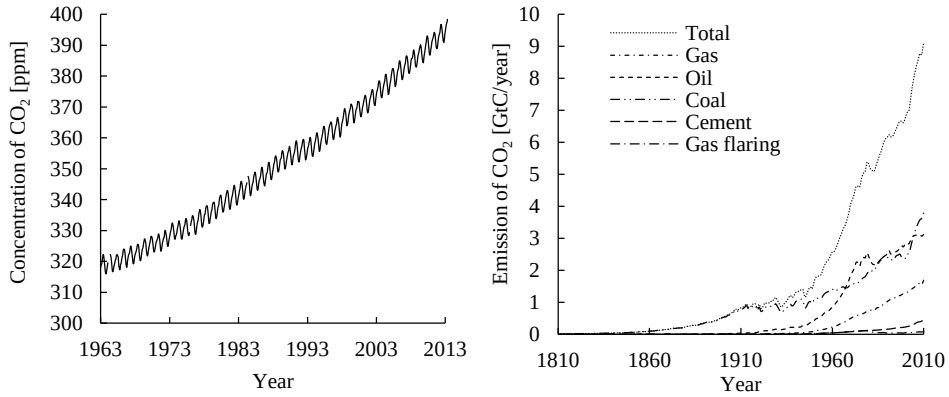

Figure 2: Plot (a) represents the average atmospheric CO_2 concentration (in ppm) measured at the Mauna Loa observatory over the past 50 years. Data taken from Keeling et al. (2009). Plot (b) presents the annual human CO_2 emission to the atmosphere since 1810. Plots were made based on data taken from Boden et al. (2012) for 1810-2009, and from Boden and Blasing (2010) for 2010.

Elevated partial pressure of CO_2 decreases the pH of the waterbody, especially oceans. This may lead to destruction of marine ecosystems by destabilization of calcite. As described by Andersson et al. (2006) many marine organisms which build their skeletons from carbonates such as corals, molluscs, foraminifera will be negatively affected by lower pH of the water and therefore the entire food chain is likely to suffer. It is evident that the rate of present human-induced ocean acidification is most likely unprecedented in the geologic record for the past 800,000 years, the time record of atmospheric CO_2 and temperature as obtained from ice cores (Jouzel et al., 2007; Lüthi et al., 2008; Mackenzie and Andersson, 2013).

Although the climate change impact on the environment has been discussed for a long time, the atmospheric CO_2 concentration is still raising and the International Energy Agency predicts that energy production will increase by 30%; furthermore according to them the fossil fuel will constitute about 80% of the total energy

production. It is estimated that by 2100 the CO_2 concentration in the atmosphere will increase even up to 570 ppm and the temperature will rise by 3.8 ℃ if economic growth will keep the same pace (IEA, 2012).

Most people are aware of the consequences of the climate change, and the price which one has to pay for the damages caused by climate change (e.g. floods, hurricanes), however, there will be no reduction in usage of fossil fuels since it is the cheapest energy source available for next decades. Also, it is not in the economic interest of countries which are the main producers of oil, gas and coal to cut down the production so there will be no support for those countries to develop and produce alternative sources of energy. In addition, the USA, China, and India which are the top-three emitters of CO_2 in the world will still use fossil fuels to sustain economic growth. It seems that engineering carbon storage is a reasonable option to stem the predicted CO_2 emission in the future and curb sea level rise and ocean acidification. However, in Europe the politics regarding Carbon Capture and Storage (CCS) is going through difficult times. A recent review by the European Commission reveals that cost and a lack of a proper long-term business case for implementing CCS are two main reasons for delay in introduction of a legal framework for the development of CCS. The economic crisis and over-allocation of emission allowances within the European Union (EU) has led to a much lower-than-expected CO_2 price. Removing and storing a tonne of CO_2 through CCS costs €30-100, depending on the type of fuel, transportation and technology of storage compared to the costs of EU-emission quota which was about €5 per tonne of CO_2 early 2013. Private operators have been forced to rely almost exclusively on private funding for their demonstration projects, due to governmental cuts on public funding. In addition some onshore pilot projects have also faced opposition from local communities and unexpected technical difficulties that have brought the projects to a halt. The Commission initiated a public consultation to explore options on how to revive CCS development in Europe. The Commission is considering a mandatory CCS certificate for carbon emitters, mandatory emission performance standards and national funding for CCS investments in demonstration projects. If this action is implemented successfully the CCS in Europe has a chance to develop an important scheme for reduced CO_2 emissions into the atmosphere (Comment Visions, 2013).

1.3. CARBON CAPTURE AND STORAGE (CCS)

Carbon capture requires immobilization of the CO_2 emitted directly from the power plants, cement production facilities, gas refineries etc. The CO_2 released from moving sources such as vehicles and airplanes will require to be captured directly from the atmosphere. Transportation of captured gas to the place where it can be safely stored is carried out by pipelines, ships and trucks. The choice of the transportation method depends on the costs, distance between the CO_2 emitter and

the storage area, present and future amount of the transported CO_2, and pressure limits of the transporting facilities. There are three main CO_2 storage methods: 1) ocean storage, 2) geological storage 3) mineral storage.

During the ocean storage, CO_2 could be injected into the ocean at depths greater than 3000 m where liquid CO_2 is denser than seawater and therefore providing isolation from the atmosphere for decades over centuries (Adams and Caldeira, 2008). The capacity of the ocean for CO_2 storage is estimated to be 10,000 Gt of C, however more realistic assessment requires taking into account the impact of the CO_2 on the marine chemistry. The CO_2 dissolution in the oceanic water results in pH decrease. However, the pH change would be initially limited to the injection points which are the largest at greater depths and therefore in the short term perspective it is safe for most of the marine organisms (Adams and Caldeira, 2008). This option of carbon storage has not been tested in a field scale and requires further study of its effect on the environment.

Geological storage requires injection of CO_2 into porous formations such as sedimentary basins, depleted oil and gas reservoirs and coal beds (Benson and Cole, 2008; Bickle et al., 2007; Haugen et al., 2013; IPCC, 2005; Kharaka et al., 2009; Pham et al., 2011). Because the CO_2 density at injection conditions is lower than surrounded pore water, the impermeable cap rock is necessary to prevent the CO_2 from escaping into the atmosphere. Because the injected CO_2 stays buoyant for a long time due to low solubility of CO_2 in formation water, monitoring of the behaviour of the CO_2 at the injection site is required for a secure geological storage. Benson et al., (2005) describe two monitoring programs that could be used during the engineered geological carbon storage which among others include geophysical and geochemical monitoring methods. They have been already implemented in some of the CCS field projects (Emberley et al., 2005; Hovorka et al., 2011; Martens et al., 2011; Mito and Xue, 2011; White, 2011; Whittaker et al., 2011).

Mineralization of CO_2 is the safest method of carbon storage. It requires interaction between silicate minerals and CO_2 leading to formation of stable carbonates such as calcite, dolomite, magnesite, and siderite (Oelkers et al., 2008). This method mimics natural weathering of silicates which plays a major role in the long term carbon cycle (Berner, 2004). The dissolution of Ca-Mg-Fe bearing silicates provides divalent cations, like Ca^{2+}, Mg^{2+}, and Fe^{2+} which after interaction with dissolved CO_2 precipitate as carbonates (see Eq. 2-7). These reaction products are stable over geological time scale minimizing the risk of CO_2 leakage into the atmosphere. It is estimated that about 0.4 Gt of CO_2 is fixed annually as bicarbonate (HCO_3^-) by silicate weathering on the continents and volcanic islands of the Earth (Gaillardet et al., 1999).

Generally, carbonatization involves several chemical reactions. First, after injection into the groundwater CO_2 dissolves in accord with:

$$CO_{2(g)} + H_2O = H_2CO_3 \quad (2)$$

Second, carbonic acid (H_2CO_3) dissociates causing liberation of protons and decreasing the pH of water:

$$H_2CO_3 = HCO_3^- + H^+ \quad (3)$$

The amount of the dissolved CO_2 depends on the partial pressure of CO_2, total hydraulic pressure of the aquifer, temperature, pH and the salinity of the water. Decreased temperature and salinity increases the solubility of CO_2.
Third, protons are consumed by dissolution of Ca,Mg-silicates during which divalent cations are released, for example:

$$\mathbf{(Mg,Fe)_2SiO_4} + 4H^+ = 2(Mg,Fe)^{2+} + SiO_{2(aq)} + 2H_2O \quad (4)$$

$$\mathbf{CaAl_2Si_2O_8} + 8H^+ = Ca^{2+} + 2Al^{3+} + 2SiO_{2(aq)} + 4H_2O \quad (5)$$

$$\mathbf{CaMgSi_2O_6} + 4H^+ = Ca^{2+} + Mg^{2+} + 2SiO_{2(aq)} + 2H_2O \quad (6)$$

Finally, similar to the simplified reaction (1) describing the silicate-carbon subcycle, released cations interact with dissolved CO_2 resulting in precipitation of carbonate that can be summarized as:

$$(Ca,Mg,Fe)^{2+} + CO_2 + H_2O = \mathbf{(Ca,Mg,Fe)CO_3} + 2H^+ \quad (7)$$

Reaction (7) can proceed to the right only if the protons are consumed by dissolution of minerals and therefore dissolution of silicates is most cases the rate limiting step for carbonatization (Oelkers et al., 2008). Mafic (basalts) and ultramafic (peridotites) rocks are rich in divalent metals, highly reactive and abundant on the Earth surface. This makes them perfect candidates for mineral trapping.

Ultramafic rocks consist of olivine $(Mg,Fe)_2SiO_4$, orthopyroxene $(Mg,Fe)_2Si_2O_6$, and clinopyroxene $(Mg,Fe)CaSi_2O_6$ and therefore are rich in divalent metals. The most common type of ultramafic rock is peridotite. It originates from the Earth upper mantle; however, due to emplacement it is observed on the Earth surface in vicinity of mid-ocean ridges, forearc regions of subduction, in ophiolite complexes, mafic and ultramafic intrusions, and in some orogenic massifs (Kelemen and Matter, 2008). During chemical weathering, peridotites react with water and CO_2 resulting in hydrous silicates (serpentinites), Fe-oxides, and carbonate precipitation. Partially carbonatized peridotites can be found on the seafloor and on land as ophicarbonates, listvenites, soapstones, and travertine. Results of recent studies indicate that peridotites have enormous potential for carbonatization (Andreani et al., 2009; Beinlich and Austrheim, 2012; Daval et al., 2011; Giammar et al., 2005; Hövelmann et al., 2011; Kelemen and Matter, 2008; King et al., 2010; Olsson et al., 2012a;

Paukert et al., 2012; Pokrovsky and Schott, 2000; Prigiobbe et al., 2009; Wolff-Boenisch et al., 2011).

Mafic rock represented by basalts are composed mainly of plagioclases $(Na,Ca)(Al,Si)_2SiO_8$, pyroxenes, e.g. augite $(CaMgFe)_2Si_2O_6$ and olivine $(Mg,Fe)_2SiO_4$. Large volumes of basalts can be found all over the world including large igneous provinces, such as the Columbia River basalts, Deccan and Siberian traps, and smaller outcrops of oceanic basaltic crust such as Iceland (McGrail et al., 2006; Oelkers et al., 2008). Furthermore, the upper oceanic crust is largely composed of basalts (Goldberg et al., 2010; Goldberg et al., 2008). According to Dessert and co-workers (2003) despite basalts covering only about 5% of the continental surface, they take up 30-35% of the CO_2 consumed by silicate weathering. Basalts are shown to be highly reactive under CO_2 conditions (Gislason et al., 2010; Gysi and Stefánsson, 2012; Munz et al., 2012; Schaef et al., 2010; Schaef et al., 2013; Wolff-Boenisch et al., 2011). Carbonates are often seen in natural basaltic groundwater and geothermal environments as a product of basalt-H_2O-CO_2 interaction (Alfredsson et al., 2013; Neuhoff et al., 2006; Rogers et al., 2006). The CO_2 originates either from the atmosphere or from magma degassing in volcanic areas. This provides a natural analogue for carbon mineral storage. The results of experimental work and analysis of naturally weathered basalts indicate carbonates and secondary Si-Al-bearing phases as alteration products of basalt-H_2O-CO_2 interaction (Kristmansdottir, 1982; Neuhoff et al., 2006).

The CO_2 mineral storage can be carried out *ex situ* or *in situ*. The *ex situ* carbon mineralization requires the CO_2-charged fluid reacting with silicates or other minerals such as MgO and CaO earlier mined and pre-treated under engineered or laboratory conditions (IPCC, 2005). This method provides an opportunity to control and accelerate the rates of carbonatization by increasing the surface area of minerals (grinding), increasing the temperature and pressure of reactors, adding chemical compounds which increase the dissolution rates of minerals. Higher reactive surface area not only provides more divalent cations released to the fluid making them available, but also creates more nucleation sites for secondary precipitation (Schott et al., 2012). Higher temperature increases the dissolution rates of primary minerals but also creates thermodynamically favourable conditions for carbonate precipitation due to their retrograde solubility. Also, elevated pressure increases the dissolution rates of basalt and peridotite (Wolff-Boenisch et al., 2011) and increases CO_2 solubility in the reactive fluid. The other advantage of *ex situ* mineralization is the possibility to reuse the mineral products of CO_2 interaction for the industry. The main disadvantages of this method are costs and energy use for maintaining the reaction vessels, mining and transportation of minerals to the “laboratory”.

During *in situ* carbonatization – CO_2 is directly injected into the subsurface where it reacts with the host rock. In contrast to the *ex situ* method, there are no

costs for maintaining the reactors, mining, and mineral transporting. However, the main disadvantage of this method is the lack of full control on the mineralization process. The choice of the target zone is critical. First, minerals have to be highly reactive and with possible minimal secondary alteration. Secondary minerals already present in the host formation can inhibit the dissolution of primary minerals. As it was mentioned above, mafic and ultramafic formations are the most suitable for mineralization trapping. Second, geological formations have to be permeable and porous enough to conduct the reactive CO_2-charged fluid at high enough injection rates far from the injection well, while at the same time require to store the reaction products and preserve the permeability. When the secondary minerals precipitate, their volume is higher comparing to the volume of primary dissolved phases and therefore alteration products can fill the pores and decrease the permeability (summarized in Putnis (2009)). There is also a possibility that the volume increase will generate fractures and therefore maintain the permeability (Jamtveit et al., 2009). Third, the redox conditions in the injection formation are critical since only Fe^{2+} has the potential to form carbonates. The Fe^{3+} can form secondary Fe(oxy)hydroxides and clays, decreasing the permeability of the aquifer and decreasing the Fe available for carbonate formation. In addition, redox state will affect the speciation of some toxic elements such as chromium (Cr). The Cr^{3+} is not dangerous for biota but the oxidized form Cr^{6+} is carcinogenic. Fourth, depth of injection will constrain the temperature of host rock-CO_2-charged fluid interaction. Greater depth and therefore higher temperature, lower than 250 °C (Wiese et al, 2008), provides better conditions for dissolution and precipitation of carbonates and also minimizes the influence of atmospheric oxidizing conditions.

Even though all factors affecting mineral dissolution-precipitation are taken into account when carrying out experiments in the laboratory, a field scale project is necessary to be conducted to check if carbonatization of basaltic rock is indeed effective and safe for the environment. *In situ* mineralization has been tested in the CarbFix pilot project, where CO_2 fully dissolved in water has been injected into basaltic formations (lava formation) in Iceland. The location of the injection site is within the geothermal power plant Hellisheiði where CO_2-H_2S mixture will be separated from geothermal gasses, mixed with groundwater taken in vicinity of the injection site and pumped down at about 550 m depth m and about 30 °C into a basaltic lava formation (Alfredsson et al., 2013; Aradóttir et al., 2012; Gislason et al., 2010; Oelkers et al., 2008). Figure 3 presents the aerial overview of the injection site at the Hellisheiði geothermal power plant. Two and three dimensional reactive transport modelling predicts that during the pilot scale injection of CO_2 (1,200 tonnes), 100% will be stored as carbonates within 10 years (Aradóttir et al., 2012). Results of modelling of the full scale CO_2 injection (400,000 tonnes) indicate that 80% of CO_2 will be stored within 100 years.

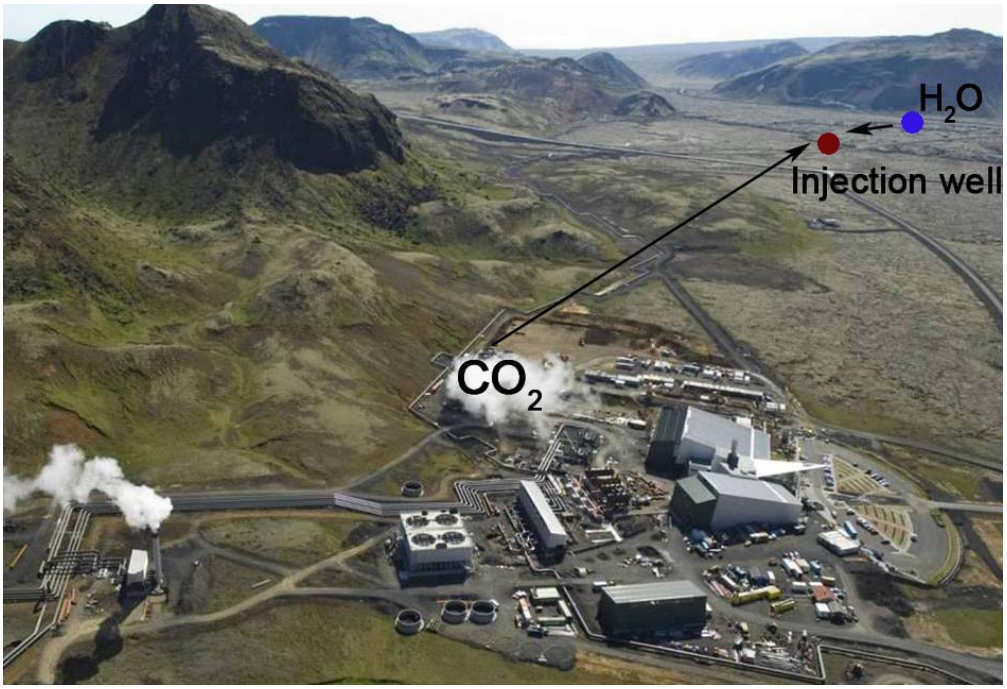

Figure 3. The overview of the Hellisheiði geothermal power plant. Water from the vicinity of the injection well and CO_2 from geothermal production will be mixed and pumped into basaltic lava flows at 550 m depth. Photo taken by Sigfús Mar Pétursson.

1.4. LABORATORY EXPERIMENT

To bridge the gap between field and laboratory scale CO_2-water-basalt interactions, a high pressure column flow reactor (HPCFR) was designed. This 2.3 meter long column enables to mimic natural processes occurring in natural and engineered systems. The column experiments can be carried out under high pressure and elevated temperature monitoring in-line vital parameters necessary to predict the progress of H_2O-CO_2-basalt interaction such as total dissolved inorganic carbon (DIC) and pH. In addition, samples of solute are taken on different horizons along the flow path within the reactor. After the experiment has finished, solid samples between different compartments along the flow path within the column can be analyzed to complement the solute chemistry analyses. The secondary alteration products will be explored at a later stage of the study. Even though the reactor was meant to mimic natural *in situ* carbon mineralization, the tool itself has a potential for *ex situ* mineralization efforts if the reactor is up-scaled.

A conceptual model of CO_2 injection into natural basaltic formation and into the column filled with basaltic glass grains was similar. In the beginning dissolution was predicted to be the dominant process due to low pH of the CO_2-charged fluid, but further along the flow path secondary carbonates were expected to form (Fig. 4).

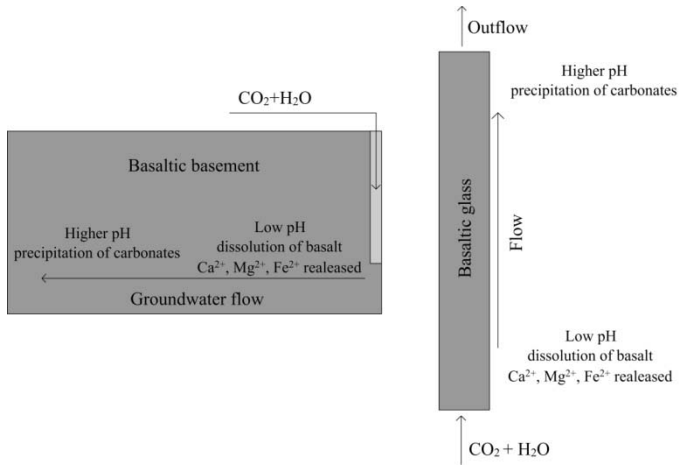

Figure 4. A conceptual model of CO_2 fixation during the field scale CarbFix project (left) and during the column flow experiment (right). In both cases, it is anticipated that in the beginning of basalt-H_2O-CO_2 interaction dissolution of rocks will be the dominant process whereas at later stages, as a result of proton consumption by basalt dissolution, pH will increase resulting in carbonates precipitation.

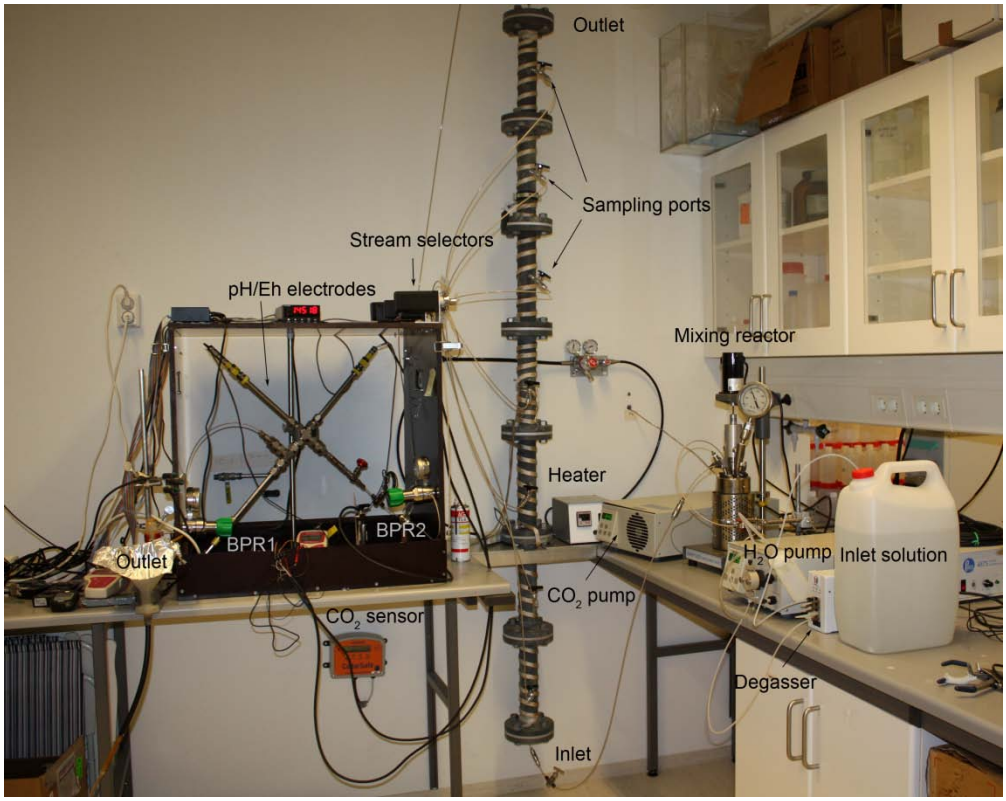

Figure 5. The experimental design. The CO_2-H_2O mixture is pumped into the mixing reactor and from there it flows through the column. From the column the reactive fluid passes a stream selectors where it is directed through pH/Eh electrodes and towards the back pressure regulator (BPR1) and finally to the outlet. The CO_2 and N_2 cylinders are placed on the other site of the wall.

Full description of the experimental design of the HPCFR is provided in the Chapter 2. The photograph of the experimental design with major components of the set-up is presented in Fig. 5. The short and long term CO_2-charged fluid injections into the column were carried out during this study and results of the fluid analyses are explored in Chapter 3 and 4. The experimental design allows for the direct evaluation of the ability of geochemical modelling codes to reproduce the solute chemistry along the flow path during CO_2-water-rock interaction. This is why reaction transport modelling of the column was performed whose results are described in Chapter 3.

The CO_2-charged fluid experiments carried out in the column not only mimic the CO_2 injection and storage but they also reflect the natural processes of CO_2 fixation in volcanic terrains. Another example of natural CO_2 storage, apart from weathering of silicates, is the fixation of CO_2 released from magmatic intrusions into groundwater, surface waters and glacier melt waters. The sub-glacial reservoirs formed due to enhanced heating from geothermal systems can be looked upon as a column flow reactor filled up with rocks of a given chemical composition and surface area, where percolating aqueous solution and external gas source react with each other and with the solid material. The fluid inside the column represents melt water whereas magmatic gases such as CO_2, SO_2, HCl and HF represent the external gas source. Waters accumulated under the ice cap periodically drain in sudden floods so called 'jökulhlaups' and depending on the triggering mechanism (volcanic or geothermal), can be more or less powerful. Their size varies from small (1,000 m^3/s) to Amazonian size (200,000 m^3/s) (Gudmundsson et al., 2008; Snorrason et al., 2002; Tomasson, 1996). In addition, depending on the heat source – they can be fertilizing and/or toxic (Gislason et al., 2002). For example if the glacial flood was triggered by volcanic eruptions, acid gas input can lead acidic flood waters and toxic metal release. If the heat source origin was geothermal, extensive, long-term fluid-rock interaction would lead to higher pH and non-toxic flood waters.

1.5. GENERAL DESCRIPTION OF JÖKULHLAUPS IN ICELAND

The glacial floods called 'jökulhlaups' in Icelandic are sudden bursts of water from a glacier dammed marginal lakes or from water reservoirs inside glaciers (Björnsson, 1975). The released water originates from melting of ice due to atmospheric processes, permanent geothermal heat or volcanic eruptions (Björnsson, 2009a). The floods can consist entirely of water or of a mixture of water, sediments, volcanic materials and ice. Depending on their frequency, topography under the glacier, amount of water, load of suspended material and ice, the impact on the flood plain and surrounding areas can be disastrous. The floods increase the erosion of land, create canyons, ridges, kettleholes and they deposit the sediments, icebergs, and boulders on outwash plain. In the Pleistocene, jökulhlaups transported enormous

amounts of sediments and icebergs over the vast glacier outwash plains which are called 'sandurs' in Icelandic. The floods can damage cultivated and vegetated areas, disrupt roads, bridges and alluvial plains, break the hydroelectric plant located on glacially fed rivers and generate enormous flood waves in coastal waters. There are two main causes of jökulhlaups in Iceland: 1) sub-glacial geothermal activity during which ice is melted continuously and accumulates in sub-glacial lakes which are periodically drained, 2) sub-glacial volcanic eruptions where the melt water is produced due to thermal energy released during fast cooling of magma (Gudmundsson et al., 2008). The chemical composition of the melt water is dictated by its interaction with surrounding rock and geothermal fluid circulating under the glacier, and overburden pressure which controls the solubility of gasses. During the eruption volcanic tephra and gasses will additionally interact with melted ice affecting the chemistry of the outburst waters. Intense melting causes lakes to expand resulting in increased basal pressure. This in turn can finally lift the ice sealing. The release of water can be slow and gradual or sudden and disruptive. The drainage of melt water can proceed within the tunnels which are created by heat of friction and heat of released water or it can be dispersed in a sheet under the glacier (Björnsson, 2009a). Steep slope of the flood channel will increase the speed of the water making the flood more powerful. If the overlying ice collapses, the flood can be terminated and accumulation of water starts again until another flood starts (Björnsson, 2009a).

The best documented glacial floods originate from the sub-glacial Grímsvötn Lake under the Vatnajökull ice cap. The peak discharge varies between 600 to 50,000 m^3/s at the outwash plain, their duration ranges up to 4 weeks and the total volume of released water is 0.5-4.0 km^3 each event (Björnsson, 2009b). The most violent Grímsvötn jökulhlaup flooded 1000 km^2 of the flood plain. Usually, the drainage starts at a water pressure around 6-7 bar lower than that exerted by the ice dam with small initial discharge within melted conduits. However, sometimes the lake level rises until the dam is floated so the discharge increases faster than the speed of melting conduits and the glacier can be lifted along the flow path (Björnsson, 2009a,b).

The glacial floods triggered by eruptions are the most violent ones. A flood which occurred in 1996 during the so called Gjálp eruption originated from the sub-glacial Grímsvötn Lake where the water melted at eruption site was being collected for a month. The discharge from the eruption site to the lake was estimated to be up to 5,000 m^3/s before the onset of the flood (Gudmundsson et al., 1997). The tremor measured at Grímsvötn started at 21:30 on Monday November 4 and the jökulhlaup came out of the glacier 11 hours later on November 5. The growth of the discharge was fast and many icebergs were floating in the flood water reaching all the way to the sea (Fig. 6). The peak discharge from the lake was attained within 16 hours and

it was 45,000 m^3/s what is around 10,000 to 15,000 m^3/s higher than during the jökulhlaups triggered by historical Grímsvötn eruptions in 1934 and 1938 (Björnsson, 2003; Snorrason et al., 2002). During the 40 hours of flood duration around 3.2 km^3 of water drained from the lake. The flood channel from Grímsvötn caldera could be clearly seen as it formed a depression-like structure on the surface of the glacier dotted with several holes. Because the glacier seal was destroyed due to melting of the ice the Grímsvötn Lake was totally emptied. This had never occurred in Grímsvötn before. The total dissolved flux during the flood was estimated to be 1 million tonnes which is the annual total dissolved solid of the biggest river in Iceland, the Ölafusa River. The dissolved CO_2 flux during the flood was 0.6 million tonnes. For comparison the estimated annual magmatic flux of CO_2 in Iceland equals to 1-2 millions tones (Arnórsson and Gislason, 1994; Gislason et al., 2002). The suspended sediment flux during the flood was 180 Mt and the suspended flux in the beginning of the flood was as high as 121 g/L (Stefánsdottir and Gislason, 2005).

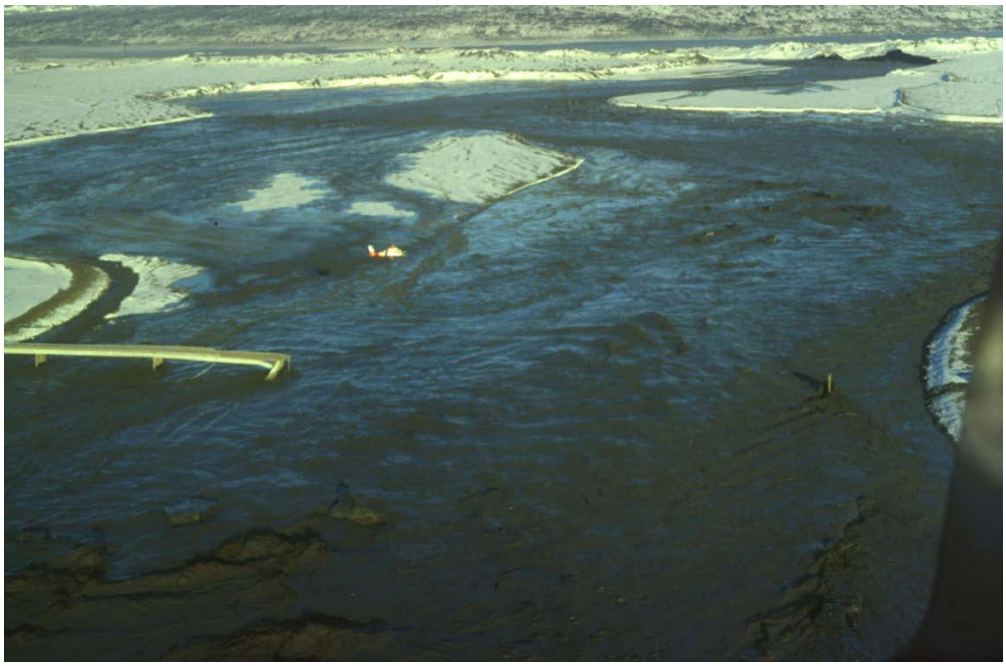

Figure 6. Overview of the jökulhlaup drained from the Grímsvötn Lake in 1996. The bridge on Gígja River on Road 1 was swept away. Photo taken by Magnús Tumi Gudmundsson.

There are many ice cauldrons on the surface of Mýrdalsjökull and Vatnajökull glaciers. The cauldrons are the depressions on the surface of the glacier caused by localized heat flux from the bedrock (Björnsson, 1975). The cauldrons may be semi-permanent or may persist only for a few years (Gudmundsson et al., 2007). Melt water is accumulated under the cauldrons and floods occur frequently from some of

them (Björnsson, 2009). Many of the smaller cauldrons do not change the surface geometry over long time period what is probably caused either by lack of water accumulation or by a constant drainage (Gudmundsson et al., 2007). The largest cauldrons formed in the western part of Vatnajökull – so called Skaftár Cauldrons and they are 2-3 km wide. Outbursts from these cauldrons can have a peak discharge of 200-1,500 m^3/s and the total volume of released water up to 0.35 km^3. Currently there are 18 cauldrons formed within Katla caldera rims on Mýrdalsjökull glacier and they are 20 to 50 m deep and 500 to 1000 m wide. Two photographs of the cauldrons can be seen in Fig. 7. In 1955, the jökulhlaup drained from eastern caldera rim reached a peak discharge of 2,500 m^3/s in 20 hours. Probably a small intrusion to the glacier base triggered the flood (Gudmundsson et al., 2007).

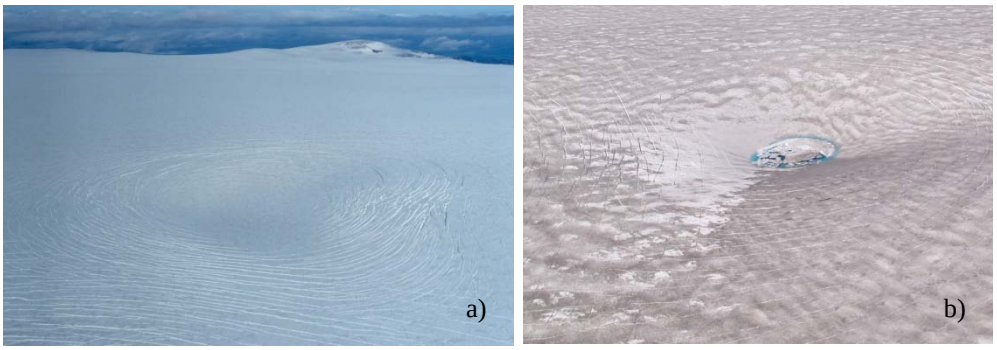

Figure 7. The cauldron nr. 7 (a) and nr. 11 (b) formed on the surface of Mýrdalsjökull ice cap. Photos were taken in August 1999 by Magnús Tumi Gudmundsson (a) and in July 2005 by Reynir Ragnarsson (b). The fresh crevasses are visible in around the depression indicating recent sub-glacial drainage (Gudmundsson et al., 2007).

The jökulhlaups can also be drained from marginal and ice-dammed lakes. Nowadays there are around 15 lakes at all the main glaciers in Iceland and most of them are located in ice-free tributary valleys (Björnsson, 1976). Due to glaciers recession, jökulhlaups have been more frequent (1-2 times a year) but smaller in volume because of thinning of the ice dams. The discharge of those jökulhlaups can ranges up to 3,000 m^3/s (Björnsson, 2009a).

The amount of melt water depends on the location of the eruption site, the input rate, chemical composition of magma and the conditions at the base of the glacier. The Katla eruptions under 600-750 m of ice release huge amounts of melt water with heavy fallout of tephra what makes it the most hazardous volcano in Iceland. In addition its location is close to inhabited areas. Large eruptions break through the ice within 2 hours. The outbursts from Katla last for 3-5 days with peak discharge of 10^5-10^6 m^3/s reached within few hours after floods start, and a total water release of 1-8 km^3.

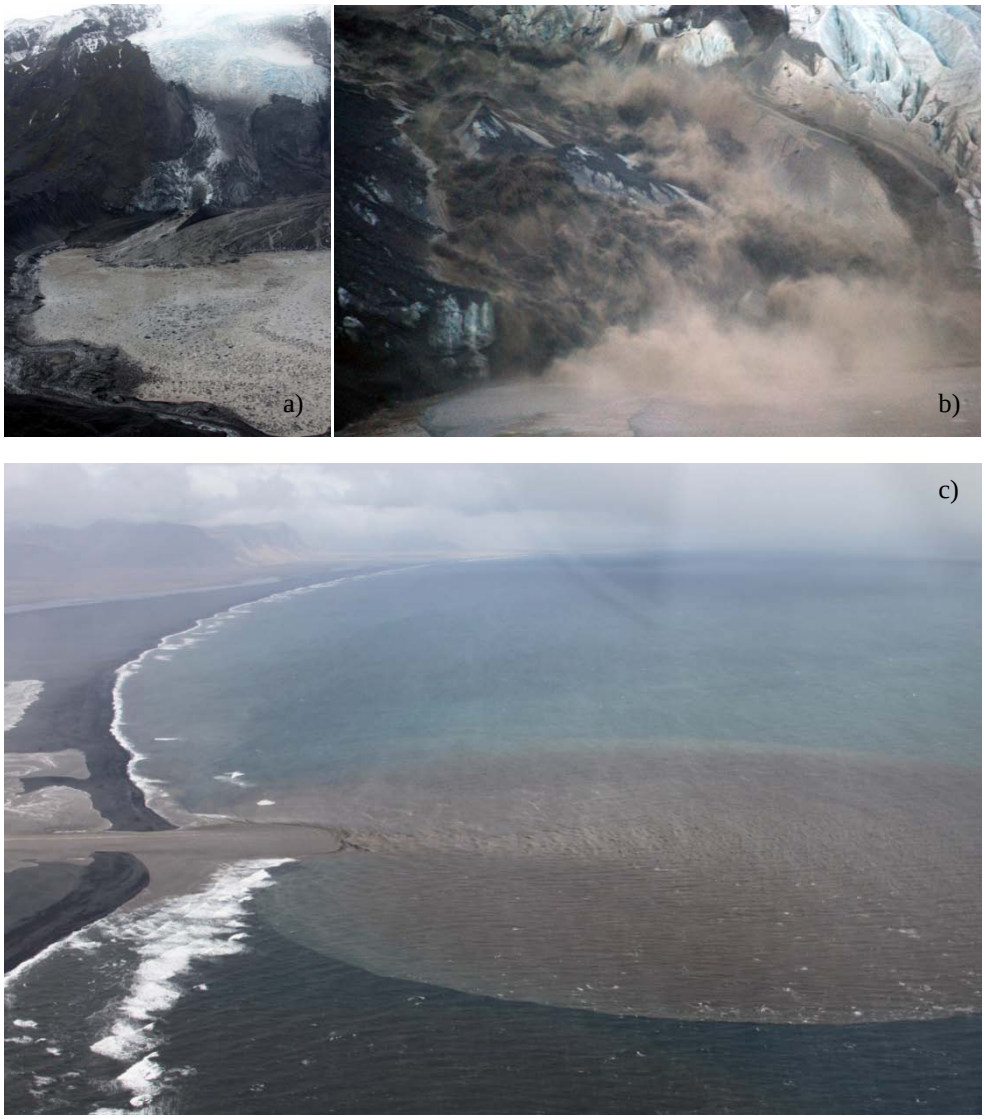

Figure 8. The jökulhlaup during the 2010 Eyjafjallajökull eruption. The melt water from eruption site came down through Gígjökull into the lagoon (a and b). Photograph (a) and (c) were taken by Þórdís Högnadóttir and photograph (b) by Eyjólfur Magnússon.

When the flood breaks through the glacier margin, the mixture of water, ice, volcanic material and sediments flows at velocities of 5-15 m/s (Björnsson, 2009b). The estimated volcanic debris carried with the single flood is 0.7-1.6 km^3 (Björnsson, 2009b). During the Katla eruption in 1918 most of the water flowed in eight hours during the initial stage of eruption. The flood might have reached a peak of 300,000 m^3/s and inundated an area of 600-800 km^2 to the east of the volcano (Tómasson, 1996; Larsen, 2000). The majority of the water came from under the glacier breaking through the tail of the glacier. The coast line advanced 3 km into the sea and the sediments caused lifting of the surface of the land up to few meters.

The total volume of drained water was estimated to be 8 km^3 (Tómasson, 1996). Witnesses saw big blocks of ice carried with the water. The other glacial floods from Katla occurred in 1955, 1999, and 2011.

The Eyjafjallajökull sub-glacial eruption in 2010 caused a significant flood. The jökulhlaup came from the Gígjökull outlet glacier, which protrudes from the main ice cap to the north, and further into Markarfljót River (Fig. 8a and b). The flood was caused by intensive localized melting of about 200 m thick ice at the eruption site. The melt water accumulated in the caldera for few hours, before the level of Gígjökull glacial lagoon began to rise on 14th April, 2010. The increased water level, conductivity and decrease in temperature in Gígjökull lagoon indicated that the inflow was affected by the summit eruption and melting of ice cap (Karlsdóttir et al. 2012). The discharge of the first flood from lagoon measured downstream of Markarfljót River was 2,500-3,000 m^3/s and the flood water covered about 57.2 km^2 of the floodplain at it maximum. The volume of melted water was estimated to be 0.03 km^3. When the eruption became subaerial, the rate of melting decreased diverting the thermal energy into the eruption plume. The second jökulhlaup was only about 30% of the volume of the first flood but it was heavily loaded with volcanic ash – 20-60% solid per volume unit and appeared as viscous, smooth-surfaced slurry, containing ice clasts, volcanic material, soil and vegetation (Karlsdóttir et al. 2012). This flood water was distinct from the first flood indicating a different propagation path. Some collapsing pits on the surface of the Gígjökull were observed showing the sub-glacial flood path (Karlsdóttir et al. 2012). The levees prevented the flood water to damage the farmlands; however the ice slurry broke part of levees along the Markarfljót River. During the event the water was diverted away from the bridge on Markarfljót by the breaches made by bulldozers (Karlsdóttir et al. 2012). The load of sediments into the sea carried by the flood water from Markarfljót can be seen in Fig. 8c.

Due to the enormous power of the flood water and its possible catastrophic effect on inhabited areas, it is crucial to be able to predict jökulhlaups and warn people of impeding events. The monitoring of the most dangerous active volcanoes and sub-glacial geothermal areas is carried out by regularly spaced seismometers, GPS stations, radio-linked river gauges, regular airborne radar profiling and inspection flights of the ice caps (Gudmundsson, 2007). It is important to map the bedrock surface under the ice cap to forecast the drainage paths and the flood plains. Based on results of the measurements, empirical and theoretical relations can be applied to estimate the possible magnitude of jökulhlaup (Gudmundsson, 2007). In addition, when a flood starts, the discharge can be predicted based on the reservoir volume and flow measured during the initial phase of the flood (Björnsson, 2009b).

Geochemical analysis of the flood water can complement the geophysical and hydrological data and help to understand what triggered the outburst. The amount of

sediments and dissolved loads carried by the flood can either fertilize or pollute the ecosystems. The possible hazard to the biota can be evaluated based on chemical composition of flood water, groundwater in the vicinity of volcanoes and through small scale experiments where dissolution of suspended matter is carried out (Aiuppa et al., 2003; Aiuppa et al., 2005; Bagnato et al., 2009; D'Alessandro et al., 2013; Federico et al., 2002; Federico et al., 2004; Flaathen and Gislason, 2007; Flaathen et al., 2009; Floor et al., 2011; Gislason et al., 2002; Stefánsdóttir and Gislason, 2005; Taran et al., 2008). Also, studying present floods help to understand jökulhlaups in late Pleistocene and early Holocene. The 2011 small foods from the Mýrdalsjökull and Vatnajökull glaciers in Iceland provided an opportunity to study the chemistry of the flood waters and to decipher whether they were caused by direct contact of magma and tephra with melt water at the base of the glacier or rather resulted from enhanced glacier melting caused by geothermal activity.

The pH is a major parameter describing fluid chemistry. Water-magmatic gas interaction decreases pH due to the dissociation of strong (H_2SO_4, HCl,) and weak acids (H_2CO_3, HF). The pH can be subsequently raised by mineral dissolution. Another indicator of the chemical evolution of the natural waters is its dissolved inorganic carbon (DIC) concentration. The DIC concentration of a fluid depends on its total pressure, temperature, pH, and salinity. The DIC concentration increases with increasing pressure and decreases with increasing temperature and salinity. Upon water-rock interaction, fluid pH tends to increase shifting carbon species from dissolved CO_2 ($CO_{2(aq)}$) and carbonic acid (H_2CO_3) towards HCO_3^- and CO_3^{2-}. The $CO_{2(aq)}$ activity will decrease with increasing pH reducing the risk of CO_2 "boiling" out of the water due to pressure drop. In natural systems decreasing pressure could be caused by fracturing or removing of the overburden, for example the ice cap. High DIC or alkalinity accompanied by increased pH is often seen in basaltic aquifers and is indicative of advanced water-rock interaction, whereas high DIC, low alkalinity, and low pH are indicative of CO_2 supply from magmatic sources with minimal water-rock interaction. After reducing the overall system pressure, CO_2 can degas lowering DIC concentration; however, the alkalinity will remain constant if carbonates do not precipitate. Apart from CO_2, magma can release other gasses including SO_2, HF, HCl, and H_2S. The HF and HCl gases are soluble in water and thus dissolved Cl^- and F^- concentrations will increase even after short water-gas interactions. Melt water caused by volcanic eruption has limited time to interact with the rock causing the pH and alkalinity to remain low, nevertheless the fluid Cl^- and F^- concentration will increase. Based on chemical analysis of the flood waters, it was possible to determine if the water accumulated in the reservoir had been in contact with intensive supply of gasses and how advanced the melt water-rock interaction was. A detailed description of the chemical composition of the glacial floods which occurred in July 2011 are provided in Chapter 5.

The sub-glacial reservoirs have a potential to store huge amounts of CO_2 originated from magmatic intrusions underneath the glacier due to high overburden pressure exerted by ice caps and interactions with the background rocks. These reservoirs are periodically drained in glacial floods releasing water from which CO_2 can either degas (if there has not been enough water-rock interactions) or it can be transported within flood channel as bicarbonate and carbonate species into the sea and eventually precipitate as stable carbonates. Assuming an ice thickness of 440 m, which is close to that in the vicinity of the Mýrdalsjökull cauldrons, the total pressure at the highest point of the lake at the base of the glacier is around 40 bars. The maximum CO_2 solubility in the water with the ionic strength similar to the water samples collected during the studied floods at this pressure and temperature of 4° C is 1.74 mol/kg and the corresponding fluid pH equals to 4.23 (calculated based on the Duan et al. (2006) CO_2 solubility model and using PHREEQC). When the total pressure decreases due to the draining of sub-glacial water (the ice cap thickness decreases as the water approaches the margin of the glacier), CO_2 degasses, decreasing DIC concentration and increasing pH. If the total hydrostatic pressure decreases only by 10 bars, the maximum CO_2 solubility decreases to 1.44 mol/kg resulting in the degassing of 0.30 moles of CO_2 per kilogram of water. According to Gudmundsson (2011) the release of water underneath the main drained cauldron was 0.014 km^3. Taking this amount of water, the total degassed volume of CO_2 would equal 0.1 km^3 which corresponds to 191,186 tonnes of CO_2. For comparison the annual CO_2 discharge of the Mt. Hekla system is between 99,380 and 257,500 tonnes (Flaathen and Gislason, 2007; Flaathen et al., 2009). If the simulation of CO_2 degassing from the water proceeds to the DIC concentration and pH close to those measured in the Múlakvísl River (about 10 mmol/kg and 7.5, respectively) the amount of CO_2 degassed would be over 1 million tonnes. This could be referred as the CO_2 carrying capacity of the flood waters and if the partial pressure of CO_2 during the flow from the cauldron to the glacier edge becomes significant greater than the total pressure, CO_2 will "boil" out of the water. This "boiling" might create low frequency seismic tremor.

Full saturation of the drained water with CO_2 was unlikely to happen, however, the calculations presented above suggest that sub-glacial lakes have the potential to store substantial quantities of CO_2. If the hydrostatic pressure is preserved, there is no CO_2 boiling from the sub-glacial lake. However, if the CO_2-saturated water is drained from beneath the glacier, the overburden pressure decreases, and if the pH remains low, CO_2 boiling is likely. Degassing of CO_2 can exert pressure on the glacier cover. For example, if we imagine a half sphere whose dimensions reflect approximately a lake under the cauldron, the decrease of total pressure by 10 bars would cause the degassing of CO_2 according to the CO_2 solubility model and the pressure exerted on the inner surface of the half sphere would equal 22 kbar. In

addition, CO_2 degassing results in the fluid becoming supersaturated with respect to carbonate minerals which could lead to carbonate precipitation and permanent CO_2 fixation. According to Gislason et al. (2002) up to 1/3 of the mass of carbon released from magma could have precipitated as Ca, Mg, Sr carbonate at the eruption site or in the Lake Grímsvötn under the glacier during the Gjálp eruption. Such precipitation can also scavenge metals such as Al, Fe, Cd, Cu, Mn, and Sr (e.g. Olsson et. al., 2012b).

1.6. SUMMARY OF SCIENTIFIC CONTRIBUTIONS

The first article presented in Chapter 2 is entitled ***'A novel high pressure column flow reactor for experimental studies of CO_2 mineral storage'.*** It describes in details the experimental set-up and testing of a large scale column flow through reactor which is designed for high gas/hydrostatic pressure applications in the laboratory. This novel technique is meant to study carbon mineralization in basalt as it refers to a current *in-situ* carbon storage project in Iceland (Carbfix). The manuscript presents the first results of H_2O-CO_2-basaltic glass interactions as a function of time and distance along the flow path within the column. This article provides a guide for those who want to design, run and study in detail supercritical fluid/gas-water-rock interactions in column flow through reactors under elevated pressures up to 10 MPa.

The second article presented in Chapter 3 is entitled '***An experimental study of basaltic glass-H_2O-CO_2 interaction at 22 and 50 °C: Implications for subsurface storage of CO_2'.*** It describes a series of long-term column experiments aimed at an improved understanding of CO_2-H_2O-basalt interaction during natural and geo-engineered processes. The study includes a detailed analysis of the evolution of the fluid phase and assessment of PHREEQC geochemical modelling code to describe accurately processes controlling the behaviour of the fluid along the flow path. The results of this study contribute to the large number of research focussing on the fate and consequences of geologic carbon storage.

The third article presented in Chapter 4 is entitled '***Experimental studies of basalt-H_2O-CO_2 interaction with a high pressure column flow reactor: The mobility of metals'.*** At the early stage of CO_2 injection due to production of carbonic acid the host rock not only releases major divalent cations but also hazardous and toxic trace metals which can pose a threat to the environment. This study describes the potential risk associated with the enhanced metal release during the short term CO_2-charged water injections into the column filled with basaltic glass grains. It explores to some extent also the potential of their immobilization during the neutralization of the system.

The fourth article presented in Chapter 5 is entitled ***'The chemistry and element fluxes of the July 2011 Múlakvísl and Kaldakvísl glacial floods, Iceland'.*** It covers

the chemistry of two sub-glacial floods, their impact on the carbon budget, poisoning and fertilizing potential. The chemical composition of the flood waters was used to decipher the possible origin of the heat causing the glacier to melt – volcanic or geothermal. This study was motivated to better understand how the heat source affects flood water chemistry and its environmental consequences. It contributes to a large number of scientific articles focusing on natural hazards resulting from volcanic activity.

1.7. CONCLUDING REMARKS AND PERSPECTIVES

During this study, the major task was to set-up a big scale high pressure column flow reactor and conduct experiments which will confirm its ability to study the H_2O-CO_2-basalt interaction as a function of time and distance along the flow path. Because of the complexity of the experimental design and long-term preparation to conduct the experiments, only the reactive fluid chemistry was analyzed. The results of water-rock interaction in the column gave a unique opportunity to study the very first reactions occurring between water and the rock. It is very important to monitor the initial water-rock interaction which often is not possible in nature, since water samples taken in the field are altered by dilution, organics, atmospheric O_2 and CO_2 etc. It is crucial to monitor these initial reactions for several reasons. First, the initial pH, Al concentration and solution saturation state with respect to the host rock dictates the dissolution rate of basaltic glass and plagioclases, the major components of basalt. Second, it is important to monitor the redox state and it influence on the speciation of redox sensitive metals. Furthermore, it is essential to monitor the relative mobility of heavy/toxic elements in the initial stage of water-rock interaction, before major precipitation of secondary minerals. For example, the initial aquatic Al and Cr concentrations could pose threats to humans and the environment. All those aspects were examined to some extent during this experimental study and the obtained results indicate that the column reactor is a good tool to investigate the CO_2 behaviour under the subsurface. However, there is a need to complement the liquid chemistry by analyzing the alteration products. This will be the major task during the future work. Characterization of secondary minerals would help with the examination of the usefulness of geochemical model and help determine the fate of mobilized elements (i.e. Mn scavenging by carbonate, Al concentration decrease due to clay precipitation, and Cr incorporation into clay phases). Before, appropriate changes to the experimental conditions have to be evaluated to enhance dissolution kinetics of the basaltic glass. This step is necessary to overcome the pH buffer capacity which was the principal cause of the stagnant low pH resulting in constant carbonate undersaturation in the column. While the application of the column reactor was tested using a carbonated solution and basaltic glass, other materials and gas mixtures such as CO_2-H_2S and/or supercritical CO_2

can be also used. Despite some limitations of the experimental set-up (complexity, possibility of preferential flow, clogging the sampling outlets, sensitivity of pH electrodes to the fluctuations in pressure etc.) the HPCFR should be extensively used to fully exploit and improve understanding of carbon storage in geological formations.

References

Adams E.E., Caldeira K. (2008) Ocean Storage of CO_2. *Elements* **4**, 319-324.

Aiuppa A., D'Alessandro W., Federico C., Palumbo B., Valenza M. (2003) The aquatic geochemistry of arsenic in volcanic groundwaters from southern Italy. *App. Geochem.* **18** 1283-1296.

Aiuppa A., Federico C., Allard P., Gurrieri S., Valenza M. (2005) Trace metal modeling of groundwater–gas–rock interactions in a volcanic aquifer: Mount Vesuvius, Southern Italy. *Chem. Geol.* **216** 289-311.

Alfredsson H.A., Oelkers E.H., Hardarsson B.S., Franzson H., Gunnlaugsson E., Gislason S.R. (2013) The geology and water chemistry of the Hellisheidi, SW-Iceland carbon storage site. *Int. J. Greenhouse Gas Control* **12**, 399-418.

Andersson A.J., Mackenzie F.T., Lerman A. (2006) Coastal ocean CO_2–carbonic acid–carbonate sediment system of the Anthropocene. *Global Biogeochem. Cycles* **20**, GB1S92.

Andreani M., Luquot L., Gouze P., Godard M., Hoisé E., Gibert B. (2009) Experimental Study of Carbon Sequestration Reactions Controlled by the Percolation of CO_2-Rich Brine through Peridotites. *Environ. Sci. Technol.* **43**, 1226-1231.

Aradóttir E.S.P., Sonnenthal E.L., Björnsson G., Jónsson H. (2012) Multidimensional reactive transport modeling of CO_2 mineral sequestration in basalts at the Hellisheidi geothermal field, Iceland. *Int. J. of Greenhouse Gas Control* **9**, 24-40.

Arnórsson S., Gislason S.R. (1994) CO_2 from magmatic sources in Iceland. *Min. Mag*. **58A**, 27-28.

Bagnato E., Aiuppa A., Parello F., D'Alessandro W., Allard P., Calabrese S. (2009) Mercury concentration, speciation and budget in volcanic aquifers: Italy and Guadeloupe (Lesser Antilles). *J. Volcanology and Geothermal Research* **179**, 96-106.

Barnola J.M., Raynaud D., Lorius C., Barkov N.I. (2003) Historical CO_2 record from the Vostok Ice Core. Carbon Dioxide Information Analysis Centre, Oak National Laboratory, U.S. Department of Energy *http://cdiac.ornl.gov/ftp/trends/co2/vostok.icecore.co2*

Beinlich A., Austrheim H. (2012) In situ sequestration of atmospheric CO_2 at low temperature and surface cracking of serpentinized peridotite in mine shafts. *Chem. Geol*. **332–333**, 32-44.

Benson S.M., Cole D.R. (2008) CO_2 Sequestration in Deep Sedimentary Formations. *Elements* **4**, 325-331.

Benson S.M., Hoversten M., Gasperikova E., Haines M. (2005) Monitoring protocols and life-cycle costs for geologic storage of carbon dioxide, in: Rubin E.S., Keith D.W., Gilboy C.F., Wilson M., Morris T., Gale J., Thambimuthu K. *Greenhouse Gas Control Technol.* **7**. Elsevier Science Ltd, Oxford, pp. 1259-1264.

Berner R.A. (2004) The phanerozoic carbon cycle: CO_2 and O_2. Oxford University Press.

Bickle M., Chadwick A., Huppert, H.E., Hallworth, M., Lyle, S., 2007. Modelling carbon dioxide accumulation at Sleipner: Implications for underground carbon storage. *Earth and Planetary Sci. Letters* **255**, 164-176.

Björnsson H. (1975) Subglacial water reservoirs, jökulhlaups and volcanic eruptions. *Jökull* **25,** 1-14.

Björnsson H. (1976) Marginal and subglacial lakes in Iceland. *Jökull* **26,** 40-51.

Björnsson H. (2003) Subglacial lakes and jökulhlaups in Iceland. *Global and Planetary Change* **35**, 255-271.

Björnsson H. (2009a) Jökulhlaup in Iceland: sources, release and drainage in Megaflooding on Earth and Mars, ed. Burr D.M., Carling P.A., Baker V.R. Published by Cambridge University Press, 50-64.

Björnsson H. (2009b) Glacial lake outburst floods in mountain environments in Megaflooding on Earth and Mars, ed. Burr D.M., Carling P.A., Baker V.R. Published by Cambridge University Press, 165-184.

Boden T.A., Marland G., Andres R.J. (2012) Global CO_2 Emission from Fossil-Fuel Burning, Cement Manufacture, and Gas Flaring: 1751-2009. Carbon Dioxide Information Analysis Centre, Oak National Laboratory, U.S. Department of Energy, *http://cdiac.ornl.gov/trends/emis/glo.html*

Boden T.A, Blasing T.J. (2010) Preliminary 2009 and 2010 global and national estimates of carbon emission from fossil-fuel combustion and cement manufacture. Carbon Dioxide Information Analysis Centre, Oak National Laboratory, U.S. Department of Energy, *http://cdiac.ornl.gov/trends/emis/prelim_2009_2010_estimates.html*

Broecker W.S. (1997) Thermohaline Circulation, the Achilles Heel of Our Climate System: Will Man-Made CO_2 Upset the Current Balance? *Science* **278**, 1582-1588.

Comment Visions. Debating the energy challenge (2013) *http://commentvisions.com/event/9266/carbon-capture-and-storage-in-europe-progress-and-prospects#sthash.XOeRk5LE.dpuf*

Crowley T.J. (2000) Causes of Climate Change Over the Past 1000 Years. *Science* **289**, 270-277.

Daval D., Sissmann O., Menguy N., Saldi G.D., Guyot F., Martinez I., Corvisier J., Garcia B., Machouk I., Knauss K.G., Hellmann R. (2011) Influence of amorphous silica layer formation on the dissolution rate of olivine at 90 °C and elevated pCO_2. *Chem. Geol.* **284**, 193-209.

Dessert C., Dupré B., Gaillardet J., François L.M., Allègre C.J. (2003) Basalt weathering laws and the impact of basalt weathering on the global carbon cycle. *Chem. Geol.* **202**, 257-273.

D'Alessandro W., Aiuppa A., Bellomo S., Brusca L., Calabrese S., Kyriakopoulos K., Liotta M., Longo M. (2013) Sulphur-gas concentrations in volcanic and geothermal areas in Italy and Greece: Characterising potential human exposures and risks. *J. Geochem. Exploration* **131**, 1-13.

Duan Z., Sun R., Zhu C., Chou, I.M. (2006) An improved model for the calculation of CO_2 solubility in aqueous solutions containing Na^+, K^+, Ca^{2+}, Mg^{2+}, Cl^-, and SO_4^{2-}. *Marine Chemistry* **98**, 131-139.

Emberley S., Hutcheon I., Shevalier M., Durocher K., Mayer B., Gunter W.D., Perkins E.H. (2005) Monitoring of fluid–rock interaction and CO_2 storage through produced fluid sampling at the Weyburn CO_2-injection enhanced oil recovery site, Saskatchewan, Canada. *App. Geochem.* **20**, 1131-1157.

Federico C., Aiuppa A., Allard P., Bellomo S., Jean-Baptiste P., Parello F., Valenza M. (2002) Magma-derived gas influx and water-rock interactions in the volcanic aquifer of Mt. Vesuvius, Italy. *Geochim. Cosmochim. Acta* **66**, 963-981.

Federico C., Aiuppa A., Favara R., Gurrieri S. and Valenza M. (2004) Geochemical monitoring of groundwaters (1998–2001) at Vesuvius volcano (Italy). *J. Volcanology and Geothermal Research* **133**, 81-104.

Flaathen T.K., Gislason S.R. (2007) The effect of volcanic eruptions on the chemistry of surface waters: The 1991 and 2000 eruptions of Mt. Hekla, Iceland. *J. Volcanology and Geothermal Research* **164**, 293-316.

Flaathen T.K., Gislason S.R., Oelkers E.H., Sveinbjörnsdóttir Á.E. (2009) Chemical evolution of the Mt. Hekla, Iceland, groundwaters: A natural analogue for CO_2 sequestration in basaltic rocks. *App. Geochem.* **24**, 463-474.

Floor G.H., Calabrese S., Román-Ross G., D´Alessandro W. Aiuppa A. (2011) Selenium mobilization in soils due to volcanic derived acid rain: An example from Mt Etna volcano, Sicily. *Chem. Geol.* **289**, 235-244.

Gaillardet J., Dupré B., Louvat P., Allègre C.J. (1999) Global silicate weathering and CO_2 consumption rates deduced from the chemistry of large rivers. *Chem. Geol.* **159**, 3-30.

Gerlach T. (2011) Volcanic versus anthropogenic carbon dioxide. *Eos, Transactions American Geophysical Union* **92**, 201-202.

Giammar D.E., Bruant Jr R.G., Peters C.A. (2005) Forsterite dissolution and magnesite precipitation at conditions relevant for deep saline aquifer storage and sequestration of carbon dioxide. *Chem. Geol.* **217**, 257-276.

Gislason S.R., Oelkers E.H. (2003) Mechanism, rates, and consequences of basaltic glass dissolution: II. An experimental study of the dissolution rates of basaltic glass as a function of pH and temperature. *Geochim. Cosmochim. Acta* **67**, 3817-3832.

Gislason S.R., Oelkers E.H., Eiriksdottir E.S., Kardjilov M.I., Gisladottir G., Sigfusson B., Snorrason A., Elefsen S., Hardardottir J., Torssander P., Óskarsson, N. (2009) Direct evidence of the feedback between climate and weathering. *Earth and Planetary Sci. Letters* **277**, 213-222.

Gislason S.R., Wolff-Boenisch D., Stefansson A., Oelkers E.H., Gunnlaugsson E., Sigurdardottir H., Sigfusson B., Broecker W.S., Matter J.M., Stute M., Axelsson G., Fridriksson T. (2010) Mineral sequestration of carbon dioxide in basalt: A pre-injection overview of the CarbFix project. *Int. J. Greenhouse Gas Control* **4**, 537-545.

Goldberg D.S., Kent D.V., Olsen P.E. (2010) Potential on-shore and off-shore reservoirs for CO_2 sequestration in Central Atlantic magmatic province basalts. *Proc. Natl. Acad. Sci.* **107**, 1327-1332.

Goldberg D.S., Takahashi T., Slagle A.L. (2008) Carbon dioxide sequestration in deep-sea basalt. *Proc. Natl. Acad. Sci.* **105**, 9920-9925.

Groisman P.Y., Knight R.W., Easterling D.R., Karl T.R., Hegerl G.C., Razuvaev V.N. (2005) Trends in Intense Precipitation in the Climate Record. *J. Climate* **18**, 1326-1350.

Gudbrandsson S., Wolff-Boenisch D., Gislason S.R., Oelkers E.H. (2011) An experimental study of crystalline basalt dissolution from $2 \leqslant pH \leqslant 11$ and temperatures from 5 to 75 °C. *Geochim. Cosmochim. Acta* **75**, 5496-5509.

Gudmundsson M.T., Sigmundsson F., Bjornsson H. (1997) Ice-volcano interaction of the 1996 Gjalp subglacial eruption, Vatnajokull, Iceland. *Nature* **389,** 954-957.

Gudmundsson, M.T., Högnadóttir, Þ., Kristinsson A.B., Gudbjörnsson S. (2007) Geothermal activity in the subglacial Katla caldera, Iceland, 1999-2005, studied with radar altimetry. *Annals of Glaciology* **45**, 66-72.

Gudmundsson M.T., Larsen G., Höskuldsson Á., Gylfason Á.G. (2008) Volcanic hazards in Iceland. *Jökull* **58**, 251-268.

Gudmundsson M.T., Högnadóttir T. (2011) Upptök of stærð jökulhlaups í Mulakvisl – niðurstöður flugmælinga. Minnisblað 13. Júlí 2011.

Gysi A.P., Stefánsson A. (2012) CO_2-water–basalt interaction. Low temperature experiments and implications for CO_2 sequestration into basalts. *Geochim. Cosmochim. Acta* **81**, 129-152.

Haugen H.A., Aagaard P., Kjärstad J., Bergmo P.E.S., Nielsen L.H., Eldrup N.H., Skagestad R., Mathisen A., Thorsen T.A., Johnsson F., Bjørnsen D. (2013) Infrastructure for CCS in The Skagerrak/Kattegat Region, Southern Scandinavia: A Feasibility Study. *Energy Procedia* **37**, 2562-2569.

Hövelmann J., Austrheim H., Beinlich A., Anne Munz I. (2011) Experimental study of the carbonation of partially serpentinized and weathered peridotites. *Geochim. Cosmochim. Acta* **75**, 6760-6779.

Hovorka S.D., Meckel T.A., Trevino R.H., Lu J., Nicot J.-P., Choi J.-W., Freeman D., Cook P., Daley T.M., Ajo-Franklin J.B., Freifeild B.M., Doughty C., Carrigan C.R., Brecque D.L., Kharaka Y.K., Thordsen J.J., Phelps T.J., Yang C., Romanak K.D., Zhang T., Holt R.M., Lindler J.S., Butsch R.J. (2011) Monitoring a large volume CO_2 injection: Year two results from SECARB project at Denbury's Cranfield, Mississippi, USA. *Energy Procedia* **4**, 3478-3485.

IEA (2012) CO_2 emission from fuel combustion, highlights. Internation Energy Agency, France.

IPCC (2005) IPCC Special Report on Carbon Dioxide Capture and Storage, prepared by Working Group III of the Intergovernmental Panel on Climate Change. In: Metz B., Davidson O., de Coninck H., Loos C.M., Meyer L.A. (Eds.), Cambridge University Press.

Jamtveit B., Putnis C., Malthe-Sørenssen A. (2009) Reaction induced fracturing during replacement processes. *Contrib. Mineral. Petrol.* **157**, 127-133.

Johns T.C., Gregory J.M., Ingram W.J., Johnson C.E., Jones A., Lowe J.A., Mitchell J.F.B., Roberts D.L., Sexton D.M.H., Stevenson D.S., Tett S.F.B., Woodage M.J. (2003) Anthropogenic climate change for 1860 to 2100 simulated with the HadCM3 model under updated emissions scenarios. *Climate Dynam.* **20**, 583-612.

Jouzel J., Masson-Delmotte V., Cattani O., Dreyfus G., Falourd S., Hoffmann G., Minster B., Nouet J., Barnola J.M., Chappellaz J., Fischer H., Gallet J.C., Johnsen S., Leuenberger M., Loulergue L., Luethi D., Oerter H., Parrenin F., Raisbeck G., Raynaud D., Schilt A., Schwander J.,

Selmo E., Souchez R., Spahni R., Stauffer B., Steffensen J.P., Stenni B., Stocker T.F., Tison J.L., Werner M., Wolff E.W. (2007) Orbital and Millennial Antarctic Climate Variability over the Past 800,000 Years. *Science* **317**, 793-796.

Karl T.R., Trenberth K.E. (2003) Modern Global Climate Change. *Science* **302**, 1719-1723.

Karlsdóttir S., Gylfason Á.G., Höskuldsson Á., Brandsdóttir B., Ilyinskaya E., Gudmundsson M.T., Högnadóttir Þ. (2012) The 2012 Ejafjallajökull eruption, Iceland. Report to ICAO – June 2012.

Keeling R.F., Piper S.C., Bollenbacher A.F., Walker S.J. (2009) Atmospheric CO2 values (ppmv) derived from in situ air samples collected at Mauna Loa, Hawaii, USA. Carbon Dioxide Information Analysis Centre, Oak National Laboratory, U.S. Department of Energy, *ftp://ftp.cmdl.noaa.gov/ccg/co2/trends/co2_mm_mlo.txt*

Kelemen P.B., Matter J. (2008) In situ carbonation of peridotite for CO_2 storage. *Proc. Natl. Acad. Sci.* **105**, 17295-17300.

Kharaka Y.K., Thordsen J.J., Hovorka S.D., Seay Nance H., Cole D.R., Phelps T.J., Knauss K.G. (2009). Potential environmental issues of CO_2 storage in deep saline aquifers: Geochemical results from the Frio-I Brine Pilot test, Texas, USA. *App. Geochem.* **24**, 1106-1112.

King H.E., Plümper O., Putnis A. (2010) Effect of Secondary Phase Formation on the Carbonation of Olivine. *Environ. Sci. Technol.* **44**, 6503-6509.

Kristmannsdottir H (1982) Alteration in the IRDP dill hole compared with other drill holes n Iceland. *J. Geophysical Research* **87**, 6525-6531.

Larsen G. (2000) Holocene eruptions within the katla volcanic system, south Iceland: Characteristics and environmental impact. *Jökul* **49**, 1-28.

Lüthi D., Le Floch M., Bereiter B., Blunier T., Barnola J.-M., Siegenthaler U., Raynaud D., Jouzel J., Fischer H., Kawamura K., Stocker T.F. (2008) High-resolution carbon dioxide concentration record 650,000-800,000 years before present. *Nature* **453**, 379-382.

Mackenzie F.T., Andersson A.J. (2013) The marine carbon cycle and ocean acidification during phanerozoic time. *Geochem. Perspectives* **2**, 1-227.

Manabe S., Stouffer R.J. (1994) Multiple-Century Response of a Coupled Ocean-Atmosphere Model to an Increase of Atmospheric Carbon Dioxide. *J. Climate* **7**, 5-23.

Martens S., Liebscher A., Möller F., Würdemann H., Schilling F., Kühn M. (2011) Progress report on the first european on-shore CO_2 storage site at ketzin (Germany) – Second year of injection. *Energy Procedia* **4**, 3246-3253.

McGrail B.P., Schaef H.T., Ho A.M., Chien Y.-J., Dooley J.J., Davidson C.L. (2006) Potential for carbon dioxide sequestration in flood basalts. *J. Geophysical Research: Solid Earth* **111**, B12201.

Mito S., Xue Z. (2011) Post-Injection monitoring of stored CO_2 at the Nagaoka pilot site: 5 years time-lapse well logging results. *Energy Procedia* **4**, 3284-3289.

Munz I.A., Brandvoll Ø., Haug T.A., Iden K., Smeets R., Kihle J., Johansen H. (2012) Mechanisms and rates of plagioclase carbonation reactions. *Geochim. Cosmochim. Acta* **77**, 27-51.

Neuhoff P.S., Rogers K.L., Stannius L.S., Bird D.K., Pedersen A.K. (2006) Regional very low-grade metamorphism of basaltic lavas, Disko–Nuussuaq region, West Greenland. *Lithos* **92**, 33-54.

Oelkers E.H., Gislason S.R., Matter J. (2008) Mineral Carbonation of CO_2. *Elements* **4**, 333-337.

Olsson J., Bovet N., Makovicky E., Bechgaard K., Balogh Z., Stipp S.L.S. (2012a) Olivine reactivity with CO_2 and H_2O on a microscale: Implications for carbon sequestration. *Geochim. Cosmochim. Acta* **77**, 86-97.

Olsson J., Stipp S., Gislason S.R. (2012b) Calcium carbonate formation at the Eyjafjallajökull volcano: a carbon capture and storage analogue. 30th Nordic Geological Winter Meeting, Reykjavik, Iceland 9-12 January 2012, 174.

Parmesan C. (2006) Ecological and evolutionary responses to recent climate change, Annual Review of Ecology Evolution and Systematics. *Annual Reviews, Palo Alto*, pp. 637-669.

Paukert A.N., Matter J.M., Kelemen P.B., Shock E.L., Havig J.R. (2012) Reaction path modeling of enhanced in situ CO_2 mineralization for carbon sequestration in the peridotite of the Samail Ophiolite, Sultanate of Oman. *Chem. Geol.* **330–331**, 86-100.

Petit J.R., Jouzel J., Raynaud D., Barkov N.I., Barnola J.-M., Basile I., Bender M., Chappellaz J., Davis M., Delayque G., Delmotte M., Kotlyakov V.M., Legrand M., Lipenkov V.Y., Lorius C.,

Pepin L., Ritz C., Saltzman E., Stievenard M. (1999) Climate and atmospheric history of the past 420,000 years from the Vostok ice core, Antarctica. *Nature* **399**, 429-436, *http://cdiac.ornl.gov/ftp/trends/temp/vostok/vostok.1999.temp.dat*

Pham T.H.V., Maast T.E., Hellevang H., Aagaard P. (2011) Numerical modeling including hysteresis properties for CO_2 storage in Tubåen formation, Snøhvit field, Barents Sea. *Energy Procedia* **4**, 3746-3753.

Pokrovsky O.S., Schott J. (2000) Kinetics and mechanism of forsterite dissolution at 25 °C and pH from 1 to 12. *Geochim. Cosmochim. Acta* **64**, 3313-3325.

Prigiobbe V., Hänchen M., Costa G., Baciocchi R., Mazzotti M. (2009) Analysis of the effect of temperature, pH, CO_2 pressure and salinity on the olivine dissolution kinetics. *Energy Procedia* **1**, 4881-4884.

Putnis, A. (2009) Mineral Replacement Reactions. Reviews in Mineralogy and Geochemistry 70, 87-124.

Rogers K.L., Neuhoff P.S., Pedersen A.K., Bird D.K. (2006) CO_2 metasomatism in a basalt-hosted petroleum reservoir, Nuussuaq, West Greenland. *Lithos* **92**, 55-82.

Schaef H.T., McGrail B.P., Owen A.T. (2010) Carbonate mineralization of volcanic province basalts. *Int. J. Greenhouse Gas Control* **4**, 249-261.

Schaef H.T., McGrail B.P., Owen A.T., Arey B.W. (2013) Mineralization of basalts in the CO_2-H_2O-H_2S system. *Int. J. Greenhouse Gas Control* **16**, 187-196.

Schott J., Oelkers E.H., Bénézeth P., Goddéris Y., François L. (2012) Can accurate kinetic laws be created to describe chemical weathering? *Comptes Rendus Geoscience* **344**, 568-585.

Snorrason Á., Jónsson P., Sigurdsson O., Pálsson S., Árnason S., Víkingsson S., Kaldal I. (2002) November 1996 jökulhlaup on Skeidarársandur outwash plan. Iceland. In: Martin P., Baker V.R. and Garzón G. eds. Flood and Megaflood Processes and Deposits. Recent and Ancient Examples. Special Publ. 32 of the International Association of Sedimentologists, Blackwell Science, Oxford, 55-67

Stefánsdóttir M.B., Gislason S.R. (2005) The erosion and suspended matter/seawater interaction during and after the 1996 outburst flood from the Vatnajökull Glacier, Iceland. *Earth and Planetary Sci. Letters* **237** 433-452.

Stott P.A., Jones G.S., Mitchell J.F.B. (2003) Do Models Underestimate the Solar Contribution to Recent Climate Change? *J. Climate* **16**, 4079-4093.

Taran Y., Rouwet D., Inguaggiato S. and Aiuppa A. (2008) Major and trace element geochemistry of neutral and acidic thermal springs at El Chichón volcano, Mexico: Implications for monitoring of the volcanic activity. *J. of Volcanology and Geothermal Research* **178**, 224-236.

Tómasson H. (1996) The Jökulhlaup from Katla in 1918. *Ann. Glaciology* **22**, 249-254.

Walker J.C.G., Hays P.B., Kasting J.F. (1981) A negative feedback mechanism for the long-term stabilization of Earth's surface temperature. *J. Geophysical Research: Oceans*, **86(C10)**, 9776-9782.

White D.J. (2011) Geophysical monitoring of the Weyburn CO_2 flood: Results during 10 years of injection. *Energy Procedia* **4**, 3628-3635.

White A.F., Blum, A.E. (1995) Effects of climate on chemical weathering in watersheds. *Geochim. Cosmochim. Acta* **59**, 1729-1747.

Wiese F., Fridriksson Th., Armannsson H. (2008) CO_2 fixation by calcite in high-temperature geothermal systems in Iceland. Report for Icelandic GeoSurvey ISOR, Reykjavik, ISOR-2008/003.

Whittaker S., Rostron B., Hawkes C., Gardner C., White D., Johnson J., Chalaturnyk R., Seeburger D. (2011) A decade of CO_2 injection into depleting oil fields: Monitoring and research activities of the IEA GHG Weyburn-Midale CO_2 Monitoring and Storage Project. *Energy Procedia* **4**, 6069-6076.

Wolff-Boenisch D., Gislason S.R., Oelkers E.H., Putnis C.V. (2004) The dissolution rates of natural glasses as a function of their composition at pH 4 and 10.6, and temperatures from 25 to 74 °C. *Geochim. Cosmochim. Acta* **68**, 4843-4858.

Wolff-Boenisch D., Wenau S., Gislason S.R., Oelkers E.H. (2011) Dissolution of basalts and peridotite in seawater, in the presence of ligands, and CO_2: Implications for mineral sequestration of carbon dioxide. *Geochim. Cosmochim. Acta* **75**, 5510-5525.

Chapter 2

A novel high pressure column flow reactor for experimental studies of CO_2 mineral storage

Iwona Galeczka, Domenik Wolff-Boenisch, Þorsteinn Jonsson, Bergur Sigfússon, Andri Stefánsson, and Sigurdur R. Gislason

Galeczka I., Wolff-Boenisch D., Jonsson Th., Sigfusson B., Stefansson A., Gislason S.R. (2013)
A novel high pressure column flow reactor for experimental studies of CO2 mineral storage.
Applied Geochemistry **30**, 91-104

Abstract:

The objective of this study was to design, build, and test a large scale laboratory high pressure column flow reactor (HPCFR) enabling experimental work on water-rock interactions in the presence of dissolved gases, demonstrated here by CO_2. The HPCFR allows sampling of a pressurized gas charged fluid along the flow path within a 2.3 m long titanium column filled with either rock, mineral, and/or glass particles. In this study, we used a carbonated aqueous solution (1.2 M $CO_{2(aq)}$) and basaltic glass grains. Given the pressure (up to 10 MPa) and temperature rating (up to 90 °C) of the HPCFR, it can also be used with different gas and/or gas mixtures, as well as for supercritical fluid applications. The scale of the HPCFR, the possibility to sample a reactive fluid at discrete spatial intervals under pressure, and the possibility to monitor the evolution of the dissolved inorganic carbon and pH *in-situ* all render the HPCFR unique in comparison with other columns constructed for studies of water-rock interactions. We hope this novel experimental device will aid in closing the gap between bench scale reactor experiments used to generate kinetics data inserted into reactive transport models and field observations related to geological carbon sequestration. A detailed description and testing of the HPCFR is presented together with first geochemical results from a mixed H_2O-CO_2 injection into a basalt slurry whose solute concentration distribution in the HPCFR was successfully modelled with PHREEQC geochemical computer code.

2.1. INTRODUCTION

Mineral sequestration is the final product of geological carbon storage which provides long-term stability for captured, industrial CO_2. In fact, mineral storage mimics the natural processes of weathering of primary silicates and magmatic CO_2 flux into groundwater systems in silicate rocks (Flaathen et al., 2009). Atmospheric carbon can be transformed into carbonate minerals either *ex-situ*, as part of an industrial process, or *in-situ*, by injection into geological formations where the elements required for carbonate-mineral formation are present (Oelkers et al., 2008). The relative amount and rate of CO_2 fixation depend on the rock type (Wolff-Boenisch et al., 2006), injection methods and temperature. Investigation of basaltic and ultramafic rocks (Garg and Shukla, 2009, Gislason et al., 1993, Gysi and Stefánsson, 2012a, Kelemen and Matter, 2008, Matter et al., 2007, McGrail et al., 2006, Prigiobbe et al., 2009, Schaef and McGrail, 2009, Wolff-Boenisch et al., 2011) demonstrate their high capacity for *in-situ* carbonatization. The CarbFix CO_2 sequestration pilot project in Iceland (Aradóttir et al., 2012, Gislason et al., 2010) has been established to investigate *in-situ* the potential for mineral carbon storage in basalt. The conceptual model of the CO_2 fixation into basaltic rocks indicates that CO_2 saturated waters will enhance basalt dissolution due to its low pH, releasing divalent metals into the solution. As a result of proton consumption by basalt dissolution, pH will increase followed by carbonate ($(Ca,Mg,Fe)CO_3$) precipitation (Aradóttir et al., 2012, Gislason et al., 2010, McGrail et al., 2006, Oelkers et al., 2008).

There have been numerous experimental studies investigating H_2O-CO_2-basalt interaction. Many of them focused on basalt dissolution rate measurements (Gislason and Eugster, 1987, Gislason et al., 1993, Gudbrandsson et al., 2011, Schaef and McGrail, 2009, Wolff-Boenisch et al., 2011), other were geared towards the effects of basalt carbonatization (Stockmann et al., 2011), whereas a third group combined basaltic dissolution and re-precipitation processes under CO_2 pressure (Gysi and Stefánsson, 2012a,c). Even though most of these experiments were carried out in small reactors of hundreds of ml volumes filled with few grams of rock, results of these experiments confirm the efficiency of basalt dissolution leading to its carbonatization under CO_2 pressure. The outcome of these experimental studies was a motivation to go a step further and bridge laboratory experiments and field observations by designing and constructing a large scale (2.3 m) high pressure column flow reactor HPCFR (alternatively called ‘plug’ or ‘plug flow reactor’ in the literature) which will combine fluid flow through porous media, dissolution and precipitation of minerals and glasses under variable CO_2 or gas mixture pressure, fluid composition, and temperature.

A HPCFR is a cylindrical container filled with solid material where fluids are pumped through. At its inlet, dissolution reactions are predominant but over time and space, as the concentrations of reagents decrease and the concentrations of products increase along the reaction path, precipitation becomes more important. Despite the advantage of high chemical reaction rates, few laboratory studies have been published on percolation of CO_2 rich fluids through columns (Andreani et al., 2009, Bateman et al., 2005, Bateman et al., 2011, Luquot and Gouze, 2009, Munz et al., 2012, Yi et al., 2011). The fact that not many column studies on pressurized water-rock interaction exist may be because large scale laboratory HPCFR of several metres are more difficult to design and maintain than their smaller batch and mixed-flow analogues, especially under elevated gas or hydraulic pressure. In a pressurized system, each connection (fittings, valves) inserted into the system poses a potential problem. Sampling procedure of a liquid under pressure is very challenging and special conditions have to be provided to obtain pH and CO_2 concentrations of a sample *in-situ*, that is, under experimental conditions. The following experimental set-up makes it possible to monitor pH, Eh and chemical composition of the fluid along the flow path within the column, and also variations over time. Furthermore, a spatial study of the solid chemistry along the flow path can be performed due to divisions of the column into compartments (see chapter 3.1 and Fig. 1). This spatial and temporal resolution at a higher scale is the most fundamental difference to common practice batch and flow-through reactor experiments. Because of this it can be used to "test" the performance of reactive transport models like PHREEQC (Parkhurst and Appelo, 1999) and TOUGHREACT (Xu et al., 2006, Xu et al., 2011). The latter was used to predict the reactive transport properties of CO_2 injection into basaltic rocks at the CarbFix site in Iceland (Aradóttir et al., 2012). Information obtained during column experiments will improve our understanding of the kinetics of basalt dissolution and solid replacement reactions under CO_2 sequestration conditions. Future characterization and quantification of secondary minerals (carbonates, clays) will yield molar volume and porosity changes as a function of time and distance along the flow path. Data provided from the experiment will be used in reactive transport models to elucidate the advance of reaction fronts, forecast porosity changes and estimate more accurately the amount of sequestered CO_2.

This study discusses in detail the HPCFR design and technical issues such that it may serve as a guide for future experimental studies of supercritical fluid/gas-water-rock interactions. The HPCFR was tested with CO_2 charged waters (1.2 M $CO_{2(aq)}$) and basaltic glass as reactive material but in fact all kinds of material and different gases or gas mixtures can be used. The first results from the column, mimicking CO_2 injection into glassy basalt at ~4 MPa pCO_2 and 22 °C are presented.

2.2. MATERIAL

The filling material for the column is basaltic glass originating from the Stapafell Mountain located in SW Iceland. This material has been utilized in previous studies on glass dissolution kinetics (Gislason and Oelkers, 2003, Oelkers and Gislason, 2001, Stockmann et al., 2011, Wolff-Boenisch et al., 2011) and its chemical composition is consistent with $Si_{1.0}Ti_{0.024}Al_{0.355}Fe_{0.207}Mg_{0.276}Ca_{0.265}Na_{0.073}K_{0.007}O_{3.381}$. The particle size fraction of 45-100 µm was dry sieved and washed by repeated gravitational settling to remove ultrafine particles. The total mass of glass inside the column is 8.3 kg, the corresponding specific BET surface area equals 22 000 cm^2/g, while the total surface area amounts to 182,160,000 cm^2. The total mass of aqueous solution is estimated as 1.84 L assuming 40% porosity, yielding a surface area to solution volume ratio of $\sim 10^5$ cm^{-1}.

2.3. EXPERIMENTAL SET-UP

Liquid CO_2 is mixed with degassed deionized (DI) water and pumped through a 2.3 m long titanium column filled with basaltic glass powder. Dissolution and precipitation reactions take place inside the HPCFR and reaction progress is monitored via solute sampling together with pH and DIC (Dissolved Inorganic Carbon) determinations in different compartments at increasing distances from the column inlet. The residence time of the fluid (total volume of the aqueous solution inside the column divided by the sum of the individual pump flow rates) can vary from few to tens of hours. Total pressure is set to 8 MPa to keep the CO_2 in liquid phase (see chapter 3.2); however this value can differ depending on the temperature, gas or gas mixtures used in experiment. The description of the HPCRF and its functioning can be divided into four subsections. The first section focuses on the column itself, containing the basalt slurry where chemical reactions between solid material and inlet solution occur. The second section depicts the reactive inlet solution supply. The third section covers the combination of electrical stream selectors and valves, gas expander, and back pressure regulators which enable sampling the outlet solution under physical and chemical conditions that prevail in the column, without alterations. The fourth section defines the in-line determination of the parameters pH, Eh and CO_2.

The CO_2 saturated inlet solution has a low pH and is therefore corrosive. Using materials with superior resistance to corrosive attack prevents changing solution chemistry caused by reaction between the corrosive liquid and plug material. Therefore, nearly the entire reactor is made either of titanium (Ti), Hastelloy® C-276 (HC), or PEEK (Polyether ether ketone). Titanium alloys can be used up to 600 °C

and pressure up to 180 MPa depending on the type and thickness of the alloy and the temperature. It shows also high corrosion resistance to brines, seawater, and high ionic strength aqueous chloride solutions. Titanium performance, however, can be limited in strong, highly reducing acid media such as moderately or highly concentrated solutions of HCl, HBr, H_2SO_4, H_3PO_4 and in HF solutions as the temperature increases. Likewise, Hastelloy® C-276 shows outstanding performance in a variety of industrial applications. It can be used up to 1000 °C and is corrosion resistant to hot contaminated media (organic and inorganic), a variety of organic acids, seawater and brines, sulphur compounds and chloride ions. In the HPCFR set-up, there are some exceptions where 316 stainless steel (SS) parts which are less corrosion resistant in acidic environments (especially at temperatures >66 °C) were used. It is assumed that in these instances contact time between SS and acidic fluid is so short that corrosion will have a negligible influence on the solute chemistry and material behaviour. Furthermore, in the CO_2-basalt system the pH will not permanently remain acid but will evolve towards a circum-neutral range with progressing chemical reactions along the flow path, resulting in less corrosion.

2.3.1. The plug

The titanium column measures 234×5.8×5.0 cm [L×OD×ID] and holds a total volume of ~4.6 L (Fig. 1). It is anticipated that in the lower part of the column, dissolution of primary basaltic material will be the dominant process whereas precipitation of secondary phases will prevail in the upper part. Thus, the column was divided into seven compartments to allow a better spatial resolution of the reaction progress (Fig. 1, Box 1). Titanium discs of 16.4×5.0 cm [OD×ID] size were welded to each pipe compartment to create a flange (Fig. 1, Box 4). Additionally, two titanium inlet and outlet discs with 1/8” compression fittings were added (Fig. 1, Box 5). All compartments together with upper and bottom discs were properly screwed together with Teflon discs and O-ring rubbers wedged in between to assure a leak-free system up to a minimum of 10 MPa total pressure (Fig. 1, Box 3). Teflon is resistant to high temperatures up to 260 °C and to many chemicals (ozone, chlorine, acetic acid, ammonia, sulfuric acid and hydrochloric acid). The only substance which could affect Teflon performance and potentially create leakage in the pressurized column is molten alkali metals and highly reactive fluorinating agents. The small ID of the column compared to its length provides long flow paths for the reactive solution.

The inlet is placed at the bottom of the vertically aligned column to spread the percolating fluid perpendicular to the flow axis and to avoid preferential flow paths via gravitational resistance and lateral spread. The column has one main outlet at the top and seven lateral sampling outlets, one in each segment (Fig. 1, Box 6).

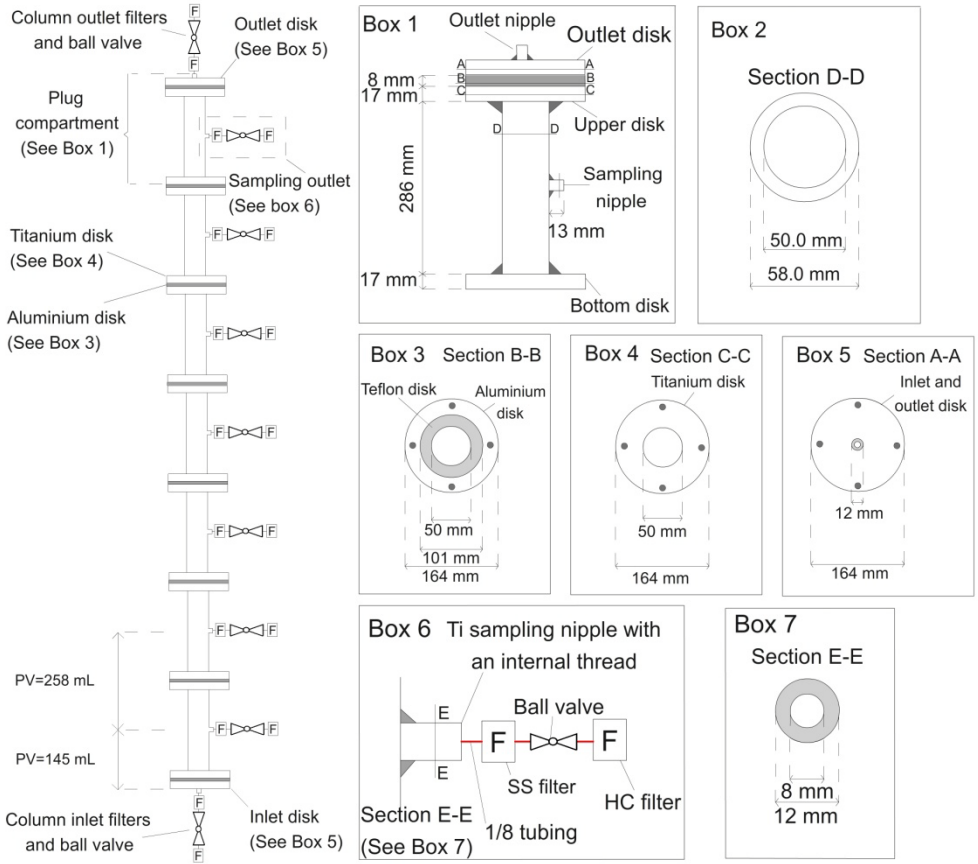

Figure 1. Overall drawing of the 2.34 m long column is shown on the far left, with details displayed in Boxes 1-7. Box 1 illustrates the column outlet compartment in frontal view. Boxes 2-5 depict, in top view, the dimensions of the various compartments presented in Box 1. Box 6 describes the sampling outlet of each compartment and Box 7 displays, in top view, the dimensions of the sampling nipple. 'PV' in the overall drawing on the left refers to the pore volume in the compartments after filling the reactor with the solid material. Total length of the column is 2.34 m, the volume is 4.6 L, and the pore volume assumed to be 40% (~1.84 L).

Solution sampling from seven compartments enables the determination of changes in concentration of individual elements including dissolved inorganic carbon (DIC) as well as pH and redox conditions along the flow path within the column. At all outlets of the column 1/8" compression fittings are connected to 1/8" SS 60 µm (Swagelok®) and HC 10 µm filters (VICI®) to avoid glass particles from the column entering and potentially clogging the sampling valves (see also chapter 3.3 and Fig. 1). A SS ball valve (Swagelok®) is placed between both filters. The HC filters clogged during the initial testing of the plug. These filters consist of frits with a small cross sectional area and thus tended to clog very rapidly. It was decided to insert SS filters (Swagelok®) which contain frits with much larger cross sectional areas before the HC filters (Fig 1, Box 6). Ball valves between the filters facilitate the replacement of the HC filter frits in case of clogging by closing the column

outlet valves (Box 6 in Fig. 1). The column inlet and outlet filters (Fig.1 far left) are connected to Ti 1/8" needle valves (Collins Instrument) because contact with the reactive fluid is quasi permanent. In contrast, the seven sampling outlets are connected to SS 1/8" ball valves (Swagelok®) as the short contact time between fluid and sampling valves is considered to exert a negligible influence on the solution chemistry. In order to avoid detrimental temperature swings in the lab, the column is wrapped with a heating Tape (HTS/Amptec) maintained at ambient temperature (22°C). This heating tape also circumvents the development of temperature gradients inside the column and enables to promote chemical reactions when used at higher system temperatures (max. 90 °C given the pressure rating for the Ti plug thickness of 0.4 cm) which was, however, not explored in this study. The total pore volume of the water inside the column is estimated as ~1.84 L assuming a porosity of 40%. This pore volume is divided into eight sections where the beginning of the section starts with the previous sampling outlet and ends with the following one. The pore volume ('PV' in Fig. 1) of the bottom and the top section of the column is 145 mL, respectively whereas the pore volumes between two adjacent sampling outlets equal 258 mL.

2.3.2. Reactive fluid supply

The liquid CO_2 cylinder is placed on a scale and its status monitored through mass loss as shown in Figure 2a. The cylinder is connected to a supercritical fluid pump (Supercritical Fluid Technologies) through SS 1/8" tubing. To provide sufficient head space delivery pressure from the CO_2 cylinder to the pump (>5.2 MPa), the distance between both has to be short and the gas cylinder kept at constant room temperature. It is recommended to use a tank heater (Power Modules, Inc.) to increase the head space cylinder pressure if low flow rates are used. To ensure thorough and complete mixing and dissolution of CO_2 in water ($CO_{2(aq)}$), liquid CO_2 ($CO_{2(l)}$) was given preference over a gaseous CO_2 ($CO_{2(g)}$) source because the solubilization kinetics of $CO_{2(l)}$ is fast (Bortoluzzi et al., 2011). The downside of $CO_{2(l)}$ is that the system pressure has to be maintained at or above 7.1 MPa, necessary to keep CO_2 liquid at room temperature. This calls for the installation of a high pressure corrosion resistant mixing device, ideally with a sufficient volume to enable longer residence time for H_2O-CO_2 mixing. This requirement was solved by a flow-through Ti reactor like the ones routinely employed in mineral dissolution studies (Wolff-Boenisch et al., 2011). The liquid $CO_{2(l)}$ and DI water enter separately through the same dip tube and are thoroughly mixed by a magnetic stirrer before exiting through a 2 µm outlet reactor Ti filter (Fig 2a). This 'mixing chamber' has the additional advantage of adjusting and controlling the mixing temperature. It should be pointed out that there are alternative ways to achieve

thorough mixing for example by coiled tubing in a water jacket (mixing loop) to dissolve $CO_{2(l)}$ (Luquot and Gouze, 2009). The advantage of a reactor versus mixing loop is the option of measuring initial dissolved inorganic carbon (DIC) *in-situ* before the fluid comes into contact with the solid. Depending on the desired overall flow rate of the experiment, which in the case of a large, meter-long plug may amount to several mL/min, a minimum mixing volume is needed to provide an adequate residence time for full dissolution of $CO_{2(l)}$ in water. At the flow rate of 5 mL/min and vigorous stirring (300 rpm) at 22 °C, the residence time of 20 min in the 100 mL Ti reactor was observed to be sufficient. Mixing efficiency was tested at different pump flow rates of H_2O and CO_2, i.e., different flow rate ratios yielding different initial DIC concentrations. A minimum of ten consecutive stable DIC determinations close to the expected, theoretical DIC concentrations indicated full dissolution of $CO_{2(l)}$ When the $CO_{2(l)}$ was not fully dissolved, large variations in the DIC measurements and deviations from the theoretical concentrations were noticed. A reactor volume of 100 ml as required in this study is a large mixing volume which puts some constraint on the option of using alternatively a mixing coil as it would, under our experimental conditions, correspond to≥55 m of inert tubing [1] that would have to be cooled/heated evenly.

When mixing $CO_{2(l)}$ and water in the mixing chamber, it is vital to avoid backflow of H_2O-CO_2 mixture into the CO_2 pump. This corrosive liquid may destroy the upper pump head check valves which are made of SS. Potential backflow into the CO_2 pump head can also cause freezing of the solution and thus create ice particles and scratch the glass pistons. In preliminary tests a regular Tee (a unit connecting two flow paths into one) was used to combine the $CO_{2(l)}$ and the DI water lines (Fig. 2a). From there, the H_2O-CO_2 mixture flowed to the mixing reactor. However, it is recommended to keep CO_2 and DI water lines separated because the water pump runs on larger flow rates that could potentially push water into the CO_2 line. Furthermore, check valves (Swagelok®) have to be inserted prior to the CO_2 and DI water reactor inlets (Fig. 2). Commonly used SS check valves have a disadvantage of rubber O-rings which are not fully resistant to CO_2 attack. Stainless steel ball check valves without O-ring or Teflon soft seated check valves (Maximator®, HiPressure Equipment Company) are better to provide longer lifetime.

Another critical issue is the flow rate ratio between the supercritical fluid pump (SCF) and water pump (high pressure liquid chromatography pump, HPLC). This ratio depends on the solubility of $CO_{2(l)}$ in water which decreases with increasing temperature and ionic strength of the solvent and increases with the CO_2 partial pressure (pCO_2) (Gislason et al., 2010). Based on the literature, the mole fraction solubility of $CO_{2(l)}$ in DI water under close-to operating conditions (25 °C and

[1] A regular 1/8“ tubing with an ID of 0.06“ yields a volume of one ml for every 55cm length.

7.5 MPa total pressure) equals 0.0244 (Teng and Yamasaki, 2002) and 0.0245 (Duan et al., 2006), respectively. This value cannot be surpassed to ensure saturation and a one-phase flow of water and $CO_{2(aq)}$ into the plug. In order to calculate the appropriate pump rate ratios the following three equations are introduced: The mole fraction X_{CO2}:

$$X_{CO_2} = \frac{n_{CO_{2(aq)}}}{n_{CO_{2(aq)}} + n_{H_2O}} \quad (1)$$

where n_{CO2} and n_{H2O} are the moles of $CO_{2(aq)}$ and H_2O, respectively. This ratio is necessary to calculate the mole ratio between H_2O and $CO_{2(aq)}$, $X_{\frac{H_2O}{CO_{2(aq)}}}$ (40.15). The molar volume ratio between H_2O and CO_2 is calculated based on the density (δ) of H_2O and CO_2 at 25°C and the molecular weight of both:

$$V_{m\frac{H_2O}{CO_2}} = \frac{\frac{m_{weight H_2O}}{\delta_{H_2O}}}{\frac{m_{weight CO_2}}{\delta_{CO_2}}} = \frac{\frac{18}{0.997}}{\frac{44}{0.77}} = 0.32 \quad (2)$$

Combining Eqs. (1, 2), the ratio between HPLC and SFC pump flow rates to reach maximum dissolved carbon concentration is:

$$\text{pump flow rate ratio}_{\frac{HPLC}{SFC}} = X_{\frac{H_2O}{CO_{2(aq)}}} * V_{m\frac{H_2O}{CO_2}} = 40.15 * 0.32 = 12.85 \quad (3)$$

This number means that at least 13 times more H_2O volume versus $CO_{2(l)}$ volume has to be delivered per time unit to ensure complete dissolution of $CO_{2(l)}$ in the Ti mixing reactor. This ratio will increase significantly when mixing a very saline solution with $CO_{2(l)}$ and when temperature is increased. Under such circumstances, a syringe pump rather than the piston pump utilized in this study is required to deliver the very small volumes of liquid/supercritical CO_2.

2.3.3. Sampling the plug

Sampling of fluids is carried out by either diverting the selected stream through a stream selector to a pressurised sampling loop and expander for DIC analysis or towards the fluid sampling outlet and pH and Eh electrodes (Figure 2). The sampling unit shown in Figures 2a-d starts with an HC multi-position 8-port stream selector (VICI®) where individual ports are connected to corresponding column compartment outlets through 1/8" tubing (PEEK). The selector outlet is connected to an HC 2-position 6-port valve (VICI®). In sampling mode, $CO_{2(aq)}$ is captured in a sampling loop of known volume. The DIC concentration is measured in a 26 mL custom-made plastic container, the so-called 'expander' equipped with a pressure transducer (OMEGA®) that records the pressure induced by CO_2 expansion.

Following the 2-position 6-port valve, the solution flows through an HC 2-position 4-port valve (VICI®) connected to a N_2 gas cylinder. This inert gas provides pressurization of the sampling path before reactive solution is sampled to avoid degassing of CO_2 from the column. The main outlet of the column as well as the 2-position 4-port valve are connected to an HC multi-position 4-port stream selector (VICI®). From this selector outlet, the fluid passes either through an SS cross (Swagelok®) with high pressure/temperature SS pH and Eh electrodes (Corr Instruments, Texas) and finally through the main back pressure regulator (BPR 1, Swagelok®) or is by-passed to a second similar BPR 2. The addition of a second BPR and two 1/8" inlet needle valves (one of Ti from Collins Instrument; one of SS from Swagelok®) provide the possibility of short-cutting the pH/Eh cross for calibration and/or maintenance purposes. Samples for the major cations are taken from the by-pass BPR 2 to avoid long contact times of the fluid with the pH/Eh cross which is made of SS.

There are four running modes of the column. During normal flow the solution flows through the column without sampling (Fig. 2a). Preparation of the system for sampling follows by pressurization of the sampling path which after previous sampling remained depressurized (Fig. 2b). The third stage is the actual sampling (Fig. 2c) followed by the last stage – expansion, when the CO_2 concentration is measured in the expander (Fig. 2d).

First stage (Fig. 2a). The solution is continuously delivered to the column. In the first stage the multi-position 8-port stream selector is oriented towards the 8^{th} port which is closed with an SS 1/8" plug (VICI®). Subsequently, the multi-position 4-port stream selector is oriented to the 1^{st} port so that, after exiting the column (ball valves on each compartment are closed), the solution flows directly via the pH and Eh cross through the BPR 1 (Fig 2a). The pressure on the additional by-pass BPR 2 is set slightly higher than the pressure on the regular BPR 1 to allow fluid through the latter.

Second stage (Fig. 2b). Sampling preparation procedure requires orienting the multi-position 8-port stream selector to any port which is connected to a specific column compartment. Nitrogen gas fills the passage through the three lower valves in Figure 2b, including the sampling loop, up to the compartment ball valve. Figure 2b depicts preparation for sampling from the forth outlet. Gas is introduced to the system until the pressure in the sampling path approaches a pressure around 2 MPa lower than the operating system pressure allowing the fluid from the column to replace the N_2 gas. During this stage the pH/Eh cross is short-cut by closing one of the two inlet cross valves and reducing the pressure on the by-pass BPR 2.

Third Stage (Fig. 2c). Sampling commences with opening the compartment ball valve. Figure 2c represents sampling from the forth outlet. Liquid flows through all valves from the forth outlet and displaces the N_2 which exits the system through the

by-pass BPR 2. It is important to run the initial part of the sampling phase through the by-pass BPR 2 to avoid displaced N_2 from entering and potentially persisting in the pH/Eh cross. Note that the positions of the multi-position 4-port stream selector and 2-position 4-port valve have to be changed between stage 2 and 3 (Figs. 2b and c) and the pressure difference between both has to be readjusted.

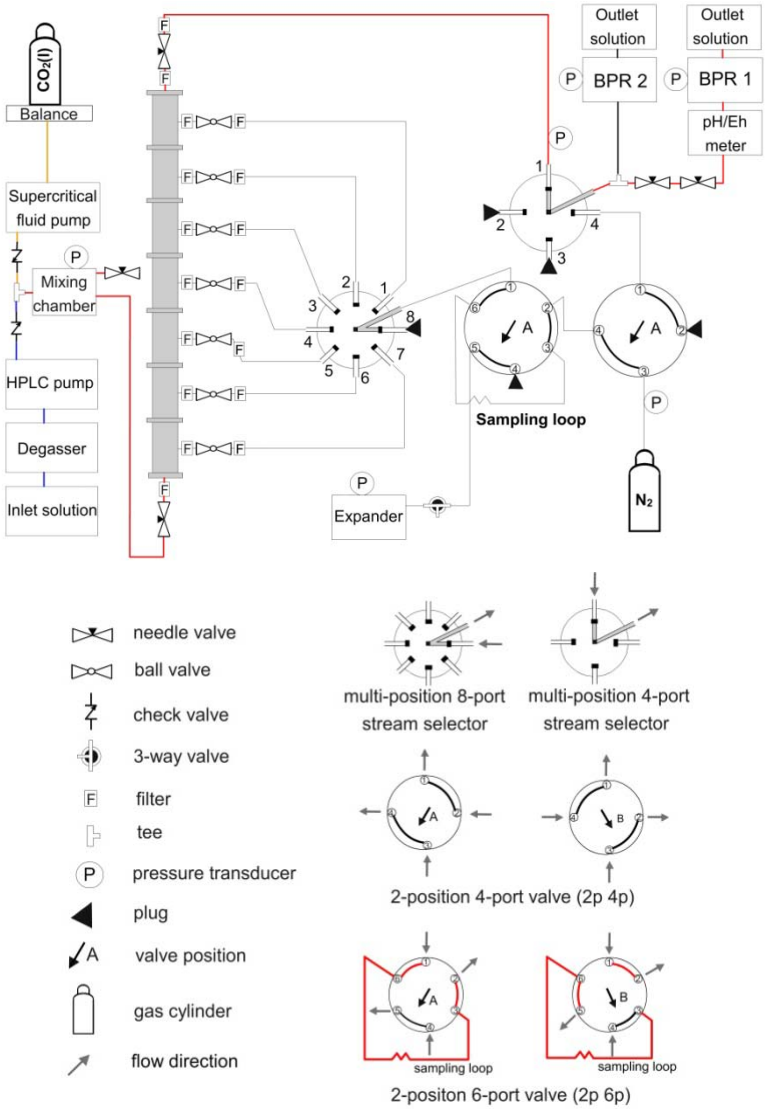

Figure 2a. Set-up for normal flow. The CO_2 is mixed with H_2O and pumped through the column. The reacted solution passes the multi-position 4-port stream selector through port 1, which is connected to the outlet port and flows through high temperature/high pressure electrodes followed by a back pressure regulator (BPR 1). The multi-position 8-port stream selector is aligned with port 8. Both, the 2-position 6-port and 2-position 4-port valves are set on position A. All the compartments outlet ball valves are closed.

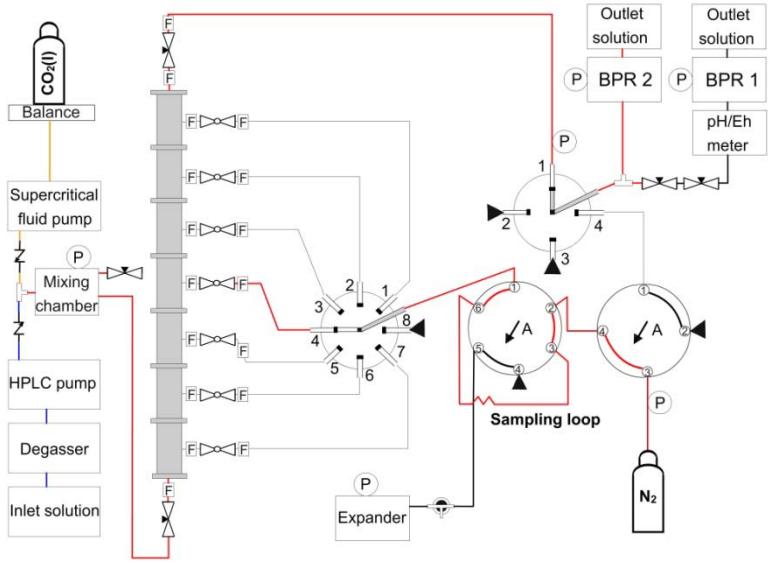

Figure 2b. Set-up for pressurization of the sampling path with nitrogen (N_2). The reacted solution flows through the multi-position 4-port stream selector and the by-pass back pressure regulator (BPR 2). The multi-position 8-port stream selector is set on a chosen sampling compartment. N_2 passes the 2-position 4-port valve, the 2-position 6-port valve with the sampling loop and reaches the ball valve on the compartment sampling outlet.

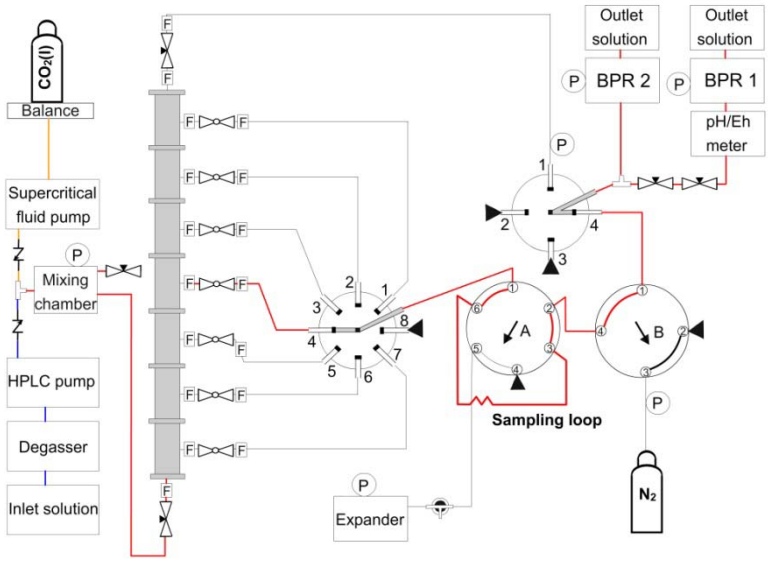

Figure 2c. Set-up for sampling mode, in this case from compartment #4. The 2-position 4-port valve is set on port 4. The solution in the column outlet line is stagnant during this stage. The ball valve of the sampled compartment is opened; solution flows through the multi-position 8-port stream selector and passes the 2-position 6-port valve in position A followed by the 2-position 4-port valve in position B. The fluid flows through the multi-position 4-port stream selector to the by-pass back pressure regulator BPR 2. After taking sample for major ions, the fluid is diverted to the cross and BPR 1 for pH/Eh measurements.

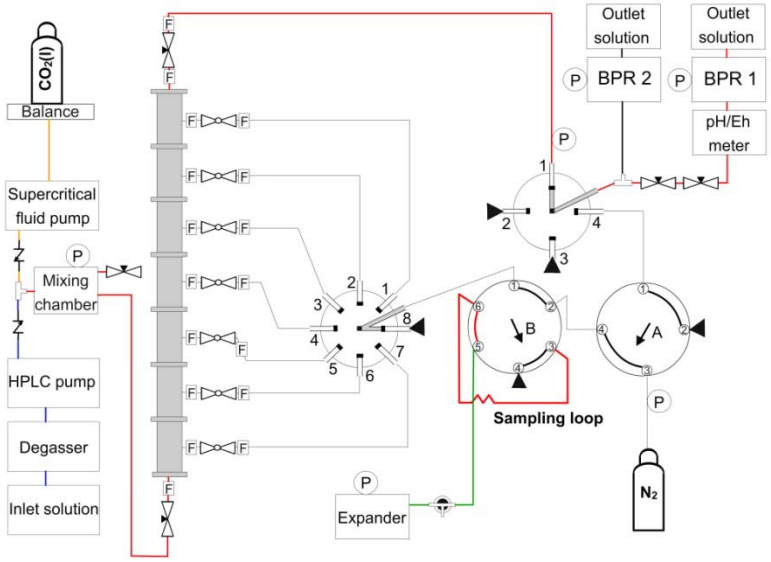

Figure 2d. Set-up for the expansion mode to measure the total dissolved inorganic carbon (DIC). The outlet solution is directed to pass through the multi-position 4-port stream selector set on port 1 and flows through the high temperature/high pressure electrodes followed by the back pressure regulator BPR 1. The multi-position 8-port stream selector is aligned with port 8. The 2-position 6-port valve is switched to position B which allows CO_2 expansion into the expander. The 2-position 4-port valve is switched back to position A after CO_2 expansion.

It is in the third position that fluid samples for subsequent elemental and ion analysis are collected from the by-pass BPR 2 and in-line pH/Eh measurements are carried out from BPR 1.

Forth stage (Fig. 2d). The fourth stage involves expansion of exsolved CO_2 ($CO_{2(g)}$) from the pressurized fluid in the sampling loop into the expander (2-position 6-port valve is set on position B). The expander is maintained at ambient pressure prior to sampling and thus the pressure increase through expansion is recorded. At the same time the settings from the normal flow mode are restored (Fig. 2d). After measuring the CO_2 concentration the 2-position 6-port valve goes back to position A. After sampling, the tubing between the column and the 8-port multi-position stream selector is filled with solution. It is vital to prevent precipitation of secondary phases in the sampling tubing. Secondary solids can not only clog the tubing but also change the chemistry of the sampled liquid by dissolving during the next sampling. The design of the set-up allows disconnecting the tubing after finishing the sampling procedure and flushing it with DI water and/or drying it with N_2 gas.

2.3.4. Analysis

To characterize chemically the H_2O-CO_2 system, two out of six parameters have to be measured: pH, pCO_2, alkalinity, DIC, HCO_3^-, and CO_3^{2-}. The selection of measured parameters is related to the experimental design and conditions. High CO_2

pressure used in carbon sequestration laboratory experiments and field applications requires the *in-situ* determination of the desired parameters before exposing the pressurized H_2O-CO_2 mixture to the atmosphere where CO_2 degassing can cause changes in these parameters. In this study we use high pressure/temperature SS pH and Eh electrodes (Corr Instruments, Texas) combined with an expander-transducer set-up to determine the pH and DIC, respectively. Precision of the pH/Eh measurements are ±0.1 log unit. When pH and DIC are known, alkalinity, pCO_2, HCO_3^-, and CO_3^{2-} can be recalculated using geochemical modelling software, such as PHREEQC (Parkhurst and Appelo, 1999). There are different analytical ways of DIC determination, e.g., titrimetry, ion chromatography, or standard addition technique. In this study, the $CO_{2(aq)}$ is captured in a sampling loop of know volume (1 mL) as depicted in Figure 2d. A pressure transducer (OMEGA®) connected directly to an expander measures the pressure change induced by CO_2 expansion. Recalculations of ΔP made by CO_2 expansion yield DIC, according to:

$$\text{volume of } CO_2\ [\text{mL}] = [(P_{exp} - P_{atm}) * \text{volume of expander}]/P_{atm} \quad (4)$$

$$\text{DIC}\left[\frac{\text{mol}}{\text{L}}\right] = \frac{\frac{\text{volume of } CO_2[\text{mL}]}{\text{molar volume of } CO_2[\frac{\text{L}}{\text{mol}}]}}{\text{volume of the sample[mL]}} \quad (5)$$

where P_{atm} is the atmospheric pressure in the expander prior to CO_2 expansion and P_{exp} is the final pressure after expansion. Both values are relayed through the transducer to an appropriate analog signal reader (DP41-B, OMEGA®). This technique is very fast, simple and gives comparable results with other analytical methods. In this study, we compared results from the expander-transducer method with the standard addition technique (SAT, Table 1). The set-up for the SAT method is shown in Figure 3. This method was successfully employed in a related study dealing with fluid carbonation (Alfredsson et al., 2011). The SAT method determines the DIC concentration by repeated pH measurements of a concentrated base (0.5 M KOH) into which CO_2 from a sampled solution has been repeatedly degassed. The pH electrode records the pH change as a function of the sampled volume. With each sample being captured into the base the pH is lowered. Delta pH is recalculated to the amount of consumed moles of OH by the dissociation of carbonic acid, H_2CO_3, thus yielding the molar carbonate concentration. This technique works only in a pH range where CO_3^{2-} is the predominant aqueous carbon species (≥12.5) and only if gas is sampled. For the expander-transducer method to work, the pH of the fluid which is sampled has to be relatively low (<5.5) such that all inorganic C species are mainly present as $CO_{2(aq)}$. If the pH increases due to fast mineral or glass dissolution in the plug, the contribution from HCO_3^- to the overall inorganic C species may become importance and other methods, e.g. titration, will

be more suitable for the DIC determination. Alternatively, acid could be injected into the loop after degassing to convert any HCO_3^- into $CO_{2(g)}$ and drive it out of the loop and into the expander.

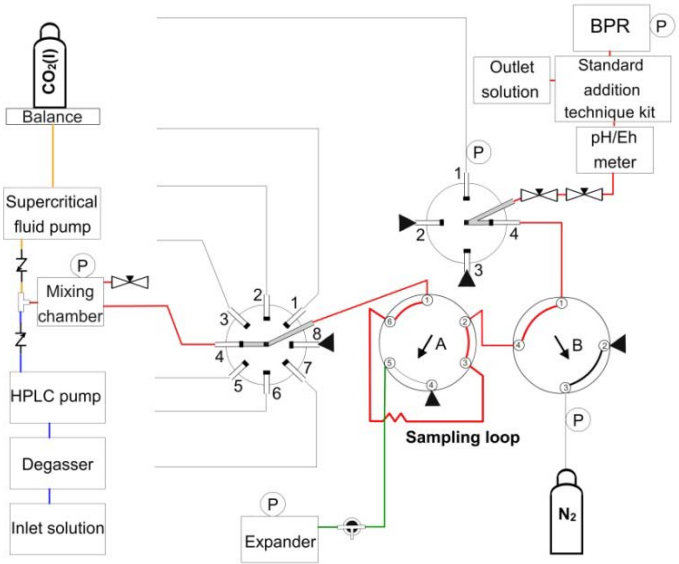

Figure 3. Set-up for DIC measurement via standard addition technique (SAT). The CO_2 is mixed with H_2O and flows in chronological order through the following key components: the multi-position 8-port stream selector, the 2-position 6-port valve (position A), the 2-position 4-port valve (position B), the multi-position 4-port stream selector, the pH/Eh cross, the standard addition technique kit (where the DIC measurement is performed), and the back pressure regulator (BPR 1). An alternative DIC analysis is carried out in the expander as shown in Figure 2d.

Further laboratory tests confirming the accuracy of the expander-transducer method were carried out at 22 °C and 8 MPa total pressure (Fig. 3). The tests (and subsequent column experiment) were performed under known H_2O/CO_2 pump ratios at 8 MPa to provide ~1 MPa pressure buffer with respect to potential CO_2 boiling of $CO_{2(l)}$ prior to mixing which is a reasonable safety margin in complicated pressure systems where small pressure fluctuations always occur.

Table 1. Comparison between calculated theoretical concentrations of DIC and concentrations determined by the standard addition technique (SAT) and the expander-transducer method (see text). The reproducibility test was performed at a H_2O/CO_2 pump ratio of 16. The percent recovery for the two methods has also been added.

DIC concentration [mol/L]			Percent recovery [%]	
Theoretical	**SAT**	**EXPANDER**	**SAT**	**EXPANDER**
1.25	1.07	1.15	86	92
1.25	1.02	1.10	81	88
1.25	1.06	1.09	85	87
1.25	1.13	1.08	90	86
1.25	1.12	1.08	89	86
1.25	1.11	1.10	88	88

According to the CO_2 solubility in water (Teng et al., 1997), theoretical DIC concentrations were calculated for selected H_2O/CO_2 pump flow rate ratios. The theoretical concentration at a H_2O/CO_2 pump flow rate ratio of 16 was compared with measured values obtained with the expander-transducer method as well as with SAT (Table 1 and Fig. 4a). Additionally, the DIC was measured with the expander-transducer method at varying initial inlet CO_2 concentrations where the H_2O pump flow rate remained constant and only the CO_2 pump flow rate was changed (Fig. 4b). Results of these tests indicate that the obtained average recovery at different H_2O/CO_2 pump flow rate ratios equals 95%. At higher H_2O/CO_2 flow rate ratios (≥22), recovery reached 100%, assuming that the H_2O pump and the CO_2 pump are delivering solutions with the same precision at different flow rate ratios (Table 2 and Fig. 4b). Average recovery at the flow rate ratio of 16 reaches only 87%. The time required to yield ≥98% recovery of the CO_2 degassing from the sampling loop into the expander is at least 20 minutes (Fig. 5).

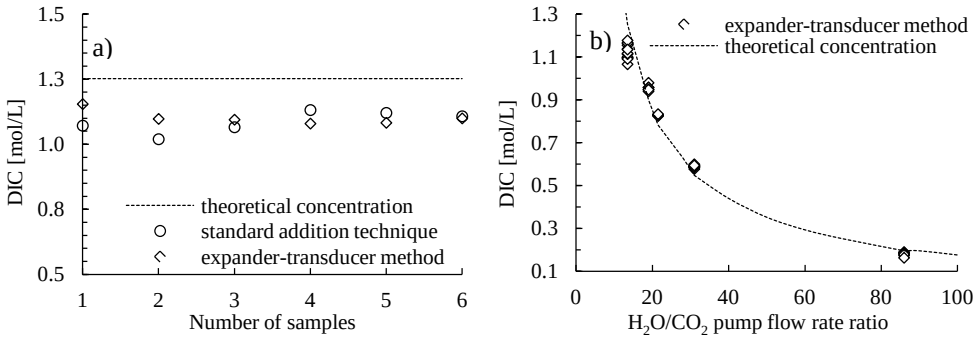

Figure 4. Plot (a) presents the comparison between theoretical and measured DIC at the H_2O/CO_2 flow rate ratio of 16. Measured concentrations were obtained with the standard addition technique and the expander-transducer method, respectively. Plot (b) shows the relationship between H_2O/CO_2 pump flow rate ratios and the DIC obtained with the expander-transducer method. At higher flow rate ratios (≥22), measured concentrations match closely the theoretical DIC. The theoretical curve was calculated based on the solubility mole fraction of CO_2, molar volume ratios of H_2O and CO_2, and theoretical pump flow ratios (cf. Eqs. (1-3)).

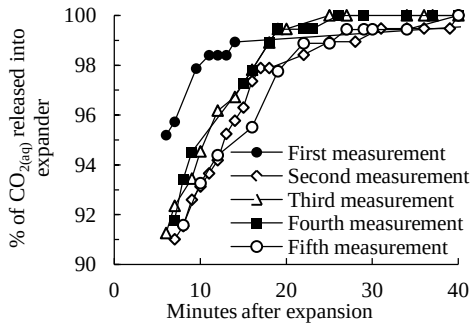

Figure 5. Efficiency of CO_2 expansion. After 20 minutes, 98% of $CO_{2(aq)}$ captured from the sampled solution degassed into the expander, indicating the critical minimum waiting time for pressure reading from the transducer which yields the DIC concentration according to Eqs. (4, 5).

Table 2. The DIC concentrations obtained with the expander-transducer method. Comparison between measured DIC (DIC_m) at different set H_2O/CO_2 flow ratios with the theoretical DIC concentrations (DIC_{th}) calculated for the tested flow rate ratios.

H_2O pump flow rate [ml/min]	CO_2 pump flow rate [ml/min]	Pump ratio H_2O/CO_2	DIC_m [mol/L]	number of measurements	standard deviation	Relative stdev [%]	DIC_{th} [mol/L]	Percent recovery [%]
5.00	0.32	16	1.10	16	0.04	3.81	1.25	87
5.00	0.23	22	0.95	6	0.01	1.44	0.90	101
5.00	0.20	25	0.83	6	0.04	0.34	0.78	101
5.00	0.14	36	0.59	10	0.01	1.42	0.55	103

2.4. RESULTS

The system was tested at 22 °C and 8 MPa total pressure. The column was filled with basaltic glass grains 40-100 μm in diameter. The DI water at a flow rate of 3.5 mL/min and $CO_{2(l)}$ at a flow rate of 0.22 mL/min were mixed and pumped through the column for 91 hours. Initial DIC concentration was ~1.2 mol/L and initial, measured pH 3.2 at 22 °C. The experiment started with DI water being pumped through the HPCFR at 22 °C and 0.1 MPa to condition the system. Then, the total/hydraulic pressure was increased to 8 MPa by adjusting the BPR 1 and BPR 2 accordingly, followed by turning on the $CO_{2(l)}$ pump. It took approximately 44 hours (5 pore volumes) to replace the initial reacted solution of pH~9 which is the result of DI water-basaltic glass interaction in the column with the H_2O-CO_2 mixture and decrease the pH to ~4.5 (Fig. 6).

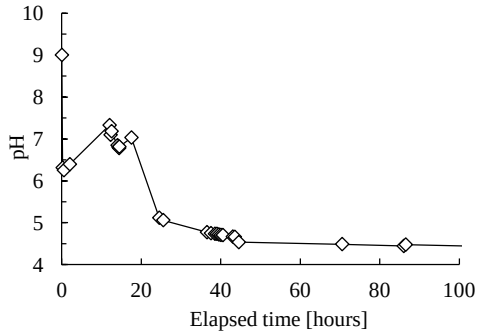

Figure 6. Evolution of the pH in the column during the replacement of the initial DI solution with the 1.2 M $CO_{2(aq)}$ solution. Values were measured in the outlet of the column. First point on the plot (pH 9) represents the column outlet pH during DI water conditioning of the basalt slurry.

First samples of the solute from all the outlets were taken after 44 hours followed by a second set after 90 hours. During the sampling the pH, Eh, and DIC were determined in-line which correspond to *in-situ* values.

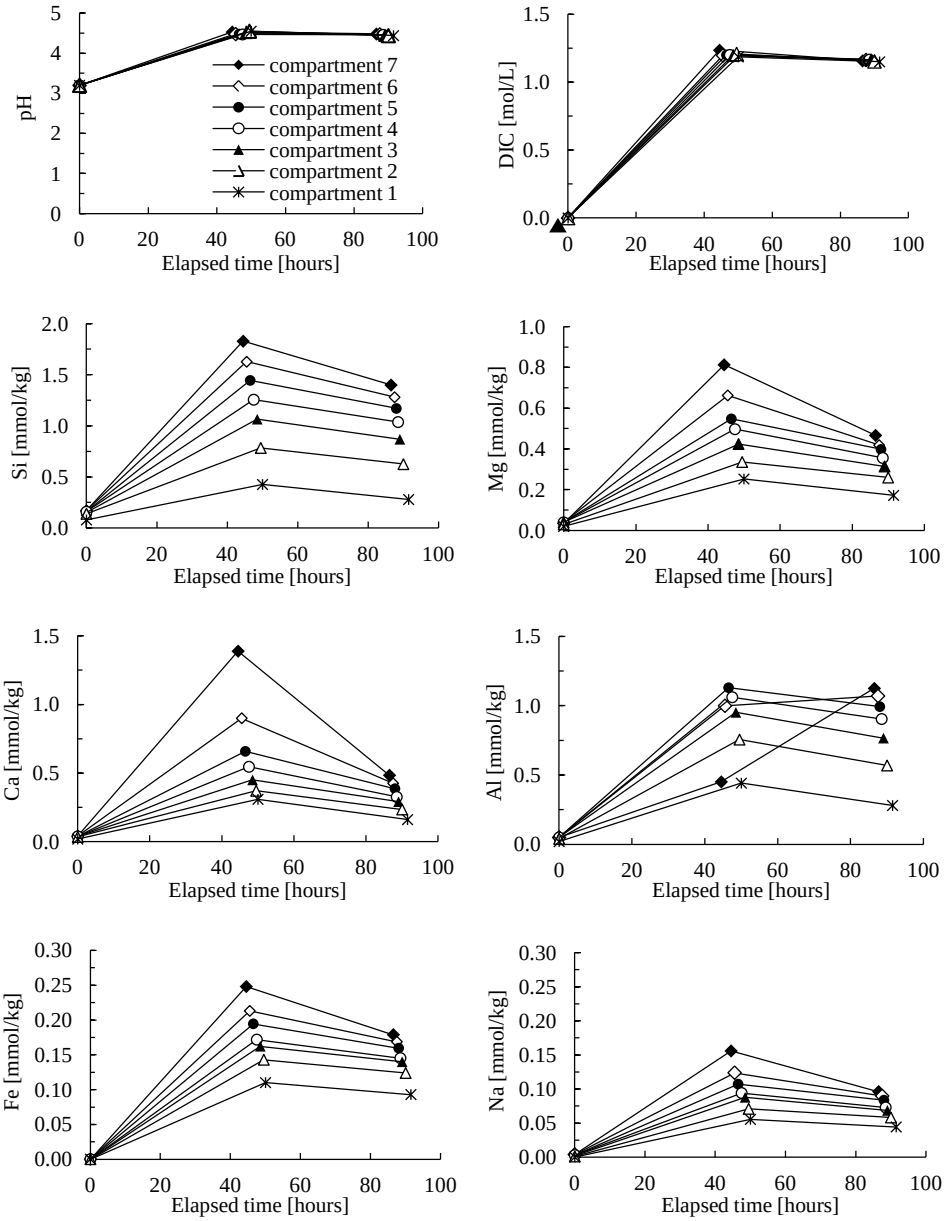

Figure 7. Results from the chemical analyses of the individual compartments during CO_2 injection. The compartment number reflects the sampling distance along the flow path inside the column, starting with compartment 1 which is the closest to the inlet of the column. The first set of points in the pH plot represents the initial pH of the H_2O-CO_2 solution in the mixing reactor before entering the column. The first set of points on the other plots represents the elemental concentrations during the conditioning of the column, when only DI water was pumped through.

The outlet solution was sampled, filtered using a 0.2 µm cellulose acetate filter, and then acidified with concentrated supra-pure HNO_3 prior to analysis for major elements with ICP-OES (Inductively Coupled Plasma Optical Emission

Spectrometer). Analytical uncertainties of ICP-OES analyses are on the order of ≤5%. Results of the chemical analyses are reported in Table 1 in Supplementary data. A comparison of major cation concentrations between individual compartments is depicted in Figure 7. Elemental concentrations for Si, Ca, Mg, Al, and Fe increased by factors of 11, 35, 20, 9, and 2500 after 48 hours and by factors of 8, 12, 12, 22, and 1800 after 90 hours of experimental duration compared to elemental concentrations during conditioning of the basaltic glass slurry with DI water. The DIC concentration and pH remained constant along the flow path.

2.5. DISCUSSION

The HPCFR was designed to monitor the evolution of the solute chemistry during different time stages along the flow path under high total/pCO_2 pressure. There are many challenges related to the experimental set-up which have to be overcome. A major problem in liquid or supercritical CO_2 experiments is the corrosive properties of the CO_2-charged water. Various kinds of less corrosion resistant materials such as O-rings and plastic seals in BPR and check valves can be irreversibly damaged when continuously exposed to $CO_{2(aq)}$ for long time. Worse, there is no possibility for replacement if needed because of the required pressure relief. Degassing of the system takes a long time and during degassing and re-launching of the experiment the chemistry of the system may change and influence secondary phase precipitation. The CO_2-charged water not only reduces the lifetime of vital parts in the experimental set-up but may also lead to damage of the pH electrodes. The CO_2 can diffuse into the inner compartment of the reference probe. Even though this does not change the probe potential, it may cause mechanical damages to the inner probe compartment during sudden pressure drops. Small pressure drops are unavoidable during the sampling procedure when the stream selectors are switched from one position to the other and therefore there is always a risk of inaccurate pH measurement. The manufacturer's recommended lifetime of the pH/Eh electrodes is about six months, heavily depended on the system temperature. Another issue is clogging of the compartment's outlet filters with fine material from the column (Fig. 1, Box 6). Clogged filters can result in 1-1.5 MPa pressure surge immediately after insertion, and if clogging persists during the whole experimental duration, it may not be possible to sample the compartment outlet and information from that particular compartment will be lost. Pumps delivering CO_2 and H_2O can also pose a problem. Especially the supercritical CO_2 pump is susceptible to damage when in-line check valves start to leak, consequently allowing backflow of the aqueous solution into the CO_2 pump. Such backflow inevitably causes deterioration of the pump leading to fluctuating flow rates, incontrollable inlet conditions, and ultimately costly downtime and repair. A syringe pump may

thus be a more suitable solution for $CO_{2(l)}$-$CO_{2(aq)}$-rock experiments, especially when dealing with low flow rates.

Other, non-technical issues involve sampling effects on the system flow. Taking a sample perturbs the overall vertical flow in the system. Therefore, sampling of the individual compartments is kept as short as possible to keep the disturbance of the flow dynamics and solute chemistry small. During sampling, fluid, which is above the sampled compartment, does not move. In order to avoid sampling a stagnant fluid the sampling protocol commences with the upper most compartment and moves downwards. Despite these technical and hydrological drawbacks, during this first phase of CO_2 pulse in the column, which mimics the onset of CO_2 injection in the field, a clear consistent elemental behaviour is observable.

After 90 hours (12 pore volumes), concentration curves start to overlap which is interpreted as approaching steady-state dissolution of the basaltic glass. Steady-state dissolution in flow through reactors is commonly defined as a constant outlet concentration of a conservative element (e.g. Si) from the solid at constant flow rate. Apparently, steady-state was not attained in the HPCFR but nonetheless the silica concentration at the second point was taken as a point of reference to determine a preliminary, close-to steady-state dissolution rate of the basaltic glass in the column and compare that value with literature rates. The experimentally determined dissolution rate normalized to geometric surface area (290 cm^2/g) yielded $10^{-13.4}$ $mol_{Si}/cm^2/s^{-1}$ and compares quite favourably with a calculated dissolution rate of $10^{-13.3}$ $mol_{Si}/cm^2/s^{-1}$ based on a rate expression given by Gislason and Oelkers (2003). So while the system may not have reached steady-state, its preliminary dissolution rate determined from the silica outlet concentration is very consistent with the far-from-equilibrium dissolution of basaltic glass of similar composition under acidic conditions of pH 4.5 and ambient temperature.

Further, one dimensional reactive transport modelling was carried out using PHREEQC 2.17 (Parkhurst and Apello, 1999) and the llnl.dat database. Results of the calculations were again compared with the experimental solute data. In the simulation, the column was divided into seven cells (dimensions of the cells represented real scale of the compartments) and the flow of the fluid was directed from the first to the seventh cell. DI water saturated with 1.2 M $CO_{2(aq)}$ was used as initial solution and allowed to react with basaltic glass in accordance with the dissolution rate expression reported by Gislason and Oelkers (2003) and previously implemented to compare dissolution rates. The total surface area of the basaltic glass used in the simulation was set as one tenth of the geometric surface area (29 cm^2/g) and the time step corresponded to one residence time in the compartment.

Results of the geochemical modelling are summarized in Figure 8 and reveal an increase of the individual elemental concentrations along the flow path from the first to the seventh compartment which agrees well in magnitude with the experimental

results. The major increase in solute concentrations is from the reactor inlet to the first cell/compartment outlet and decreases further along the flow path which is also reflected in the experimental data. The only discrepancy appears in the pH which is between 0.6 (in the seventh compartment) and 1.0 (in the first compartment) log units lower than experimental values. In addition, in the geochemical simulation steady-state is attained already after 10 hours of experimental duration, in stark contrast to the +90 hours in the experiment. Reducing the geometric surface area from 290 to 29 cm^2/g resulted in exceptional agreement between major elemental concentrations along the flow path in the model calculations versus the experimental data. The real reactive surface area of basaltic glass inside the column is unknown due to possible preferential flow, changes in the grain morphology and size during experimental duration, secondary phase precipitation and hydraulic pressure exerted on the solid. Gysi and Stefansson (2012b) described that a ten-fold decrease in geometric surface area of their basaltic glass used in the simulation resulted in shifting the overall reaction path for over 100 days indicating that the reactive surface area plays a pivotal role in controlling basaltic glass dissolution kinetics. In the reactive transport modelling simulating of a field CO_2 injection into basaltic basement, Aradóttir et al. (2012) assumed a reactive surface area of minerals and glasses to be 20 cm^2/g alike, which is close to the surface area applied in this study. Occurrence of preferential flow in the column is a major unknown and cannot be ruled out unambiguously. However, if preferential flow indeed happened, only a fraction of the total basaltic glass surface area would be in contact with the carbonated water. It can be expected that under such conditions, the scale of dissolution and reaction kinetics would be reduced proportionately to the available reduced reactive surface area and therefore steady-state could be approached much earlier than +90 hours. Likewise, the consistent solute chemistry evolution in Fig. 7 undermines partial preferential flow inside the column unless it affected the entire reactor uniformly, compartment by compartment, which seems unlikely.

Interestingly, the main change in the measured pH occurs in the first compartment where the initial pH of 3.2 increases to 4.5 and remains constant thereafter. This observation is all the more intriguing because the surface area of the basaltic glass up to the first compartment outlet is only 8% of the remainder of the column. Constant pH along the flow path is not surprising if taking the buffer capacity of the solution into account. The buffer capacity β is mathematically defined as ΔA or ΔB divided by ΔpH and describes the resistance of a solution to a pH change when acid (A) or base (B) are added incrementally (Urbanski and Schock, 2000). In the case of the HPCFR, basaltic glass is the base used to titrate the carbonic acid created by $CO_{2(aq)}$ to a pH range amenable to carbonate precipitation.

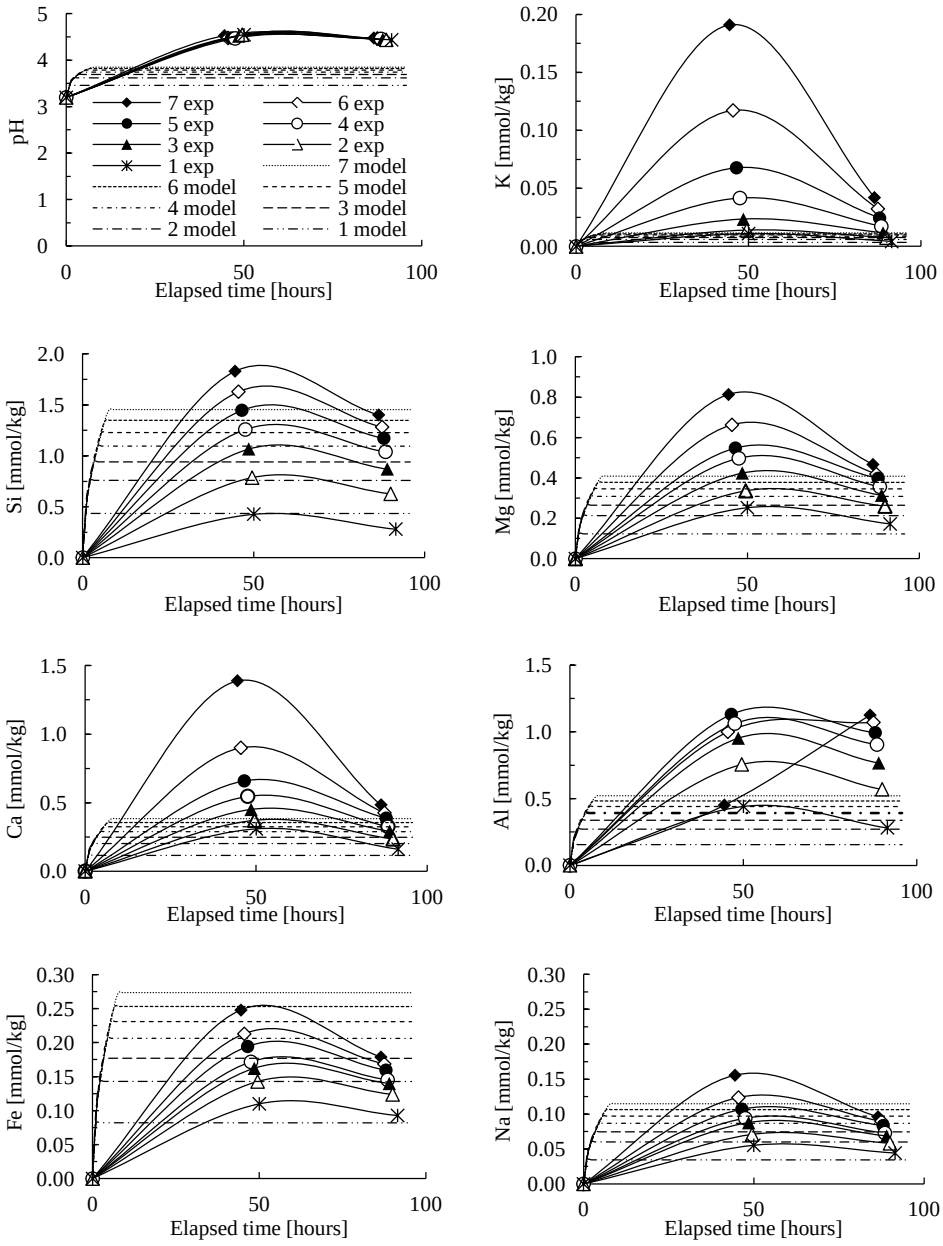

Figure 8. Comparison between results of geochemical modelling and experiment showing the concentration of major cations and pH. The symbols represent the experimental results ('exp' in the legend) and the dashed lines represent outcome of reactive transport modelling ('model' in the legend) for each compartment. The initial DIC concentration used in the simulation was 1.2 M and the total surface area of the basaltic glass implemented in the simulation was one tenth of the geometric surface area (29 cm^2/g). The dissolution rate expression for basaltic glass was taken from Gislason and Oelkers (2003). The first set of points represents the initial concentration of the H_2O-CO_2 solution in the mixing reactor before entering the column.

At an initial inlet pH around 3, the pH buffer capacity of the CO_2 charged solution is very low (~10^{-3} eq/kg) because DI water has no alkalinity and the dissolution of CO_2 does not add any alkalinity. Thus, proton consumption of this unbuffered inlet solution through dissolution reactions with the basaltic glass leads to a noticeable pH rise in the lowest part of the column. However, the pH buffer capacity of the solution rises exponentially with increasing pH such that over time, a constant pH evolves when the protons production by carbonic acid dissociation equal that of proton consumption by basaltic glass dissolution (Gislason and Eugster 1987, Wolff-Boenisch, 2011). Based on acidity titrations performed with PHREEQC, raising the pH from 3.2 to 4.5 through dissolution reactions with the basaltic glass increases the buffer capacity β from $10^{-2.9}$ to $10^{-2.1}$ eq/kg. A further, apparently small rise in pH from 4.5 to only 4.7 causes, however, a similar increase in β to $10^{-1.4}$ eq/kg. To enable a further increase in pH, vital for carbonate precipitation, dissolution rates of basalt and thus proton consumption have to be increased significantly. An increase in temperature from 25 to 50 °C at pH 3.5 enhances basaltic glass dissolution two-fold (Gislason and Oelkers, 2003). Another way to promote basaltic dissolution kinetics is the addition of fluoride to the inlet solution. Fluoride has the capability of forming aqueous complexes with aluminium, diminishing the dissolution rate inhibitory effect of aqueous Al^{3+}. Addition of 90 µmol of F^- to a pH 4 solution increases the dissolution rate of basaltic glass by nearly one order of magnitude (Wolff-Boenisch et al., 2004). Wolff-Boenisch (2011) discussed different scenarios on how to overcome the pH buffer hurdle, including dilution of the $CO_{2(aq)}$ solution. The constant pH observed during the experiment indicates the need for chemical and/or temperature changes to the column experiment to overcome this stalemate and induce precipitation reactions at higher pH.

2.6. CONCLUSIONS

The HPCFR is designed to sample pressurized gas loaded fluid along the flow path within a column filled with mineral or glass particles. While its application is exemplified in this study using a carbonated solution and basaltic glass, it should also work for supercritical CO_2 applications because the system pressure is higher than the supercritical pressure of CO_2 and the experimental temperature can be regulated up to 90 °C. Furthermore the inlet part of the plug can be adjusted to accommodate gas mixtures such as CO_2-H_2S and/or CO_2-SO_2.

Sampling reactive liquid at spatial intervals and under pressure makes the HPCFR unique in comparison with other columns constructed for studies of water-rock interactions. Measuring the evolution of the crucial parameters DIC and pH in-line which correspond to *in-situ* values in H_2O-*p*CO_2 or H_2O-scCO_2 systems

gives the set-up additional and crucial advantage over other experimental reactor systems. Due to its complexity and size, technical challenges of the HPCFR remain and it requires daily attention and dedication during the entire experimental duration.

The solute chemistry resulting from H_2O-CO_2-basaltic glass interaction inside the column was successfully modelled with 1D reactive transport modelling indicating that the reactor is a reliable tool to investigate the behaviour of pressurized CO_2 in the subsurface. Likewise, the experimentally determined dissolution rate, based on silicon and normalized to the geometric surface area corresponds well with literature rates.

A first conclusion from the preliminary run with $CO_{2(aq)}$ is that the pH of the reactive fluid inside the column remains low along the flow path such that carbonate saturation is not attained. Appropriate changes to the experimental conditions are being evaluated to enhance dissolution kinetics of the basaltic glass and to overcome the buffer capacity which is deemed the principal cause of the stagnant pH.

Acknowledgements

The authors would like to thank all colleagues and co-workers, in particular Helgi Alfredsson, Eydis Eiriksdottir, Kiflom Gebrehiwot, Snorri Gudbrandsson, Nicole Keller, Hanna Kassalainen, Gabrielle Stockmann, Kevin Padilla, Alejandro Rodriguez, Alexander Gysi, Niels Oskarsson, and Sveinbjörn Steinthorsson. Anna Sigurdottir and Birnir Sigurdsson are acknowledged for their help with sieving the huge amounts of basaltic glass material. The first author would like to thank Lukasz Kowolik for his endless patience and personal support. This study is part of the CarbFix project (www.carbfix.com) in Iceland and was funded by the European Union through the European Marie Curie network Delta-Min (Mechanisms of Mineral Replacement Reactions; Grant# PITN-GA-2008-215360) and SP1-Cooperation (FP7-ENERGY-2011-1; Grant# 283148), Reykjavík Energy, University of Iceland and RANNÍS, Icelandic Fund for Research Equipment; Grant# 10/0293).

References

Alfredsson H.A., Wolff-Boenisch D., Stefánsson A. (2011) CO_2 sequestration in basaltic rocks in Iceland: Development of a piston-type downhole sampler for CO_2 rich fluids and tracers. *Energy Procedia* **4**, 3510-3517.

Andreani M., Luquot L., Gouze P., Godard M., Hoisé E., Gibert B. (2009) Experimental Study of Carbon Sequestration Reactions Controlled by the Percolation of CO_2-Rich Brine through Peridotites. *Environ. Sci. Technol.* **43**, 1226-1231.

Aradóttir E.S.P., Sonnenthal E.L., Björnsson G., Jónsson H. (2012) Multidimensional reactive transport modeling of CO_2 mineral sequestration in basalts at the Hellisheidi geothermal field, Iceland. *Int. J. Greenhouse Gas Control* **9**, 24-40.

Bateman K., Turner G., Pearce J.M., Noy D.J., Birchall D., Rochelle C.A. (2005) Expérimentation de longue durée sur grandes colonnes, dans le contexte du stockage géologique de CO_2: étude

des interactions eau-roche et modélisation. *Oil & Gas Science and Technology* - Rev. IFP 60, 161-175.

Bateman K., Rochelle C., Lacinska A., Wagner D. (2011) CO_2-porewater-rock reactions–Large-scale column experiment (Big Rig II). *Energy Procedia* **4**, 4937-4944.

Bortoluzzi D., Cinquemani C., Torresani E., Spilimbergo S. (2011) Pressure-induced pH changes in aqueous solutions – On-line measurement and semi-empirical modelling approach. *J. Supercritical Fluids* **56**, 6-13.

Duan Z., Sun R., Zhu C., Chou I.M. (2006) An improved model for the calculation of CO_2 solubility in aqueous solutions containing Na^+, K^+, Ca^{2+}, Mg^{2+}, Cl^-, and SO_4^{2-}. *Marine Chemistry* **98**, 131-139.

Flaathen T.K., Gislason S.R., Oelkers E.H., Sveinbjörnsdóttir Á.E. (2009) Chemical evolution of the Mt. Hekla, Iceland, groundwaters: A natural analogue for CO_2 sequestration in basaltic rocks. *Appl. Geochem.* **24**, 463-474.

Garg A., Shukla P.R. (2009) Coal and energy security for India: Role of carbon dioxide (CO_2) capture and storage (CCS). *Energy* **34**, 1032-1041.

Gislason S.R., Eugster H.P. (1987) Meteoric water-basalt interactions. I: A laboratory study. *Geochim. Cosmochim. Acta* **51**, 2827-2840.

Gislason S.R., Veblen D.R., Livi K.J.T. (1993) Experimental meteoric water-basalt interactions: Characterization and interpretation of alteration products. *Geochim. Cosmochim. Acta* **57**, 1459-1471.

Gislason S.R., Oelkers E.H. (2003) Mechanism, rates, and consequences of basaltic glass dissolution: II. An experimental study of the dissolution rates of basaltic glass as a function of pH and temperature. *Geochim. Cosmochim. Acta* **67**, 3817-3832.

Gislason S.R., Wolff-Boenisch D., Stefansson A., Oelkers E.H., Gunnlaugsson E., Sigurdardottir H., Sigfusson B., Broecker W.S., Matter J.M., Stute M., Axelsson G., Fridriksson T. (2010) Mineral sequestration of carbon dioxide in basalt: A pre-injection overview of the CarbFix project. *Int. J. Greenhouse Gas Control* **4**, 537-545.

Gudbrandsson S., Wolff-Boenisch D., Gislason S.R., Oelkers E.H. (2011) An experimental study of crystalline basalt dissolution from $2 \leqslant pH \leqslant 11$ and temperatures from 5 to 75 °C. *Geochim. Cosmochim. Acta* **75**, 5496-5509.

Gysi A.P., Stefánsson A. (2012a) CO_2-water–basalt interaction. Low temperature experiments and implications for CO_2 sequestration into basalts. *Geochim. Cosmochim. Acta* **81**, 129-152.

Gysi A.P., Stefánsson A. (2012b) Experiments and geochemical moedling of CO_2 sequestration during hydrothermal basalt alteration. *Chem. Geol.* **306–307**, 10-28.

Gysi A.P., Stefánsson A. (2012c) Mineralogical aspects of CO_2 sequestration during hydrothermal basalt alteration — An experimental study at 75 to 250 °C and elevated pCO_2. *Chem. Geol.* **306–307**, 146-159.

Kelemen P.B., Matter J. (2008) In situ carbonation of peridotite for CO_2 storage. *Proc. Natl. Acad. Sci.* **105**, 17295-17300.

Luquot L., Gouze P. (2009) Experimental determination of porosity and permeability changes induced by injection of CO_2 into carbonate rocks. *Chem. Geol.* **265**, 148-159.

Matter J.M., Takahashi T., Goldberg D. (2007) Experimental evaluation of in situ CO_2-water-rock reactions during CO_2 injection in basaltic rocks: Implications for geological CO_2 sequestration. *Geochem. Geophys. Geosyst.* **8,** Q02001.

McGrail B.P., Schaef H.T., Ho A.M., Chien Y.-J., Dooley J.J., Davidson C.L. (2006) Potential for carbon dioxide sequestration in flood basalts. *J. Geophys. Res.* **111**, B12201.

Munz I.A., Brandvoll O., Haug T.A., Iden K., Smeets R., Kihle J., Johansen H. (2012) Mechanisms and rates of plagioclase carbonation reactions. *Geochim. Cosmochim. Acta* **77**, 27-51.

Oelkers E.H., Gislason S.R. (2001) The mechanism, rates and consequences of basaltic glass dissolution: I. An experimental study of the dissolution rates of basaltic glass as a function of aqueous Al, Si and oxalic acid concentration at 25°C and pH = 3 and 11. *Geochim. Cosmochim. Acta* **65**, 3671-3681.

Oelkers E.H., Gislason S.R., Matter J. (2008) Mineral Carbonation of CO_2. *Elements* **4**, 333-337.

Parkhurst D.L., Appelo C.A.J. (1999) User's guide to PHREEQC (Version 2) – A computer program for speciation, batch-reaction, one-dimensional transport, and inverse geochemical calculations. USGS-Report 99-4259.

Prigiobbe V., Hänchen M., Costa G., Baciocchi R., Mazzotti M. (2009) Analysis of the effect of temperature, pH, CO_2 pressure and salinity on the olivine dissolution kinetics. *Energy Procedia* **1**, 4881-4884.

Schaef H.T., McGrail B.P. (2009) Dissolution of Columbia River Basalt under mildly acidic conditions as a function of temperature: Experimental results relevant to the geological sequestration of carbon dioxide. *Appl. Geochem.* **24**, 980-987.

Stockmann G.J., Wolff-Boenisch D., Gislason S.R., Oelkers E.H. (2011) Do carbonate precipitates affect dissolution kinetics? 1: Basaltic glass. *Chem. Geol.* **284**, 306-316.

Teng H., Yamasaki A., Chun M.K., Lee H. (1997) Solubility of liquid CO_2 in water at temperatures from 278 K to 293 K and pressures from 6.44 MPa to 29.49 MPa and densities of the corresponding aqueous solutions. *J. Chem. Thermodynam.* **29**, 1301-1310.

Teng H., Yamasaki A. (2002) Pressure-mole fraction phase diagrams for CO_2-pure water system under temperatures and pressures corresponding to ocean waters at depth to 3000 m. *Chem. Eng. Commun.* **189**, 1485-1497.

Urbanski E.T., Schock M.R. (2000) Understanding, Deriving, and Computing Buffer Capacity. *J. Chem. Education* **77**, 1640-1644.

Wolff-Boenisch D., Gislason S.R., Oelkers E.H. (2004) The effect of fluoride on the dissolution rates of natural glasses at pH 4 and 25°C. *Geochim. Cosmochim. Acta* **68**, 4571-4582.

Wolff-Boenisch D., Gislason S.R., Oelkers E.H. (2006) The effect of crystallinity on dissolution rates and CO_2 consumption capacity of silicates. *Geochim. Cosmochim. Acta* **70**, 858-870.

Wolff-Boenisch D., (2011) On the buffer capacity of CO_2-charged seawater used for carbonation and subsequent mineral sequestration. *Energy Procedia* **4**, 3738-3745.

Wolff-Boenisch D., Wenau S., Gislason S.R., Oelkers E.H. (2011) Dissolution of basalts and peridotite in seawater, in the presence of ligands, and CO_2: Implications for mineral sequestration of carbon dioxide. *Geochim. Cosmochim. Acta* **75**, 5510-5525.

Xu T., Sonnenthal E., Spycher N., Pruess K. (2006) TOUGHREACT – A simulation program for non-isothermal multiphase reactive geochemical transport in variably saturated geologic media: Applications to geothermal injectivity and CO_2 geological sequestration. *Computers & Geosciences* **32**, 145-165.

Xu T., Spycher N., Sonnenthal E., Zhang G., Zheng L., Pruess K. (2011) TOUGHREACT Version 2.0: A simulator for subsurface reactive transport under non-isothermal multiphase flow conditions. *Computers & Geosciences* **37**, 763-774.

Yi W.-T., Yan C.-Y., Ma P.-H. (2011) Kinetic study on carbonation of crude Li_2CO_3 with CO_2-water solutions in a slurry bubble column reactor. *Korean J. Chem. Engineering* **28**, 703-709.

Supplementary data for Chapter 2

Table 1. Results of H_2O-CO_2-basaltic glass interaction in different compartments within the column. The pH and Eh were measured in-line and major cations with ICP-OES. The DIC concentration was obtained with the expander-transducer technique. Initial cation concentrations correspond to the conditioning phase of the column, when only DI water was pumped through.

		Elapsed time	pH		Eh	DIC	Si		Ca	
Sample	compartment	[hours]	Initial	CO_{2exp}	[mV]	[mol/L]	Initial	CO_{2exp}	Initial	CO_{2exp}
							[mmol/kg]			
P 7 1	7	44.5	9.27	4.53	164	1.24	0.17	1.83	0.04	1.39
P 6 1	6	45.5	9.32	4.48	175	1.20	0.17	1.63	0.04	0.9
P 5 1	5	46.5	9.31	4.48	169	1.20	0.16	1.45	0.04	0.66
P 4 1	4	47.5	9.37	4.47	179	1.20	0.16	1.26	0.04	0.55
P 3 1	3	48.5	9.39	4.52	177	1.20	0.15	1.07	0.04	0.45
P 2 1	2	49.5	9.34	4.55	196	1.21	0.14	0.78	0.03	0.37
P 1 1	1	50	9.12	4.55	189	1.19	0.07	0.43	0.02	0.31
P 7 2	7	86.5	9.27	4.48	186	1.16	0.17	1.40	0.04	0.48
P 6 2	6	87.5	9.32	4.47	187	1.16	0.17	1.28	0.04	0.43
P 5 2	5	88	9.31	4.46	184	1.16	0.16	1.17	0.04	0.39
P 4 2	4	88.5	9.37	4.46	184	1.17	0.16	1.04	0.04	0.33
P 3 2	3	89	9.39	4.45	191	1.17	0.15	0.87	0.04	0.29
P 2 2	2	90	9.34	4.44	179	1.15	0.14	0.63	0.03	0.23
P 1 2	1	91.5	9.12	4.44	192	1.15	0.07	0.28	0.02	0.16

Table 1. Continuation.

		Mg		Al		K		Na		Fe	
Sample	compartment	Initial	CO_{2exp}	Initial	CO_{2exp}	Initial	CO_{2exp}	Initial	CO_{2exp}	Initial	CO_{2exp}
		[mmol/kg]									
P 7 1	7	0.04	0.81	0.05	0.45	0.00	0.19	0.00	0.16	0.00	0.25
P 6 1	6	0.04	0.66	0.05	1.00	0.00	0.12	0.00	0.12	0.00	0.21
P 5 1	5	0.04	0.55	0.05	1.13	0.00	0.07	0.00	0.11	0.00	0.19
P 4 1	4	0.04	0.5	0.05	1.06	0.00	0.04	0.01	0.09	0.00	0.17
P 3 1	3	0.04	0.42	0.05	0.95	0.00	0.02	0.00	0.09	0.00	0.16
P 2 1	2	0.03	0.34	0.04	0.76	0.00	0.01	0.00	0.07	0.00	0.14
P 1 1	1	0.02	0.25	0.02	0.44	0.00	0.01	0.00	0.06	0.00	0.11
P 7 2	7	0.04	0.47	0.05	1.12	0.00	0.04	0.00	0.10	0.00	0.18
P 6 2	6	0.04	0.42	0.05	1.07	0.00	0.03	0.00	0.09	0.00	0.17
P 5 2	5	0.04	0.4	0.05	0.99	0.00	0.02	0.00	0.08	0.00	0.16
P 4 2	4	0.04	0.36	0.05	0.90	0.00	0.02	0.01	0.07	0.00	0.14
P 3 2	3	0.04	0.31	0.05	0.77	0.00	0.01	0.00	0.07	0.00	0.14
P 2 2	2	0.03	0.26	0.04	0.57	0.00	0.01	0.00	0.06	0.00	0.12
P 1 2	1	0.02	0.17	0.02	0.28	0.00	0.00	0.00	0.04	0.00	0.09

Chapter 3

An experimental study of basaltic glass-H_2O-CO_2 interaction at 22 and 50 °C: Implications for subsurface storage of CO_2

Iwona Galeczka, Domenik Wolff-Boenisch, Eric H. Oelkers,
and Sigurdur R. Gislason

Geochimica and Cosmochimica Acta, in review

Abstract:

A novel high pressure column flow reactor was used to investigate the evolution of solute chemistry along a 2.3 meter flow path during 37-104 days of pure water- and CO_2-charged water-basaltic glass interaction experiments at 22 and 50 °C and at $10^{-5.7}$ to 22 bars partial pressure of CO_2. Experimental results and geochemical modelling showed that the pH of injected pure water evolved rapidly from 6.7 to 9-9.5 and most of the dissolved iron was consumed by secondary minerals, similar to natural meteoric water-basalt systems. In contrast to natural systems, however, the aqueous aluminium concentration remained relatively high along the entire flow path. The aqueous fluid was undersaturated with respect to basaltic glass and carbonate minerals, but supersaturated with respect to zeolites, clays, and Fe(oxy)hydroxides. As CO_2-charged water replaced the alkaline fluid within the column, the fluid became supersaturated with respect to siderite for a short time, but once the entire column was filled with the CO_2-charged water and the pH decreased to 4.5, the fluid remained undersaturated with respect to all carbonates. Once the CO_2-charged fluid exited the pressurized column, carbonates precipitated in the degassing water at the outlet.

Basaltic glass dissolution in the CO_2-charged water was closer to stoichiometry than in pure water. The mobility and concentration of several metals increased significantly in the fluid phase and some of the toxic/heavy metals, including Mn, Fe, Cr, Al, and As exceeded the allowable drinking water limits. Iron became mobile and the aqueous Fe^{2+}/Fe^{3+} ratio increased along the flow path. Basaltic glass dissolution in the CO_2-charged water did not overcome the pH buffer capacity of the reactive fluid. The pH rose from an initial pH of 3.4 to 4.5 during the first

40 minutes of CO_2-charged water-basaltic glass interaction along the first 18.5 cm of the column but remained constant during the remaining 2.1 meters of the flow path. Raising the temperature of the CO_2-charged fluid from 22 to 50 °C increased the relative amount of iron present as Fe^{2+} in the fluid phase. Dissolved Al was incorporated into secondary minerals and pH was lower compared to the 22 °C experiment, resulting in enhanced basaltic glass dissolution rates. The dissolved Cr concentration evolution mimicked that of Al at 50 °C, suggesting substitution of trivalent Cr for Al in secondary phases. The CO_2-charged fluid was always undersaturated with respect to basaltic glass and carbonate minerals within the experimental column, but supersaturated with respect to clays and Fe(oxy)hydroxides at 22 °C and with respect to clays and Al(oxy)hydroxides at 50 °C.

3.1. INTRODUCTION

This study focuses on the improved understanding of CO_2-charged fluid-basalt interaction. This process is of current attention due to its potential application to sub-surface carbon storage efforts. Engineered *in situ* mineral carbonatization attempts to combine injected CO_2 with divalent cations such as Ca^{2+}, Mg^{2+}, and Fe^{2+} to form stable carbonate minerals (Broecker, 2012; Gislason et al., 2010; IPCC, 2005; Kelemen and Matter, 2008; Oelkers et al., 2008;). Because basalts and ultramafic rocks are 1) rich in divalent cations, 2) abundant on the Earth surface, and 3) highly reactive - they have large potential for CO_2 mineral storage (Goldberg et al., 2008; McGrail et al., 2006). This possibility is currently being tested as part of the CarbFix CO_2 storage pilot project in Iceland (Alfredsson et al., 2013; Aradóttir et al., 2012; Gislason et al., 2010). Moreover, the interaction of CO_2-charged fluids with basalts plays a major role in the global carbon cycle. Carbon dioxide released from the crust and the mantle during continental drift is balanced, on a geological time scale by weathering of Ca, Mg-silicates, formation of carbonates and burial of organic carbon (Berner, 2004; Marini, 2007; Mackenzie and Andersson, 2013). Part of the CO_2 released from volcanoes and crustal intrusions never reaches the atmosphere. It dissolves in groundwater and geothermal waters, making the water corrosive and provoking carbonate mineral precipitation. This 'short-cut' in the carbon cycle provides a natural analogue for industrial *in situ* CO_2 storage (Beinlich and Austrheim, 2012; Brady and Gislason, 1997; Flaathen et al., 2009; Gislason et al., 2002; Kelemen and Matter, 2008; Olssen et al., 2012a; Wiese et al., 2008).

Most laboratory studies investigating the potential efficiency of *in situ* CO_2 storage in basalts and ultramafic rocks have focused on secondary products and CO_2-H_2O/CO_2-H_2S/$scCO_2$ interactions and/or the effects of secondary mineral coatings on primary mineral dissolution rates (e.g. Andreani et al., 2009; Daval et al., 2009; Daval et al., 2011; Giammar et al., 2005; Gysi and Stefánsson, 2012;

Hövelmann et al., 2011; Miller et al., 2013; Munz et al., 2012; Olsson et al., 2012; Rani et al., 2013; Schaef and McGrail, 2009; Schaef et al., 2010; Schaef et al. 2011; Schaef et al., 2013; Stockmann et al., 2011, Stockmann et al., 2013). In contrast, this study focusses on the solute chemistry evolution during water-basaltic glass and CO_2-charged water-basaltic glass interaction. Such results can be applied to engineered *in situ* mineral carbonatization as well as to volcanic systems where CO_2 is degassed from magma into groundwater (Aiuppa et al., 2005; Federico et al., 2002; Federico et al., 2004; Flaathen and Gislason, 2007; Flaathen et al., 2009; Fridriksson et al., 2006; Olsson et al. 2012a). A major difference between this study and previous studies of water-basalt interaction is the experimental design; in this study we follow the fluid compositional evolution within a 2.3 meter long high pressure column flow reactor (HPCFR) (Galeczka et al., 2013) using sampling ports located along the column. This reactor makes it possible to sample the reactive fluid along the flow path at both ambient and at elevated pressure and temperature, providing insight into the temporal and spatial evolution of reactive fluid composition. This reactor, thereby, allows for the direct assessment of the ability of geochemical modelling codes to reproduce the solute chemistry along the flow path during CO_2-water-rock interaction. Such model assessment is an essential step to validate our ability to predict the fate of CO_2 injected into the subsurface during carbon storage efforts. The purpose of this paper is to present the results of this experimental study and to apply these to the improved understanding of carbon storage in basalts, and to the fate of CO_2 in natural volcanic systems.

3.2. METHODS

3.2.1. Materials

The basaltic glass used in this study was collected from the Stapafell Mountain located in SW Iceland. The composition of the material is similar to that of mid-ocean ridge basalt (MORB) and its dissolution kinetics was reported in previous studies (Gislason and Oelkers, 2003; Oelkers and Gislason, 2001; Stockmann et al., 2011; Wolff-Boenisch et al., 2011). Its chemical composition is consistent with $Si_{1.0}Ti_{0.024}Al_{0.355}Fe_{0.207}Mg_{0.276}Ca_{0.265}Na_{0.073}K_{0.007}O_{3.381}$ (Table 1 in Supplementary data 1). The material was crushed in a jaw crusher and dry sieved to obtain the 45-100 μm particle size fraction, which was subsequently washed by repeated gravitational settling to remove ultrafine particles. The resulting powder was dried at 50 °C for 2 days. The cleaned glass was poured into the column reactor. The total mass of glass inside the column reactor was ~8.3 kg. The void fraction of the material, which is randomly and loosely packed, was estimated to be ~0.4 (Weltje and Alberts, 2011). The powdered glass was inserted into the reactor as a slurry making it difficult to measure directly the void fraction. The BET specific surface

area (A_{BET}) before the experiment was 22,000 cm^2/g, as measured by six-point N_2 adsorption using a Quantachrome Gas Sorption system. The specific geometric surface area (A_{geo}), calculated assuming the glass powder to be identical cubes was 290.4 cm^2/g (Wolff-Boenisch et al., 2011), resulting in a surface roughness factor (A_{BET}/A_{geo}) of 76. The total BET surface area in the column amounted thus to ~182,000,000 cm^2, and the corresponding geometric surface area was ~2,410,000 cm^2. Taking into account an estimated porosity of 40%, the total fluid volume in the reactor was 1.84 L, yielding a surface area to fluid volume ratio of ~10^5 cm^{-1}.

3.2.2. Experimental design

Fluid-basaltic glass interaction experiments were performed in a high pressure column flow reactor (HPCFR). A detailed description of the column reactor is provided in (Galeczka et al., 2013). Due to the corrosive nature of CO_2-charged water, nearly the entire reactor was made of a combination of titanium, Hastelloy, and PEEK (Polyether ether ketone). The titanium column measured 234 cm in length, 5.0 cm in inner diameter and held a total volume of ~4.6 L. During the CO_2-charged water experiments, liquid CO_2 was delivered through a supercritical fluid pump (SCF) and the degassed deionized H_2O through a high pressure liquid chromatography pump. The complete mixing and dissolution of CO_2 into the water was assured by a mixing chamber (mixed-flow-through Ti reactor) installed before the column reactor inlet. The initial *in situ* DIC (Dissolved Inorganic Carbon) concentration during the CO_2-charged water experiments was measured in the mixing chamber every 2-3 days to verify the H_2O/CO_2 ratio. The HPCFR had seven lateral sampling ports, which were used to sample the fluid along the flow path. Fluid sampling from these ports allowed determination of the elemental concentrations as well as DIC, pH, and Eh along the flow path within the column. The column reactor was wrapped with a heating tape to control temperature. Fluid sampling was performed by diverting the sampled fluid from the column outlet to a pressurized sampling loop connected to an 'expander' for DIC analysis and towards in-line pH and Eh electrodes. The 'expander' was equipped with a pressure transducer that recorded the pressure induced from CO_2 expansion and therefore the DIC concentration. Further samples were collected for measurement of major and trace cations. Details of this reactor are presented by Galeczka et al. (2013).

3.2.3. Geochemical modelling

The standard state adopted in this study was that of unit activity for pure minerals and H_2O at any temperature and pressure. The standard state for aqueous species was that of a hypothetical 1 molal solution referenced to infinite dilution at

any temperature and pressure. Aqueous speciation, mineral saturation states, and reactive transport modelling were performed using the PHREEQC 2.17 geochemical code (Parkhurst and Apello, 1999) and the standard *phreeqc.dat* database, which was updated with selected aqueous speciation and mineral solubility constants from (Gysi and Stefánsson, 2011). The thermodynamic properties of the hydrated basaltic glass surface were estimated from the stoichiometrically weighted sum of the hydrolysis reactions of amorphous SiO_2 and amorphous $Al(OH)_3$ (Bourcier 1990; Wolff-Boenisch et al., 2004). The equilibrium constant and enthalpy of individual hydrolysis reactions were taken from the *phreeqc.dat* database. The logarithm of the equilibrium constant at 25 °C calculated for the hydrated basaltic glass dissolution reaction given by

$$Si_{1.0}Al_{0.35}O_2(OH)_{1.05} + 1.05H^+ + 0.95H_2O = 0.35Al^{3+} + H_4SiO_4 \quad (1)$$

is 1.07. For aqueous speciation and mineral saturation state calculations, chemical composition of the sampled fluid together with measured in-line DIC and pH were used. In cases where DIC measurements were missing, PHREEQC calculations were performed to estimate DIC concentrations using measured *in situ* pH assuming charge balance. Resulting DIC estimates were used for further calculations. Aqueous speciation and saturation state calculations with PHREEQC included measured Fe^{2+} and Fe^{3+} concentrations as redox indicators for the CO_2-charged water experiments, but calculated dissolved O_2 from the degassed inlet fluid for the pure water experiments.

The saturation state of the reactive fluid with respect to the hydrated basaltic glass is given as the Gibbs free energy of reaction, ΔG_r, but the saturation state of the experimental fluid with respect to secondary minerals is given as saturation index, SI. The relationship between these two functions is given by

$$\Delta G_r = RT\, 2.303 \log (Q/K) = RT\, 2.303\, SI \quad (2)$$

where R corresponds to the gas constant, T designates the temperature, Q stands for the reaction quotient (also called ion activity product), and K denotes the equilibrium constant of the hydrolysis reaction at the temperature of interest. Both ΔG_r and SI are zero at equilibrium and negative when the fluid is undersaturated with respect to the dissolving phase.

The dissolution rate of basaltic glass can be described using (Gislason and Oelkers, 2003)

$$r_{+,geo} = A_A exp^{\left(\frac{-E_A}{RT}\right)} \left(\frac{a_{H^+}^3}{a_{Al^{3+}}}\right)^{\frac{1}{3}} (1 - \exp\left(\frac{\Delta G_r}{\sigma RT}\right)) \quad (3)$$

where r_{+geo} signifies the geometric surface area normalized steady-state basaltic glass in moles of Si/cm^2/s, A_A designates a pre-exponential factor ($10^{-5.6}$ mol of Si/cm^2/s), E_A refers to a pH independent activation energy (25.5 kJ/mol), and σ corresponds to the Temkin parameter, equal to 1 for basaltic glass when its formula is normalized to one Si atom (Daux et al., 1997). The ΔG_r symbolizes the Gibbs free energy of the hydrated basaltic glass dissolution (Eq. 1). The term $(1 - \exp\left(\frac{\Delta G_r}{\sigma RT}\right))$ reflects the saturation state of the fluid with respect to the hydrated basaltic glass in accord with reaction (1). The basaltic glass dissolution rates along the flow path were calculated using Eq. 3. The activities of Al^{3+} and H^+ were calculated from the measured fluid chemistry using PHREEQC. Apparent basaltic glass dissolution rates during the experiments were also determined from measured fluid Si concentration using:

$$r_{+,Si} = \frac{(Si_1 - Si_0) fr}{A_{geo} m} \quad (4)$$

where $r_{+,Si}$ designates the basaltic glass dissolution rate in moles of Si/cm^2/s, Si_1 stands for the measured outlet fluid Si concentration, Si_0 refers to the initial Si concentration, and *fr*, A_{geo}, and *m* stand for fluid flow rate, geometric surface area, and the mass of basaltic glass, respectively. Note that precipitation of Si into secondary minerals within the column will diminish apparent dissolution rates calculated with equation (4).

The fluid compositional evolution in the reactor was modelled using a one dimensional reactive transport simulation with the aid of PHREEQC. The fluid phase was allowed to react with basaltic glass in accord with Eq. 3, taking into account the fluid composition and its saturation state with respect to the hydrated basaltic glass surface. The inlet fluid chemistry used in the model was set equal to the inlet fluid chemistry used during the experiments (see chapter below) and the basaltic glass was assumed to dissolve stoichiometrically. The one dimensional reactive transport model consisted of seven cells. The flow of the fluid was directed from the first towards the seventh cell and the time step of the simulation corresponded to the fluid residence time within each cell (the fluid residence time is equal to the total fluid volume inside the cell divided by its flow rate). The basaltic glass surface area used in the model was the initial A_{geo}. In the first scenario, the basaltic glass was allowed to dissolve according to the rate expression (Eq. 3). In the second scenario basaltic glass dissolution was also calculated with Eq. 3, but secondary minerals commonly forming in basaltic groundwater systems were assumed to form at local equilibrium. The local equilibrium assumption was used instead of distinct mineral precipitation rates since 1) such rates are generally unavailable, 2) there is no constraint on secondary mineral surface area, and 3) precipitation rate expressions, predicted by transition state theory, have been

shown to fail (Saldi et al., 2012; Schott et al., 2012). Although the assumption of partial equilibrium between fluid and secondary phases has been questioned (c.f. Zhu and Lu, 2009), it was used in the present study for illustrative purpose only to provide insight into potential processes causing the evolution of the fluid chemistry, and the potential application of geochemical models to predict the evolution of CO_2-rock interaction in laboratory and geo-engineered systems.

3.2.4. Experiment

The experiment performed in this study was divided into 3 stages. In the first stage deionized water (DI water) was pumped through the column at a flow rate of 5 ml/min, at 22 °C and ambient pressure for 2500 hours. This experiment will be referred to as the pure water experiment. The residence time of the fluid inside the column was ~6 hours. The second stage of the experiment started after completion of the pure-water experiment. The total/hydraulic pressure in the reactor was increased to 8 MPa and CO_2-charged water was injected. This experiment will be referred to as the CO_2-charged water or CO_2-charged fluid experiment at 22 °C. The total pressure and the flow rates of water and liquid CO_2 were set to ensure that the CO_2 was fully dissolved in the water before entering the column reactor. In this instance it was set at ~25% of the CO_2 solubility limit to fully dissolve in the fluid at this pressure and temperature. The CO_2 solubility was calculated based on the Duan et al. (2006) model. This CO_2 concentration thus avoids degassing even if there were some fluctuations in the set total pressure due to sampling. In the third stage of the experiment the temperature of the HPCFR was increased to 50 °C ±0.5. This experiment will be referred to as the CO_2-charged water or CO_2-charged fluid experiment at 50 °C. In both CO_2-charged water experiments, the $CO_{2(l)}$ and water flow rates were set to 0.13 and 3.5 ml/min, respectively resulting in an average fluid residence time of ~8 hours in the column. The duration of the two CO_2-charged water experiments were 1000 hours each. The velocity of the fluid through the pores was ~7 m/day which is 100 times faster than natural groundwater flow at the CarbFix injection site (Aradóttir et al., 2012). The initial measured DIC concentration and calculated pH of the CO_2-charged inlet fluid was ~300 mmol/L and ~3.4, respectively. The fluid phase pH, Eh, and DIC were measured in samples collected from seven positions along the column reactor. The precision of the pH measurements during the CO_2-rich fluid experiments obtained using high P/T electrodes was estimated to be ±0.1 pH unit but was ±0.05 pH unit for measurements made at ambient pressure during the pure water experiment. The sampling of the reactor involved taking samples from all seven sampling ports in a single day, within 8 to 9 hours. Samples were taken a minimum of 6 residence times from each other (see Fig. 1). In total, 347 fluid samples were collected: 191 during the pure water experiment, 79 during the CO_2-charged water experiment at 22 °C

and 77 during the CO_2-charged water experiment at 50 °C. The sampling affected somewhat the fluid flow in the column; the fluid above the sampling port was stagnant during sampling. To sample fresh fluids, sampling was always started from the uppermost sampling port and continued downwards. The outlet fluid sampled for major and trace elemental composition was filtered using a 0.2 µm cellulose acetate filter, and then acidified with concentrated supra-pure HNO_3 (0.5 vol. %) prior to analysis by ICP-OES (Inductively Coupled Plasma Optical Emission Spectrometer). Analytical uncertainties of ICP-OES analyses are on the order of≤5%. During the CO_2-experimental runs the concentrations of Fe species (Fe^{2+} and Fe^{3+}) were measured by ion chromatography (Dionex IC 3000). These samples were captured directly from the filtered outflow into a syringe filled with 0.1 M HCl, thus avoiding any contact of the fluid with the atmosphere. This method takes advantage of the slow oxidation of Fe^{2+} to Fe^{3+} at low pH (Stumm and Morgan, 1996).

3.3. RESULTS

3.3.1. Pure water-basaltic glass interaction experiment

The HPCFR provides the opportunity to study the temporal fluid chemistry evolution along the flow path. Figure 1 shows an example of results obtained during the pure water injection at 22 °C. The inlet fluid percolated through the column passing sequentially the first, second, third, fourth, fifth, sixth and seventh sampling port, respectively. The vertical axis, labelled 'residence time' in Figure 1, shows the average time it took the fluid to flow from the inlet to each sampling port at a flow rate of 5 ml/min. The horizontal axis labelled 'elapsed time' represents the duration of the experiment. In case of the pure water-basaltic glass experiment, deionized water was pumped through the column continuously for 2500 hours (104 days). Elapsed time is expressed as hours since the beginning of the pure water inflow into the reactor. The dissolved constituent concentrations attained steady-state first in the first outlet and then later in the higher outlets, as shown for Mg in Fig. 1. Steady-state is defined as constant fluid composition within experimental uncertainty for at least 10 residence times.

Major elemental concentrations and the pH evolution along the flow path are shown at elapsed times of 500 and 2200 hours, respectively in Fig. 2. These two elapsed times were chosen because after 500 hours the concentrations of most elements were increasing. After 2200 hours, the dissolved major element concentrations attained steady-state in all outlets. The initial pH of the degassed, deionized water injected into the column was 6.7 at 22 °C. The fluid pH increased to more than 9 during the first 30 minutes of water-rock interaction indicating consumption of protons by basaltic glass dissolution (see Fig. 2a). After 2-3 hours,

the pH slightly decreased consistent with proton production by secondary phase precipitation or dissociation of monomeric uncharged silica species.

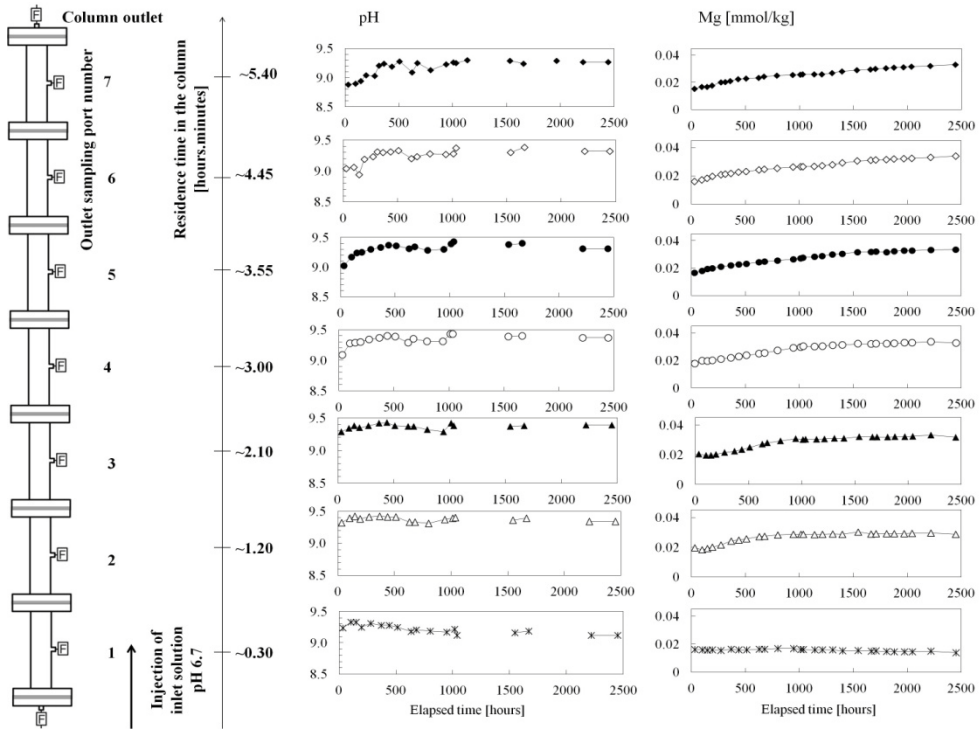

Figure 1. Example of the data collected from the different outlet sampling ports during the pure water-basaltic glass interaction experiment. The inlet fluid of pH 6.7 was pumped bottom-up through the column continuously for 2500 hours (elapsed time) and it is shown on the horizontal axis. The calculated residence time from the inlet to each sampling outlet is displayed on the vertical axis. Seven fluid samples were collected during each sampling session, one from each outlet port.

Along the flow path, the concentrations of most major elements increased during the first two hours of water-rock interaction at both elapsed times, as sampled in the first three reactor outlets (see Fig. 2b and c). Major element concentrations continued to increase with further fluid-basaltic glass interaction but at a slower rate as the fluid continued through the column. After three hours, the Mg concentration in the fluid phase in the reactor decreased suggesting preferential incorporation of Mg into secondary phases. The slowing of the release rates of other elements (Si, Al, Ca, Na) suggests precipitation of Mg-Ca-aluminosilicates. The stoichiometric coefficients (the ratio between measured element concentration normalized to Na in the fluid and in the dissolving glass) of Si, Al, Ca, Mg were close to 1. Sodium is considered as a conservative element in basaltic groundwater systems due to its negligible incorporation into secondary phases and it was the only measurable mobile element during this early part of the experiment. Despite these ratios being close to unity, the concentration curves level off significantly along the flow path in Fig. 2b and c. The

slowing of metal release rates is consistent with either 1) a slowing of basaltic glass dissolution rates along the flow path stemming potentially from fluid channelling or 2) the incorporation of all elements into secondary phases.

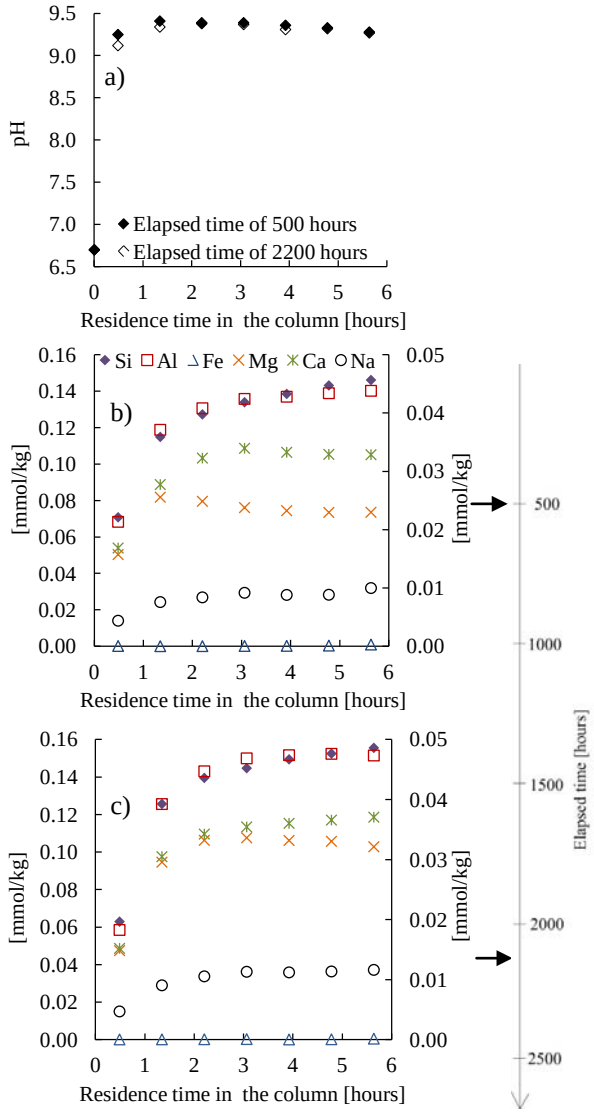

Figure 2. The pH (a) and concentration of major elements from the pure water-basaltic glass interaction experiment along the flow path at elapsed times of 500 (b) and 2200 hours (c), respectively. The silicon concentration is shown on the left axis whereas all other element concentrations are displayed on the right axis. The increase in the pH along the first, second and third outlet sampling ports indicate proton consumption by basalt dissolution. The subsequent pH decrease indicates proton release. The Fe concentration was below detection limit of analysis, revealing precipitation of Fe phases.

The Al concentration was still comparatively high in the fluid phase after 6 hours of water-basaltic glass interaction (around 40 µmol/kg) whereas in natural basaltic

groundwater systems aqueous Al ranges up to few µmol/kg (Alfredsson et al., 2013; Gislason et al., 1996). The Fe concentration along the flow path was close to or below the detection limit of the analytical method: <0.36 µmol/kg. Very low concentrations (usually up to 1 µmol/kg) of Fe is seen in natural basaltic groundwater systems due to Fe^{2+} oxidation and precipitation of Fe(oxy)hydroxides (Alfredsson et al., 2013; Gislason and Eugster, 1987).

3.3.2. CO_2-charged water-basaltic glass interaction experiment at 22 °C

The injection of a CO_2-charged fluid was started after 2500 hours of the pure water-basaltic glass experiment. The pH decrease stemming from the injection of the CO_2-charged water into alkaline fluid is shown in Figure 3a. During the first hours following the start of the injection of the CO_2-charged fluid, it was difficult to measure *in situ* pH in all outlets because of the time required for sampling. A steady-state pH of ~4.5 was attained after ~200 hours of elapsed time. The pH increased from the initial inlet fluid value of 3.4 to 4.5 in the samples obtained from the first outlet port; fluid samples from this port experienced only 40 minutes of water-basaltic glass interaction (see Figure 4a). Further interaction between basaltic glass and CO_2-charged water along the flow path was not sufficient to overcome the pH buffering capacity of the fluid, resulting in a steady-state between proton consumption and proton production at pH ~4.5 (see Fig. 3a and Fig 4a). The DIC concentration in the column was similar to the inlet DIC concentration of ~300 mmol/L and it remained constant along the flow path (Fig. 3b).

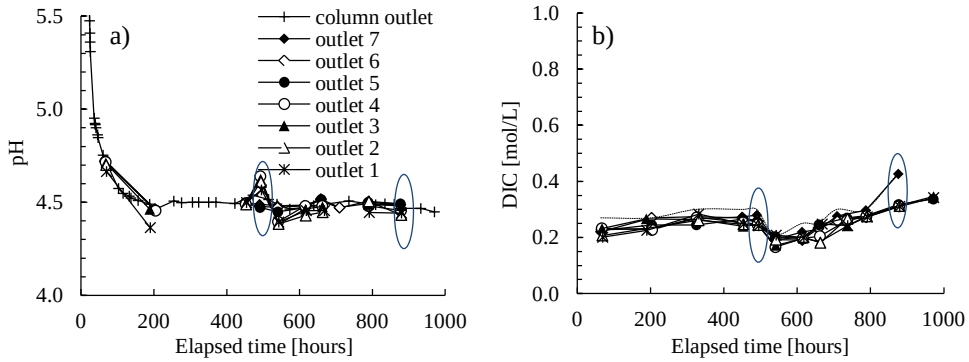

Figure 3. The pH (a) and DIC (b) measured in-line in the fluid collected from the sampling ports indicated in the legend during the CO_2-charged fluid-basaltic glass experiment at 22 °C. Due to complexity of the sampling procedure, only the column outlet fluid pH was determined during the first 60 hours of the experiment when the alkaline solution inside the column was replaced by CO_2-charged water. The dotted curve represents initial measured DIC concentration in the mixing chamber before entering the column. Fluctuations of the initial DIC concentration were related to the fluctuations in delivery of CO_2 by the supercritical fluid pump. Circles on the lines represent the samples that were singled out for further discussion in the text.

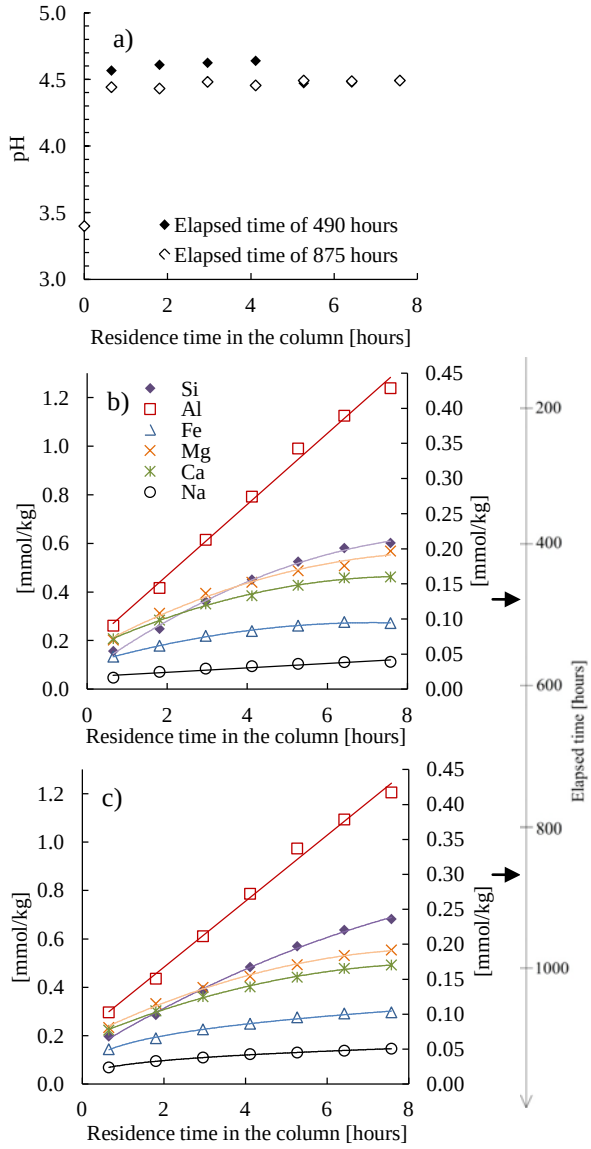

Figure 4. The pH (a) and major elemental concentrations during the CO_2-charged fluid-basaltic glass experiment at 22 °C at elapsed times of 490 (b) and 875 hours (c), respectively. Silicon concentration is shown on the left axis whereas all other element concentrations are displayed on the right axis. Element release versus flow distance was more linear compared to the release during the pure water experiment.

The constant concentration of DIC along the flow path confirms that there was no CO_2 degassing through the column. Decrease of DIC at elapsed time of 500 hours was caused by fluctuation in delivery of the liquid CO_2 by the injection pump system. Dissolved element concentrations along the flow path at elapsed times of 490 and 875 hours since the beginning of the CO_2-charged fluid injection showed different patterns of element release (Fig. 4b and c) compared to the pure water

experiment (see Fig. 2b and c). We chose to show the results after 490 hours of elapsed time as at this time the initial DIC concentration had been stable for almost 300 hours (see Fig. 3b). The second elapsed time of 875 hours was selected for illustration because at this time the pH had been stable for ~300 hours in all fluid samples (Fig. 3a).

The abundance of major elements in the fluid phase agreed with the abundance of major elements in the basaltic glass: Si> Al> Mg> Ca> Fe> Na. This observation is in contrast to the results of the pure water experiment where the abundance of elements was: Si> Al> Ca> Mg> Na> Fe. The enrichment pattern of the fluid along the flow path is consistent with their linear concentration increase with increasing duration of fluid-basaltic glass interaction as indicated by the straight lines in Figs. 4b and c. During the pure water-basaltic glass interaction experiment, concentration curves were non-linear along the flow path (Fig. 2b and c), consistent with secondary phase precipitation and/or a slowing of basaltic glass dissolution rates. In contrast, element releases along the flow path in this experiment were more constant. There is a slight non-linearity in Si, Ca, Mg, and Fe concentrations versus flow distance, whereas the Al concentration versus flow distance curve is linear. These observations suggest the precipitation of secondary Si-bearing phases. At an elapsed time of ~875 hours Si, Ca, Mg, and Fe showed preferential retention in the solid phase at all sampled fluids (stoichiometric coefficient <1 compared with Na) confirming secondary phase precipitation. The Al stoichometric coefficient was <1 at first and second sampling outlet port.

Outflow chemistry in this CO_2-charged fluid experiment exhibited higher trace element concentrations compared to the pure water experiment. For example, the outflow fluid in the latter experiment contained more than 40 times Mn and 6 times Sr than the former (Fig. 5). Elements which were close to or below detection limits during the pure water-basalt experiment were detectable during the CO_2-charged fluid experiment. This observation is consistent with faster basaltic glass dissolution rates at acidic pH of 4.5 compared to those in the basic fluids present in the pure water experiment. Concentrations of B, Mn, and Sr after 875 hours showed a linear increase along the flow path similarly to the major elements. Concentrations of some of the metals in the sampled fluids exceeded WHO drinking water limits (WHO, 2008). Aluminium, iron, and chromium concentrations were always higher than the drinking water limits (>3.7 µmol/kg for Al, >36 µmol/kg for Fe, and >0.1 µmol/kg for Cr). Manganese exceeded the WHO drinking water limit (7.3 µmol/kg) during the first 40 hours after the pure water inlet fluid was replaced by the CO_2-charged fluid. The As concentration was close to the WHO drinking water limit of 0.13 µmol/kg.

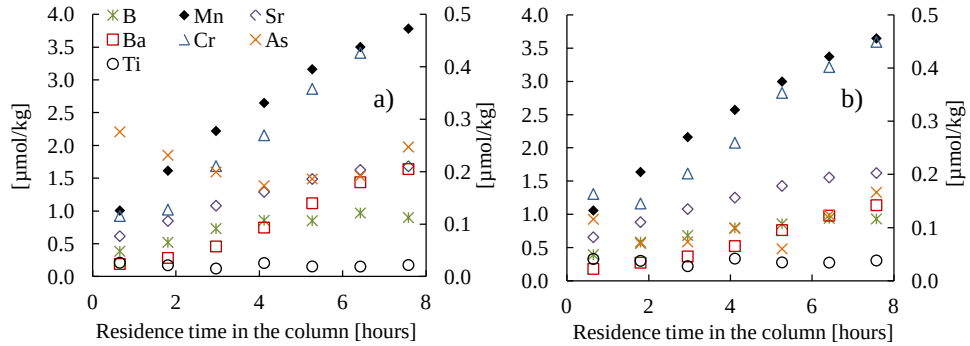

Figure 5. Trace elemental concentrations during the CO_2-charged fluid-basaltic glass experiment at 22 °C at elapsed times of 490 (a) and 875 hours (b), respectively. The B and Mn concentrations are shown on the left axis; other elements are displayed on the right axis.

3.3.3. CO_2–charged water-basaltic glass interaction experiment at 50 °C

After approximately 1000 hours of CO_2-charged water-basaltic glass interaction at 22 °C, deionized water was pumped through the column at 3.5 ml/min for ~900 hours to neutralize the system. After this time, liquid CO_2 was again mixed with DI water at the same ratio as during the CO_2 experiment at 22 °C (H_2O at 3.5 ml/min, $CO_{2(l)}$ at 0.13 ml/min) and pumped through the column reactor. The temperature of the column was increased to 50 °C. The pH and DIC evolution during this final experiment is shown in Fig. 6.

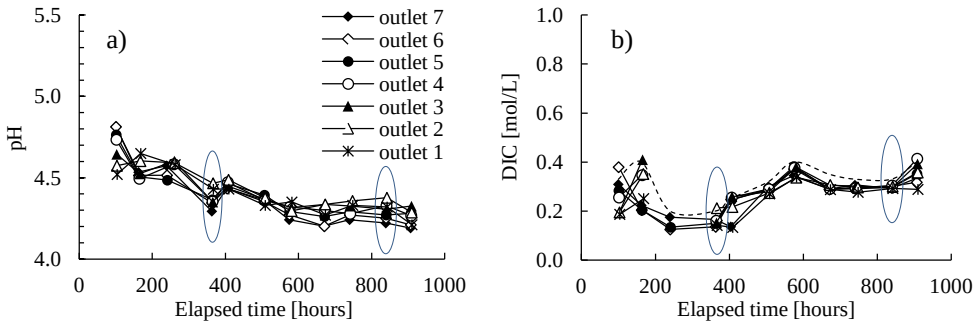

Figure 6. The pH (a) and DIC (b) measured in the fluid collected from the sampling ports indicated in the legend during the CO_2-charged fluid-basaltic glass experiment at 50 °C. Measurement of pH was performed at ambient temperature and recalculated to 50 °C with PHREEQC. The dotted line represents the initial measured DIC concentration in the mixing chamber before entering the column. Fluctuations of the initial DIC concentration were related to the variations of CO_2 delivery by the supercritical pump. Circles on the lines represent the samples that were singled out for further discussion in the text.

The pH was measured at ambient temperature and recalculated to *in situ* pH at 50 °C using PHREEQC. The pH decreased gradually with time, possibly related to an unintentional increase in initial DIC concentration due to fluid injection system variations. Even though DIC concentration was homogeneous throughout the column (and close to the initial DIC concentration), pH varied more between the

fluids obtained from the various outlet sampling ports than during the CO_2 experiment at 22 °C (Figs. 4a and 7a). At 50 °C, pH reached its maximum after two hours of water-basaltic glass interaction in outlet samples 2 and 3 (pH of 4.4 at elapsed time of 840 hours), and then it decreased along the rest of the flow path down to 4.2.

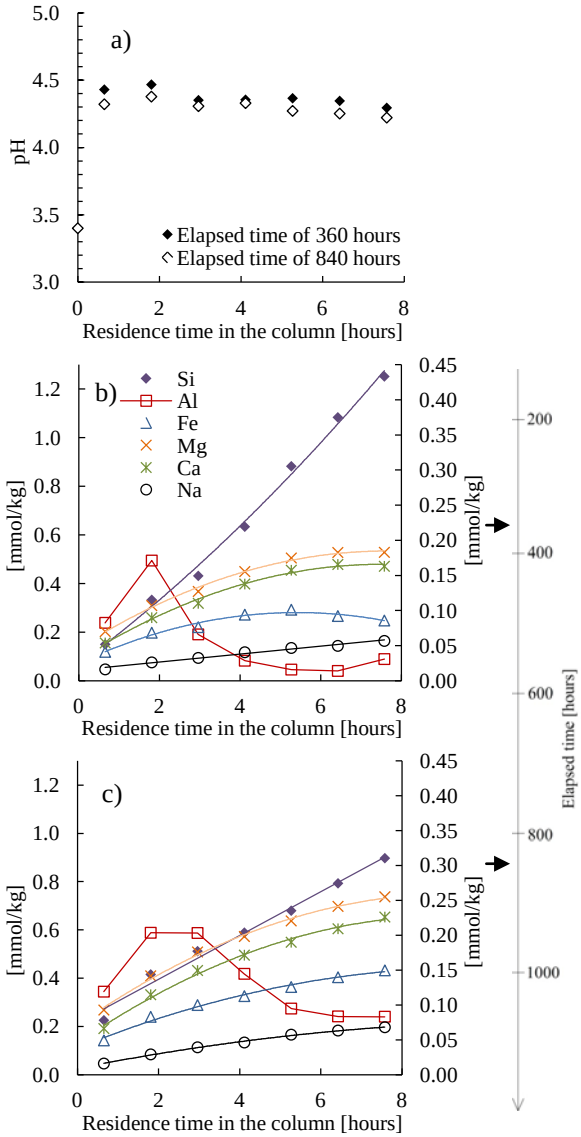

Figure 7. The pH (a) and major elemental concentrations during the CO_2-charged fluid-basaltic glass experiment at 50 °C at elapsed times of 360 (b) and 840 hours (c), respectively. Silicon concentration is shown on the left axis; other element concentrations are presented on the right axis. The aluminium concentration profile suggests precipitation, with Al enrichment in the fluid at the beginning of the column and a decline further along the flow path.

The increase in temperature did not enhance basaltic glass dissolution rates sufficiently to overcome the pH buffer capacity of the CO_2-charged fluid.

Solute concentrations along the flow path at elapsed time of 360 and 840 hours following the start of the injection of CO_2-charged fluid at 50 °C were distinct from those observed during the CO_2-charged fluid experiment at 22 °C (compare Figs. 4b and c with Figs. 7b and c). These two elapsed times were chosen because the initial DIC concentration was stable for ~200 hours prior to these chosen elapsed times. The element stoichiometry of the fluid was different from that of the basaltic glass. During the first 2-3 hours, the Al concentration increased significantly, followed by rapid decrease after ~3-4 hours of water-basaltic glass interaction. The dissolved Al concentration at elapsed time of 360 hours, after 7.5 hours of CO_2-charged water-basaltic glass interaction, was lower than Si, Mg, Ca, Fe, and Na (see Fig. 7b). This indicates significant precipitation of an Al-bearing secondary phase from the fluid. High Si concentrations along the flow path after 360 hours (Fig. 7b) decreased after 840 hours of elapsed time (Fig. 7c), in contrast with Mg and Ca which increased later. The pattern of Ca and Mg enrichment along the flow path was similar to that observed during the CO_2-charged fluid experiment at 22 °C. The stoichiometric coefficient for Si at elapsed time of 840 was <1 compared to Na at all sampling outlet ports. According to the stoichiometric coefficients, Ca and Mg were preferentially released to the fluid up to fourth sampling outlet port, Al up to third sampling outlet port and Fe just in the first sampling outlet port. Later along the flow path, these elements were preferentially retained in the solid.

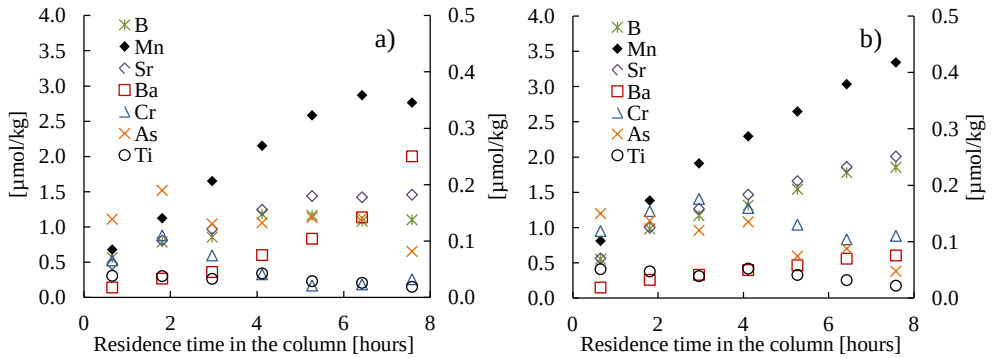

Figure 8. Trace elemental concentrations during the CO_2-charged fluid-basaltic glass experiment at 50 °C at elapsed times of 360 (a) and 840 (b) hours, respectively. The B and Mn concentrations are shown on the left axis; other elements are presented on the right axis.

The Sr and Mn concentrations increased along the flow path (see Fig. 8), however, there was no gradual increase between compartments as it was seen during CO_2 experiment at 22 °C (Fig. 5b). This might indicate incorporation of these elements into secondary phases. The Cr release pattern was similar to that of Al along the flow path which is consistent with its incorporation into Al secondary

minerals. Concentrations of toxic metals in the sampled fluids exceeded WHO drinking water limits for a number of elements (WHO, 2008). Aluminium and iron concentrations were always higher than acceptable limits (>3.7 µmol/kg for Al, >36 µmol/kg for Fe). The Cr concentration consistently exceeded acceptable limits (>0.1 µmol/kg) in the first and second sampling port but likely due to co-precipitation and substitution for Al in secondary phases, its concentration decreased such that Cr was close to or below acceptable limits in the last three outlet ports. Manganese exceeded drinking water limit (7.3 µmol/kg) during the first 200 hours of the experiment in all outlet samples. The As concentration was very close to the WHO drinking water limit of 0.13 µmol/kg.

3.3.4. Iron chemistry and redox conditions

According to Oelkers and Gislason (2001), around 90% of the total Fe in the basaltic glass used in the experiment was in divalent form. The inlet fluids were originally saturated with atmospheric O_2 at 22 °C, but much of this was degassed before the inlet fluid entered the column reactor (Galeczka et al., 2013). Thus, mostly reduced iron was dissolved from the basaltic glass although some was oxidized by the remaining O_2 present in the inlet fluid. The dissolved Fe concentration was low during the pure water experiment at 22 °C in all sampling ports (Figs. 2b and c and Table 1 in Supplementary data 2). The concentrations were too low for Fe species measurements (<0.36 µmol/kg). This suggests that most of the dissolved iron was oxidized with what O_2 remained in the inlet solution, forming insoluble Fe(oxy)hydroxide since Fe^{2+} oxidation kinetics is fast at elevated pH (c.f. Stumm and Morgan, 1996). The Fe^{3+} could be also incorporated into secondary clays. The dissolved Fe concentration was sufficiently high for total dissolved Fe and Fe speciation measurements during both CO_2-charged fluid experiments. To confirm the quality of the analysis, the sum of Fe^{2+} and Fe^{3+} measured with ion chromatography was compared with Fe_{tot} measured with ICP-OES. The differences between the concentrations measured with both methods were between 0-15%, but most of the time were less than 10%. Note, that during sampling for Fe^{2+}/Fe^{3+} analysis, minor oxidation could have occurred. Hence, the concentrations of Fe species reported in this study are the minimum for Fe^{2+} and maximum for Fe^{3+}.

The evolution of the iron chemistry, along the flow path during the CO_2-charged fluid experiment at 22 °C is shown in Fig. 9a and b. During the first two hours of water-basaltic glass interaction, Fe was mostly present as Fe^{3+}, but the concentration of Fe^{2+} increased along the flow path and became more abundant in the upper part of the column. A similar pattern was observed during the CO_2-charged fluid experiment at 50 °C but Fe^{2+} became the dominant species earlier than in the CO_2-charged fluid experiment at 22 °C (Fig. 9c and d and Table 1 in the Supplementary data 2).

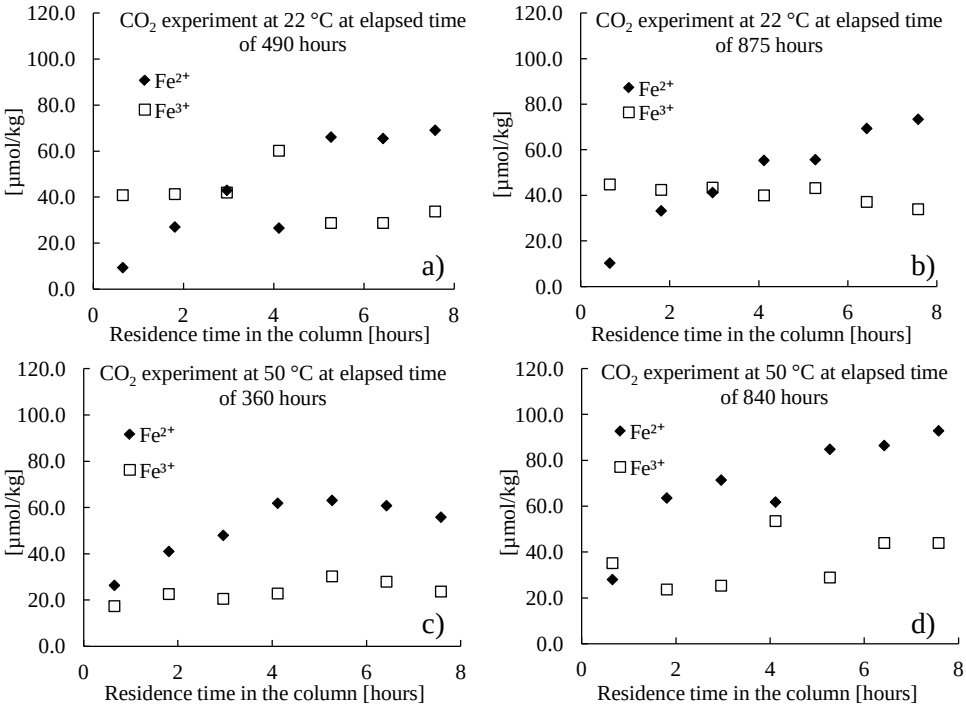

Figure 9. Distribution of Fe species along the flow path during the CO_2-charged fluid-basaltic glass experiments at 22 °C (a, b) and 50 °C (c, d). Predominance of Fe^{3+} in the lower part of the column could be a result of Fe oxidation due to remaining O_2 in the inlet fluid. Later along the flow path, Fe^{2+} became the predominant species showing no further oxidation reactions proceeding in the column.

The measured Eh prior to injecting the CO_2-charged water into the column reactor at 22 °C was ~200-300 mV (Fig. 1 in Supplementary data 1). After an elapsed time of ~200 hours during the CO_2 experiment at 22 °C, the Eh dropped to ~-200 mV and remained constant thereafter. During the CO_2-charged fluid experiment at 50 °C, the measured Eh increased continuously from ~-200 to ~-90 mV. The measured in-line Eh at ambient temperature differed from *in situ* Eh calculated with PHREEQC based on the Fe^{2+}/Fe^{3+} ratio. Measured Eh was about 800 mV and 600 mV lower than calculated during the CO_2-charged fluid experiment at 22 °C and 50 °C, respectively. The reason for this difference is likely lack of equilibrium between different redox couples in the sampled fluids (see Stefánsson et al., 2005) and the analytical difficulties in Eh measurements with a Pt-electrode (Appelo and Postma, 2005; Lindberg and Runnells, 1984).

Aqueous speciation and mineral saturation state calculations with PHREEQC used measured Fe^{2+} and Fe^{3+} species to fix the redox conditions for the CO_2-charged fluid experiments but used the calculated dissolved O_2 for the pure water experiment. These choices lead to an uncertainty for the calculations where the Fe^{2+}/Fe^{3+} ratio was used since there was no overall redox equilibrium within the

fluid in the column. In any case, the water phase evolved to a more reduced state along the flow path during the CO_2 experiments.

3.3.5. Relative mobility of elements

The relative mobility of the elements was calculated by dividing the measured dissolved element concentrations in the sampled fluids by the elemental concentrations in the dissolving basaltic glass. Relative mobility calculated for major and trace elements after elapsed time of 2200, 875, and 840 hours for pure water experiment, CO_2 experiment at 22 °C, and CO_2 experiment at 50 °C experiment, respectively is illustrated in Figure 10. Figures 10a, c, and e show the relative mobility in fluids collected from the seventh outlet sampling port. Figures 10 b, d, and f display the evolution of this relative mobility at the same elapsed times as a function of length of fluid-basaltic glass interaction along the flow path. The most mobile elements were As and B in all experiments. The least mobile measured element was Ti, an element frequently considered immobile in basaltic groundwater systems (e.g. Alfredsson et al., 2013; Gislason et al., 1996). The log mobility of the major elements Si, Ca, Mg, Na, and K during the pure water experiment was ~-4.7 and during both CO_2-charged fluid experiments ~-4.0, indicating that the presence of CO_2 in the fluid rather than a temperature increase from 22 °C to 50 °C was a major factor enhancing element mobility. The highest mobility of Al (log mobility ~-3.8) was during the CO-charged fluid experiment at 22 °C. During the pure water experiment and during the CO_2-charged fluid experiment at 50 °C, the Al log mobility was ~-4.9 and ~-4.5, respectively. When the CO_2-charged water was injected, the log mobility of Fe increased from ~-7.0 to ~-4.0. Similarly, trace elemental mobility increased with the injection of CO_2-charged fluids; the relative mobility of As, Sr, Cr, Mn, Ba, and V increased by a factor of 5, 7, 20, 45, 156, and 160 by changing the inlet fluid from pure water to a CO_2-charged fluid.

3.3.6. Saturation state of basaltic glass and secondary minerals

PHREEQC was used to calculate the *in situ* saturation state of the sampled fluids with respect to basaltic glass (Fig. 11) and selected secondary minerals (see Fig. 2 in Supplementary data 1 and Supplementary data 3). As described in the method section, the saturation state for basaltic glass is expressed as the Gibbs free energy of reaction, ΔG_r. When the absolute values of ΔG_r is low, basaltic glass dissolution may slow as equilibrium is approached (c.f. Schott and Oelkers 1995); based on transition state theory one would expect a substantial decrease in basaltic glass dissolution rates when ΔG_r exceeds -10 kJ/mol at 25 °C and -11 kJ/mol at 50 °C. At lower ΔG_r, the $\left(1 - \exp\left(\frac{\Delta G_r}{\sigma RT}\right)\right)$ term from the rate expression (3) is >0.98 and therefore does not influence the overall dissolution rate significantly.

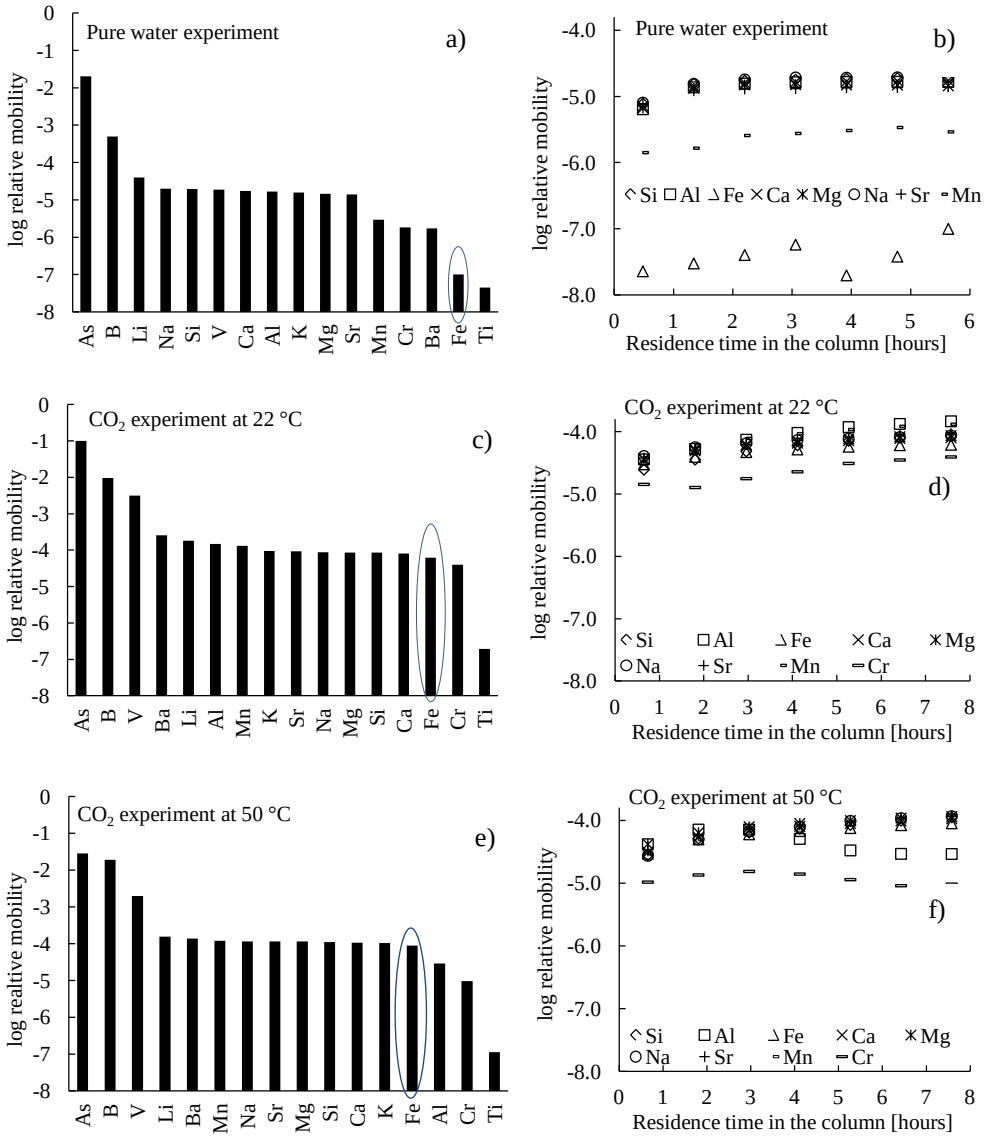

Figure 10. The relative mobility of elements sampled from the seventh outlet port after an elapsed time of 2200 hours for the pure water-basaltic glass experiment (a), 875 hours for the CO_2-charged fluid-basaltic glass interaction experiment at 22 °C (c) and 840 hours for the CO_2-charged fluid-basaltic glass interaction experiment at 50 °C (e), respectively. Plots (b), (d), and (f) represent relative mobility of major elements along the flow path during pure water experiment, CO_2 experiment at 22 °C, and CO_2 experiment at 50 °C, respectively, at the same elapsed times as (a), (c), and (e). Circles focus on the mobility of Fe.

The percent of slowing down of basaltic glass dissolution is given as horizontal lines in Figure 11. During the pure water experiment, the dissolution rate of basaltic glass was independent of the saturation state during the first 30 minutes of water-rock interaction (e.g. only in samples collected from the first sampling outlet). The fluid became less undersaturated with respect to basaltic glass along the flow path,

causing the dissolution rate to be slowed down by up to 4% (Fig. 11a). During the CO_2-charged fluid experiment at 22 °C, the dissolution rate depended on the basaltic glass saturation state along the whole flow path, and the dissolution rate was calculated to have slowed by up to 13% after ~7.5 hour of water-rock interaction (e.g. in fluid sampled from the last sampling port) as displayed in Fig. 11b.

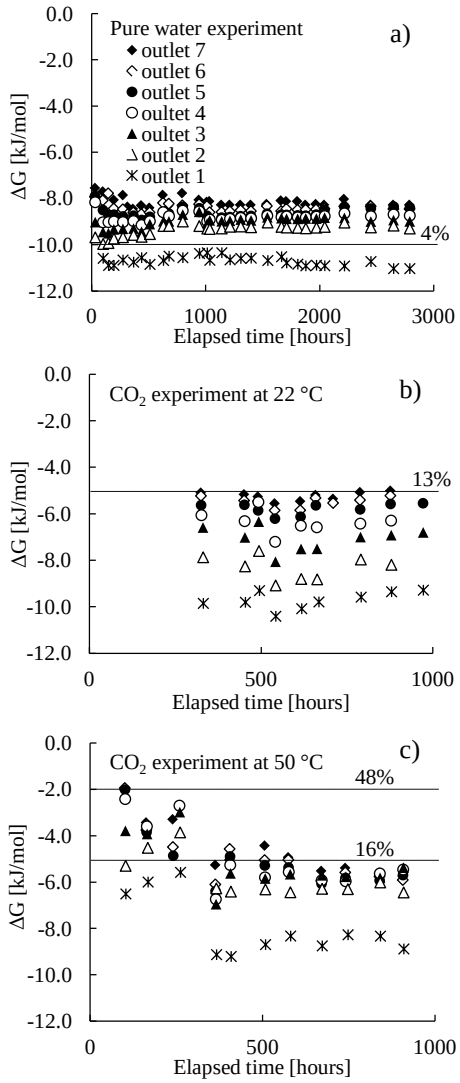

Figure 11. The saturation state of collected fluids with respect to the hydrated basaltic glass calculated with PHREEQC. Example of calculations can be found in Wolff-Boenisch et al. (2004). The horizontal line represents percentage slowdown of the basaltic glass dissolution due to saturation state according to Eq. (2).

During the CO_2 experiment at 50 °C, the dissolution rate was dependent on basaltic glass saturation state along the whole flow path, and the dissolution rate was calculated to have slowed by up to 48% after ~7.5 hour of water-basaltic glass

interaction at the beginning of this experiment but no more than 16% at the latter stages (e.g. in fluid sampled from the last sampling port at elapsed time from 600 hours) - see Fig. 11c.

The reactive fluid during the pure water experiment was basic (pH ~9.3) and supersaturated with respect to the secondary minerals commonly found in natural basaltic systems such as zeolites (here represent by heulandite), clay minerals (here represent by Mg-clay, Ca-montmorillonite, gibbsite, imogolite, kaolinite) and Fe-phases such as goethite, amorphous goethite and $Fe(OH)_{3(am)}$ (see Fig. 2 in Supplementary data 1 and Supplementary data 3). The fluid was undersaturated with respect to amorphous and cryptocrystalline phases such as $Al(OH)_{3(am)}$ and chalcedony, respectively. During the CO_2-charged fluid experiment at 22 °C, the fluid was undersaturated with respect to zeolites but supersaturated with respect to Ca-montmorillonite after 2-3 hours of water-basaltic glass interaction. It was supersaturated with respect to amorphous phases such as $Fe(OH)_{3(am)}$, $goethite_{(am)}$, chalcedony and undersaturated with respect to amorphous $Al(OH)_{3(am)}$. During the CO_2-charged fluid experiment at 50 °C, the fluid was again undersaturated with respect to zeolites but supersaturated with respect to Ca-montmorillonite. The fluid was close to and/or in equilibrium with amorphous and cryptocrystalline phases such as $Al(OH)_{3(am)}$, $goethite_{(am)}$ and chalcedony. The fluid was undersaturated with respect to amorphous $Fe(OH)_{3(am)}$. Supersaturation with respect to amorphous phases such as $Al(OH)_{3(am)}$, $Fe(OH)_{3(am)}$ and chalcedony suggests that precipitation of these phases controlled the mobility of Al, Fe, and Si in the fluid phase. In natural systems, amorphous phases are the first to precipitate (Gislason et al., 1997). Slight supersaturation with respect to siderite occurred only at the beginning of the CO_2-charged fluid experiments, when the pH was still high ~5. Also, the PHREEQC simulation of the degassing of the outlet fluid indicated supersaturation with respect to siderite and ankerite. Carbonates precipitated at the reactor outlet and their presence was confirmed by simple HCl test. According to model calculations approximately 6 grams of carbonates (siderite, ankerite, and calcite) precipitated at the outlet of column reactor during the 1000 hours of the CO_2-charged fluid experiment at 50 °C.

3.3.7. Basaltic glass apparent dissolution rates

Figure 12 shows a comparison between basaltic glass dissolution rates calculated using Eq. 3 and that obtained experimentally based on Eq. 4. The latter was potentially affected by Si consumption into secondary minerals along the flow path and fluid channelling. Rates shown in Fig. 12 were normalized to the total geometric surface area from the bottom of the column to the specific outlet port. According to the calculations, experimentally obtained apparent dissolution rates were always slower than those calculated using Eq. (3) (see Fig. 12). This difference

increased along the flow path and it was the largest in the CO_2-charged fluid experiment at 50 °C. The difference between the calculated basaltic glass dissolution rates and the apparent rates determined from the measured Si concentration of reactive fluids indicates Si-bearing secondary phases precipitated in the column and/or significant fluid channelling occurred.

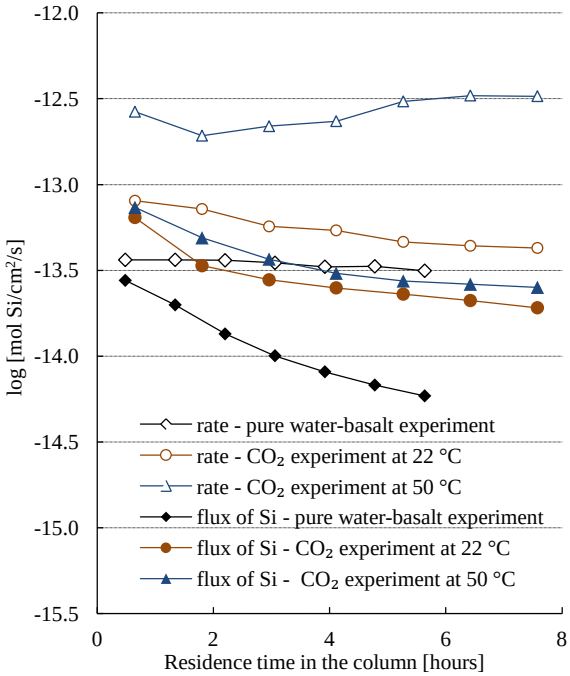

Figure 12. Release rate of Si along the flow path at elapsed time of 2200, 875, and 840 hours for the pure water-basaltic glass interaction experiment, the CO_2-charged fluid-basaltic glass interaction experiment at 22 °C, and for the CO_2-charged fluid-basaltic glass interaction experiment at 50 °C, respectively. Open symbols represent the Si release rates calculated using the rate expression from Gislason and Oelkers (2003) and filled symbols represent experimentally obtained Si release rates calculated from sampled fluid compositions. These latter values were normalized to the surface area of the material from the bottom of the column to the specific sampling outlet.

The minimum amount of basaltic glass dissolved inside the column during the experiment was calculated based on the Si outlet concentration at the highest compartment and the amount of water pumped through the column during individual stages of the experiment. This excludes precipitation of secondary Si-phases. The total amount of dissolved glass was time dependent. For 1000 hours of experimental duration, around 40 g of basaltic glass dissolved during the CO_2 experiment at 50 °C, around 13 g during the CO_2 experiment at 22 °C, and around 6 g during the pure water experiment. The total amount of dissolved basaltic glass during whole experimental duration (2500 hours of pure water experiment and 2000 hours for CO_2 experiments) was ~68 g which was ~0.8% of the total basaltic glass in the column.

3.4. DISCUSSION

3.4.1. Chemical trends during the experiments

The pure water-basaltic glass interaction experiment provides insight into natural basaltic groundwater systems. The pH in the column was similar to that in natural basaltic groundwaters (e.g. Alfredsson et al., 2013; Arnorsson et al., 2002; Gislason and Eugster, 1987; Gislason et al., 1996). The experimental mobility of elements reflected the mobility of the elements in natural basaltic systems with the exception of Al (Fig. 10a). The low Al mobility commonly observed in natural environments indicates the precipitation of Al(oxy)hydroxides at low pH and clays and zeolites at high pH (e.g. Crovisier et al. 1992; Gislason and Eugster, 1987; Gislason et al., 1996; Kristmannsdottir, 1979; Kristmanndottir, 1982; Stefánsson and Gislason, 2001). Iron concentrations measured in the column were close to or below detection limit of the analyses. Released Fe^{2+} from the basaltic glass most likely precipitated as Fe(oxy)hydroxides due to fast iron oxidation kinetics at alkaline pH. This likelihood is corroborated by calculated fluid supersaturation with respect to trivalent Fe-phases. It seems likely that some aluminosilicate minerals precipitated along the entire column since the fluids collected from the first sampling port were supersaturated with respect to some clays (gibbsite, imogolite, Mg-clay) and as the fluid travelled further it became supersaturated with respect to additional phases such as chalcedony, clays (Ca-montmorillonite) and zeolites (heulandite) (Fig. 2 in Supplementary data 1). The Si release rate decreased as the fluid continued to flow in the column reactor (Fig. 12) suggesting silica incorporation into secondary phases. The Na concentration curve also levelled off indicating Na consumption by secondary phases (e.g. zeolites). This observation is in contrast with the assumption that Na is a conservative element in natural alkaline basaltic groundwater systems.

During the CO_2-charged fluid experiment at 22 °C, the pH decreased from alkaline to acidic (~4.5) causing enhanced basaltic glass dissolution (Fig. 3a and 4a). The inlet pH of the fluid was 3.4 and its pH increased to 4.5 during the first 40 minutes after the beginning of water-basaltic glass interaction. A further pH increase did not occur because the pH buffer capacity of the fluid at pH ~4.5 was approximately an order of magnitude higher ($\sim 10^{-2}$) than that of the glass. Although the inlet fluid DIC concentration fluctuated somewhat during the first part of this experiment (Fig. 3b), the overall sampled fluid pH was constant along the flow path giving the confidence in measured fluid chemistry. Due to low pH, the mobility of all elements increased (Fig. 10c and d) compared to the pure water experiment (Fig. 10a and b). Iron, manganese, and chromium became more mobile compared to results from the pure water experiment. Also, other elements which were close to the detection limit of the analyses during the pure water experiment increased in concentrations (e.g. Mn, B, Sr, Ba, As Ti) (see Fig. 5). The Si release rates obtained

from this experiment were lower than rates calculated using Eq. 3 (Fig. 12) during the first 40 minutes of water-basaltic glass interaction suggesting the precipitation of a secondary Si-bearing phase as the fluid flowed to the first outlet, consistent with supersaturation of the fluid with respect to chalcedony, quartz, and other Si-bearing phases such as clays (Fig. 2 in Supplementary data 1). Note also the calculated stoichiometric coefficients for Si, Ca, Mg, and Fe which were below 1 indicating their preferential retention in the solid. Rogers et al. (2006) reported that amorphous silica is the common silica phase formed via low-temperature alteration of basalts by CO_2-rich fluids. Iron chemistry showed that Fe^{3+} was the dominant Fe aqueous species during the first two hours of water-basaltic glass interaction (Fig. 9a and b) suggesting that most of the Fe^{2+} released from basaltic glass was oxidized to Fe^{3+} during the initial stage of water-basaltic glass interaction, probably due to O_2 remaining in the inlet degassed fluid. Later along the flow path Fe^{2+} became the major iron species. Furthermore, the Fe^{3+} concentration did not increase with time but slowly decreased in concentration consistent with Fe^{3+} precipitation; this likelihood is consistent with the observed supersaturation of the fluid phase with respect to amorphous $Fe(OH)_3$ (Fig. 2 in Supplementary data 1). Later along the flow path there was no O_2 left to oxidize Fe^{2+}, allowing the Fe^{2+} concentration to increase gradually, while Fe^{3+} decreased. Although the kinetics of iron oxidation at pH <~6 is slow (Stumm and Morgan, 1996), during the first minutes of water-basaltic glass interaction in which the pH changed from 3.4 to 4.5 nearly 80% of the Fe^{2+} released from the basaltic glass was oxidized to Fe^{3+}.

Element mobility in the CO_2-charged inlet fluid at 50 °C was similar to that measured at 22 °C (see Fig. 10c and e). This temperature increase did not enhance the basaltic glass dissolution rates sufficiently to raise pH and it was stable at ~4.2 along the flow path (Fig. 6a and 7a). After a significant initial rise during the first 2-3 hours of water-basaltic glass interaction along the flow path, aluminium concentrations decreased consistent with the precipitation of an Al-bearing secondary phase (Fig. 7b and c). In addition, the fluid was supersaturated with respect to amorphous $Al(OH)_3$ in the first two outlet fluids suggesting that it might have precipitated (see Fig. 2 in Supplementary data 1). The discrepancy between measured and calculated Si release rate (Fig 12) suggests incorporation of Si into secondary phases, consistent with the supersaturation of the fluid with respect to chalcedony and clay minerals (see Fig. 2 in Supplementary data 1). In addition, the stoichiometric coefficients for major elements confirm their preferential retention in the solid phase. The Cr concentration followed the Al concentration pattern consistent with Cr incorporation into an Al hydroxide phase (Kaasalainen and Stefánsson, 2012).

3.4.2. Reactive transport modelling

The results of geochemical reactive transport modelling are compared to the experimental results in Fig. 13 and 14. Modelled fluid concentrations assuming no secondary minerals formed for the pure water-basaltic glass interaction experiment were higher by a factor of ~8 from those measured in samples collected from the seventh sampling port but by only a factor of ~3 from those measured in the first sampling outlet for Si, Ca, Mg, Na, and Al (see Fig. 13a). Corresponding modelled fluid concentrations for the CO_2-charged fluid-basaltic glass interaction experiment at 22 °C yielded concentrations 3-4 times higher than their experimental counterparts for all major elements (see Fig. 13c). Corresponding modelled fluid concentrations of the CO_2-charged fluid-basaltic glass interaction experiment at 50 °C were ~6 times higher than those measured in the first sampling outlet and ~3 times higher than in the seventh sampling outlet for Si, Ca, Mg, Na, and Fe (see Fig. 13e).

The saturation state of hydrated basaltic glass, when using a log K of 1.07 calculated based on the hydrolysis reaction (1) did not affect significantly the results of modelling of the pure water-basaltic glass and CO_2-charged fluid-basaltic glass interaction experiment at 22 °C. However, there was some effect of saturation state on the modelled concentrations for the 50 °C experiment; the relatively high fluid saturation state slowed basaltic glass dissolution rates somewhat. The saturation state of hydrated basaltic glass decreased modelled fluid concentrations starting from the second sampling port consistent with experimental results. The non-linearity of the modelled curves during the CO_2-charged fluid-basaltic glass interaction experiment at 22 °C stemmed from the effect of increasing fluid Al concentration along the flow path which decreased basaltic glass dissolution rate.

Result of the modelling including the assumption that common secondary minerals precipitated at local equilibrium yielded lower estimates of fluid element concentrations for some elements compared to those made assuming no secondary minerals precipitated (see Fig. 13 b, d, and f). During the pure water-basaltic glass interaction experiment, many phases were supersaturated in the fluid phase including various clays, zeolites, and Fe and Al (oxy)hydroxides. In the simulation imogolite, goethite, heulandite, and Mg-saponite were chosen to precipitate at local equilibrium as these are common secondary minerals found in natural basaltic systems (e.g. Alfredsson, 2013) and the thermodynamic properties of these phases are available (Gysi and Stefánsson, 2011). Results of the modelling show that the fluid attained equilibrium with imogolite, goethite, and Mg-saponite causing a decrease in Si, Mg, Al, and Fe concentrations compared to model calculations performed assuming that secondary minerals did not precipitate (Fig. 13b).

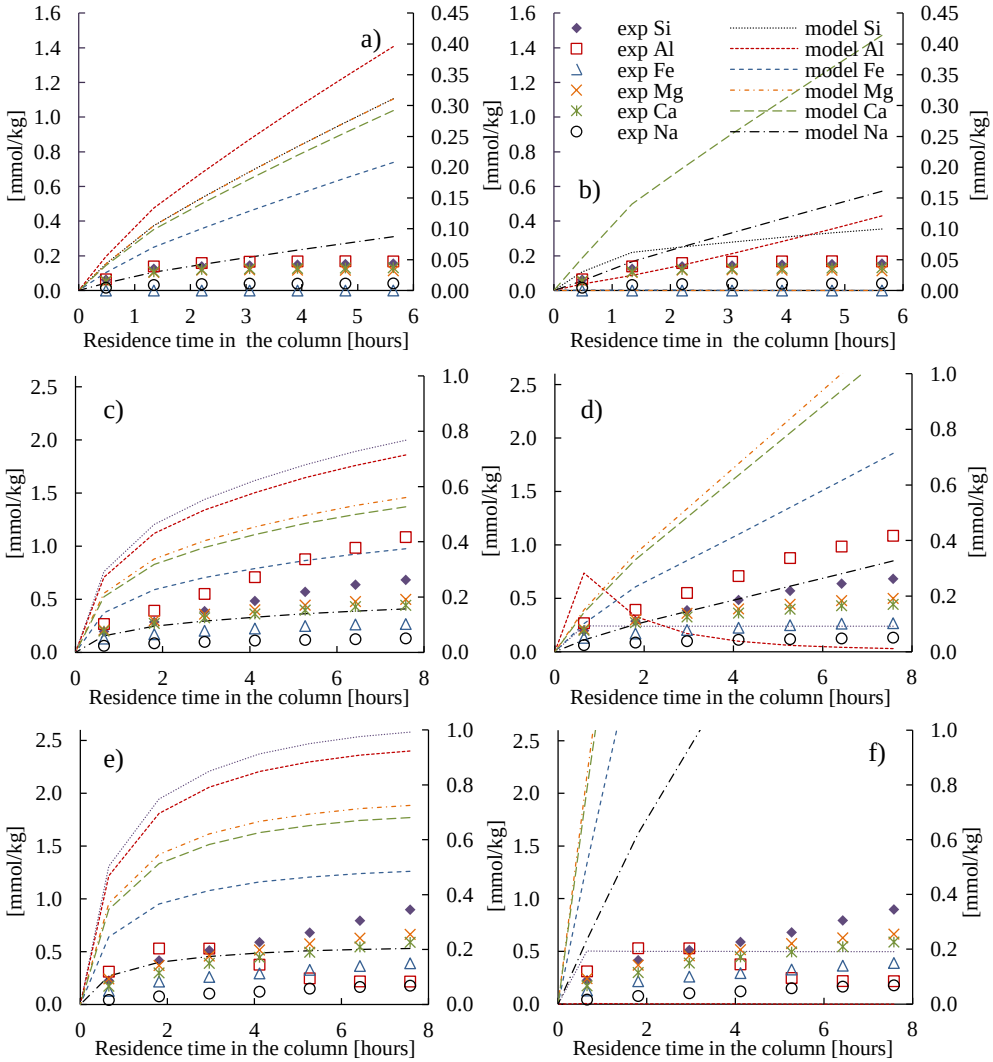

Figure 13. Comparison of the results of reactive transport modelling calculations with measured fluid concentrations for the pure water-basaltic glass interaction experiment at elapsed time of 2200 hours (a, b), for the CO_2-charged fluid-basaltic glass interaction experiment at 22 °C at elapsed time of 875 hours (c, d), and for the CO_2-charged fluid-basaltic glass interaction experiment at 50 °C at elapsed time of 840 hours (e, f). The symbols correspond to the experimental results. The Si concentration is shown on the left axis and the rest of the elements are displayed on the right axis. Plots (a), (c), and (e) represent reactive transport modelling assuming basaltic glass dissolved according to the rate expression given by Gislason and Oelkers (2003). The logarithm of equilibrium constant for the hydrated basaltic glass was 1.07. Plots (b), (d), and (f) represent reactive transport modelling under the same conditions but additionally assuming local equilibrium with imogolite, goethite, heulandite, and Mg-saponite for the pure water experiment, and goethite$_{(am)}$, chalcedony, and gibbsite for both CO_2 experiments, respectively. The right y axis scale in (d) and (f) was decreased to give better comparison between modelled concentration curves and thus the curves are cut.

As, however, basaltic glass dissolution rates increase with decreasing aqueous Al concentration, the aqueous concentrations of some metals, including Ca and Na increase when secondary mineral precipitation is considered.This latter result stems from the fact that the precipitation of secondary minerals decreases modelled fluid Al concentration leading to accelerated basaltic glass dissolution rates as calculated using Eq. (3).

A comparison between modelled and measured fluid pH is provided in Fig. 14. Although calculated pH is similar to corresponding measured pH for the case of the CO_2-charged fluid-basaltic glass interaction experiment at 22 ºC, differences of more than a pH unit are evident between the modelled and measured pH for the other two experiments.

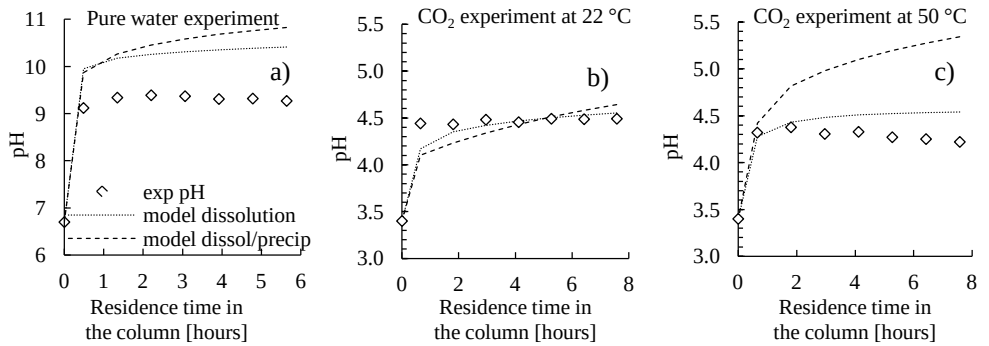

Figure 14. Comparison of the fluid pH obtained from reactive transport modelling calculations with those measured during the pure water-basaltic glass interaction experiment at elapsed time of 2200 hours (a), for the CO_2-charged fluid-basaltic glass interaction experiment at 22 °C at elapsed time of 875 hours (b), and for the CO_2-charged fluid-basaltic glass interaction experiment at 50 °C at elapsed time of 840 hours (c). The symbols correspond to the experimental results. The simulation was performed assuming basaltic glass dissolution according to the rate expression given by Gislason and Oelkers (2003) ('model dissolution') and dissolution consistent with this rate expression assuming local equilibrium with imogolite, goethite, heulandite, and Mg-saponite for pure water experiment, and goethite$_{(am)}$, chalcedony, and gibbsite for both CO_2 experiments, respectively ('model dissol/precip').

The relative simplicity of the pure water-basaltic glass interaction experiment allows some assessment of the sensitivity of the calculations to the input parameters. In the absence of secondary mineral precipitation calculated fluid compositions are a function of three parameters: 1) the dissolution rate constant of the basaltic glass, 2) basaltic glass surface-fluid interaction area and 3) the equilibrium constant (log *K*) for the basaltic glass surface hydrolysis reaction. Of these parameters the equilibrium constant is likely the poorest constrained; in this study it was estimated from the sum of amorphous oxides solubilities assuming the surface contains only Si and Al. As can be seen in Fig. 15, by decreasing the value of log *K* in Eq. (1) from 1.07 to -0.85 yields a close agreement between the modelled and measured element concentrations during pure water-basaltic glass interaction experiment. Nevertheless,

if secondary mineral precipitation is considered the model calculations begin to fail significantly (see Fig 15b). Using this same log *K* to describe the two CO_2-charged fluid basaltic glass dissolution experiments also yields a closer match between modelled and measured element concentrations; however, the model results fail to reproduce the variation of fluid concentrations as a function of distance along the flow path (e.g. the strong increases in the fluid concentrations of numerous elements along the flow path – see Fig. 15c, d, e, and f). The description of these fluid concentrations variations is critical to modelling the distribution and quantity of precipitated secondary minerals including carbonates along the flow path.

Overall there is a poor match between geochemical modelling and experimental results. This poor description of the measured fluid compositions underscores the challenges to predicting the fate and consequences of CO_2 injected into the subsurface during carbon storage efforts. There are likely a number of sources of these observed discrepancies. First is the poor choice of secondary minerals. The selection of secondary phases attaining local equilibrium with the fluid controls to a large extent the mobility of modelled element concentrations and the dissolution rate of the basaltic glass. A second factor influencing the modelling results is the poor understanding of the thermodynamic properties of minerals such as clays and zeolites (c.f. Oelkers et al., 2009). Gysi and Stefánsson (2011) attempted to construct a thermodynamic database for the clays and zeolites commonly observed in natural basaltic systems. The diversity of the structures and compositions of clays and zeolites, however, leads to significant uncertainties in these results. Simulation performed with a distinct log *K* for the hydrated basaltic glass surface layer (see Fig. 15) illustrates how variations in thermodynamic properties can alter model results. A third factor is the lack of precipitation rate expressions for secondary minerals; such are a prerequisite for the accurate modelling of the temporal and spatial composition of reactive fluids. Even if the fluid is supersaturated with respect to the secondary phase, precipitation rates may be sluggish avoiding the nucleation and crystal growth (e.g. Saldi et al., 2009, Schott et al., 2012). Also as reported by Schott et al. (2012) rates close to equilibrium are dependent on the availability of reactive surface sites for the nucleation which is closely related to the history of the mineral surface which often is not known. The limitation of the modelling related to the nucleation and precipitation kinetics were discussed among others in Hellevang et al. (2013), Pham et al. (2011), Zhu and Lu (2009). Finally, estimation of glass-fluid interfacial surface area, due in part to fluid channelling can contribute to the discrepancies between modelled and experimental outlet concentrations. As mentioned by many authors, mineral-fluid interfacial surface area is crucial to predict not only rates measured in the laboratory but also the rates of natural processes (e.g. Anbeek et al., 1994, Aradóttir et al., 2012; Gysi and Stefansson, 2012; Maher et al., 2009; Navarre-Sitchler et al., 2011; Navarre-Sitchler et al., 2013,

Paukert et al., 2012; White and Brantley, 2003; Trautz et al. 2012; Zheng et al., 2012; Zhu et al., 2006).

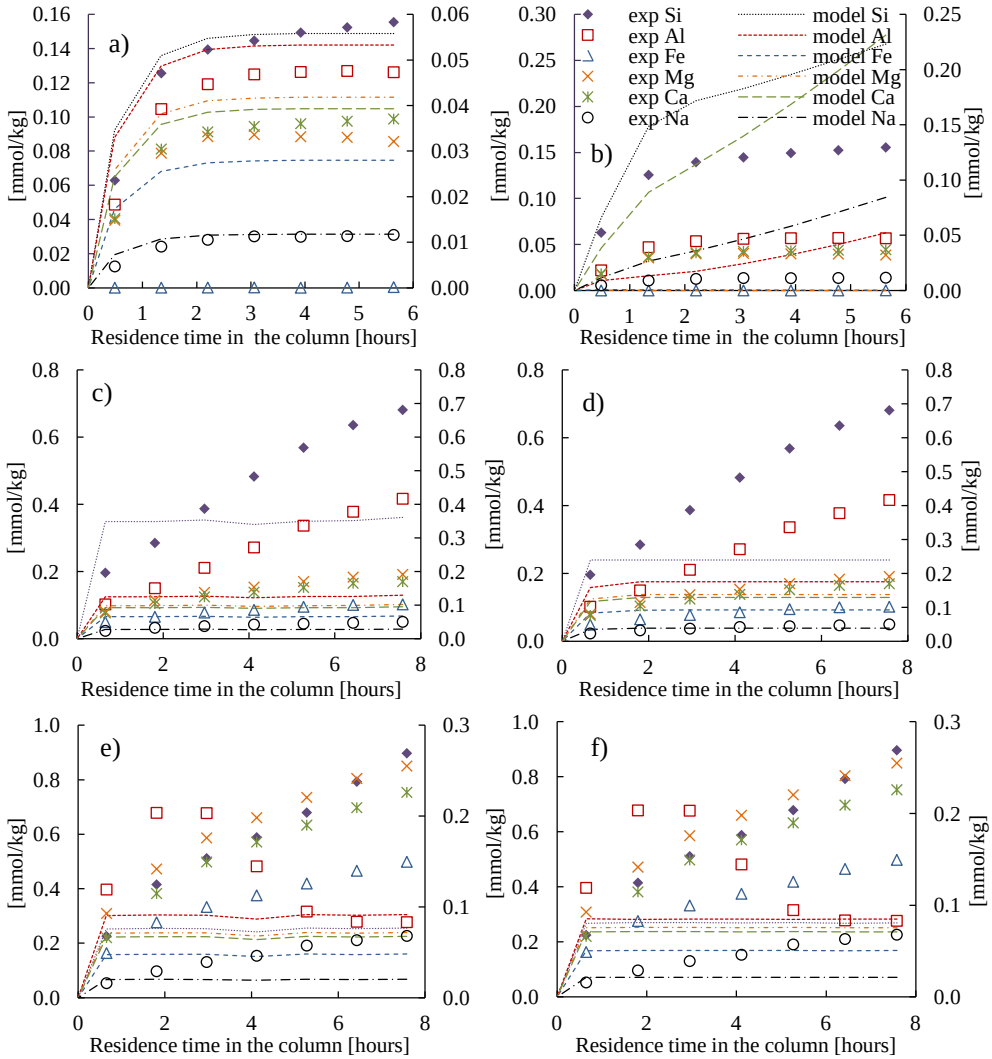

Figure 15. Comparison of the results of reactive transport modelling calculations with measured reactive fluid concentrations for the pure water-basaltic glass interaction experiment at elapsed time of 2200 hours (a, b), for the CO_2-charged fluid-basaltic glass experiment at 22 °C at elapsed time of 875 hours (c, d), and for the CO_2-charged fluid-basaltic glass experiment at 50 °C at elapsed time of 840 hours (e, f). The symbols correspond to the experimental results. The Si concentration is shown on the left axis and all other concentrations are presented on the right axis. The model calculations were performed using a logarithm of the equilibrium constant for hydrated basaltic glass surface layer of -0.85, generated by a best fit of the data shown in graph (a). Plots (a), (c), and (e) represent reactive transport modelling assuming basaltic glass dissolved according to the rate expression given by Gislason and Oelkers (2003). Plots (b), (d), and (f) represent reactive transport modelling including this basaltic glass dissolution expression and assuming local equilibrium with imogolite, goethite, heulandite, and Mg-saponite for the pure water experiment, and goethite$_{(am)}$, chalcedony and gibbsite for both CO_2 experiments, respectively.

3.4.3. Implications for CO_2 mineral storage

The results presented above provide insight into *in situ* mineral storage efforts in basaltic rocks. As the experimental results and natural observations reveal, CO_2 will not be fixed as carbonates during the first hours of water-basalt interaction in flow systems. In contrast, this region is dominated by primary rock dissolution. This observation favours the industrial scale injection of CO_2 into subsurface basalts as the injection will tend to increase porosity and permeability near the well outlet. Nevertheless some Si-Al bearing phase precipitation cannot be excluded. A potential risk associated with such secondary Si-Al bearing phase formation is the passivation of the primary rock minerals, slowing its further dissolution (e.g. Daval et al., 2011, Schaef et al., 2013). The only potential for carbonate precipitation near the injection well is at the beginning of CO_2-charged fluid injection, where mixing with natural alkaline groundwater could lead to carbonate precipitation. This was evidenced by the reactive fluid composition during the first hours of the CO_2-charged fluid experiment at 22 °C, which was the only time during the CO_2-charged experiment that the fluid became supersaturated with respect to carbonate minerals due to the mixing of the injected fluid with the alkaline-rich fluid already present in the reactor. The potential for carbonate formation via dilution and mixing of CO_2-charged waters and alkaline groundwater was previously discussed as means to overcome the critical buffer capacity which stabilizes the column pH below carbonate saturation (Wolff-Boenisch, 2011).

The column reactor is a natural analogue for the magmatic CO_2 rich groundwater in vicinity of volcanoes or geothermal systems (e.g. Flaathen and Gislason 2007, Olsson et al., 2012a). When the CO_2-charged groundwater emerges to the surface, the CO_2 dissolved in the water degasses leading to the supersaturation with respect to carbonates and resulting in their precipitation (e.g. travertine deposits). During the two CO_2-water-basalt interaction experiments ~10 grams of carbonates were calculated to have precipitated as a result of CO_2 degassing at the outlet (~4 g during the 22 ºC and ~6 g during the 50 ºC experiment) suggesting that divalent cation harvesting from basalts using CO_2-charged waters could be used for CO_2 storage. Such precipitation can also scavenge some metals such as Al, Fe, Cd, Cu, Mn, and Sr (e.g. Olsson et. al., 2012a).

3.5. CONCLUSIONS

This experimental study of CO_2-charged fluid-basaltic glass interaction provides a number of insights relevant to mineral carbonatization efforts and natural CO_2-rich systems:

1. The neutralization of the CO_2-rich fluid from pH of 3.4 to ~4.5 does not immobilize toxic elements at ambient temperature but immobilizes Al and

Cr at elevated temperature. This indicates that further neutralization of CO_2-charged water is required for decreased toxic element mobility.

2. The CO_2-charged water injection enhances the mobility of redox sensitive Fe^{2+} significantly making it available for the storage of injected carbon as iron carbonate minerals.
3. The precipitation of aluminosilicates likely occurred at a pH of 4.2-4.5 in CO_2-charged fluids. These secondary phases can 1) fill the available pores and therefore clog the efficient porosity in vicinity of the injection well, 2) incorporate some divalent cations limiting their availability for carbon storage.
4. The inability of simple reactive transport models to describe accurately the fluid evolution in this well constrained one dimensional flow system suggests that significant improvements need to be made to such models before we can predict with confidence the fate and consequences of injecting carbon dioxide into the subsurface.
5. Column reactors such as that used in this study could be used to facilitate *ex situ* carbon mineral storage. Carbonate precipitation at the outlet of the reactor suggests that the harvesting of divalent metals from rocks using CO_2-charged waters could potentially be upscaled to an industrial carbonatization process.

Acknowledgments

This study is part of the CarbFix project (www.carbfix.com) in Iceland and was funded by the European Union through the European Marie Curie network Delta-Min (Mechanisms of Mineral Replacement Reactions; Grant# PITN-GA-2008-215360) and SP1-Cooperation (FP7-ENERGY-2011-1; Grant# 283148), Reykjavík Energy, University of Iceland and RANNÍS, Icelandic Fund for Research Equipment; Grant# 10/0293 and 121071-0061. The authors would like to thank all colleagues and co-workers at University of Iceland and Reykjavik Energy, in particular: Þorsteinn Jonsson, Eydis Eiriksdottir, Kiflom Gebrehiwot, Snorri Gudbrandsson, Helgi Alfredsson, Nicole Keller, Niels Oskarson. The first author would like to thank Lukasz Kowolik for his endless patience and personal support.

References

Aiuppa A., Federico C., Allard P., Gurrieri, S., Valenza M. (2005) Trace metal modeling of groundwater–gas–rock interactions in a volcanic aquifer: Mount Vesuvius, Southern Italy. *Chem. Geol.* **216**, 289-311.

Alfredsson H.A., Oelkers E.H., Hardarsson B.S., Franzson H., Gunnlaugsson E., Gislason S.R. (2013) The geology and water chemistry of the Hellisheidi, SW-Iceland carbon storage site. *Int. J. Greenhouse Gas Control* **12**, 399-418.

Anbeek C., Van Breemen N., Meijer E.L., Van Der Plas L. (1994) The dissolution of naturally weathered feldspar and quartz. *Geochim. Cosmochim. Acta* **58**, 4601-4613.

Andreani M., Luquot L., Gouze P., Godard M., Hoisé E., Gibert B. (2009) Experimental Study of Carbon Sequestration Reactions Controlled by the Percolation of CO_2-Rich Brine through Peridotites. *Environ. Sci. Technol.* **43**, 1226-1231.

Appelo C.A.J., Postma D. (2005) Geochemistry, groundwater and pollution. 2nd ed. Amsterdam, CRC Press.

Aradóttir E.S.P., Sonnenthal E.L., Björnsson G., Jónsson H. (2012) Multidimensional reactive transport modeling of CO_2 mineral sequestration in basalts at the Hellisheidi geothermal field, Iceland. *Int. J. Greenhouse Gas Control* **9**, 24-40.

Arnórsson S., Gunnarsson I., Stefánsson A., Andrésdóttir A. and Sveinbjörnsdóttir Á.E. (2002) Major element chemistry of surface- and ground waters in basaltic terrain, N-Iceland.: I. primary mineral saturation. *Geochim. Cosmochim. Acta* **66**, 4015-4046.

Beinlich A., Austrheim H. (2012) In situ sequestration of atmospheric CO_2 at low temperature and surface cracking of serpentinized peridotite in mine shafts. *Chem. Geol*. **332–333**, 32-44.

Berner R.A. (2004) The phanerozoic carbon cycle: CO_2 and O_2. Oxford University Press.

Bourcier W.L., Peiffer D.W., Knauss K.G., McKeegan K.D., Smith D.K. (1990) A kinetic model for borosilicate glass dissolution based on the dissolution affinity of a surface alteration layer. *Mat. Res. Soc. Symp. Proc.* **176**, 209-216.

Brady P.V., Gislason S.R. (1997) Seafloor weathering controls on atmospheric CO_2 and global climate. *Geochim. Cosmochim. Acta* **61**, 965-973.

Broecker W.S. (2012) The carbon cycle and climate change: Memoirs of my 60 years in science. *Geochem. Perspectives* **1,** 221-351.

Crovisier J.L., Honnorez J., Fritz B. and Petit J.C. (1992) Dissolution of subglacial volcanic glasses from Iceland: laboratory study and modelling. *App. Geochem.*, **7**, Supplement **1**, 55-81.

Daux V., Guy C., Advocat T., Crovisier J.-L., Stille P. (1997) Kinetic aspects of basaltic glass dissolution at 90 °C: role of aqueous silicon and aluminium. *Chem. Geol.* **142**, 109-126.

Daval D., Martinez I., Corvisier J., Findling N., Goffé B., Guyot F. (2009) Carbonation of Ca-bearing silicates, the case of wollastonite: Experimental investigations and kinetic modeling. *Chem. Geol.* **265**, 63-78.

Daval D., Sissmann O., Menguy N., Saldi G.D., Guyot F., Martinez I., Corvisier J., Garcia B., Machouk I., Knauss K.G., Hellmann R. (2011) Influence of amorphous silica layer formation on the dissolution rate of olivine at 90 °C and elevated pCO_2. *Chem. Geol.* **284**, 193-209.

Duan, Z., Sun, R., Zhu, C., Chou, I.M. (2006) An improved model for the calculation of CO_2 solubility in aqueous solutions containing Na^+, K^+, Ca^{2+}, Mg^{2+}, Cl^-, and SO_4^{2-}. *Marine Chemistry* **98**, 131-139.

Federico C., Aiuppa A., Allard P., Bellomo S., Jean-Baptiste P., Parello F., Valenza M. (2002) Magma-derived gas influx and water-rock interactions in the volcanic aquifer of Mt. Vesuvius, Italy. *Geochim. Cosmochim. Acta* **66**, 963-981.

Federico C., Aiuppa A., Favara R., Gurrieri S., Valenza M. (2004) Geochemical monitoring of groundwaters (1998–2001) at Vesuvius volcano (Italy). *J. Volcanol. Geothermal Res.* **133,** 81-104.

Flaathen T.K., Gislason S.R. (2007) The effect of volcanic eruptions on the chemistry of surface waters: The 1991 and 2000 eruptions of Mt. Hekla, Iceland. *J. Volcanol. Geothermal Res.* **164**, 293-316.

Flaathen T.K., Gislason S.R., Oelkers E.H., Sveinbjörnsdóttir Á.E. (2009) Chemical evolution of the Mt. Hekla, Iceland, groundwaters: A natural analogue for CO_2 sequestration in basaltic rocks. *App. Geochem.* **24**, 463-474.

Fridriksson T., Kristjánsson B.R., Ármannsson H., Margrétardóttir E., Ólafsdóttir S., Chiodini G. (2006). CO_2 emissions and heat flow through soil, fumaroles, and steam heated mud pools at the Reykjanes geothermal area, SW Iceland. *App. Geochem.* **21**, 1551-1569.

Galeczka I., Wolff-Boenisch D., Jonsson T., Sigfusson B., Stefansson A., Gislason S.R. (2013) A novel high pressure column flow reactor for experimental studies of CO_2 mineral storage. *App. Geochem.* **30**, 91-104.

Giammar D.E., Bruant Jr R.G., Peters C.A. (2005) Forsterite dissolution and magnesite precipitation at conditions relevant for deep saline aquifer storage and sequestration of carbon dioxide. *Chem. Geol.* **217**, 257-276.

Gislason S.R. and Eugster H.P. (1987) Meteoric water-basalt interactions. II: A field study in N.E. Iceland. *Geochim. Cosmochim. Acta* **51**, 2841-2855.

Gislason S.R., Arnorsson S., Armannsson H. (1996) Chemical weathering of basalt in Southwest Iceland; effects of runoff, age of rocks and vegetative/glacial cover. *Am. J. Sci.* **296**, 837-907.

Gislason S.R., Heaney P.J., Oelkers E.H., Schott J. (1997) Kinetic and thermodynamic properties of moganite, a novel silica polymorph. *Geochim. Cosmochim. Acta* **61**, 1193-1204.

Gislason S.R., Snorrason Á., Kristmannsdóttir H.K., Sveinbjörnsdóttir Á.E., Torsander P., Ólafsson J., Castet S., Dupré B. (2002) Effects of volcanic eruptions on the CO_2 content of the atmosphere and the oceans: the 1996 eruption and flood within the Vatnajökull Glacier, Iceland. *Chem. Geol.* **190**, 181-205.

Gislason S.R., Oelkers E.H. (2003) Mechanism, rates, and consequences of basaltic glass dissolution: II. An experimental study of the dissolution rates of basaltic glass as a function of pH and temperature. *Geochim. Cosmochim. Acta* **67**, 3817-3832.

Gislason S.R., Wolff-Boenisch D., Stefansson A., Oelkers E.H., Gunnlaugsson E., Sigurdardottir H., Sigfusson B., Broecker W.S., Matter J.M., Stute M., Axelsson G., Fridriksson T. (2010) Mineral sequestration of carbon dioxide in basalt: A pre-injection overview of the CarbFix project. *Int. J. Greenhouse Gas Control* **4**, 537-545.

Goldberg D.S., Takahashi T., Slagle A.L. (2008) Carbon dioxide sequestration in deep-sea basalt. *Proc. Natl. Acad. Sci.* **105**, 9920-9925.

Guidelines for Drinking-water Quality, third edition incorporating the first and second agenda, volume 1, recommendation, WHO, Geneva 2008.

Gysi A.P., Stefánsson A. (2011) CO_2–water–basalt interaction. Numerical simulation of low temperature CO_2 sequestration into basalts. *Geochim. Cosmochim. Acta* **75**, 4728-4751.

Gysi A.P., Stefánsson A. (2012) Experiments and geochemical modeling of CO_2 sequestration during hydrothermal basalt alteration. *Chem. Geol.* **306–307**, 10-28.

Hellevang H., Pham V.T.H., Aagaard P. (2013) Kinetic modelling of CO_2–water–rock interactions. *Int. J. Greenhouse Gas Control* **15**, 3-15.

Hövelmann J., Austrheim H., Beinlich A., Anne Munz I. (2011) Experimental study of the carbonation of partially serpentinized and weathered peridotites. *Geochim. Cosmochim. Acta* **75**, 6760-6779.

IPCC, 2005. IPCC Special Report on Carbon Dioxide Capture and Storage, prepared by Working Group III of the Intergovernmental Panel on Climate Change. In: Metz B., Davidson O., de Coninck H., Loos C.M., Meyer L.A. (Eds.), Cambridge University Press.

Kaasalainen H., Stefánsson A. (2012) The chemistry of trace elements in surface geothermal waters and steam, Iceland. *Chem. Geol.* **330-331**, 60-85.

Kelemen P.B., Matter J. (2008) In situ carbonation of peridotite for CO_2 storage. *Proc. Natl. Acad. Sci. USA* **105**, 17295-17300.

Kristmannsdottir H. (1979) Alteration of Basaltic Rocks by Hydrothermal-Activity at 100-300°C. In: M.M. Mortland and V.C. Farmer (Editors), Developments in Sedimentology. Elsevier, pp. 359-367.

Kristmannsdottir H. (1982) Alteration in the IRDP dill hole compared with other drill holes n Iceland. *J. Geophys. Res.* **87**, 6525-6531.

Lindberg R.D., Runnells D.D. (1984) Ground Water Redox Reactions: An Analysis of Equilibrium State Applied to Eh Measurements and Geochemical Modeling. *Science* **225**, 925-927.

Mackenzie F.T., Andersson A.J. (2013) The marine carbon cycle and ocean acidification during phanerozoic time. *Geochem. Perspectives* **2,** 1-227.

Maher K., Steefel C.I., White A.F., Stonestrom D.A. (2009) The role of reaction affinity and secondary minerals in regulating chemical weathering rates at the Santa Cruz Soil Chronosequence, California. *Geochim. Cosmochim. Acta* **73**, 2804-2831.

Marini L. (2007) Geological sequestration of carbon dioxide. Thermodynamics, kinetics and reaction path modeling. Developments in Geochemistry. 1st ed. Amsterdam, Elsevier.

McGrail B.P., Schaef H.T., Ho A.M., Chien Y.-J., Dooley J.J., Davidson C.L. (2006) Potential for carbon dioxide sequestration in flood basalts. *J. Geophys. Res.* **111**, B12201.

Miller Q.R.S., Thompson C.J., Loring J.S., Windisch C.F., Bowden M.E., Hoyt D.W., Hu J.Z., Arey B.W., Rosso K.M., Schaef H.T. (2013). Insights into silicate carbonation processes in water-bearing supercritical CO_2 fluids. *Int. J. Greenhouse Gas Control* **15**, 104-118.

Munz I.A., Brandvoll Ø., Haug T.A., Iden K., Smeets R., Kihle J., Johansen H. (2012) Mechanisms and rates of plagioclase carbonation reactions. *Geochim. Cosmochim. Acta* **77**, 27-51.

Navarre-Sitchler A., Steefel C.I., Sak P.B., Brantley S.L. (2011) A reactive-transport model for weathering rind formation on basalt. *Geochim. Cosmochim. Acta* **75**, 7644-7667.

Navarre-Sitchler A.K., Cole, D.R., Rother G., Jin L., Buss H.L., Brantley S.L. (2013) Porosity and surface area evolution during weathering of two igneous rocks. *Geochim. Cosmochim. Acta* **109**, 400-413.

Oelkers E.H., Gislason S.R. (2001) The mechanism, rates and consequences of basaltic glass dissolution: I. An experimental study of the dissolution rates of basaltic glass as a function of aqueous Al, Si and oxalic acid concentration at 25°C and pH = 3 and 11. *Geochim. Cosmochim. Acta* **65**, 3671-3681.

Oelkers E.H., Gislason S.R., Matter J. (2008) Mineral Carbonation of CO_2. *Elements* **4**, 333-337.

Oelkers E.H., Benezeth P., Pokrovski G.S. (2009) Thermodynamic Databases for Water-Rock Interaction in Reviews in Mineralogy & Geochemistry: Thermodynamics and Kinetics of Water-Rock Interaction. Mineralogical Society of America, **70**, 1-46.

Olsson J., Stipp S., Gislason S.R. (2012a) Calcium carbonate formation at the Eyjafjallajökull volcano: a carbon capture and storage analogue. 30th Nordic Geological Winter Meeting, Reykjavik, Iceland 9-12 January 2012, 174.

Olsson, J., Bovet, N., Makovicky, E., Bechgaard, K., Balogh, Z., Stipp, S.L.S. (2012b) Olivine reactivity with CO_2 and H_2O on a microscale: Implications for carbon sequestration. *Geochim. Cosmochim. Acta* **77**, 86-97.

Parkhurst D.L., Appelo C.A.J. (1999) User's guide to PHREEQC (Version 2) - a computer program for speciation, batch-reaction, one-dimensional transport, and inverse geochemical calculations: U.S. In: Geological Survey Water-Resources Investigations Report 99-4259, 312.

Paukert A.N., Matter J.M., Kelemen P.B., Shock E.L., Havig J.R. (2012) Reaction path modeling of enhanced in situ CO_2 mineralization for carbon sequestration in the peridotite of the Samail Ophiolite, Sultanate of Oman. *Chem. Geol*. **330-331**, 86-100.

Pham V.T.H., Lu P., Aagaard P., Zhu C., Hellevang H. (2011) On the potential of CO_2–water–rock interactions for CO_2 storage using a modified kinetic model. *Int. J. Greenhouse Gas Control* **5**, 1002-1015.

Rani N., Pathak V., Shrivastava J.P. (2013) CO_2 Mineral Trapping: An Experimental Study on the Carbonation of Basalts from the Eastern Deccan Volcanic Province, India. *Proc. Earth Planetary Sci*.**7**, 806-809.

Rogers, K.L., Neuhoff, P.S., Pedersen, A.K., Bird, D.K. (2006) CO_2 metasomatism in a basalt-hosted petroleum reservoir, Nuussuaq, West Greenland. *Lithos* **92**, 55-82.

Saldi G.D., Schott J., Pokrovsky O.S., Gautier Q., Oelkers E.H. (2012) An experimental study of magnesite precipitation rates at neutral to alkaline conditions and 100–200 °C as a function of pH, aqueous solution composition and chemical affinity. *Geochim. Cosmochim. Acta* **83**, 93-109.

Schaef H.T., McGrail B.P. (2009) Dissolution of Columbia River Basalt under mildly acidic conditions as a function of temperature: Experimental results relevant to the geological sequestration of carbon dioxide. *App. Geochem.* **24**, 980-987.

Schaef, H.T., McGrail, B.P., Owen, A.T. (2010) Carbonate mineralization of volcanic province basalts. *Int. J. Greenhouse Gas Control* **4**, 249-261.

Schaef H.T., McGrail B.P., Owen A.T. (2011) Basalt Reactivity Variability with Reservoir Depth in Supercritical CO_2 and Aqueous Phases. *Energy Procedia* **4**, 4977-4984.

Schaef, H.T., McGrail, B.P., Owen, A.T., Arey, B.W. (2013) Mineralization of basalts in the CO_2-H_2O-H_2S system. *Int. J. Greenhouse Gas Control* **16**, 187-196.

Schott J., Oelkers E.H. (1995) Dissolution and crystallization rates of silicate minerals as a function of chemical affinity. *Pure & Appl. Chem*. **67**, 903-910.

Schott, J., Oelkers, E.H., Bénézeth, P., Goddéris, Y., François, L. (2012) Can accurate kinetic laws be created to describe chemical weathering? *Comptes Rendus Geoscience* **344**, 568-585.

Stefánsson A., Gislason S.R. (2001) Chemical Weathering of Basalts, Southwest Iceland: Effect of Rock Crystallinity and Secondary Minerals on Chemical Fluxes to the Ocean. *Am. J. Sci.* **301**, 513-556.

Stefánsson A., Arnórsson S., Sveinbjörnsdóttir Á.E. (2005) Redox reactions and potentials in natural waters at disequilibrium. *Chem. Geol.* **221**, 289-311.

Stockmann G.J., Wolff-Boenisch D., Gislason S.R., Oelkers E.H. (2011) Do carbonate precipitates affect dissolution kinetics? 1: Basaltic glass. *Chem. Geol*. **284**, 306-316.

Stockmann G.J., Wolff-Boenisch D., Gislason S.R., Oelkers E.H. (2013) Do carbonate precipitates affect dissolution kinetics?: 2: Diopside. *Chem. Geol.* **337-338**, 56-66.

Stumm W., Morgan J.J. (1996) Aquatic chemistry. Chemical Equilibria and Rates in Natural Waters. 3rd ed. New York, John Wiley & Sons, p. 683.

Trautz R.C., Pugh J.D., Varadharajan C., Zheng L., Bianchi M., Nico P.S., Spycher N.F., Newell D.L., Esposito R.A., Wu Y., Dafflon B., Hubbard S.S., Birkholzer J.T. (2012) Effect of Dissolved CO_2 on a Shallow Groundwater System: A Controlled Release Field Experiment. *Environ. Sci. Technol* **47**, 298-305.

Weltje G.J., Alberts L.J.H. (2011) Packing states of ideal reservoir sands: Insights from simulation of porosity reduction by grain rearrangement. *Sedimentary Geol.* **242**, 52-64.

White A.F., Brantley S.L. (2003) The effect of time on the weathering of silicate minerals: why do weathering rates differ in the laboratory and field? *Chem. Geol.* **202**, 479-506.

WHO (2008) Guidelines for Drinking-water Quality. Third edition incorporating the first and second agenda. Volume 1, Recommendations. Geneva.

Wiese F., Fridriksson Th., Armannsson H. (2008) CO_2 fixation by calcite in high-temperature geothermal systems in Iceland. Report for Icelandic GeoSurvey ISOR, Reykjavik, ISOR-2008/003.

Wolff-Boenisch D. (2011) On the buffer capacity of CO_2-charged seawater used for carbonation and subsequent mineral sequestration. *Energy Procedia* **4**, 3738-3745.

Wolff-Boenisch D., Gislason S.R., Oelkers E.H., Putnis C.V. (2004) The dissolution rates of natural glasses as a function of their composition at pH 4 and 10.6, and temperatures from 25 to 74 °C. *Geochim. Cosmochim. Acta* **68**, 4843-4858.

Wolff-Boenisch D., Wenau S., Gislason S.R., Oelkers E.H. (2011) Dissolution of basalts and peridotite in seawater, in the presence of ligands, and CO_2: Implications for mineral sequestration of carbon dioxide. *Geochim. Cosmochim. Acta* **75**, 5510-5525.

Zheng L., Apps J.A., Spycher N., Birkholzer J.T., Kharaka Y.K., Thordsen J., Beers S.R., Herkelrath W.N., Kakouros E., Trautz R.C. (2012) Geochemical modeling of changes in shallow groundwater chemistry observed during the MSU-ZERT CO_2 injection experiment. *Int. J. Greenhouse Gas Control* **7**, 202-217.

Zhu C., Veblen D.R., Blum A.E., Chipera S.J. (2006) Naturally weathered feldspar surfaces in the Navajo Sandstone aquifer, Black Mesa, Arizona: Electron microscopic characterization. *Geochim. Cosmochim. Acta* **70**, 4600-4616.

Zhu C., Lu P. (2009) Alkali feldspar dissolution and secondary mineral precipitation in batch systems: 3. Saturation states of product minerals and reaction paths. *Geochim. Cosmochim. Acta* **73**, 3171-3200.

Chapter 4

Experimental studies of basalt-H_2O-CO_2 interaction with a high pressure column flow reactor: The mobility of metals

Iwona Galeczka, Domenik Wolff-Boenisch and Sigurdur R. Gislason

Galeczka I., Wolff-Boenisch D., Gislason S.R. (2013) Experimental studies of basalt-H_2O-CO_2 interaction with a high pressure column flow reactor: the mobility of metals.
Energy Procedia **37**, 5823-5833

Abstract

Here, we report on the mobility of metals at the early stage of CO_2 injection into basalt, before significant precipitation of secondary minerals. Short-lived pulses (50-100 hours) of CO_2-charged water were injected into a high pressure column flow reactor filled with basaltic glass grains at 22 °C, 8 MPa of total pressure and a velocity of ~0.5 cm/min. The residence time of the water within the column ranged from 8 to 10 hours. The column was conditioned with pure water, resulting in alkaline outflow (pH ~9). The pH of the inlet CO_2-charged water was ~3.2, and the lowest pH measured in the column was 4.5, after less than 10 hours of water/rock interaction. The dissolved metal concentrations and metals relative mobility increased dramatically during the CO_2-pulses; more than 100 times for Sr, Fe, Al, Ca, Ba, Mn, and Mg. Of these elements, all but Al can bind with CO_2 to form carbonate minerals. Only the dissolved Al, Fe, Mn and Cr concentrations exceeded allowable drinking water limits. After the CO_2-pulses, all of the elemental concentrations decreased close-to or even below what was measured during the conditioning of the column. The pH never reached ~9 which was the initial pH before CO_2-pulses.

4.1. INTRODUCTION

The safest way of carbon sequestration is mineral carbonatization, when CO_2 is fixed as stable carbonate minerals (IPCC, 2005; Oelkers et al., 2008). Mineral storage requires combining CO_2 with divalent cations such as Ca^{2+}, Mg^{2+} and Fe^{2+} which are the constituents of the host rock. Basalts and ultramafic rocks are the

largest and the most efficient sources of these elements on Earth (e.g. McGrail et al., 2006). This is underscored by the fact that despite basalt covering less than 10% of the Earth's continental surface its weathering consumes up to 33% of all the CO_2 fixed during weathering of Earth's terrestrial silicates (Dessert et al., 2003). The oceanic floor covering about 70% of the Earth's surface is mostly made of basalt. The large volumes of mafic (basalt) and ultramafic rocks on the Earth's surface have large CO_2 sequestration capacities. Examples of locations where CO_2 could be injected and allowed to react with the host rock to form carbonates are large igneous provinces, such as the Columbia River basalts, Deccan and Siberian traps, and smaller outcrops of oceanic basaltic crust such as Iceland (Oelkers et al., 2008). The CarbFix CO_2 sequestration pilot project in Iceland (Gislason et al., 2010; Arádottir et al., 2012) has been established to investigate the potential for *in situ* mineral carbon storage in basalt. The injected CO_2-saturated waters are predicted to enhance basalt dissolution, leading to the release of divalent metals into the percolating solution. As a result of proton consumption by basalt dissolution, pH increases followed by carbonate ($(Ca,Mg,Fe)CO_3$) precipitation (Arádottir et al., 2012; Gislason et al., 2012; McGrail et al., 2006; Oelkers et al., 2008). Another field project, the Wallula Basalt Sequestration Pilot Project in the USA, was designed to confirm the feasibility of safe sequestration of large quantities of supercritical CO_2 within a deep flood basalt formation (McGrail et al., 2011). Laboratory studies investigating the efficiency of *in situ* CO_2 storage have mainly focused on the secondary products of the basalt/CO_2-H_2O/CO_2-H_2S/CO_2/$scCO_2$ interaction (Gysi and Stefánsson, 2012; Schaef et al., 2010; Schaef et al., 2011). The basalt, when reacting with the CO_2-charged water, does not only release divalent cations that end up in carbonates, but also releases other metals that can be harmful to biota. The main metals of concern are Al and Cr. Some other elements such as Fe and Mn, for example, can be both essential for life and toxic depending on their concentration. The toxic metal release is the most dangerous at the early stage of injection, when the CO_2-charged water is still at low pH, 3-5, and the metals are mobile. This is before significant precipitation of carbonates, clays, Al- and Fe- oxides and hydroxides that will eventually scavenge the metals (Flaathen et al., 2009).

A novel high pressure column flow reactor (Galeczka et al., 2013) provides an opportunity to study the relative mobility of metals at the early stage of the CO_2 injection into basalt. In this study we report on the consequences of short-lived (50-100 hours) CO_2-pulses injected into the column filled with basaltic slurry at 22 °C and 8 MPa of total pressure. Results of this study will help the understanding of how the basalt-water system responds to sudden changes caused by CO_2 flux and how it returns to pH neutrality after the CO_2-pulse ends. The outcome of this experiment is not only applicable to industrial CO_2 storage but also to natural

processes such as sudden magmatic CO_2 fluxes into groundwater systems in volcanic terrains such as Iceland (Flaathen et al., 2009).

4.2. MATERIALS AND METHODS

The experiment was carried out in a high pressure column flow reactor (HPCFR) (Galeczka et al., 2013). Liquid CO_2 was mixed with degassed deionized (DI) water and pumped through a vertical column filled with basaltic glass powder. Dissolution and precipitation reactions took place inside the HPCFR and reaction progress was monitored via outlet solute sampling together with pH/Eh measurement (Fig. 1). Basaltic glass used in this study was collected from the Stapafell Mountain located in SW Iceland. The composition of the material is similar to that of mid-ocean ridge basalt (MORB) and its dissolution kinetics was reported in previous studies (Oelkers and Gislason, 2001; Stockmann et al., 2011; Wolff-Boenisch et al., 2011). Its chemical composition is consistent with $Si_{1.0}Ti_{0.024}Al_{0.355}Fe_{0.207}Mg_{0.276}Ca_{0.265}Na_{0.073}K_{0.007}O_{3.381}$. The material was crushed in a jaw crusher and dry sieved to obtain the particle size fraction of 45-100 µm which was subsequently washed by repeated gravitational settling to remove ultrafine particles. The total mass of dry glass particles inside the column was 8.3 kg, the corresponding specific BET surface area equalled 22,000 cm^2/g, while the total surface area amounted to ~182,000,000 cm^2. The total mass of aqueous solution, within the column at a given time during the experiment, was 1.84 L assuming 40% porosity, yielding a surface area to solution volume ratio of ~10^5 cm^{-1}.

Due to corrosive nature of CO_2-charged water, nearly the entire reactor was made either of titanium (Ti), Hastelloy® C-276 (HC), or PEEK. The titanium column measures 234×5.8×5.0 cm [L×OD×ID] and holds a total volume of ~4.6 L. The inlet is placed at the bottom of the vertically aligned column to spread the percolating fluid perpendicular to the flow axis and thus to avoid preferential flow paths via gravitational resistance and lateral spread. In this study sampling of the solution was done just through the main outlet; however the HPCFR has additionally seven lateral sampling outlets, one in each compartment which can be used to sample the solution along the flow path as it is described in Galeczka et al. (2013). From the column the solution flowed through a pH and Eh electrode cross (Corr Instruments) where pH and Eh were determined in-line which corresponded to *in situ* pH and Eh. The elevated pressure in the reactor was maintained with a back pressure regulator (BPR, Swagelok®) at the end of the sampling line. The column was wrapped with a heating Tape (HTS/Amptec) keeping the experimental temperature at 22 °C ± 1°. The liquid CO_2 cylinder was placed on a scale and its status was monitored through mass loss. The cylinder was connected to a supercritical fluid pump (Supercritical Fluid Technologies). Degassed DI (deionized water) water was delivered by high pressure liquid chromatography pump, HPLC (Supercritical Fluid Technologies). Both fluids

were mixed in a flow-through Ti reactor like the ones routinely employed in mineral dissolution studies (Wolff-Boenisch et al., 2011).

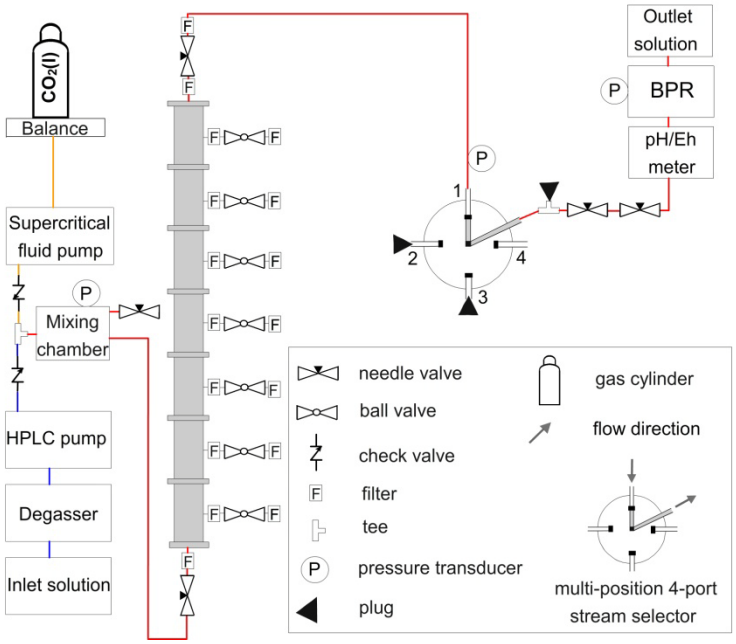

Figure 1. The high pressure column flow reactor (HPCFR). The CO_2 was dissolved in DI water in the mixing chamber and flowed through the column followed by a multi-position 4-port stream selector, and through the pH/Eh cross where pH/Eh was determined in-line. Liquid samples for major and trace elements were eventually collected at ambient pressure from the back pressure regulator (BPR).

The experiment started with DI water being pumped through the column at 5 ml/min, 22°C and 0.1 MPa for 2500 hours to condition the system. Then, the total/hydraulic pressure was increased to 8 MPa followed by $CO_{2(l)}$ injection. The total pressure and the flow rates of water and liquid CO_2 were set to ensure that the $CO_{2(l)}$ was fully dissolved in the water before entering the column. During the first CO_2-pulse the water was pumped at 3.5 mL/min and $CO_{2(l)}$ at 0.22 mL/min for 100 hours. The residence time of the CO_2-charged water within the column was ~8.5 hours. The residence time is calculated by the total volume of the solution inside the column divided by the sum of the individual pump flow rates. During the second CO_2-pulse water was delivered at 3.0 ml/min and $CO_{2(l)}$ at 0.13 ml/min which corresponds to the residence time of ~10 hours. The duration of the second pulse was 50 hours. Initial measured dissolved inorganic carbon (DIC) concentration was ~1.2 mol/L during the first CO_2-pulse and ~0.8 mol/L during the second CO_2-pulse. Based on the initial DIC concentration, the calculated pH of the CO_2-charged water was 3.14 during the first pulse and 3.24 during the second pulse. It took approximately 44 hours (~5 pore volumes) to replace the initial reacted solution of pH ~9, which was the result of pure water-basaltic glass interaction, with the CO_2-charged water and to decrease the *in situ* pH to ~4.5. The outlet solution

was sampled, filtered using a 0.2 μm cellulose acetate filter, and then acidified with concentrated supra-pure HNO_3 prior to analysis for major elements with Inductively Coupled Plasma Optical Emission Spectrometer (ICP-OES). Analytical uncertainties of ICP-OES analyses are in the order of ≤5%. Selected samples were analyzed for trace elements and rare earth elements (REE) by Inductively Coupled Plasma Quadrupole Mass Spectrometer (ICP-QMS) and/or Sector Field Inductively Coupled Plasma Mass Spectrometer (ICP-SFMS).

The saturation state of the basaltic glass and selected secondary minerals with respect to the solution was determined with the PHREEQC 2.17 computer code (Parkhurst and Appelo, 1999) based on the outlet chemical composition, *in situ* pH and Eh. The database used in this study was *phreeqc.dat* which was updated with Cr thermodynamic properties from *llnl.dat* and the minerals of interest from Gysi and Stefánsson (2011). Secondary phases were chosen based on natural analogues and previous experimental work (Gysi and Stefánsson, 2012; Rogers et al., 2006; Stefánsson and Gislason, 2001). The dissolved inorganic carbon concentration (DIC) in the outlet was determined by PHREEQC, using the measured chemical composition together with the *in situ* pH and forcing a charge balance. The inlet DIC concentration was measured directly from the mixing chamber with the expander transducer method (Galeczka et al., 2013).

4.3. RESULTS AND DISCUSSION

The experiment can be divided into five stages. The first stage corresponds to pure water (DI water) conditioning of the column when DI water was pumped through the reactor. The solute chemistry is represented by the steady-state elemental concentrations of the last samples taken during this stage and it is shown by the first data point on the diagrams in Fig. 2 and 4. The water chemistry at this stage is similar to the chemistry of the groundwater in basaltic terrains which are characterized by high pH 9-10 (Gislason and Eugster, 1987). The second stage was the first CO_2-pulse, lasting for 100 hours (four days) when the CO_2-charged water entered the system which had been conditioned with DI water during the first stage. During this stage, the *in situ* pH dropped to 4.5 as shown in Fig. 2. In the third stage DI water replaced the CO_2-charged water and the pH rose towards neutrality. The fourth stage is the second CO_2-pulse lasting for 50 hours. This pulse started about two months after the first CO_2-pulse had ended. In the fifth stage DI water replaced the CO_2-charged water. Similar to the third stage, the system returned to its pH neutrality due to the DI water replacement of the CO_2-charged water from the second pulse.

Time series for the pH and selected dissolved elements in the outlet, during the five stages are shown in Fig. 2. The pH decreased rapidly when CO_2-charged water

was pumped through the column, resulting in enhanced release of the elements from the rock. The lowest pH measured during both CO_2-pulses was 4.5.

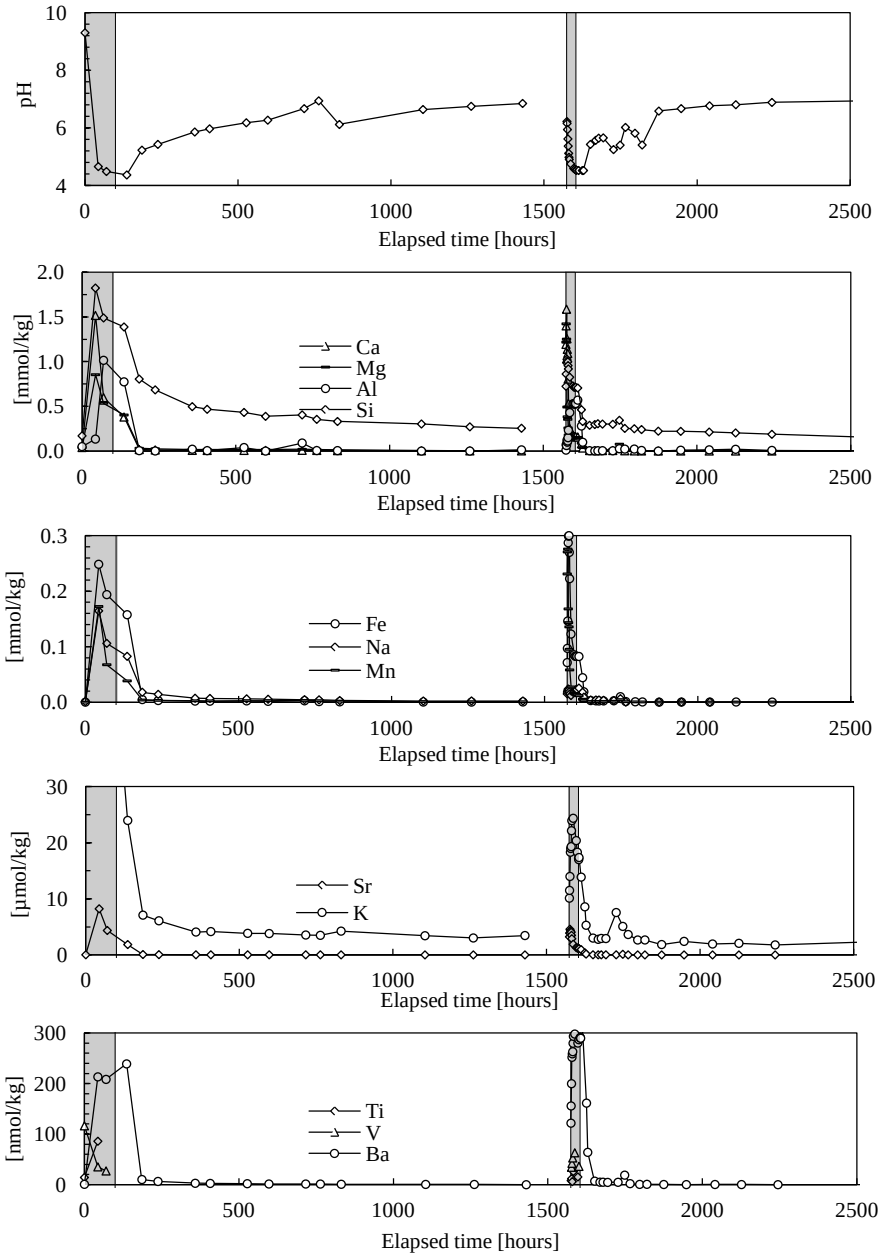

Figure 2. Results of chemical analyses of samples taken during the five stages of the experiment. First data points in all the plots represent the chemistry of the first stage of the experiment during pure water conditioning of the column. Data points in the shadowed fields correspond to the first and the second CO_2-pulse respectively. All other data points represent the third and fifth stage of the experiment when the system returned to its pH neutrality due to pure water replacement of CO_2-charged water pumped during the CO_2-pulses.

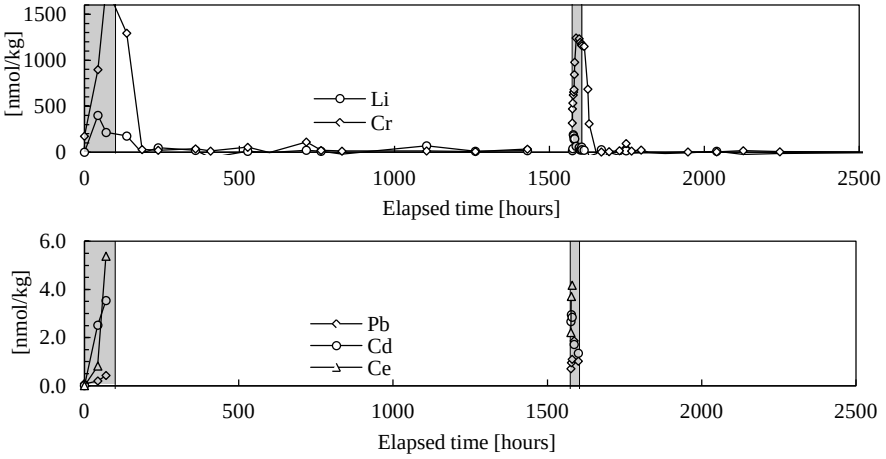

Figure 2. Continuation.

The concentrations of all elements increased significantly compared to the concentrations before and after the CO_2-pulses.The sampling resolution during the second CO_2-pulse allowed assignment of the highest concentrations of the elements to the pH. The highest concentrations of major elements were detected at pH 6.2 for Mg (1.42 mmol/kg); 5.9 for Ca (1.59 mmol/kg), Sr (4.58 µmol/kg) and Mn (275.8 µmol/kg); 5.6 for Si (1.03 mmol/kg) and Na (0.024 mmol/kg); 5.1 for Fe (0.3 mmol/kg); 4.7 for Ti (26.1 nmol/kg), Ba (298.2 nmol/kg) and Cr (1.24 µmol/kg); 4.6 for Al (0.53 mmol/kg). The relative mobility (the water concentration divided by the rock composition, of major, minor and trace elements) increased considerably during the CO_2-pulses compared to the mobility before and after the CO_2-pulses (Figs. 3a, b and c). The mobility of individual elements was time dependent, reflecting the pH dependence of the maximum concentrations of the elements in the CO_2-charged water as described in the previous paragraph. The elements with the highest (B, Mo, K,) and the lowest (Al, Fe, Ti) mobility during the water conditioning of the column (Fig. 3b) are also among the most and the least mobile elements in natural basaltic groundwater and surface water systems (Eiriksdottir et al., 2008; Gislason et al., 2002). During the CO_2-pulses the relative mobility for all but one element (V) increased, as shown in Fig. 3a. The most mobile elements were Sr, Mn, K, Cd, Mo, B, and Ti is still among the least mobile elements. Many dissolved elements with the concentrations below the detection limits during the conditioning of the column (Cd, As and REE) increased considerably in concentrations during the CO_2-pulses. The enrichment ratio (the relative mobility during the CO_2-pulses, divided by the relative mobility during the DI water conditioning of the column) is shown in Fig. 3c. The relative mobility increased more than 100 times for Sr, Fe, Al, Ca, Ba, Mn, and Mg. Of these elements, all but Al, can bind with carbonate to form carbonate minerals.

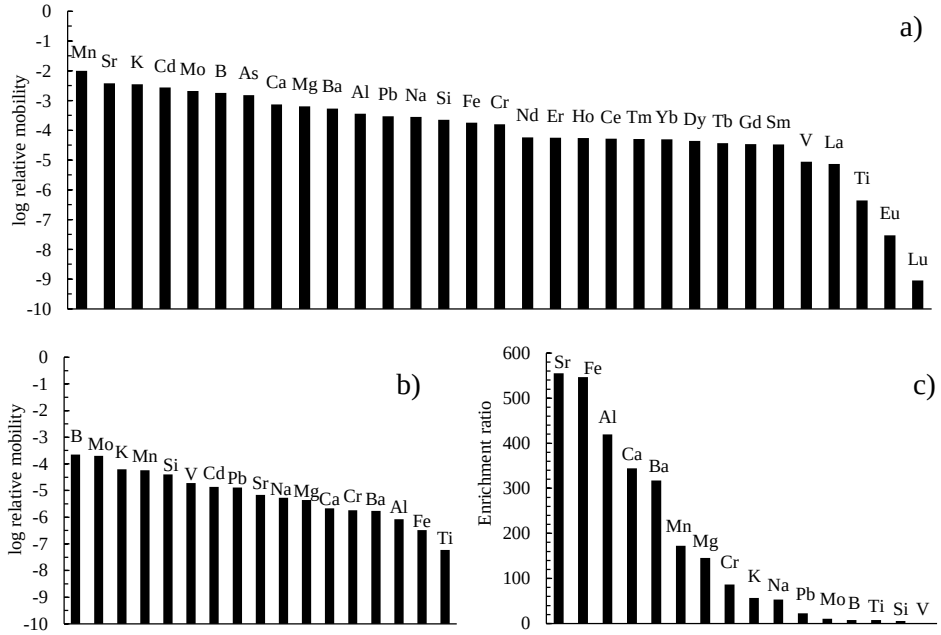

Figure 3. The relative mobility of the measured elements in sampled solution: a) the maximum relative mobility during the CO_2-pulses, b) the steady-state relative mobility during the conditioning of the column, c) the enrichment ratio of the measured elements during both CO_2-pulses.

According to the European Directive relating to the quality of the water intended for human consumption (80/778/EEC, 1980), only the dissolved Al, Fe, Cr and Mn, exceeded allowable drinking water limits (Fig. 4). All of the other measured elemental concentrations were below the drinking water limits. Dissolved Al^{3+} is toxic to plants and animals (Gensemer and Playle, 1999). High concentration of manganese affects the human nervous system, respiratory tract and the brain. Similarly, iron can accumulate in vital organs, such as the pancreas, liver and heart. Stored iron produces free radicals, which can cause tissue damage, inflammation and organ failure. High concentration of chromium in the surface waters can damage the gills of fish. In animals chromium can cause respiratory problems, a lower ability to fight diseases, birth defects, infertility and tumour formation. The health hazards associated with exposure to chromium are dependent on its oxidation state. The hexavalent form is toxic and carcinogenic (Chandra Babu et al., 2005). According to the PHREEQC modelling of the outlet solution, the most abundant dissolved Al species was the toxic Al^{3+}. This is due to the low pH, during the CO_2-pulses. During the recovery of the system to its pH neutrality, the dissolved Al species changed to less toxic Al-OH species and the overall concentration decreased (Fig. 4).

Speciation of the dissolved Cr did not change during the experimental stages and it was mostly in the Cr^{3+} form, which is not dangerous for human health. Mixing of the CO_2-pulse water with oxygen rich water can make the dissolved Cr carcinogenic

by oxidizing it to Cr^{6+}. On the other hand mixing with oxygen rich water will oxidize Fe^{2+} to Fe^{3+}, which will cause the less soluble Fe^{3+} to precipitate as Fe-oxy-hydroxides and lower Fe concentration in the solution. The Fe-oxy-hydroxides could furthermore scavenge toxic metals like the Cr^{6+}.

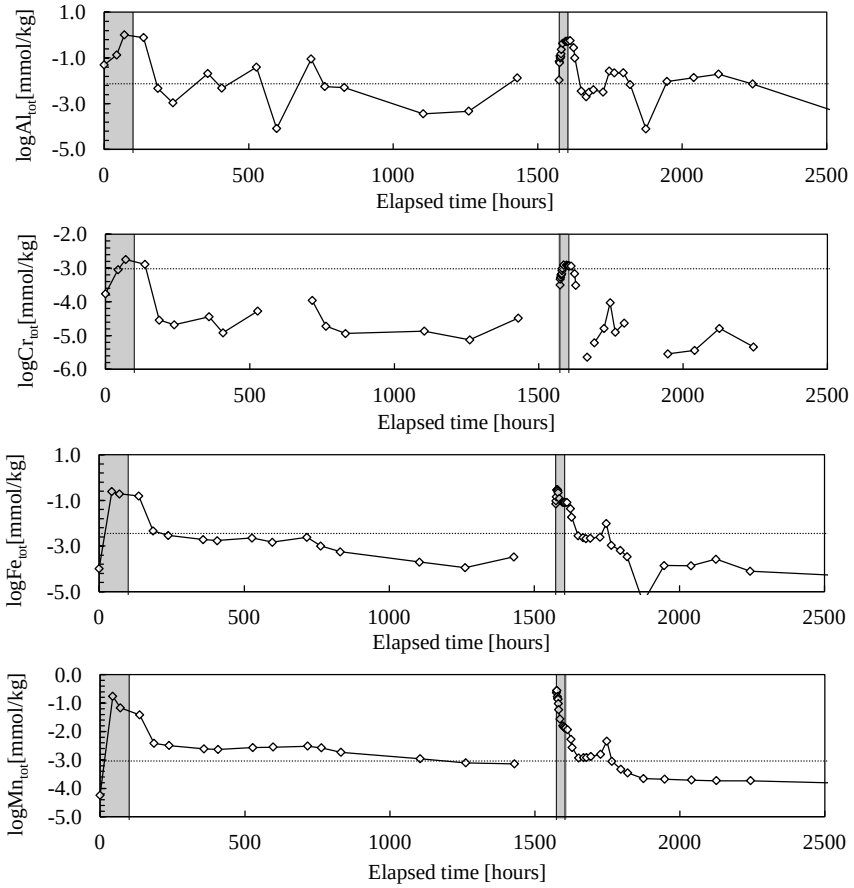

Figure 4. Total concentrations of the measured elements which exceeded the drinking water limits during the experiment according to the European Directive (80/778/EEC). First data points in all the plots represent the elemental concentrations during the DI water conditioning of the column. Data points in the grey fields correspond to the first and the second CO_2-pulse respectively. All other data points represent the third and the fifth stage when DI water was replacing the CO_2-charged water injected during the CO_2-pulses. Horizontal line is the upper limit for drinking water established by European Commission.

The pH can govern the mobility of the toxic metals through its effect on the surface charge. At low pH metals show zero sorption to surfaces (Appelo and Postma, 2005). The surfaces are positively charged meaning that the cations will not be adsorbed, despite the fact that secondary Al-, Fe-, Si- phases can potentially precipitate and create a surface to adsorb the metals on. When the pH increases, due to dilution/dissolution of basalt along the flow path – surfaces become negatively

charged resulting in adsorption of metals. The concentrations of the toxic metals Pb, Cd, As and Hg were low during the CO_2-pulses, 1.85, 3.5, 2.5 and 0.05 nmol/kg respectively and were below the drinking water limits. After the CO_2-pulses ended, all the elemental concentrations decreased close-to or even below the concentrations measured during the conditioning of the column. The pH never reached ~9 which was the initial *in situ* pH during the conditioning of the system.

The saturation states of the aqueous solution with respect to the most important secondary minerals during and after the CO_2-pulses are shown in Fig. 5. The sampled solution was supersaturated with respect to the carbonates: siderite, ankerite and $(Ca,Mg,Fe)CO_3$ just during the first hours of the second CO_2-pulse when the CO_2 was already in the system but the pH was still high enough (~6) to make the water supersaturated with respect to these phases. The solution was supersaturated with respect to gibbsite during all the experimental stages. The water was most often supersaturated with respect to Si-, Al-, Fe- phases such as amorphous $Al(OH)_3$, goethite, kaolinite and imogolite; however when the pH reached its minimum at ~4.5 the solutions became undersaturated with respect to these phases and supersaturated again after the pH increased to ~5.5-6.

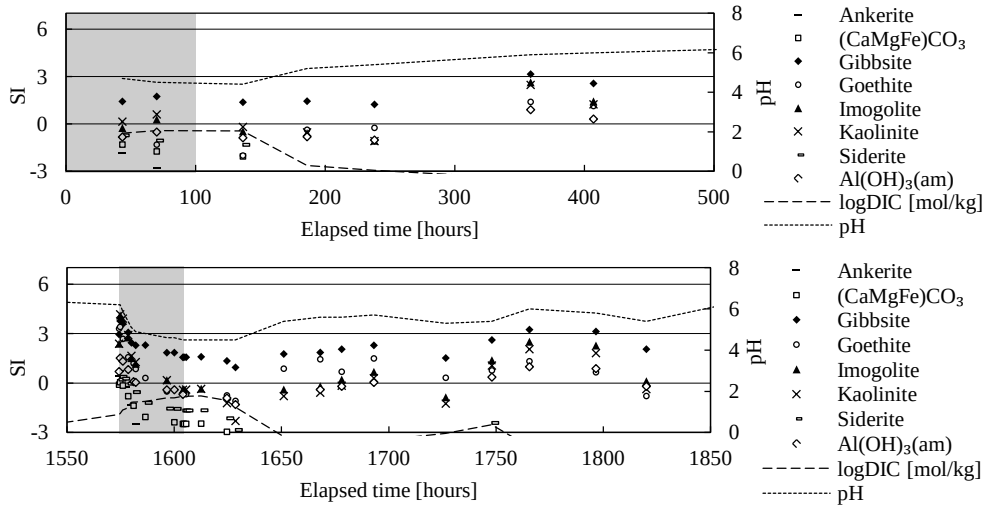

Figure 5. The saturation indices (SI) of the chosen minerals with respect to the water samples taken during the CO_2-pulses (data points in the shadowed field) and during the recovery of the system when DI water was replacing the CO_2-charged water injected previously. The concentration of DIC was calculated using PHREEQC.

When the second CO_2-pulse started and pH decreased, these secondary Si-, Al-, Fe-phases may have dissolved releasing Si, Al, Fe and also other minor elements which were perhaps scavenged by these secondary phases. According to Kaasalainen and Stefánsson (2012) mineral phases scavenging Cr, Fe and Mn observed in low to neutral pH basaltic environments are among others: goethite, amorphous $Fe(OH)_3$

and hematite. In these environments, most of the Al is consumed by amorphous $Al(OH)_3$ and gibbsite limiting Al concentration in solution.

4.4. CONCLUSIONS

The injection of the CO_2-charged water into the high pressure column flow reactor filled with the basalt slurry increased the elemental mobility of basaltic glass constituents significantly. The dissolution rate of basaltic glass is pH dependant. The CO_2-charged water changed the pH conditions from basic/neutral to acidic causing faster dissolution of the rock. The laboratory experimental CO_2-pulses described in this study mimicked very well natural processes such as magmatic CO_2 admixture into the groundwater systems or industrial CO_2 storage when the CO_2-charged water is injected into basaltic aquifers (Arádottir et al., 2012; Flaathen et al., 2009; Gislason et al., 2010). Basalt releases not only elements essential for life but also those that are toxic and dangerous for the environment. Results of the experiment showed high concentrations of potentially harmful elements such as Cr and Al. Other elements such as Fe and Mn can be dangerous if the concentrations exceed the drinkable limit and this happened during the experimental CO_2-pulses. Elements released from the host rock can pose an environmental problem and their mobility and fate have to be considered and monitored when designing the CO_2 injection system for CO_2 storage.

Saturation state calculations indicate that carbonate precipitation could happen just in the beginning of the CO_2-pulse when the water was still at neutral pH but the release rate of divalent elements such as Fe, Ca, and Mg was high enough to reach saturation with respect to the carbonate minerals. Similar conditions may occur during the industrial injection of CO_2 at some distance from the injection well when dilution and/or H_2O-CO_2-basalt interaction will increase the pH in presence of CO_2. Other phases which could precipitate from the experimental solution were Fe-, Al-, Si- phases which immobilize the toxic Al and in addition can scavenge other toxic elements such as Cr. The pH and Eh conditions will play a crucial role in elemental speciation and have to be considered during the CO_2 injection.

Acknowledgements

This study is part of the CarbFix project (www.carbfix.com) in Iceland and was funded by the European Union through the European Marie Curie network Delta-Min (Mechanisms of Mineral Replacement Reactions; Grant# PITN-GA-2008-215360) and SP1-Cooperation (FP7-ENERGY-2011-1; Grant# 283148), Reykjavík Energy, University of Iceland and RANNÍS, Icelandic Fund for Research Equipment; Grant# 10/0293 and 121071-0061). The authors would like to thank all colleagues and co-workers at University of Iceland and Reykjavik Energy.

References

Appelo C.A.J., Postma D. (2005) Geochemistry, groundwater and pollution. 2nd ed. Amsterdam, CRC Press.

Aradóttir E.S.P., Sonnenthal E.L., Björnsson G., Jónsson H. (2012) Multidimensional reactive transport modeling of CO_2 mineral sequestration in basalts at the Hellisheidi geothermal field, Iceland. *Int. J. Greenhouse Gas Control* **9**, 24-40.

Chandra Babu N.K., Asma K., Raghupathi A., Venba R., Ramesh R., Sadulla S. (2005) Screening of leather auxiliaries for their role in toxic hexavalent chromium formation in leather-posing potential health hazards to the users. *J. Cleaner Production* **13** 1189-1195.

Dessert C., Dupré B., Gaillardet J., François L.M., Allègre C.J (2003) Basalt weathering laws and the impact of basalt weathering on the global carbon cycle. *Chem. Geol.* **202**, 257-273.

Eiriksdottir E.S., Louvat P., Gislason S.R., Óskarsson N., Hardardóttir J. (2008) Temporal variation of chemical and mechanical weathering in NE Iceland: Evaluation of a steady-state model of erosion. *Earth and Planetary Sci. Letters* **272** 78-88.

European Community. Council directive 80/778/EC of 15 July 1980 relating to the quality of water intended for human consumption as amended by Council Directives 81/858/EEC and 91/692/EEC (further amended by Council Regulation 1882/2003/EC).

Flaathen T.K., Gislason S.R., Oelkers E.H., Sveinbjörnsdóttir Á.E. (2009) Chemical evolution of the Mt. Hekla, Iceland, groundwaters: A natural analogue for CO_2 sequestration in basaltic rocks. *App. Geochem.* **24**, 463-474.

Galeczka I., Wolff-Boenisch D., Jonsson T., Sigfusson B., Stefansson A., Gislason S.R. (2013) A novel high pressure column flow reactor for experimental studies of CO_2 mineral storage. *App. Geochem.* **30**, 91-104.

Gensemer R.W., Playle R.C. (1999) The Bioavailability and Toxicity of Aluminum in Aquatic Environments. Critical Reviews in *Environ. Sci. Technol.* **29**, 315-450.

Gislason S.R. and Eugster H.P. (1987) Meteoric water-basalt interactions. II: A field study in N.E. Iceland. *Geochim. Cosmochim. Acta,* **51**, 2841-2855.

Gislason S.R., Snorrason Á., Kristmannsdóttir H.K., Sveinbjörnsdóttir Á.E., Torsander P., Ólafsson J., Castet S., Dupré B. (2002) Effects of volcanic eruptions on the CO_2 content of the atmosphere and the oceans: the 1996 eruption and flood within the Vatnajökull Glacier, Iceland. *Chem. Geol.* **190**, 181-205.

Gislason S.R., Wolff-Boenisch D., Stefansson A., Oelkers E.H., Gunnlaugsson E., Sigurdardottir H., Sigfusson B., Broecker W.S., Matter J.M., Stute M., Axelsson G., Fridriksson T. (2010) Mineral sequestration of carbon dioxide in basalt: A pre-injection overview of the CarbFix project. *Int. J. Greenhouse Gas Control* **4**, 537-545.

Gysi A.P., Stefánsson A. (2011) CO_2-water-basalt interaction. Numerical simulation of low temperature CO_2 sequestration into basalts. *Geochim. Cosmochim. Acta* **75**, 4728-4751.

Gysi A.P., Stefánsson A. (2012) Mineralogical aspects of CO_2 sequestration during hydrothermal basalt alteration – An experimental study at 75 to 250 °C and elevated pCO_2. *Chem. Geol*. **306-307**, 146-159.

IPCC, 2005. IPCC Special Report on Carbon Dioxide Capture and Storage, prepared by Working Group III of the Intergovernmental Panel on Climate Change. In: Metz B., Davidson O., de Coninck H., Loos C.M., Meyer L.A. (Eds.), Cambridge University Press.

Kaasalainen H., Stefánsson A. (2012) The chemistry of trace elements in surface geothermal waters and steam, Iceland. *Chem. Geol.* **330-331**, 60-85.

McGrail B.P., Schaef H.T., Ho A.M., Chien Y.-J., Dooley J.J., Davidson C.L. (2006) Potential for carbon dioxide sequestration in flood basalts. *J. Geophys. Res.* **111**, B12201.

McGrail B.P., Spane F.A., Sullivan E.C., Bacon D.H, Hund G. (2011) The Wallula basalt sequestration pilot project. *Energy Procedia* **4**, 5653-5660.

Oelkers E.H., Gislason S.R. (2001) The mechanism, rates and consequences of basaltic glass dissolution: I. An experimental study of the dissolution rates of basaltic glass as a function of aqueous Al, Si and oxalic acid concentration at 25°C and pH = 3 and 11. *Geochim. Cosmochim. Acta* **65**, 3671-3681.

Oelkers E.H., Gislason S.R., Matter J. (2008) Mineral Carbonation of CO_2. *Elements* **4**, 333-337.

Parkhurst D.L., Appelo C.A.J. (1999) User's guide to PHREEQC (Version 2) - a computer program for speciation, batch-reaction, one-dimensional transport, and inverse geochemical calculations: U.S. In: Geological Survey Water-Resources Investigations Report 99-4259, 312.

Rogers K.L., Neuhoff P.S., Pedersen A.K., Bird D.K. (2006) CO_2 metasomatism in a basalt-hosted petroleum reservoir, Nuussuaq, West Greenland. *Lithos* **92**, 55-82.

Schaef H.T., McGrail B.P., Owen A.T. (2010) Carbonate mineralization of volcanic province basalts. *Int. J. Greenhouse Gas Control* **4**, 249-261.

Schaef H.T., McGrail B.P., Owen A.T. (2011) Basalt Reactivity Variability with Reservoir Depth in Supercritical CO_2 and Aqueous Phases. *Energy Procedia* **4**, 4977-4984.

Stefánsson A., Gislason S.R. (2001) Chemical Weathering of Basalts, Southwest Iceland: Effect of Rock Crystallinity and Secondary Minerals on Chemical Fluxes to the Ocean. *Am. J. Sci.* **301**, 513-556.

Stockmann G.J., Wolff-Boenisch D., Gislason S.R., Oelkers E.H. (2011) Do carbonate precipitates affect dissolution kinetics? 1: Basaltic glass. *Chem. Geol*. **284**, 306-316.

Wolff-Boenisch D., Wenau S., Gislason S.R., Oelkers E.H. (2011) Dissolution of basalts and peridotite in seawater, in the presence of ligands, and CO_2: Implications for mineral sequestration of carbon dioxide. *Geochim. Cosmochim. Acta* **75**, 5510-5525.

Chapter 5

The chemistry and element fluxes of the July 2011 Múlakvísl and Kaldakvísl glacial floods, Iceland

Iwona Galeczka, Eric H. Oelkers and Sigurdur R. Gislason

Submitted to Journal of Volcanology and Geothermal Research, August 26, 2013

Abstract

This study describes the chemical composition and fluxes of two ~2,000 m^3/s glacial floods which emerged from the Icelandic Mýrdalsjökull and Vatnajökull glaciers into the Múlakvísl and Kaldakvísl Rivers in July 2011. Water samples collected during both floods had neutral to alkaline pH and a conductivity from 100 to 900 µS/cm. Alkalinity, present mostly as HCO_3^-, was ~9 meq/kg during the flood peak in Múlakvísl but stabilized at around 1 meq/kg; a similar behaviour was observed at Kaldakvísl. Up to 1.5 µmol/kg of H_2S was detected. Concentrations of most of dissolved constituents in the flood waters were comparable to those commonly observed in these rivers. In contrast, particulate suspended material concentration increases dramatically during the floods and dominates chemical transport during these events. Waters were supersaturated with respect to a number of clays, zeolites, carbonates, and Fe(oxy)hydroxides. The most soluble elements were Na, Ca, K, Sr, Mn, and Mg whereas the least soluble were Ti, Al, and REE. This is consistent with typical basaltic surface waters and the composition of global rivers in general. The concentrations of toxic metals were below drinking water limits suggesting that there was no detrimental effect of flood water chemistry on the environment. Increased concentration of DOC, formate, and acetate in the flood waters suggests substantial sub-glacial microbiological activity in the melt water prior to the floods. Reaction path modelling of the flood water chemical evolution suggests that it experienced sub-glacial water-rock interaction over at least a few years in the presence of limited amounts of acid gases (e.g. H_2SO_4, HCl and HF). This suggests that the heat source for glacier melting forming the flood water was geothermal rather than volcanic.

5.1. INTRODUCTION

Iceland is the largest part of the mid-ocean ridges located above sea level. There are 30 active volcanic systems with a total average eruptive frequency of at least 20 eruptions per century and magma output rate of 5 km^3 per century (Thordarson and Höskuldsson, 2008). High-temperature geothermal systems are located in the central parts of active volcanism and rifting belts except for three located close to their margin (Arnórsson et al., 2008). The most active volcanoes and geothermal areas in Iceland are covered by glaciers. The heat from sub-glacial magma intrusions and exothermic rock alteration reactions melts the overlying ice, forming depressions in the glaciers called cauldrons (Steinthórsson and Óskarsson, 1986; Björnsson, 2003). Melt water often collects at the base of the glacier; eventually there may be sufficient melt water to lift the ice, resulting in a sub-glacial flood. There are two main causes of glacial floods – called jökulhlaups in Icelandic[1]: 1) sub-glacial geothermal activity during which ice is melted continuously and accumulates in periodically drained sub-glacial lakes and, 2) sub-glacial volcanic eruptions where the melt water is produced rapidly due to thermal energy released during magma cooling (Gudmundsson et al., 2008). The former tend to be smaller and more common than floods originating during volcanic eruptions (Gudmundsson et al., 2005; 2008). Drainage occurs in semi-regular intervals and not all flood events are recorded. During sub-glacial volcanic eruptions, floods can be abrupt, loaded with suspended matter, and sometimes contain high concentrations of dissolved metals and volatiles (Kristmannsdóttir et al., 1999; Gislason et al., 2002; Snorrason et al., 2002; Stefánsdóttir and Gislason, 2005; Sigfússon, 2009). Some of these floods can be of "Amazonian" size; with maximum flow rates of 3,000-700,000 m^3/s (Tómasson, 1996; Snorrason et al. 2002; Waitt, 2002; Gudmundsson et al. 2005; Russell et al., 2010). Because of their potentially large impact on the environment, jökulhlaups have been extensively studied (Gudmundsson et al., 1997; Kristmannsdóttir et al., 1999; Maizels, 1997; Björnsson, 1998; Geirsdóttir et al., 2000; Roberts et al., 2000; Gislason et al., 2002; Björnsson, 2003; Alho et al., 2005; Stefánsdóttir and Gíslason, 2005; Russell et al., 2006; Russell et al., 2010).

The chemical composition of waters affected by geothermal and volcanic activity (groundwaters, surface waters and flood waters) is influenced by its interaction with surrounding rocks, heat and gas supply, and overburden pressure which affects gas solubility. During "open air" volcanic eruptions, tephra and the proton and metal salts adsorbed on their surface, if present, will dissolve when exposed to surface waters. The metal salts are commonly fluorides, chlorides, and sulphates which originate from magmatic gasses such as HF, HCl and SO_2 (Óskarsson, 1980; Frogner et al, 2001; Delmelle et al., 2007; Flaathen and Gislason,

[1] In Icelandic 'jökull' is a glacier, and 'hlaup' means flood

2007; Jones and Gislason, 2008; Gislason et al. 2011). During sub-glacial eruptions, magmatic gases dissolve directly into melt waters which will influence flood water chemical composition, and leading to fluids which could either fertilize or pollute the surrounding ecosystems. Numerous studies have focussed on the effects of volcanic activity on natural water compositions (e.g. Federico et al., 2002; Aiuppa et al., 2003; Cioni et al., 2003; Marini et al., 2003; Federico et al., 2004; Aiuppa et al., 2005; Stefánsdóttir and Gislason, 2005; Flaathen and Gislason, 2007; Taran et al., 2008; Bagnato et al., 2009; Flaathen et al., 2009; Ambrosio et al., 2010; Floor et al., 2011; D'Alessandro et al., 2013). These studies confirm that the input of magmatic gasses, including CO_2, and/or the release of salts adsorbed on tephra promotes host rock dissolution and toxic metal release. Increased host rock dissolution may, however, have a positive impact on the biota due to the addition of limiting elements to the fluid, potentially leading to short lived overall net negative flux of CO_2 to the atmosphere (Gislason et al., 2002). If water-rock interaction is sufficient, the water can be neutralized leading to the precipitation of metal scavenging (oxy)hydroxides and other secondary phases (Aiuppa et al., 2000a,b; Aiuppa et al., 2005; Flaathen and Gislason, 2007; Flaathen et al., 2009, Kaasalainen and Stefansson, 2012).

An improved understanding of sub-glacial floods is of wide interest for several reasons. First, the heat source origin is critical to the potential environmental impact of the flood. If the heat was sourced by volcanic eruptions, acid gas input can lead to acidic flood waters and toxic metal release from the host rock. If the heat source origin was geothermal activity, extensive, long-term fluid-rock interaction would lead to higher pH and less toxic flood waters. Secondly, the process triggering the flood can potentially be used to design systems to forewarn the public in the potential inundated area. Third, glacial floods may play an important role in global cycle of elements. Large number of studies have shown that particulate transport in rivers contribute significantly into the global cycle of elements (e.g. Stefánsdottir and Gislason, 2005; Oelkers et al., 2011, 2012; Jones et al., 2012a,b). Glacial floods are heavily loaded with suspended material having large surface areas, making it especially reactive once it settles in estuaries. Moreover, particulate flux is far more dependent on runoff than is the dissolved element flux; glacial floods can thus increase dramatically particulate fluxes to the ocean (Gislason et al., 2006). This particulate material can influence greatly primary productivity along the coast and in lakes (Gislason and Eiriksdottir, 2004).

In this study we focus on the chemical composition of two small Icelandic glacial floods which emerged in July 2011: the Mýrdalsjökull and the Vatnajökull. This study was motivated to better understand the origin of the heat source that melted the glacier and its affect on the flood water chemistry. This study also helps illuminate the potential significance of glacial floods on suspended particulate material transport on a local scale.

5.2. GENERAL DESCRIPTION OF THE STUDY AREA

5.2.1. Mýrdalsjökull and Katla

The Mýrdalsjökull glacier is located in southern Iceland within the Eastern Volcanic Zone (Fig. 1a). It covers almost 600 km^2 with the maximum ice thickness of ~740 m in the northern part of the caldera (Björnsson et al., 2000). There is an active central volcano beneath the glacier with a large caldera located approximately 650 m above sea level. The caldera, together with an 80 km long northeast-trending fissure swarm, comprises the Katla volcanic system. The volcano circular base is about 30 km in diameter and the highest peaks reach 1,380 m above sea level (Björnsson et al., 2000). The caldera is oval shaped with its longest axis trending 14 km NW-SE. The area and volume of ice inside the caldera is 100 km^2 and 45 km^3, respectively. On the caldera rims, the ice cap thickness ranges between 150 and 200 m (Björnsson et al., 2000). Ablation in summer lowers the glacier surface elevation by 4-8 m from spring to autumn. Snow accumulation restores this elevation during the winter. The central volcano is one of the most seismically active in Iceland. The epicentres are usually located within the caldera and beneath the western rim at Goðabunga. Katla erupts roughly twice a century. It produces high Fe-Ti basalts of the transitional-alkaline magma suite. Katla activity is dominated by explosive sub-glacial eruptions producing numerous and widespread tephra layers with volumes from ~0.01 to ~1 km^3 (Thordarson and Larsen, 2007; Óladóttir et al., 2008).

The last major jökulhlaup from Katla occurred in 1918 and was triggered by an eruption within the caldera. Most of the flood water flowed during an eight hour period at the initial stages of the eruption. The total flood water volume was estimated to be 8 km^3 (Tómasson, 1996). The majority of the water came from beneath the glacier, breaking the glacial tail. Witnesses reported that large blocks of ice were carried with the flood water. The flood was estimated to have peaked at 300,000 m^3/s and inundated an area of 600-800 km^2 to the east of the volcano (Tómasson, 1996; Larsen, 2000). The coastline moved 4 km towards the sea as the sediments carried by the flood water were deposited. Other smaller glacial floods from Katla, each with a peak discharge of about 2000 m^3/s, occurred in 1955, 1999, and 2011 (Gudmundsson et al., 2013).

5.2.2. Vatnajökull and Hamarinn

The Vatnajökull glacier is the largest in Iceland and covers 8,100 km^2. It is situated in the Eastern Volcanic Zone. The ice thickness is generally 600-800 m with a maximum thickness of 950 m (Björnsson and Pálsson, 2008). There are several central volcanoes beneath the glacier including the Grímsvötn, Bárðarbunga, Gjálp,

and Hamarinn (Gudmundsson and Högnadóttir, 2007). Hamarinn is a central volcano (Fig. 1b) and belongs to the Bárðarbunga – Veidivötn tholeitic volcanic system. This volcanic system is 190 km long and 28 km wide, and it covers an area of 2,500 km^2 (Thordarson and Larsen, 2007). Most of the historical eruptions, which account for 14% of the verified historical eruptions in Iceland, took place on the ice-covered part of the system forming small to moderate volumes of basaltic tephra.

A recent jökulhlaup originating from the Vatnajökull glacier occurred in November 1996. The eruption which triggered the flood – the Gjálp eruption – produced 0.4 km^3 of magma, making it the fourth largest eruption in Iceland during the twentieth century (Gudmundsson et al., 1997). Melt water accumulated for a month in the Grímsvötn Lake prior to its release, when 3.2 km^3 of water drained from the lake within 40 hours. The peak discharge was 40,000-50,000 m^3/s (Snorrason et al., 2002; Björnsson, 2003) and most of the water drained into the Skeidará and Gígjukvísl Rivers. The total suspended flux in the flood water was at least 180 million tonnes (Snorrason et al., 2002; Stefánsdóttir and Gislason 2005). This amounted to close to 1% of the total annual global river suspended flux to the oceans (Milliman and Syvitski, 1992; Stefánsdóttir and Gislason 2005). The dissolved flux was estimated to be 1 million tonnes, equal to the total annual dissolved load of the largest Icelandic river, the Ölfusá River (Gislason et al., 1996, Gislason et al., 2002). The CO_2 flux during the flood was estimated to be 0.6 million tonnes (Gislason et al., 2002). For comparison, the estimated annual average magmatic CO_2 flux in Iceland is estimated to be 1-2 millions tones (Arnórsson and Gislason, 1994) indicating major impact of this flood on carbon budget.

5.3. THE JULY 2011 FLOODS

5.3.1. Múlakvísl flood

Several of the Mýrdalsjökull glacier caldrons shown in Figure 1a grew in size due to increasing geothermal activity from 2001 to 2004 (mainly cauldrons 16 and 9, IMO, 2013). Their growth was accompanied by intensified seismicity, possibly caused by magma accumulation under the Katla caldera (IMO, 2013). After 2004, the seismic activity declined until a sudden increase on 9 July, 2011 (IMO, 2013). The jökulhlaup originated from three ice cauldrons in the SE part of the Katla caldera: caldrons 9, 10, and 16 (Gudmundsson and Högnadóttir, 2011). The Mýrdalsjökull flood monitoring system of the Icelandic Meteorological Office (IMO, 2013) operates two gauging stations on the Múlakvísl River, which is the main drainage of the Katla glacier (Kötlujökull, Fig. 1a). Fluid monitoring at the bridge on Road 1 began to show increased conductivity during the early evening of July 8, around the time of peak seismicity (Fig. 2b). The increased water level and sediment flux affected the temperature and conductivity sensors around midnight

and the sensors were eventually swept away with the bridge few hours later. The photograph of damaged Road 1 and the data recorded by the monitoring station located on the bridge can be seen in Fig. 2a and b. The photograph of damaged Road 1 and the data recorded by the monitoring station located on the bridge can be seen in Fig. 2a and b.

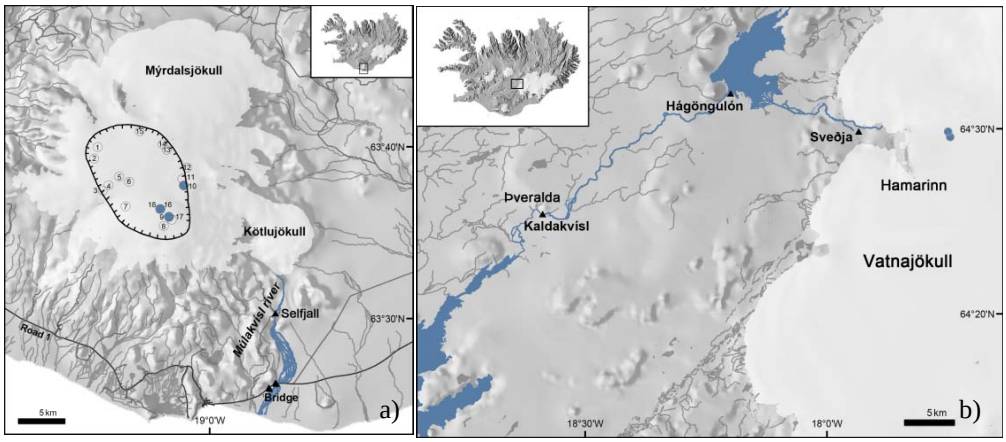

Figure 1. Location of the sampling sites (black triangles) during Múlakvísl (a) and Kaldakvísl (b) floods. The blue colour underscores the flood path. The white circles represent the cauldrons existing up to now and the blue circles represent cauldrons which were drained. Hatched curve indicates the Katla caldera. The uppermost black triangle on Figure (a) shows the location of the background sample for the Múlakvísl River and also the location of the gauge station at Léreftshöfuð (see text).

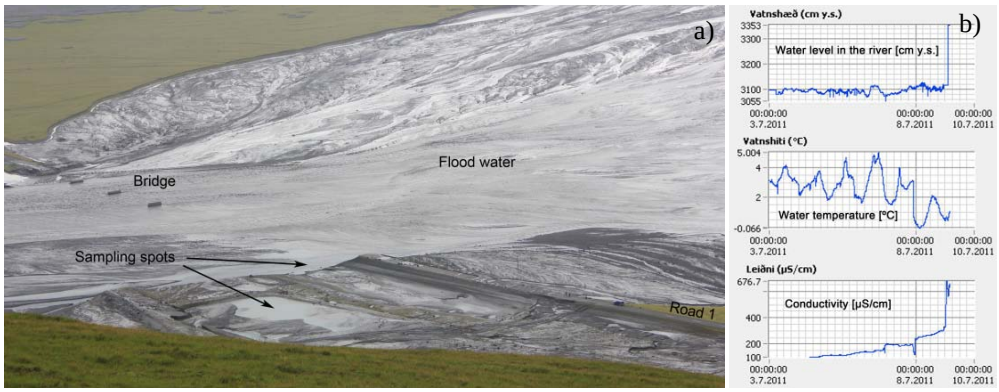

Figure 2. The Múlakvísl River at the waning stage of the flood. Some of the sampling spots, the remaining of the bridge which was swept away by the flood and Road 1 are highlighted on the photo which was taken on July 10, 2011 at 15:00 GMT. The diagram (b) shows the Icelandic Meteorological Office continuous monitoring of the water level, temperature and conductivity of the Múlakvísl River which was carried out by the gauge station located on the bridge (IMO, 2013). The plots are cut at 5:10 GMT due to the destruction of the monitoring station by the glacial outburst.

Another monitoring station, located at Léreftshöfuð, is normally not in water. Around 4:00 GMT on July 9, it began showing a rising water level, and within minutes the water level rose by more than 5 meters. Experience has shown that when the flood peaks at Léreftshöfuð, it reaches Road 1 in about an hour, and may have

swept away the bridge on Road 1 at around 5:10 GMT. The seismicity recorded prior to the flood continued, but diminished significantly on July 10 (IMO, 2013).

5.3.2. Kaldakvísl flood

Flood water drained from the Hamarinn cauldrons to the Sveðja River and reached the Hágöngulón reservoir on July 13, 2011 (Fig. 1b). The height of the water level in Hágöngulón reservoir on July 12 was 816.54 m above sea level and increased to a maximum of 817.33 m above sea level at 12:00 GMT July 13. The water discharge filling the reservoir from Sveðja River increased from 80 m^3/s before midnight on July 12 to 2,200 m^3/s at ~3:00 GMT on July 13. The recharge into the reservoir decreased again to ~80 m^3/s at ~18:00 GMT that day. The total volume of the flood water was 20 Gl (Hannesdóttir, 2011). When the water level increased in the Hágöngulón reservoir, water was discharged into the Kaldakvísl River at a rate of ~240 m^3/s. The water surface subsidence of the Hamarinn cauldrons was not measured. The seismometer in the vicinity of Hágöngulón detected higher activity around midnight July 13 (IMO, 2013). A similar outburst into the Kaldakvísl River occurred in 1972 with the total volume of 20 Gl (Freysteinsson, 1972).

5.4. METHODS

5.4.1. Sampling and analyses of flood water and suspended inorganic particulate material

Samples of water and suspended material during the Múlakvísl flood were collected from the Múlakvísl River close to the main bridge on Road 1 and from high standing ponds in the vicinity of the bridge (see Fig. 1 and 2a). The high standing ponds represent the chemical composition of the flood water at its highest discharge. The sampling locations are shown in Figs. 1a and 2a. Samples of water and suspended material during the Kaldakvísl flood were collected from 1) the Kaldakvísl River near Þeralda Mountain, 2) from the outlet of the Hágöngulón reservoir, and 3) from the Sveðja River directly at the glacier outlet (Fig. 1b). The average flood water discharge from the Hágöngulón reservoir into the Kaldakvísl River was 240 m^3/s. The sample names reflect the sampling time. The 'resolution time' is the estimated arrival time of the water at the Þveralda sampling station in Kaldakvísl, calculated from time required for the sample water to travel from the Hágöngulón Reservoir to this sampling point.

Conductivity and temperature were measured *in situ* at the time of sampling. Samples were collected in high density polyethylene buckets and poured into 2 L high density polyethylene containers which were sealed after they were filled completely. The buckets and containers were rinsed several times with flood water

prior to sampling. Water from the containers was filtered through 0.2 µm Millipore cellulose acetate membranes using a peristaltic pump, silicone tubing, and a 140 mm Sartorius® polypropylene filter holder. At least 1 L of sampled water was pumped through the filtration unit before the samples were collected, and all the air in the unit was expelled through an air valve. This filtered sample was divided and stored differently depending on the analysis. Acid washed high density polypropylene bottles were used to collect samples for cations and trace metal. Low and high density polyethylene bottles were used to collect samples for other dissolved elements. The containers for dissolved nutrients and dissolved organic carbon were acid washed. During the Kaldakvísl flood, the first samples were collected in plastic Coca-Cola bottles by a field hydrogeologist present at the site. These bottles were first rinsed several times in hot and cold tap water and then several times with the flood water. This was done to maximize sampling during the flood. These samples were otherwise, treated like the rest of the samples. Water samples collected for major and trace element analysis were acidified using Suprapur® 0.5% (v/v) HNO_3. Amber glass bottles were used to collect filtrated samples for pH and alkalinity measurements. Samples collected for DOC were acidified with 1.2 M concentrated HCl 2% (v/v).

A variety of methods were used to chemically analyse the sampled flood waters. Dissolved H_2S was measured on-site by titration using mercury acetate and dithizone as indicator (Arnórsson, 2000). The pH was later determined in the laboratory using an Oakton pH electrode. The dissolved inorganic carbon (DIC) was determined from measured pH and alkalinity. The end point of the alkalinity titration was determined by the Gran function. Dissolved F^-, Cl^-, SO_4^{2-}, $S_2O_3^{2-}$, NO_3^-, acetate, and formate concentrations were quantified using a DIONEX, IC-2000 ion chromatograph. Cations and trace metals were measured using a Spectro Cirus Vision inductive coupled plasma optical emission spectrometer ICP-OES, with an in-house standard and checked against the SPEX Certified Reference Standard. Rare earth elements (REE) and some additional trace metals were measured in selected samples by inductive coupled plasma sector field mass spectrometer ICP-SFMS at ALS Scandinavia, Luleå, Sweden. The dissolved organic carbon (DOC) was measured at Umeå Marine Sciences Centre, Sweden. Analytical measurements had an inter-laboratory reproducibility of within 5.0%.

The inorganic suspended particulate material was collected at the same time as the flood water samples. The remaining unfiltrated water sample from the 2 L high density polyethylene containers were shaken vigorously and poured into 1 L high density polyethylene bottles. Water samples containing suspended matter was centrifuged at 15 °C and 10,000 rpm, and the remaining solids were freeze-dried for 24 hours at 40 °C and 3 PSI pressure. Selected samples of suspended matter were analysed by ICP-SFMS at ALS Scandinavia, Luleå, Sweden.

During the Múlakvísl flood, ice blocks from the glacier were transported by the flood water and spread over an area delimited by the maximum discharge. An ice block sample was collected into a clean heavy wall, low density polyethylene bag and kept frozen. A few days after sampling, the ice sample was melted in the sampling bag. Melted water was filtered through 0.2 µm Millipore cellulose acetate membranes into bottles identical to those used for flood water sampling. Four months after the flood, additional river water samples were taken in the Múlakvísl valley, close to the Léreftshöfuð monitoring station (Fig. 1).

5.4.2. Discharge measurements and dissolved flux calculations

Water discharge during the Múlakvísl flood was estimated by the Icelandic Meteorological Office using the HEC-RAS model which included the cross section and the height of the water table in the flood channel (Brunner, 2010; Jónsson and Þórarinsdóttir, 2011). The water velocity was 3-4 m/s and the average discharge was ~2,500 m^3/s. The total discharge during the flood peak, between 4-6:30 GMT on July 9, was 7-8 Gl at Léreftshöfuð (Jónsson and Þórarinsdóttir, 2011). The total volume of water released from the cauldrons based on ice cap surface measurements before and after the flood was estimated to be 18 Gl (Gudmundsson and Högnadóttir, 2011). Based on this assessment, it is estimated that 10 Gl of flood water was discharged after the flood peak. Total major element fluxes (Si, Ca, Mg, Na, K, Al, Fe, Mn, Sr, Cl, SO_4, F, DIC) were calculated from measured sample water element concentrations and the total discharge. The total dissolved flux carried by the flood waters were a combination of background fluxes, dissolved fluxes during the flood peak, and dissolved fluxes during the rest of the flood. The dissolved fluxes during the flood peak were calculated by multiplying the average element concentrations of the first four samples (samples: 2011-09-07_0234; 2011-09-07_1220; 2011-09-07_1350; 2011-09-07_1725) by the total flood peak discharge of 8 Gl. The dissolved fluxes during the rest of the flood were calculated by multiplying the average elemental concentrations of other three samples (samples: 2011-09-07_1625; 2011-09-07_2105; 2011-10-07_0955) by the post-peak discharge of 10 Gl. The background fluxes were calculated by multiplying the major element concentrations of the sample taken 3.5 months after the flood from the Múlakvísl River (sample 2011-21-11_1400) by the average discharge measured in Múlakvísl River in July 1998 (Kristmannsdottir et al., 2006). The effect of the flood on element fluxes was determined by subtracting the background fluxes from the total dissolved fluxes during the entire flood.

The water discharge during the Kaldakvísl flood was measured directly at the Landsvirkjun Power Company monitoring station located at the Hágöngulón Reservoir. The total discharge into the Hágöngulón during the flood was estimated to be 30 Gl, of which around 20 Gl were assigned to the glacial flood and 10 Gl

were assigned to other sources recharging the reservoir (Hannesdóttir, 2011). The total dissolved fluxes were calculated by multiplying the average major elemental concentrations of sampled waters by the discharge of 30 Gl. To estimate the background fluxes - the average major elemental concentrations measured in Sveðja river in 1998 (Hjartarson, 1994) were multiplied by the discharge of 10 Gl. The effect of the flood on element fluxes was determined by subtracting the background fluxes from the total dissolved fluxes during the entire flood.

5.4.3. Saturation state and dissolution rate calculations

The standard state adopted in this study is unit activity for pure minerals and H_2O at any temperature and pressure. The standard state for aqueous species is a hypothetical 1 molal solution referenced to infinite dilution at any temperature and pressure. Aqueous speciation, charge balance, mineral saturation state were calculated using the PHREEQC 2.17 geochemical code (Parkhurst and Apello, 1999) with the standard *phreeqc.dat* database updated with selected aqueous complex formation and mineral solubility constants taken from Gysi and Stefánsson, 2011, and using measured water sample compositions, pH, and temperature. The thermodynamic properties of the hydrated Katla and Grímsvötn glass surface were estimated from the stoichiometrically weighted sum of the hydrolysis reactions of amorphous SiO_2 and amorphous $Al(OH)_3$ (Bourcier, 1990; Wolff-Boenisch et al., 2004). The equilibrium constants of individual hydrolysis reactions were taken from *phreeqc.dat*. The logarithm of the equilibrium constant for the hydrated basaltic glass surface hydrolysis reaction:

$$Si_{1.0}Al_{0.32}O_2(OH)_{0.96} + 0.96H^+ + 1.04H_2O = 0.32Al^{3+} + H_4SiO_4 \qquad (1)$$

was calculated to be 0.76 for both glasses at 25 °C. The saturation state of the reactive solution with respect to the hydrated glasses is reported as the Gibbs free energy of reaction, ΔG_r, but the saturation state of the flood water with respect to secondary minerals is reported as the saturation index, SI. The relationship between these parameters is given by:

$$\Delta G_r = RT\ 2.303 \log (Q/K) = RT\ 2.303\ SI \qquad (2)$$

where R (J/K/mol) corresponds to the gas constant, T designates the temperature in Kelvin, Q stands for the reaction quotient (also called ion activity product), and K denotes the equilibrium constant of the relevant reaction at the temperature of interest. Both ΔG_r and SI are zero at equilibrium and negative when the fluid is undersaturated with respect to the solid.

The dissolution rate of basaltic glass can be described using (Oelkers and Gislason, 2001)

$$r_{+,BET} = k\left(\frac{a_{H^+}^3}{a_{Al^{3+}}}\right)^{0.35} \quad (3)$$

where r_{+BET} signifies the BET (Brunauer et al., 1938) surface area normalized steady-state dissolution rate, k refers to a rate constant equal to $10^{-11.65}$ moles of Si/cm^2/s, and a_i represents the activity of subscripted aqueous species. Note that hydrated basaltic glass dissolution rates slow when equilibrium is approached (c.f. Oelkers and Gislason, 2001). This effect, however, only begins to become substantial when ΔG_r exceeds -10 kJ/mol at 25 °C, and is thus negligible in this study.

The reaction path modelling with the aid of PHREEQC 2.17 was used to evaluate the possible origin of the dissolved constituents in the Múlakvísl flood waters. The aim of the modelling was to match modelling results of water-basalt interaction with measured flood water chemistry. The modelling was performed assuming either reduced or oxidized conditions. The redox conditions in reduced system was set by Fe^{2+}/Fe^{3+} equilibrium due to the composition of the dissolving basalt and precipitating goethite/siderite. The redox conditions in the oxidized system were set by assuming the food water was in equilibrium with atmospheric O_2. The initial fluid used in the model was pure water, since the water originated from melted ice was very dilute with total dissolved solids (TDS) of 1.3 mg/kg (Table 1), to which CO_2, HF, SO_2, HCl gases were added until the concentrations of the dissolved gas corresponded to the highest measured DIC, F, SO_4, and Cl in the water samples collected during the Múlakvísl flood; in total 9; 0.02; 0.1; 0.2 mmol/kg, respectively of DIC, F, SO_4, Cl were added. The fluid was allowed to react with Katla basalt (Óladóttir et al., 2008) and secondary minerals were allowed to precipitate at local equilibrium. Secondary phases were chosen based on natural analogues and the saturation state of sampled flood water with respect to secondary minerals. Results are plotted below as functions of the mass of basalt dissolved into each kg of water.

5.5. RESULTS

5.5.1. Flood water chemistry

5.5.1.1. Múlakvísl flood

The results of chemical analysis of the Múlakvísl flood samples are shown in Tables 1 and 2, Fig. 3 and Fig. 1 in the Supplementary data. The average charge imbalance of the analyzed samples was -0.9%, and most were within 2%. The highest charge imbalance was calculated for sample 2011-10-07_0955 and it equalled -10.5%. The charge imbalance for the melted ice (2011-09-07_2200) equalled 19.7% which is not unusual in waters with very low TDS (1.3 mg/kg).

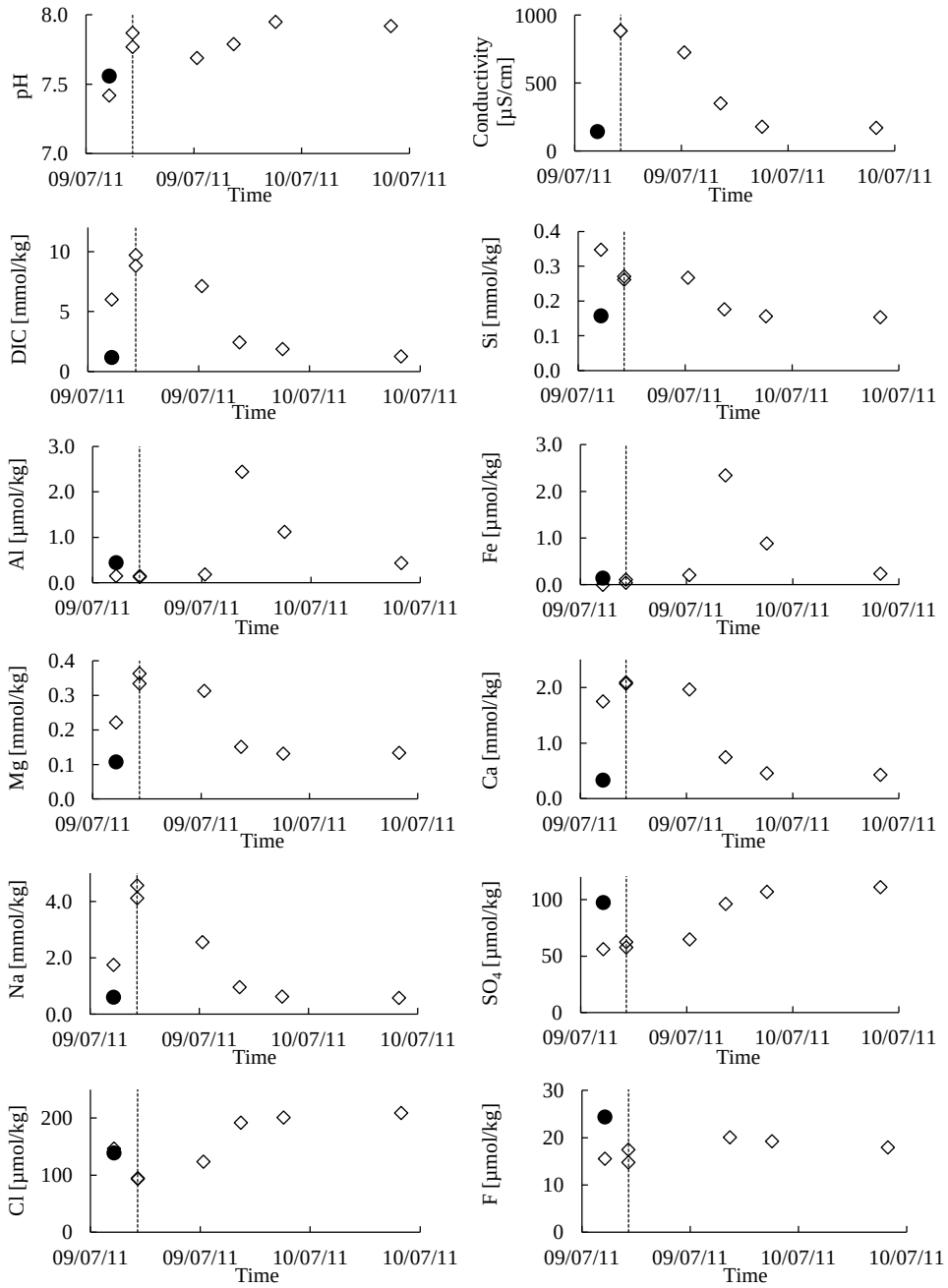

Figure 3. The pH, conductivity and dissolved constituents in the sampled waters during the Múlakvísl flood. The filled circles represent the element concentrations in the sample obtained four months after the flood. They reflect the background chemical composition of the Múlakvísl River. The vertical line represents the peak of the flood.

The average measured flood water temperature was 5 °C whereas the average measured air temperature at the time of sampling was 9.4 °C. There was no

significant rainfall during the sampling. The highest sampled conductivity was in the pond water which represent the flood peak and it equalled ~890 µS/cm. The pH of the samples was between 7.4 and 8. The concentration of all elements but F and SO_4^{2-} increased during the flood compared to the post-flood background sample and river monitoring in 1997 and 1998 (Kristmannsdóttir et al. 2006). The average dissolved H_2S concentration in the sampled waters was 0.6 µmol/kg – close to the detection limit. There was no characteristic H_2S smell; however, there was an unidentified smell in the air. The gas sensors did not detect either H_2S or SO_2 in the air at the sampling site but traces of CO (5-6 ppm) were detected in the air at the Léreftshöfuð site. Dissolved $S_2O_3^{2-}$, acetate, and formate were measured in the water samples with the highest concentration at the beginning of the flood (16, 37.2, and 22.3 µmol/kg, respectively) and decreased gradually to zero with time. The highest DIC, F, and B concentrations were measured during the flood peak and equalled 9.7 mmol/kg, 20 µmol/kg, and 3.7 µmol/kg, respectively. Conversely, SO_4, Cl, and P concentrations increased at the end of the flood and their maximum concentrations were 111, 209, and 1.0 µmol/kg, respectively. The highest concentrations of the major dissolved elements Na, Ca, Mg, Si and K were observed during the first few hours of the flood. Similar trends were observed for some of the trace element concentrations including Sr, Co, Cu, Ni, Zn, Mo, and As. The concentrations of Al, Fe, and Ti increased continuously up to 14 hours after the flood peak. The highest REE concentrations in collected waters from the Múlakvísl flood were measured in sample 2011-09-07-1655 – almost 12 hours after the water peak reached the bridge. Similar trends were observed for Al, Fe, and Ti – the highest concentrations were measured in this sample.

According to the saturation state calculations, the flood water samples were supersaturated with respect to the carbonates: calcite, aragonite, and dolomite at the beginning of the flood when the DIC concentration was >6 mmol/kg (Fig 5a). The partial pressure of CO_2 in sampled flood water was higher than atmospheric indicating its degassing (Fig. 6). The flood waters were supersaturated with respect to the less soluble Al-bearing secondary phases including gibbsite imogolite, kaolinite, Ca-montmorillonite and zeolites (stilbite, heulandite, and chabazite) (Fig. 7). Flood waters were undersaturated with respect to siderite, $Al(OH)_3$, moganite, allophane and fluorite, but close to saturation with respect to chalcedony. All the flood water samples but one were supersaturated with respect to goethite and amorphous $Fe(OH)_3$.

5.5.1.2. Kaldakvísl flood

The results of chemical analysis of the Kaldakvísl flood samples are shown in Table 1 and 2, Fig. 4, and Fig. 2 in Supplementary data. The average charge imbalance of the analyzed samples was 1.54% and most were within 3%.

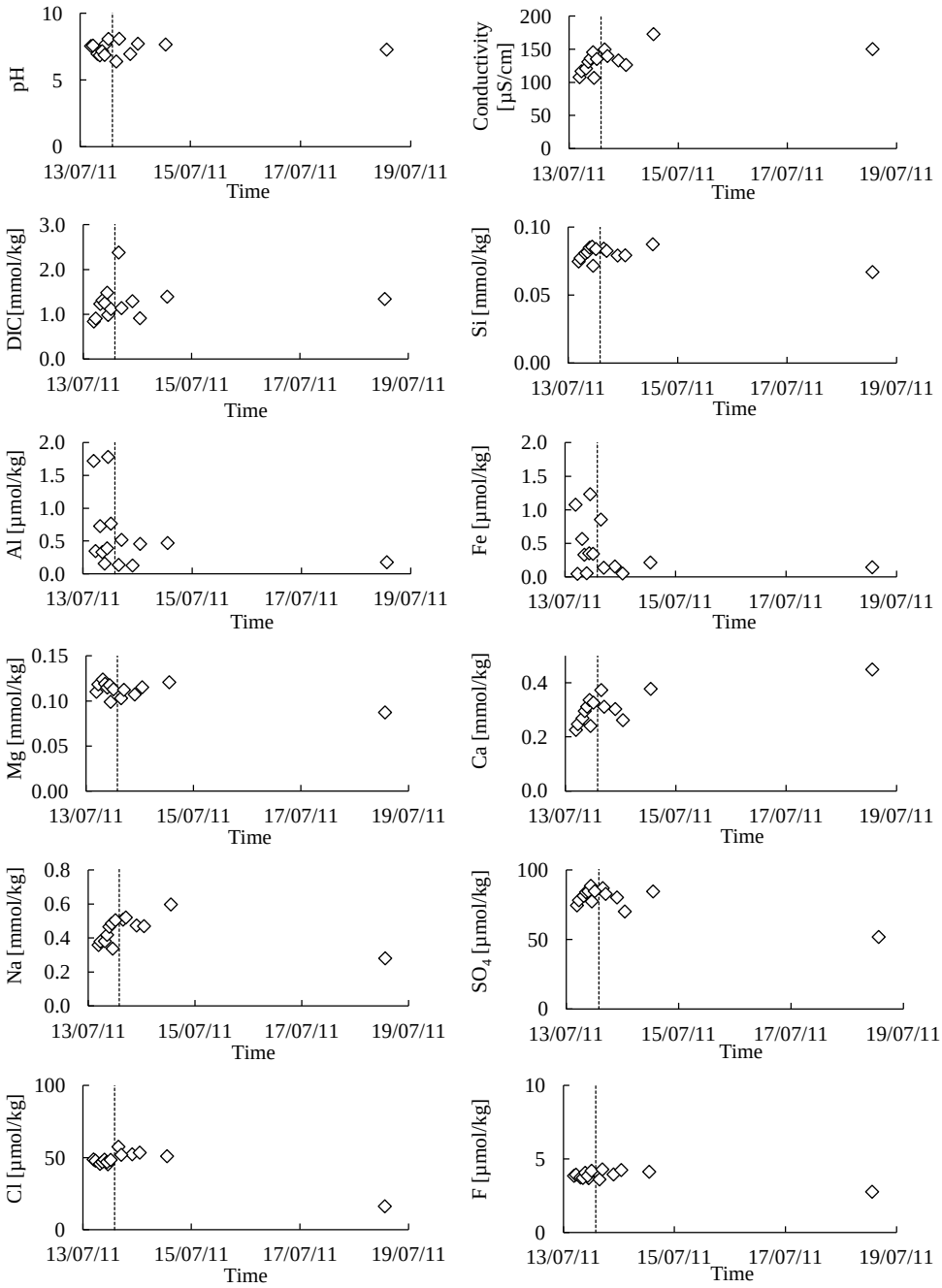

Figure 4. The pH, conductivity and dissolved constituents in the sampled water during the Kaldakvísl flood. The last sample taken on July 18, 2011 represents the chemical composition of the undiluted water from the Sveðja River. The other samples represent the chemical composition of the mixture of flood water and water from the Hágöngulón reservoir before flood started (Fig.1b). The vertical line represents the flood peak.

The average measured flood water temperature was 6.4 °C whereas the average measured air temperature was 8.4 °C. A maximum conductivity of 173 µS/cm was measured in the Hágöngulón, 26 hours after the flood started (sample: 2011-14-07_1310) and it did not correlate with the flood peak. The measured flood water pH was between 6.4 and 8.1. The concentrations of most elements increased with time during the flood. The average H_2S concentration of the flood water was 0.7 µmol/kg, close to the detection limit. The $S_2O_3^{2-}$ concentration in the flood waters was below the detection limit of 0.1 µmol/kg with exception of the sample collected from the Sveðja River five days after the flood started (sample: 2011-18-07_1900). The concentration of acetate and formate was also the highest in this sample (Table 2). Similar to the Múlakvísl flood, the partial pressure of CO_2 in the flood water was higher than atmospheric leading to its degassing. There was an undefined odour noticed at the Hágöngulón reservoir. The measured concentrations of most of the elements including Si, Ca, Mg, Na, K, Sr, Mn, Co, Ni, Zn, B, SO_4, B and DIC increased with time during the first 12 hours of the flood. Concentrations subsequently decreased until the last sample, which was taken 26 hours after the flood started (2011-14-07_1310) when they again increased.

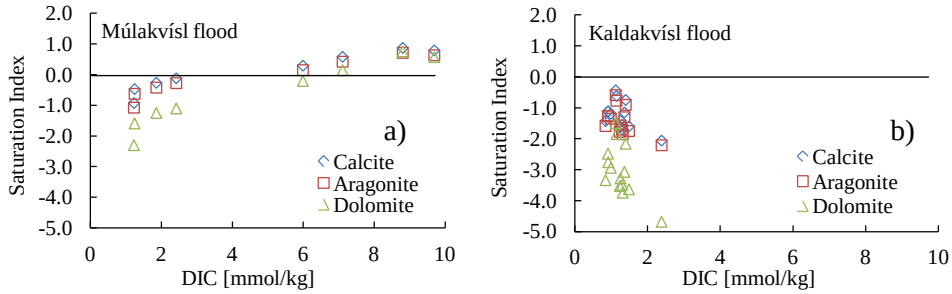

Figure 5. The saturation state of the sampled water with respect to carbonates during Múlakvísl (a) and Kaldakvísl floods (b). During Múlakvísl flood most of the samples taken during the first hours of the flood were supersaturated with respect to carbonates.

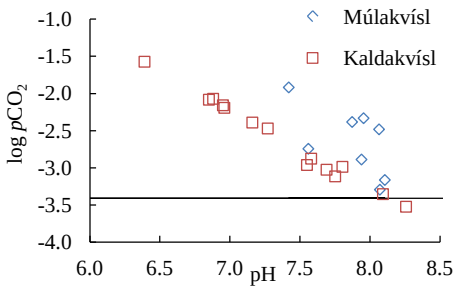

Figure 6. The in situ pH dependence of the saturation state of the sampled waters with respect to CO_2 presented in terms of partial pressure of CO_2 (pCO_2). Horizontal line represents the atmospheric CO_2 concentration also depicted as partial pressure.

The Al, Fe, Ti, V, and H_2S concentrations show a different pattern with the highest concentrations at the beginning of the flood. Concentrations of the trace metals As, Cr, Cu, Cd, Mo and Pb are the highest in the last sample collected on July 14 (2011-14-07_1310). The REE concentrations are the highest in the sample taken closest to the source of the flood in Sveðja, five days after the flood started (2011-18-07_1900). In contrast with the Múlakvísl flood, where Al, Fe, and Ti concentrations correlated with REE, there was no correlation between REE and Al, Fe, and Ti concentrations in the Kaldakvísl flood water samples. Moreover, there was no correlation between REE concentrations other with the other measured elements.

According to saturation state calculations, all flood water samples were undersaturated with respect to the carbonates calcite, aragonite, dolomite, and siderite (Fig. 5b). The partial pressure of CO_2 in sampled water was higher than atmospheric indicating its degassing (Fig. 6). Water was supersaturated with respect to the less soluble Al-bearing secondary phases including gibbsite imogolite, kaolinite and Ca-montmorillonite (Fig. 8a and b). Flood water samples were supersaturated with respect to the zeolites stilbite, heulandite, chabazite during first several hours of the flood. Samples were mostly undersaturated with respect to chalcedony, moganite, allophane and amorphous $Al(OH)_3$. Samples taken within first several hours of the flood and the sample taken 5 days after the flood in Sveðja were supersaturated with respect to goethite and amorphous $Fe(OH)_3$.

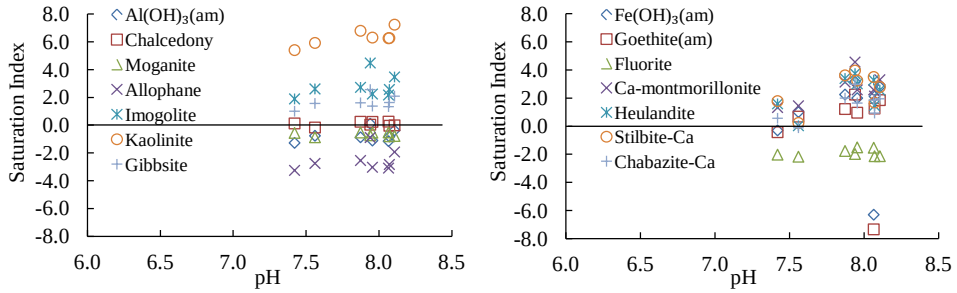

Figure 7. The in situ pH dependence of the saturation state of sampled waters with respect to the selected secondary minerals during Múlakvísl flood depicted in terms of saturation index.

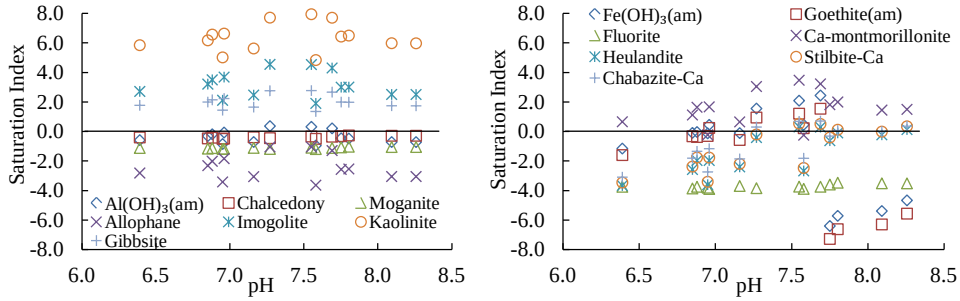

Figure 8. The in situ pH dependence of the saturation state of sampled waters with respect to the selected secondary minerals during Kaldakvísl flood depicted in terms of saturation index.

Table 1. Sample names, location, time of sampling (GMT), temperature, charge imbalance, measured pH and conductivity at temperature given in the table (T(°C)/pH), T(°C)/conductivity), total dissolved solids (TDS), and dissolved inorganic carbon (DIC). The charge imbalance was calculated with the PHREEQC computer code at in situ temperature (Parkhurst and Apello, 1999).

Sample	Location	GPS	Date	Time sampling	Time resolution
Múlakvísl					
2011-09-07 0234	West end of bridge over Múlakvísl		7/9/2011	2:34	2:34
2011-09-07 1220	From the west bank of Múlakvísl	63 25 57,6N 18 52 12,7W	7/9/2011	12:20	12:20
2011-09-07 1350	Pond from the peak discharge	63 26 01,4N 18 52 16,9W	7/9/2011	13:50	5:10
2011-09-07 1625	West end of "bridge" over Múlakvísl	63 26 15,4N 18 51 20,1W	7/9/2011	16:25	16:25
2011-09-07 1725	Highest pond northwest of "bridge"	63 26 18,3N 18 51 27,4W	7/9/2011	17:25	5:10
2011-09-07 2105	West end of "bridge" over Múlakvísl	63 26 15,4N 18 51 20,1W	7/9/2011	21:05	21:05
2011-10-07 0955	West end of "bridge" over Múlakvísl	63 26 15,4N 18 51 20,1W	7/10/2011	9:55	9:55
2011-21-11 1400	Background sample	63 30 21,1N 18 51 26,2W	11/21/2011	14:00	14:00
2011-09-07 2200	Ice block, ca 5 l, close to bond		7/9/2011	22:00	
Kaldakvísl					
2011-13-07 1100	Hágöngulón		7/13/2011	11:00	11:00
2011-13-07 1240	Þveralda		7/13/2011	12:40	4:40
2011-13-07 1330	Þveralda		7/13/2011	13:30	5:30
2011-13-07 1530	Þveralda		7/13/2011	15:30	7:30
2011-13-07 1540	Hágöngulón		7/13/2011	15:40	15:40
2011-13-07 1630	Þveralda		7/13/2011	16:30	8:30
2011-13-07 1730	Þveralda		7/13/2011	17:30	9:30
2011-13-07 1835	Þveralda		7/13/2011	18:35	10:35
2011-13-07 2015	Þveralda	64 25 44,7N 18 35 03,9W	7/13/2011	20:15	12:15
2011-13-07 2145	Hágöngulón	64 53 59,5N 18 19 01,8W	7/13/2011	21:45	21:45
2011-14-07 0055	Þveralda	64 25 44,7N 18 35 03,9W	7/14/2011	0:55	16:55
2011-14-07 0905	Þveralda	64 25 44,7N 18 35 03,9W	7/14/2011	9:05	1:05
2011-14-07 1310	Hágöngulón	64 32 09,6N 18 11 24,2W	7/14/2011	13:10	13:10
2011-18-07 1900	Hágöngulón	64 30N 17 55,4W	7/18/2011	13:30	13:30

Table 1. Continuation.

Sample	Discharge (m^3/s)	Temperature Air	Temperature Water	Charge imbalance	pH	T(°C) /pH	Conduct. (µS/cm)	T(°C) Conduct.	TDS (mg/kg)	DIC (mmol/kg)
Múlakvísl										
2011-09-07 0234		7.5		-0.4	7.42	22.5			493.7	6.0
2011-09-07 1220		8.9	3.8	0.6	7.69	22.5	727	4.5	599.2	7.1
2011-09-07 1350		8.6	3.7	-0.9	7.77	22	886	5.6	806.9	9.7
2011-09-07 1625		10.5	6.1	0.9	7.79	21.7	352	6	239.9	2.4
2011-09-07 1725		10.8	3.6	1.6	7.87	22	885	6	749.6	8.8
2011-09-07 2105		9.6	5.6	-10.5	7.95	20.6	180	5.4	189.1	1.9
2011-10-07 0955		9.7	7.1	1.8	7.92	22	172	7	150.9	1.2
2011-21-11 1400				0.1	7.56	18.3	144.5	17.8	133.1	1.2
2011-09-07 2200				19.7	6.69	13.8			1.3	0.0
Kaldakvísl										
2011-13-07 1100	240			-5.2	7.69	6.4	107	6.7	97.9	1.0
2011-13-07 1240	210			2.9	7.55	6.7	108	7.4	88.6	0.8
2011-13-07 1330	220			2.2	7.58	20.2	117	5.4	95.5	0.9
2011-13-07 1530	233			-1.0	6.96	20.6	121.1	8.9	105.0	1.2
2011-13-07 1540	240			1.8	6.39	15.7	149.9	6.1	126.0	2.4
2011-13-07 1630	235			1.9	6.85	20.2	131.1	7.7	107.6	1.3
2011-13-07 1730	237			1.4	7.16	15.2	136.3	11.4	114.5	1.3
2011-13-07 1835	240			1.6	6.88	17.9	145.7	7.25	120.4	1.5
2011-13-07 2015	240	8.1	6.4	2.2	8.08	22	135.5	6.2	118.6	1.1
2011-13-07 2145	230	7.2		2.2	6.95	21.4	133.3	6	111.1	1.3
2011-14-07 0055	235	5.8	6.2	1.3	8.09	6.2	140	6.1	118.4	1.1
2011-14-07 0905	227	10	6.8	7.1	7.72	9.7	126.5	6.8	98.3	0.9
2011-14-07 1310	190	11	6.3	1.4	7.66	22	173.0	6.6	136.7	1.4
2011-18-07 1900	100			1.9	7.27	12.2	151.6	21.9	113.2	1.4

n.a. = not analyzed; b.d. = below detection limit

values marked with the shadowed background are below accreditation limit of the ALS Scandinavia Laboratory

Table 2. Concentrations of dissolved constituents in flood water measured during Múlakvísl and Kaldakvísl floods.

Sample	Alkalinity (meq./kg)	DOC	Cl	S_2O_3	SO_4	H_2S	Acetate (µmol/kg)	Formate	NO_3	F	B	P
Múlakvísl												
2011-09-07 0234	5.6	n.a.	146.5	16.2	56.1	n.a.	37.20	22.35	2.2	15.5	3.7	0.2
2011-09-07 1220	6.9	n.a.	123.6	3.6	64.7	0.5	13.85	7.75	2.0	14.8	1.6	0.1
2011-09-07 1350	9.5	67.4	94.6	10.4	62.3	0.1	25.70	13.05	0.8	20.1	2.4	0.2
2011-09-07 1625	2.4	15.0	191.8	1.2	96.2	0.5	b.d	b.d	2.9	17.5	1.3	0.3
2011-09-07 1725	8.7	85.8	93.5	9.8	57.6	1.5	23.30	14.25	0.8	19.2	2.8	0.4
2011-09-07 2105	1.8	91.6	200.9	b.d	106.9	0.7	b.d	b.d	2.9	17.9	1.1	0.9
2011-10-07 0955	1.2	37.5	208.9	b.d	111.0	0.5	b.d	b.d	2.7	18.8	1.2	1.0
2011-21-11 1400	1.2	31.6	138.9	b.d	97.4	0.4	b.d	b.d	7.1	24.4	1.5	0.7
2011-09-07 2200	0.0	20.8	1.3	b.d	2.1	0.6	b.d	b.d	b.d	0.2	b.d	b.d
Kaldakvísl												
2011-13-07 1100	0.9	19.1	45.3	b.d	77.4	1.0	1.10	1.39	0.0	3.7	0.8	0.5
2011-13-07 1240	0.8	35.0	48.7	b.d	74.5	1.5	1.33	1.38	0.0	3.9	0.8	0.6
2011-13-07 1330	0.9	38.3	47.9	b.d	78.2	0.7	b.d	b.d	0.0	3.9	0.8	0.6
2011-13-07 1530	1.0	47.5	45.7	b.d	81.3	0.8	1.46	1.55	0.0	3.7	0.7	0.3
2011-13-07 1540	1.2	38.3	57.5	b.d	87.0	0.7	1.02	1.07	0.0	3.6	0.8	0.4
2011-13-07 1630	1.0	82.4	47.0	b.d	84.0	0.5	1.13	1.61	0.0	3.7	0.8	0.2
2011-13-07 1730	1.1	97.4	48.6	b.d	84.7	0.4	b.d	b.d	1.4	4.1	0.8	0.4
2011-13-07 1835	1.1	85.8	46.9	b.d	88.6	0.5	1.21	1.64	0.0	3.9	0.8	0.2
2011-13-07 2015	1.1	33.3	48.4	b.d	84.8	0.5	1.94	b.d	0.0	4.2	0.8	0.4
2011-13-07 2145	1.0	44.1	52.3	b.d	80.2	0.5	b.d	b.d	0.0	3.9	0.8	0.0
2011-14-07 0055	1.1	60.8	51.9	b.d	82.8	0.7	1.28	b.d	0.0	4.3	1.1	0.5
2011-14-07 0905	0.9	20.0	53.4	b.d	70.1	0.5	b.d	b.d	0.0	4.2	0.8	0.5
2011-14-07 1310	1.3	42.5	51.0	b.d	84.6	0.6	1.32	1.61	0.0	4.1	0.9	0.4
2011-18-07 1900	1.2	40.8	16.5	2.1	48.1	0.6	5.04	2.53	1.4	2.7	0.5	0.3

Table 2. Continuation.

	Si	Ca	Mg	Na	K	Al	Fe	Mn	Sr	As	Ba	Br	Co	Cr	Cu
Sample		(mmol/kg)					(µmol/kg)					(nmol/kg)			
Múlakvísl															
2011-09-07 0234	0.3	1.7	0.2	1.7	92.5	0.1	b.d.	6.8	2.7	6.5	11.8	472.1	1.7	1.4	16.2
2011-09-07 1220	0.3	2.0	0.3	2.6	97.0	0.2	0.2	7.6	3.6	1.5	11.3	b.d	3.3	b.d.	3.9
2011-09-07 1350	0.3	2.1	0.3	4.6	138.4	0.1	0.1	5.9	5.3	2.0	15.1	b.d	3.4	0.4	2.3
2011-09-07 1625	0.2	0.7	0.2	1.0	47.4	2.4	2.3	2.6	1.3	1.7	7.3	724.7	2.9	0.9	5.5
2011-09-07 1725	0.3	2.1	0.4	4.1	137.3	0.1	0.0	6.8	5.3	2.1	16.0	b.d	5.5	b.d.	8.1
2011-09-07 2105	0.2	0.5	0.1	0.6	33.0	1.1	0.9	0.7	0.8	1.2	1.8	380.0	1.0	0.5	3.3
2011-10-07 0955	0.2	0.4	0.1	0.6	31.6	0.4	0.2	0.5	0.7	0.7	1.8	571.7	0.9	b.d.	2.6
2011-21-11 1400	0.2	0.3	0.1	0.6	32.8	0.4	0.1	1.6	0.5	n.a.	0.9	183.9	n.a.	n.a.	n.a.
2011-09-07 2200	0.0	0.0	0.0	0.0	0.2	0.1	0.1	0.1	0.0	n.a.	b.d	238.9	n.a.	5.4	n.a.
Kaldakvísl															
2011-13-07 1100	0.1	0.2	0.1	0.3	7.7	1.8	1.2	0.6	0.1	n.a..	n.a..	47.8	n.a.	n.a.	n.a.
2011-13-07 1240	0.1	0.2	0.1	0.4	8.9	1.7	1.1	0.3	0.1	1.4	0.4	289.7	1.2	1.8	6.9
2011-13-07 1330	0.1	0.2	0.1	0.4	9.5	0.3	0.0	0.3	0.1	n.a..	n.a.	431.1	n.a.	n.a.	n.a.
2011-13-07 1530	0.1	0.3	0.1	0.4	9.8	0.7	0.6	0.5	0.1	n.a..	n.a.	146.8	n.a.	n.a.	n.a.
2011-13-07 1540	0.1	0.4	0.1	0.5	11.7	0.1	0.9	1.6	0.2	2.7	0.5	76.0	5.8	n.a.	5.4
2011-13-07 1630	0.1	0.3	0.1	0.4	10.3	0.3	0.3	0.7	0.1	n.a..	n.a.	220.1	n.a.	n.a.	n.a.
2011-13-07 1730	0.1	0.3	0.1	0.5	10.7	0.2	0.1	0.7	0.2	n.a..	n.a.	229.4	n.a.	n.a.	n.a.
2011-13-07 1835	0.1	0.3	0.1	0.5	11.4	0.4	0.4	0.9	0.2	n.a..	n.a.	10.5	n.a.	n.a.	n.a.
2011-13-07 2015	0.1	0.3	0.1	0.5	11.5	0.8	0.3	0.5	0.2	3.0	0.5	b.d	0.6	0.6	6.4
2011-13-07 2145	0.1	0.3	0.1	0.5	11.8	0.1	0.2	0.9	0.2	n.a..	n.a.	309.1	n.a.	n.a.	n.a.
2011-14-07 0055	0.1	0.3	0.1	0.5	10.5	0.5	0.1	0.4	0.2	2.8	0.5	b.d	0.7	2.0	6.2
2011-14-07 0905	0.1	0.3	0.1	0.5	9.3	0.5	0.1	0.3	0.1	2.4	0.7	548.8	0.7	n.a.	4.3
2011-14-07 1310	0.1	0.4	0.1	0.6	12.0	0.5	0.2	0.7	0.3	3.5	1.2	70.1	1.1	2.7	7.9
2011-18-07 1900	0.1	0.4	0.1	0.3	9.7	1.8	1.4	2.0	0.2	1.9	1.2	326.6	3.6	1.9	5.1

n.a. = not analyzed; b.d. = below detection limit

values marked with the shadowed background are below accreditation limit of the ALS Scandinavia Laboratory

Table 2. Continuation.

Sample	Sb	Ti	V	W	Cd	Hg	Mo	Ni	Pb	Zn	Th	La	Ce
							(nmol/kg)						
Múlakvísl													
2011-09-07 0234	39.8	2.4	122.3	b.d	0.1	b.d	9.1	20.8	0.2	60.8	b.d.	0.007	0.010
2011-09-07 1220	b.d	19.3	49.5	13.5	0.1	b.d	10.9	13.8	0.1	12.9	b.d.	0.040	0.062
2011-09-07 1350	b.d	28.4	58.3	18.9	0.1	0.0	20.8	17.0	0.2	6.4	b.d.	0.061	0.106
2011-09-07 1625	b.d	724.9	84.2	27.6	0.1	b.d	9.2	7.7	0.2	26.0	b.d.	0.652	1.492
2011-09-07 1725	b.d	401.1	64.4	17.5	0.0	b.d	18.2	22.0	0.2	63.8	b.d.	0.395	0.821
2011-09-07 2105	b.d	137.9	116.6	33.2	b.d.	b.d	8.7	4.9	0.1	13.0	b.d.	0.086	0.198
2011-10-07 0955	b.d	71.2	126.2	32.0	0.0	b.d	8.8	4.0	0.1	3.9	b.d.	0.068	0.131
2011-21-11 1400	b.d	31.9	72.4	b.d	n.a.	n.a.	n.a.	n.a.	n.a.	n.a.	n.a.	n.a.	n.a.
2011-09-07 2200	30.2	10.0	28.3	b.d	n.a.	n.a.	n.a.	n.a.	n.a.	n.a.	n.a.	n.a.	n.a.
Kaldakvísl													
2011-13-07 1100	b.d	285.4	80.9	36.3	n.a.	n.a.	n.a.	n.a.	n.a.	n.a.	n.a.	n.a.	n.a.
2011-13-07 1240	b.d	161.9	98.0	b.d	b.d.	b.d	2.6	4.4	0.1	24.3	b.d.	0.071	0.153
2011-13-07 1330	b.d	12.7	124.7	b.d	n.a.	n.a.	n.a.	n.a.	n.a.	n.a.	n.a.	n.a.	n.a.
2011-13-07 1530	4.6	80.2	95.2	49.1	n.a.	n.a.	n.a.	n.a.	n.a.	n.a.	n.a.	n.a.	n.a.
2011-13-07 1540	b.d	26.1	76.6	35.9	0.0	b.d	2.9	10.8	0.1	15.2	b.d.	0.019	0.036
2011-13-07 1630	b.d	42.0	95.0	5.4	n.a.	n.a.	n.a.	n.a.	n.a.	n.a.	n.a.	n.a.	n.a.
2011-13-07 1730	40.0	10.2	126.2	12.0	n.a.	n.a.	n.a.	n.a.	n.a.	n.a.	n.a.	n.a.	n.a.
2011-13-07 1835	b.d	67.3	124.3	11.9	n.a.	n.a.	n.a.	n.a.	n.a.	n.a.	n.a.	n.a.	n.a.
2011-13-07 2015	7.3	65.4	93.2	45.0	0.0	b.d	2.9	4.4	0.1	27.4	b.d.	0.030	0.056
2011-13-07 2145	36.9	14.4	94.2	b.d	n.a.	n.a.	n.a.	n.a.	n.a.	n.a.	n.a.	n.a.	n.a.
2011-14-07 0055	21.8	72.9	97.2	22.4	0.0	b.d	3.0	5.1	0.1	181.9	b.d.	0.026	0.056
2011-14-07 0905	b.d	76.9	110.5	20.5	0.0	b.d	3.1	3.5	0.1	15.4	b.d.	0.031	0.071
2011-14-07 1310	b.d	80.4	90.9	28.2	0.1	b.d	3.3	6.8	0.2	98.9	b.d.	0.044	0.091
2011-18-07 1900	b.d	468.0	65.2	55.9	b.d.	b.d	1.4	9.2	0.1	20.5	b.d.	0.207	0.475

Table 2. Continuation.

Sample	Pr	Nd	Sm	Eu	Gd	Tb	Dy	Ho	Er	Tm	Yb	Lu
						(nmol/kg)						
Múlakvísl												
2011-09-07 0234	0.002	0.005	0.001	0.001	0.003	0.001	0.005	0.001	0.003	0.001	0.005	0.002
2011-09-07 1220	0.008	0.038	0.008	0.002	0.01	0.001	0.01	0.002	0.011	0.001	0.011	0.004
2011-09-07 1350	0.015	0.062	0.014	0.009	0.009	0.002	0.013	0.004	0.012	0.002	0.016	0.004
2011-09-07 1625	0.202	0.756	0.157	0.045	0.099	0.015	0.086	0.016	0.043	0.004	0.029	0.007
2011-09-07 1725	0.113	0.44	0.082	0.025	0.054	0.009	0.058	0.01	0.03	0.005	0.025	0.005
2011-09-07 2105	0.027	0.116	0.026	0.005	0.014	0.002	0.012	0.002	0.007	0.001	0.005	0.001
2011-10-07 0955	0.018	0.073	0.021	0.005	0.01	0.002	0.012	0.001	0.004	0	0.002	0.001
2011-21-11 1400	n.a.	n.a.	n.a.	n.a.	n.a.	n.a.	n.a.	n.a.	n.a.	n.a.	n.a.	n.a.
2011-09-07 2200	n.a.	n.a.	n.a.	n.a.	n.a.	n.a.	n.a.	n.a.	n.a.	n.a.	n.a.	n.a.
Kaldakvísl												
2011-13-07 1100	n.a.	n.a.	n.a.	n.a.	n.a.	n.a.	n.a.	n.a.	n.a.	n.a.	n.a.	n.a.
2011-13-07 1240	0.026	0.087	0.028	0.009	0.016	0.004	0.017	0.004	0.011	0.002	0.01	0.002
2011-13-07 1330	n.a.	n.a.	n.a.	n.a.	n.a.	n.a.	n.a.	n.a.	n.a.	n.a.	n.a.	n.a.
2011-13-07 1530	n.a.	n.a.	n.a.	n.a.	n.a.	n.a.	n.a.	n.a.	n.a.	n.a.	n.a.	n.a.
2011-13-07 1540	0.008	0.026	0.005	0.003	0.003	0.001	0.004	0.001	0.002	0.001	0.004	0.001
2011-13-07 1630	n.a.	n.a.	n.a.	n.a.	n.a.	n.a.	n.a.	n.a.	n.a.	n.a.	n.a.	n.a.
2011-13-07 1730	n.a.	n.a.	n.a.	n.a.	n.a.	n.a.	n.a.	n.a.	n.a.	n.a.	n.a.	n.a.
2011-13-07 1835	n.a.	n.a.	n.a.	n.a.	n.a.	n.a.	n.a.	n.a.	n.a.	n.a.	n.a.	n.a.
2011-13-07 2015	0.01	0.038	0.01	0.002	0.008	0.002	0.006	0.002	0.004	0.001	0.004	0.002
2011-13-07 2145	n.a.	n.a.	n.a.	n.a.	n.a.	n.a.	n.a.	n.a.	n.a.	n.a.	n.a.	n.a.
2011-14-07 0055	0.008	0.035	0.01	0.003	0.008	0.001	0.009	0.002	0.006	0	0.004	0.005
2011-14-07 0905	0.009	0.046	0.01	0.001	0.006	0.001	0.007	0.001	0.003	0	0.004	0.002
2011-14-07 1310	0.013	0.065	0.013	0.005	0.01	0.002	0.008	0.002	0.006	0.001	0.005	0.002
2011-18-07 1900	0.065	0.297	0.065	0.025	0.046	0.009	0.053	0.011	0.028	0.004	0.026	0.005

n.a. = not analyzed; b.d. = below detection limit

values marked with the shadowed background are below accreditation limit of the ALS Scandinavia Laboratory

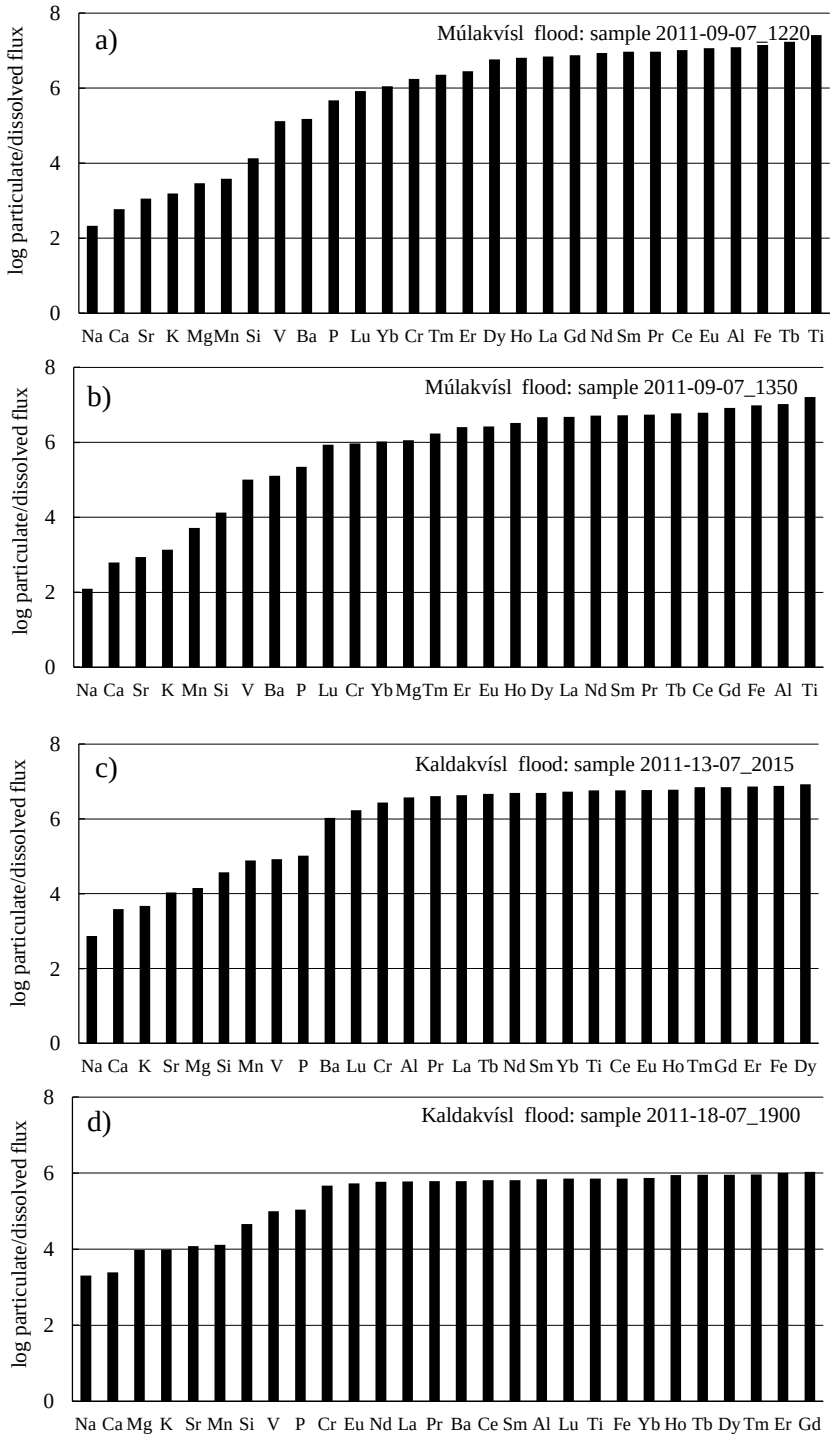

Figure 9. Ratio of particulate flux to the dissolved flux of selected elements in Múlakvísl (a, b) and Kaldakvísl floods (c, d).

5.5.2. Dissolved element fluxes and particulate material transport

The total dissolved fluxes carried by the flood waters in the Múlakvísl River were estimated to be 5,100 tonnes, and the total dissolved fluxes carried by the flood waters in the Kaldakvísl River were estimated to be 2,300 tonnes. For comparison, the annual dissolved fluxes carried by the Ölfusa River, the biggest river in Iceland is estimated to be 1 million tonnes/year (Gislason et al., 1996).

Total flux of CO_2, mainly in form of dissolved bicarbonate (HCO_3^-) during the Múlakvísl and Kaldakvísl floods were 3,300 and 1,400 tonnes, respectively. For comparison, the annual magmatic flux of CO_2 into the atmosphere and surface waters in Iceland, originated mostly from the long-term degassing of volcanoes and geothermal systems, has been estimated to be 1-2 million tonnes (Arnórsson and Gislason, 1994). According to Gislason et al. (1996), the annual transient fixation of atmospheric CO_2 by chemical weathering in Iceland is 3.3 million tonnes and the annual permanent CO_2 fixation by carbonate precipitation is 900,000 tonnes.

The effect of glacial floods on particulate material transport is far greater than that of the dissolved transport. Due to high discharge during the floods, flood waters can carry greater amounts of particulates increasing the suspended load. This is evident in the samples collected in this study. For example, the suspended material concentration in sample 2011-09-07_1220, collected 5 hours after the flood peak in Múlakvísl was 47 g/L whereas this concentration in sample 2011-10-07_0955, collected 29 hours after the flood peak, was only 30 mg/L. This latter concentration is within the range typically measured in Icelandic rivers (Pálsson and Vigfússon 1996; Eiriksdottir et al., 2011, 2012, 2013b). The ratio of particulate to the dissolved flux for various elements in the flood waters was calculated for four samples for which suspended particulate material was collected and its chemical composition was measured; the results of these calculations are shown in Fig. 9. These ratios were calculated by dividing the measured particulate element concentrations by the corresponding dissolved element concentrations. The element most transported in dissolved form was Na followed by Ca, Sr, Mn, Mg, K, and Si. The elements most transported by the particulates were Fe, Ti, Al, and REE. Note that that the concentrations of C, S, Cl, F, B, As, and Mo were not measured in the suspended material.

5.6. DISCUSSION

5.6.1. Comparison of chemical composition of flood water with background Icelandic surface and groundwater element concentrations

Water samples collected during both floods were alkaline and enriched in DIC; the DIC of the Múlakvísl and Kaldakvísl flood waters were as high as 9.7 and

2.4 mmol/kg, respectively. The typical DIC concentration of Icelandic river waters is less than 2 mmol/kg, (Gislason et al., 1996; Eiriksdottir, 2007; Louvat et al., 2008; Pogge von Strandmann et al., 2008; Vigier et al., 2009; Oskarsdottir et al. 2011) but some surface geothermal waters can have DIC as high as 8 mmol/kg (Arnórsson et al., 1982; Arnórsson et al., 1983). The background DIC concentration in the Múlakvísl River measured in the summers of 1997 and 1998 ranged between 0.7 and 2.7 mmol/kg (Kristmannsodttir et al., 2006). The average background DIC concentration of the Sveðja River is 0.56 mmol/kg (Hjartarson, 1994). The concentrations of other major anions in the Múlakvísl flood water were within the range of concentrations commonly observed in the river water: 49-140, 9-22, and 87-279 µmol/kg, respectively for SO_4^{2-}, F^- and Cl^-. The concentrations of these anions in the Kaldakvísl flood waters collected directly from Sveðja River were close to the background concentrations.

In water collected from the ponds representing high discharge of the Múlakvísl flood waters, Ca, Na, and K exceeded the upper range of the background concentrations (Krismansdottir et al., 2006) by factors of 3, 4, and 2, respectively. The major cations Si, Al, and, Fe were within the normal seasonal variation. Concentrations of Sr and Mn were higher than the background range during first hours of the flood. The concentrations of major cations in the water samples collected during the Kaldakvísl flood directly from Sveðja River were slightly higher than the background concentrations reported by Hjartarson (1994). The maximum measured concentrations of Mg, K, Na, Ca, Sr, and Mn exceeded the background concentrations by factors of 1.5, 1.5, 2, 3.8, 4.5, and 8, respectively. The Si, Al, and Fe concentrations in sampled waters were close to or slightly below their background concentrations.

The concentration of dissolved organic matter (DOC) during the Múlakvísl flood was higher than typically found in Icelandic river waters (Gislason et al., 2003; Eiriksdottir et al. 2011; 2012; 2013a, 2013b). In addition, formate and acetate were present in the flood waters. These observations suggest that active microbiological communities were present in some of the Katla sub-glacial reservoirs similar to that observed in the Skaftar sub-glacial lakes in western Vatnajökull (Marteinsson, et al., 2012).

The degree of supersaturation of the flood waters with respect to secondary minerals during Múlakvísl and Kaldakvísl floods were typical for basaltic ground and surface waters. According to saturation state calculations, the potential phases which could precipitate from the flood waters included aluminosilicates such as clays (gibbsite, imogolite, and kaolinite) and zeolites (heulandites, stilbite, and chabazite). The supersaturation of the flood waters with respect to carbonates during the Múlakvísl flood indicates its potential to precipitate and permanently fix carbon. The low concentration of Al in flood waters, similar to that commonly observed in

natural basaltic waters, is consistent with the precipitation of Al bearing clays and zeolites at high pH (Kristmannsdottir, 1979; Gislason and Eugster, 1987; Kristmannsdottir, 1982; Crovisier et al., 1992; Gislason et al., 1996; Stefánsson and Gislason, 2001). The low concentration Fe in the sampled flood waters indicates that released Fe^{2+} most likely precipitated as Fe(oxy)hydroxides due to fast oxidation kinetics at alkaline pH (Stumm and Morgan, 1996). This conclusion is consistent with the calculated flood water supersaturation with respect to trivalent Fe-phases.

5.6.2. Reaction path modelling

Insight of the origins of the Múlakvísl flood waters are obtained in this study through geochemical modelling. The results of reaction path modelling are summarized in Figures 10 and 11. The initial reactive fluid pH was ~3.4 and DIC concentration of 9 mmol/kg which corresponds to pCO_2 of 0.14 bar at 4 °C. The pH of this initial fluid was acidic due to the fact that it was assumed to be in equilibrium with CO_2, SO_2, HCl and HF consistent with the measured flood water chemistry. As this fluid reacted with basaltic glass, the pH evolved towards and passed neutrality reaching pH of ~8 after dissolution of ~0.02 mol of basaltic glass (equal to 2.5 g) per kg of water. The water became supersaturated with respect to secondary minerals such as carbonates, clays, and Fe(oxy)hydroxides. The amount of secondary phases precipitating during basaltic glass-water interaction is presented in Fig. 11. In the reduced system the first minerals that precipitate were siderite and smectite, whereas in the oxidized system goethite was the first to form. As the reaction progressed towards alkaline pH, calcite, Ca-Mg-Fe clays, Mg-clays were predicted to precipitate. It can be seen in Fig. 10 that modelled fluid composition, in general, approximated well those measured in the flood waters. Modelled Fe concentration for the reduced system matched measured flood water composition far better than those obtained from the oxidized system. This result suggests that the fluid-basalt interaction occurred primarily below the glacier cap, isolated from atmospheric oxygen. The common minerals found in low temperature basaltic soils are imogolite and allophone (Wada et al. 1992) which according to the modelling did not precipitate; however, all the other secondary minerals predicted by the simulation were in agreement with field observations (e.g. Kristmansdottir, 1982; Gislason and Eugster, 1987; Gislason et al., 1996; Stefánsson and Gislason, 2001; Alfredsson, 2013). Curiously, the measured Al composition of the fluid phase exceeded the modelled flood water Al concentration, suggesting that the stability of aluminium secondary minerals may be somewhat lower than in the thermodynamic database used for the calculations, Alternatively this difference could indicate sluggish precipitation kinetics for Al-phases (c.f. Schott et al., 2012; Zhu and Lu, 2009). Close agreement between modelled and measured Ca concentration indicates that there was no significant calcite dissolution within the reservoir which could increase

concentration of Ca and alkalinity in the sampled waters. This observation suggests that the increased alkalinity measured during the peak flood was mainly due to basalt dissolution. In addition, the modelled and measured Na concentrations confirm that the basalt dissolution was the major source of Na in the flood water.

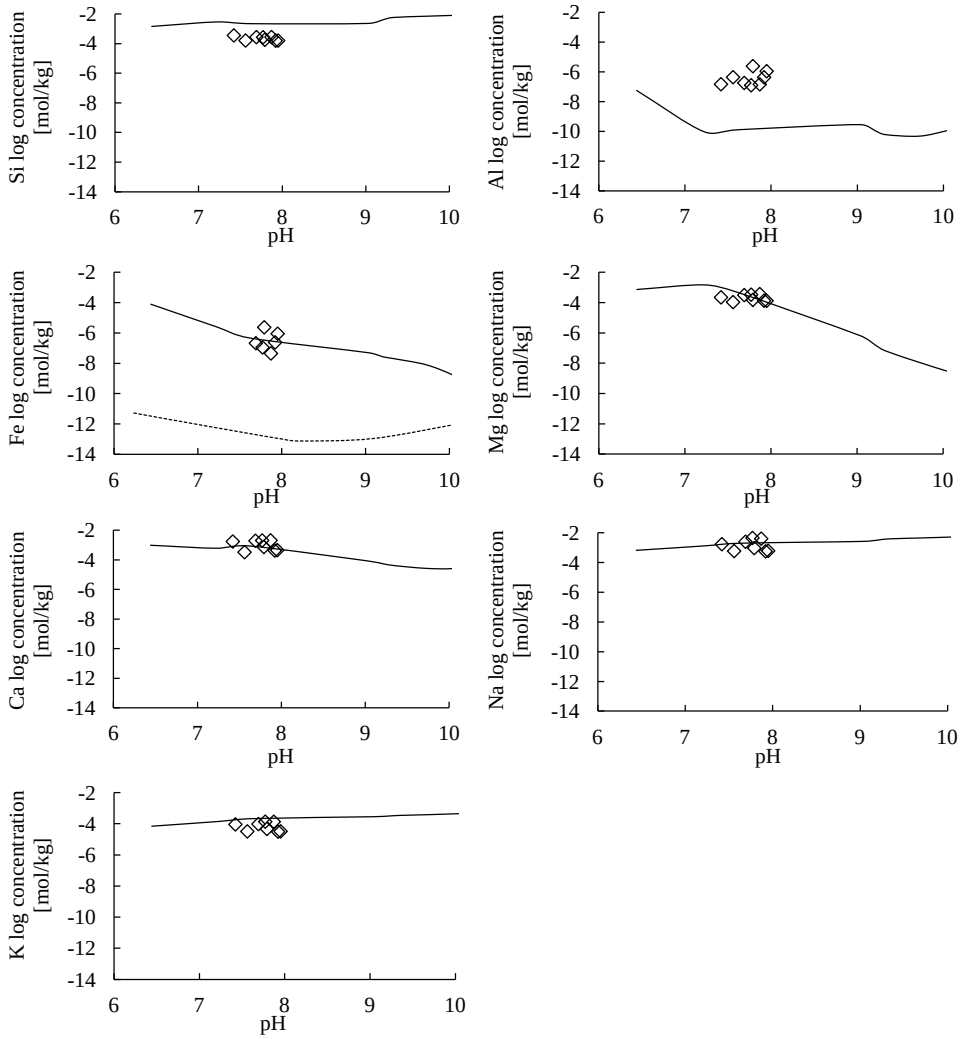

Figure 10. A comparison of the concentration of major elements in the Múlakvísl flood water (open diamonds) with those obtained by reaction path modelling (solid curves). The dotted curve on the Fe diagram represents modelled element concentrations assuming oxidized conditions whereas solid curves in all the plots show chemical composition evolution in reducing conditions.

According to the reaction path simulation, ~0.02 mol (2.5 g) of basaltic glass per kg of water dissolved to obtain an agreement between modelled and observed flood water compositions (Fig. 10 and 11). Taking account the Oelkers and Gislason (2001) basaltic glass dissolution rate expression (Eq. 3), the duration of fluid-basalt interaction can be estimated if the basalt surface area is known. By multiplying the

maximum measured suspended particulate concentration of 47 g/L with its BET surface area of 22.5 m^2/g, as measured in sample 2011-09-07_1220, one obtains a basalt surface area of 1,057 m^2/l. By adopting this surface area, approximately 2 years would have been required to dissolve 0.02 mol basaltic glass. Note these time estimates are likely minimum estimates, as riverine suspended particles have high surface areas compared to other natural particles and rocks (Gislason and Eugster, 1987; Eiriksdottir et al. 2013b). For example, the hydraulic conductivity of post glacial lava flows and pillow lavas is similar to gravel, but gravel has orders of magnitude less surface area than river suspended material (Gislason and Eugster 1987; Sigurdsson and Ingimarsson 1990). These time estimates and element concentrations comparisons suggest that the chemical composition of the flood water evolved for a non-negligible time within the sub-glacial reservoir prior to the flood. This is consistent with the frequency of flood events; the previous flood from Katla occurred in 1999.

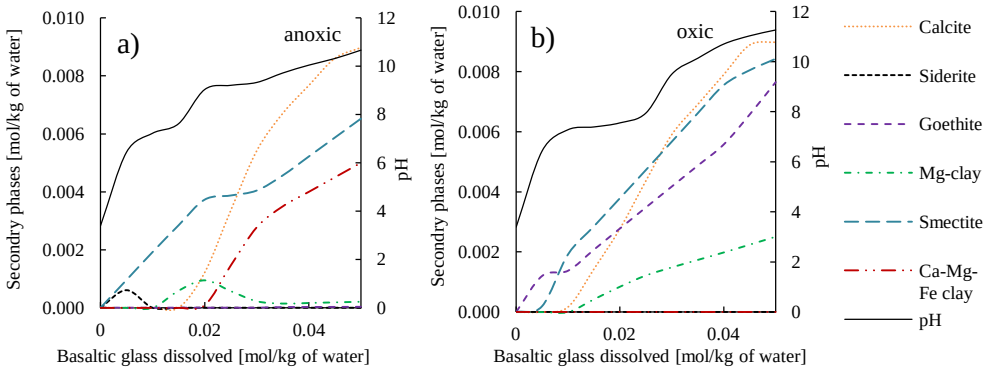

Figure 11. Results of the reaction path modeling where basaltic glass was allowed to dissolve in closed system and secondary phases were precipitating at local equilibrium. Plot (a) presents the amount of secondary phases precipitated in anoxic conditions whereas plot (b) shows the amount of secondary phases precipitated in oxic conditions.

5.6.3. Controls on the toxicity of flood water chemistry

The heat driving glacier melting can have geothermal and/or volcanic origin. Volcanic activity has been shown to lead to toxic surface waters. For example, Flaathen and Gislason (2007) confirmed the increased toxicity in surface waters associated with the 1999 and 2000 Mt. Hekla eruption. The interaction of melted snow with fresh ash increased dissolved Fe, Al, and F concentrations in surface waters so that they exceeded the allowable drinking water standards prescribed by the European Community (1998) by factors of 1350, 650, and 560, respectively. When the rainwater dissolved the salts from pristine volcanic ash originating from the 2000 Mt. Hekla eruption, F, Al, Fe, Mn, and Pb in local river waters exceeded drinking water standards given by European Community (1998). Aiuppa et al.

(2000) studied the influence of magmatic gasses, especially CO_2, on groundwater chemical composition in vicinity of the Mt. Etna volcano. They showed that the inflow of magmatic CO_2 into shallow groundwaters increased basaltic host rock dissolution leading to increased trace element concentrations, which they referred to as 'natural pollution'. Some dissolved elements, notably As, Se, Mo, and Cd concentrations exceeded WHO (World Health Organisation) drinking water limits (WHO, 2008).

Waters released during both glacial floods considered in this study were alkaline and non-toxic; all measured element concentrations were below WHO drinking water standards (WHO, 2008) or the Icelandic Directorate threshold for category III surface water (IcD, 1999). This suggests that 1) the direct input of acid gases (e.g. CO_2, SO_2, HCl, HF) to the flood waters was limited and/or 2) sufficient water-basalt interaction occurred to neutralize the fluids. If magmatic gases were present directly in abundance, their dissolution and dissociation would lower water pH and provoke the release of toxic metals from dissolving basalt. The higher the quantity of dissolved acid gas concentration, the more basalt dissolution required for its neutralization. The composition of the flood waters described in this study, having high alkalinity and low SO_4, Cl and F concentrations, were similar to Icelandic geothermal waters (e.g. Kaasalainen 2012; Kaasalainen and Stefánsson, 2012) confirming their neutralization by long term water-rock interaction and the potential for co-precipitation of toxic metals in secondary phases such as Al-, Fe-(oxy)hydroxides and clays.

5.6.4. Particulate material transport

Studies on the global cycles of the elements have been focused mainly on the dissolved fluxes. However, dissolved transport of elements to the ocean is more significant only for Na (Oelkers et al., 2012). The transport of other metals is dominated by the particulates; approximately 1Gt/year of dissolved flux and 15-20 Gt/year of the suspended flux are carried by the rivers (Gaillardet et al., 1999, 2003). The ratios of the concentration of selected elements in the flood water transported in particulate and in dissolved form varied from 10^2 to $10^{7.5}$. The most soluble elements such as Na, Ca, Sr, and K had the lowest ratios, up to 10^4, whereas the most immobile elements such as Ti, Al, and Fe had the highest ratios, more than 10^6 (Fig. 9). These high ratios indicate that the element flux during the floods was mostly transported as particulates; dissolved fluxes were significantly less important in overall transport budget. Due to the importance of suspended particle transport the movement of insoluble elements such as Ti, Al, and Fe were far more affected by the floods than soluble elements such as Na, Ca, Sr, and K.

Comparison of the particulate to dissolved flux ratios of selected elements during the floods to the average global flux ratios reported by Oelkers et al. (2011) shows that ratios were two to six orders of magnitude higher depending on element. For example, the ratio of element concentrations in suspended particulate and in dissolved form for Si, Ca, Mg, Na, and K during the floods were only 2-2.5 orders of magnitude higher than their corresponding global ratios, whereas for trace elements such as Fe, Ti, Al, V, Mn, Sr, Ba, Cr the ratios were 3-6 orders of magnitude higher, revealing that floods increased significantly the trace elements suspended flux. This implies that the high discharge during the flood increases both macro and micro nutrients suspended flux but the latter is far more affected. Micronutrients play an important role in primary production, serving as catalysts for biochemical reactions (White, 1999; Eiriksdottir et al., 2013c). The highest measured concentration of suspended material during Múlakvísl flood was 47 g/L in sample 2011-09-07_1220, however, the suspended particle concentration could have been even higher at the flood peak. Nevertheless, even measured values are dramatically higher than that commonly observed in Icelandic rivers, which depending on the discharge ranges up to a few of g/L, but does not usually exceed 1 g/L (Eiriksdottir et al., 2011, 2012, 2013b). In addition, the major phase in the suspended particulate material was basaltic glass which is highly reactive (Gislason and Oelkers, 2003; Wolff-Boenisch et al., 2004). This particulate material, once deposited along the coast can serve as slow release fertilizer, promoting primary production for extended time periods (Eiriksdottir and Gislason, 2004, Eiriksdottir et al., 2013c). In addition, the divalent cations especially Ca transported in suspended material into the sea will finally dissolve and part of it will precipitate as carbonates affecting the global carbon cycle (Gislason et al., 2006).

Results presented above confirm the sensitivity of element suspended flux to the discharge. Increased rivers discharge/runoff due to intensified rainfall and glacier melting as a result of climate change will affect the amount of suspended particulates deposited at the seacoast and therefore seawater chemistry. This will further affect the primary production and therefore carbon and nitrogen global cycle.

5.7. CONCLUSIONS

There are several major conclusions that can be drawn from this study of the composition of the Múlakvísl and Kaldakvísl flood waters:

1. The flood waters were non-toxic. Although some limited quantity of acid gases, mainly CO_2, was apparently added to these waters sub-glacially, sufficient fluid-rock interaction occurred to neutralize them.
2. As indicated by reaction transport modelling – this neutralization likely occurred sub-glacially and took substantial time. These observations

confirm lack of direct contact of magma with the sub-glacial water the day before the floods.

3. Compared to larger scale Icelandic floods associated with sub-glacial volcanic eruptions; there was no major flux of CO_2 or fixation during Múlakvísl and Kaldakvísl floods.
4. Although there was no major increase in overall dissolved fluxes in Múlakvísl and Kaldakvísl Rivers during the floods, due to increased discharge there was a major increase in particulate flux. This will influence significantly the metal and nutrients budget at the seacoast over the long term.

Acknowledgements

The authors would like to thank all colleagues and co-workers in particular: Eydis Eiriksdottir, Niels Óskarsson, Domenik Wolff-Boenisch, Kiflom Gebrehiwot, Snorri Gudbrandsson, Nicole Keller and Hanna Kaasalainen. Sigurður P. Ásólfsson, Eric Sturkell and Reynir Ragnarsson are acknowledged for their help in collecting the water samples. Rósa Ólafsdóttir and Þórdís Högnadóttir are gratefully thanked for their assisting in preparing the figures. The Icelandic Metoerological Office is thanked for permission to publish Figure 2b.The work was funded by the Icelandic Science Foundation RANNÍS 121071-0061, the European Union through the European Marie Curie network Delta-Min Grant#PITN-GA-2008-215360, Landsvirkjun and Institute of Earth Sciences, University of Iceland.

References

Aiuppa A., Dongarrà G., Capasso G., Allard P. (2000a) Trace elements in the thermal groundwaters of Vulcano Island (Sicily). *J. Volcanol. Geothermal Res.* **98**, 189-207.

Aiuppa A., Allard P., D'Alessandro W., Michel A., Parello F., Treuil M.,Valenza M. (2000b) Mobility and fluxes of major, minor and trace metals during basalt weathering and groundwater transport at Mt. Etna volcano (Sicily). *Geochim. Cosmochim. Acta*, **64**, 1827-1841.

Aiuppa A., D'Alessandro W., Federico C., Palumbo B., Valenza M. (2003) The aquatic geochemistry of arsenic in volcanic groundwaters from southern Italy. *App. Geochem.* **18**, 1283-1296.

Aiuppa A., Federico C., Allard P., Gurrieri S., Valenza M. (2005) Trace metal modeling of groundwater–gas–rock interactions in a volcanic aquifer: Mount Vesuvius, Southern Italy. *Chem. Geol.* **216**, 289-311.

Alfredsson H.A., Oelkers E.H., Hardarsson B.S., Franzson H., Gunnlaugsson E., Gislason S.R. (2013) The geology and water chemistry of the Hellisheidi, SW-Iceland carbon storage site. *Int. J. Greenhouse Gas Control* **12**, 399-418.

Alho P., Russell A.J., Carrivick J.L., Käyhkö J. (2005) Reconstruction of the largest Holocene jökulhlaup within Jökulsá á Fjöllum, NE Iceland. *Quaternary Science Reviews* **24**, 2319-2334.

Ambrosio M., Doveri M., Fagioli M.T., Marini L., Principe C., Raco B. (2010) Water–rock interaction in the magmatic-hydrothermal system of Nisyros Island (Greece). *J. Volcanol. Geothermal Res.* **192**, 57-68.

Arnórsson S. (2000) Isotopic and chemical techniques in geothermal exploration, developmnent and use. Sampling methods, data handling, interpretation. International Atomic Energy Agency, Vienna, 2000.

Arnórsson S., Sigurdsson S., Svavarsson H. (1982) The chemistry of geothermal waters in Iceland. I. Calculation of aqueous speciation from 0 to 370 °C. *Geochim. Cosmochim. Acta* **46**, 1513-1532.

Arnórsson S., Gunnlaugsson E., and Svavarsson H. (1983) The chemistry of geothermal waters in Iceland. II. Mineral equilibria and independent variables controlling water compositions. *Geochim. Cosmochim. Acta* **47**, 547-566.

Arnórsson S., Gislason S.R. (1994) CO_2 from magmatic sources in Iceland. *Min. Mag.* **58,** 27-28.

Arnórsson S., Axelsson G., Sæmundsson K. (2008) Geothermal systems in Iceland. *Jökull* **58,** 269-302.

Björnsson H. (1998) Hydrological characteristics of the drainage system beneath a surging glacier. *Nature* **395**, 771-774.

Björnsson H. (2003) Subglacial lakes and jökulhlaups in Iceland. *Global and Planetary Change* **35**, 255-271.

Björnsson H., Pálsson F., Gudmundsson M.T. (2000) Surface and bedrock topography of Mýrdalsjökull ice cap, Iceland: The Katla caldera, eruption sites and routes of Jökulhlaups. *Jökull* **49**, 29-46.

Björnsson H., Pálsson F. (2008) Icelandic glaciers. *Jökull* **58**, 365-386.

Bourcier W.L., Peiffer D.W., Knauss K.G., McKeegan K.D., Smith, D.K. (1990) A kinetic model for borosilicate glass dissolution based on the dissolution affinity of a surface alteration layer. *Mat. Res. Soc. Symp. Proc.* **176**, 209-216.

Brunauer S, Emmett P.H., Teller E. (1938) Adsorption of gases in multimolecular layers. *J. Am. Chem. Society* **60**, 309–319.

Brunner G.W. (2010) HEC-RAS River Analysis System. User's Manual, Version 4.1. US Army Corps of Engineers. Hydrologic Engineering Center.

Cioni R., Guidi M., Raco B., Marini L., Gambardella B. (2003) Water chemistry of Lake Albano (Italy). *J. Volcanol. Geothermal Res.* **120**, 179-195.

Crovisier J.L., Honnorez J., Fritz, B., Petit, J.C. (1992) Dissolution of subglacial volcanic glasses from Iceland: laboratory study and modelling. *App. Geochem.* **7**, *Supplement 1*, 55-81.

Daux V., Guy C., Advocat T., Crovisier J.-L., Stille P. (1997) Kinetic aspects of basaltic glass dissolution at 90 °C: role of aqueous silicon and aluminium. *Chem. Geol.* **142**, 109-126.

D'Alessandro W., Aiuppa A., Bellomo S., Brusca L., Calabrese S., Kyriakopoulos K., Liotta M., Longo M. (2013) Sulphur-gas concentrations in volcanic and geothermal areas in Italy and Greece: Characterising potential human exposures and risks. *J. Geochem. Exploration* **131**, 1-13.

Delmelle P., Lambert M., Dufrene Y., Gerin P., Oskarsson N. (2007) Gas/aerosol-ash interaction in volcanic plumes: new insights from surface analyses of fine ash particles. *Earth and Planetary Sci. Lett.* **259**, 159-170.

Eiriksdottir E.S. (2007) Chemical and mechanical weathering of basalt: Measured and modelled data from North-East Iceland. Master Thesis at Faculty of Science, University of Iceland.

Eiriksdottir E.S., Gislason S.R., Snorrason Á., Harðardóttir J., Þorláksdóttir S.B., Axelsson E., Sveinbjörnsdóttir Á.E. (2011) Efnasamsetning, rennsli og aurburður straum-vatna á Austurlandi VIII. Gagnagrunnur Jarðvísindastofnunar of Veðurstofnunar. Report RH-04-2011.

Eiriksdottir E.S., Gislason S.R., Snorrason Á., Harðardóttir J., Þorláksdóttir S.B., Sveinbjörnsdóttir Á.E. (2012) Efnasamsetning, rennsli og aurburður straum-vatna á Austurlandi IX. Gagnagrunnur Jarðvísindastofnunar of Veðurstofnunar. Report RH-05-2012.

Eiriksdottir E.S., Gislason S.R., Oelkers, E.H. (2013a). Does temperature or runoff control the feedback between chemical denudation and climate? Insights from NE Iceland. *Geochim. Cosmochim. Acta* **107**, 65-81.

Eiriksdottir E.S., Gislason S.R., Harðardóttir J., Þorláksdóttir S.B. (2013b) Efnasamsetning, rennsli og aurburður straum-vatna á Suðurlandi XVI. Gagnagrunnur Jarðvísindastofnunar of Veðurstofnunar. Report RH-14-2013.

Eiriksdottir E.S., Gislason S.R. and Oelkers, E.H. (2013c) *Min. Mag.* **77(5)**, 1032.

European Community (1998) Council directive 98/83 Official Journal of the European Communities.

Federico C., Aiuppa A., Allard P., Bellomo S., Jean-Baptiste P., Parello F., Valenza M. (2002) Magma-derived gas influx and water-rock interactions in the volcanic aquifer of Mt. Vesuvius, Italy. *Geochim. Cosmochim. Acta* **66**, 963-981.

Federico C., Aiuppa A., Favara R., Gurrieri S., Valenza M. (2004) Geochemical monitoring of groundwaters (1998–2001) at Vesuvius volcano (Italy). *J. Volcanol. Geothermal Res*. **133**, 81-104.

Floor G.H., Calabrese S., Román-Ross G., D´Alessandro W., Aiuppa, A. (2011) Selenium mobilization in soils due to volcanic derived acid rain: An example from Mt Etna volcano, Sicily. *Chem. Geol*. **289**, 235-244.

Flaathen T.K., Gislason S.R. (2007) The effect of volcanic eruptions on the chemistry of surface waters: The 1991 and 2000 eruptions of Mt. Hekla, Iceland. *J. Volcanol. Geothermal Res.* **164**, 293-316.

Flaathen T.K., Gislason S.R., Oelkers, E.H., Sveinbjörnsdóttir, Á.E. (2009) Chemical evolution of the Mt. Hekla, Iceland, groundwaters: A natural analogue for CO_2 sequestration in basaltic rocks. *App. Geochem.* **24,** 463-474.

Freysteinsson S. (1972) Jokulhlaup í Koldukvisl. *Jökull* **22**, 83-88.

Frogner P., Gislason S.R., Óskarsson N. (2001) Fertilizing potential of volcanic ash in ocean surface water. *Geology* **26**, 487-490.

Geirsdóttir Á., Hardardóttir J., Sveinbjörnsdóttir Á.E. (2000) Glacial extent and catastrophic meltwater events during the deglaciation of Southern Iceland. *Quaternary Sci. Reviews* **19**, 1749-1761.

Gaillardet J., Dupré B., Allégre C. (1999) Geochemistry of large river suspended sediments: silicate weathering or recycled tracers? *Geochim. Cosmochim. Acta* **63**, 4037-4051.

Gaillardet J., Viers J., Dupré B. (2003) Trace elements in river waters. In: J.I. Drever, (Ed.). Surface and Groundwater, Weathering, and Soils, vol. 5. In: Holland, H.G., Turekian, K.K., (Exec. Eds.), Treatise on Geochemistry. Elsevier.

Gislason S.R., Eugster H.P. (1987) Meteoric water-basalt interactions. II: A field study in N.E. Iceland. *Geochim. Cosmochim. Acta* **51**, 2841-2855.

Gislason S.R., Arnorsson S. and Armannsson H. (1996) Chemical weathering of basalt in Southwest Iceland; effects of runoff, age of rocks and vegetative/glacial cover. *Am. J. .Sci.* **296**; 837-907.

Gislason S.R., Snorrason Á., Kristmannsdóttir H.K., Sveinbjörnsdóttir Á.E., Torsander P., Ólafsson J., Castet S., Dupré B. (2002) Effects of volcanic eruptions on the CO_2 content of the atmosphere and the oceans: the 1996 eruption and flood within the Vatnajökull Glacier, Iceland. *Chem. Geol*. **190**; 181-205.

Gislason S.R., Snorrason Á., Eiriksdottir Sigfússon B., Elefsen S.Ó., Harðardóttir J., Gunnarsson Á., Hreinsson E.Ö., Torssander P., Kardjilov M.I., Óskarsson N. (2003) Efnasamsetning, rennsli og aurburður straumvatna á Austurlandi, IV. Gagnagrunnur Raunvísindastofnunar of Orkustofnnunar. Raunvísindastofnun, Reykjavík. RH-04-2003, 97 bls.

Gislason S.R., Oelkers, E.H. (2003) Mechanism, rates, and consequences of basaltic glass dissolution: II. An experimental study of the dissolution rates of basaltic glass as a function of pH and temperature. *Geochim. Cosmochim. Acta* **67**, 3817-3832.

Gislason S.R., Eiriksdottir E.S. (2004) Molybdenum control of primary production in the terrestrial environment. Water-Rock Interaction, Proceedings of the Eleventh International Symposium on Water-Rock Interaction, 27 June-2 July 2004, Saratoga Springs, New York, USA. Edited by Richard B. Wanty, Robert R. Seal II.

Gislason S.R., Oelkers E.H., Snorrason Á. (2006) Role of river-suspended material in the global carbon cycle. *Geology* **34**, 49-52.

Gislason S. R., Hassenkam T., Nedel S., Bovet N., Eiriksdottir E. S., Alfredsson H. A., Hem C. P., Balogh Z. I., Dideriksen K., Óskarsson N., Sigfusson B., Larsen G., Stipp S. L. S. **(**2011) Characterization of Eyjafjallajökull volcanic ash particles and a protocol for rapid risk assessment. *PNAS* **108**, 7307-7312.

Gudmundsson M.T., Sigmundsson F., Bjornsson H. (1997) Ice-volcano interaction of the 1996 Gjalp subglacial eruption, Vatnajokull, Iceland. *Nature* **389**, 954-957.

Gudmundsson M. T., Elíasson J., Larsen G., Gylfason Á. G., Einarsson P., Jóhannesson T., Hákonardóttir K. M., Torfason H. (2005) Yfirlit um hættu vegna eldgosa og hlaupa frá vesturhluta Mýrdalsjökuls og Eyjafjallajökli. Í: Magnús T. Guðmundsson og Ágúst Gunnar

Gylfason (ritstj.): Hættumat vegna eldgosa og hlaupa frá vestanverðum Mýrdalsjökli og Eyjafjallajökli. Ríkislögreglustjórinn og Háskólaútgáfan. 11-44.

Gudmundsson M.T., Högnadóttir T. (2007) Volcanic systems and calderas in the Vatnajökull region, central Iceland: Constraints on crustal structure from gravity data. *J. Geodynamics* **43**, 153-169.

Gudmundsson M., Larsen G., Höskuldsson Á., Gylfason Á.G. (2008) Volcanic hazards in Iceland. *Jökull* **58**, 251-268.

Gudmundsson M.T., Högnadóttir T. (2011) Upptök of stærð jökulhlaups í Mulakvisl – niðurstöður flugmælinga. Minnisblað 13. Júlí 2011.

Gudmundsson M.T., Larsen G., Sigmarsson O. (2013) Katla. In: Sólnes, J., Sigmundsson F., Bessason B.,Náttúruvá Á Íslándi. Eldgos og Jarðskjálftar. Viðlagatrygging Íslands/Háskólaútgáfan 2013.

Gysi A.P., Stefánsson A. (2011) CO_2–water–basalt interaction. Numerical simulation of low temperature CO_2 sequestration into basalts. *Geochim. Cosmochim. Acta* **75**, 4728-4751.

Hannesdottir L.B. (2011) Minnisblað: Flód í Hagongulon 13. Júlí 2011. Report for Landsvirkjun Power Company.

Hjartarson Á. (1994) Vatnafarskort og grunnvatnskortlagning. Master Thesis at Faculty of Science, University of Iceland.

IcD, 1999. Reglugerð: um varnir gegn mengun vatns. Icelandic Directive, Reykjavik. *http://www.reglugerd.is/interpro/dkm/Webguard.nsf/lookByNumber/7961999?OpenDocument, 4.7*

IMO, Icelandic Meteorological Office (2013) *http://en.vedur.is/*

Jones M.T., Gislason S.R. (2008) Rapid releases of metal salts and nutrients following the deposition of volcanic ash into aqueous environments. *Geochim. Cosmochim. Acta* **72**, 3661-3680.

Jones M.T., Pearce C.R., Jeandel C., Gislason S.R., Eiriksdottir E.S., Mavromatis V., Oelkers, E.H. (2012a) Riverine particulate material dissolution as a significant flux of strontium to the oceans. *Earth and Planetary Sci. Lett.* **355–356**, 51-59.

Jones M.T., Pearce C.R., Oelkers, E.H. (2012b) An experimental study of the interaction of basaltic riverine particulate material and seawater. *Geochim. Cosmochim. Acta* **77**, 108-120.

Jónsson G.Þ., Þórarinsdóttir T. (2011) Hlaup í Múlakvísl 8-10. Júlí 2011. Report for Icelandic Meteorological Office.

Kaasalainen H. (2012) Chemistry of metals and sulphur in geothermal fluids, Iceland. Doctoral thesis at Faculty of Science, University of Iceland.

Kaasalainen H., Stefánsson A. (2012) The chemistry of trace elements in surface geothermal waters and steam, Iceland. *Chem. Geol*. **330-331**, 60-85.

Kristmannsdottir H. (1979) Alteration of Basaltic Rocks by Hydrothermal-Activity at 100-300 °C. In: M.M. Mortland and V.C. Farmer (Editors), Developments in Sedimentology. Elsevier, pp. 359-367.

Kristmannsdottir H. (1982) Alteration in the IRDP dill hole compared with other drill holes n Iceland. *J. Geophysical Res*. **87**, 6525-6531.

Kristmannsdóttir H., Björnsson A., Pálsson S., Sveinbjörnsdóttir Á.E. (1999) The impact of the 1996 subglacial volcanic eruption in Vatnajökull on the river Jökulsá á Fjöllum, North Iceland. *J. Volcanol. Geothermal Res*. **92**, 359-372.

Kristmannsdóttir H., Gislason S. R., Snorrason Á., Elefsen S. Ó., Hauksdóttir S., Sveinbjörnsdóttir Á. and Haraldsson H. (2006) Þróun efnavöktunarkerfis til varnar mannvirkjum við umbrot í jökli. Orkustofnun, Vatnamælingar, Reykjavík, OS-2006/014, ISBN 9979-68-206-X, 54 bls.

Larsen G. (2000) Holocene eruptions within the Katla volcanic system, south Iceland: Characteristic and environmental impact. *Jökull* **49**, 1-28.

Louvat P., Gislason S.R., Allégre C.J. (2008) Chemical and mechanical erosion ratesin Iceland as deduced from river dissolved and solid material. *Am. J. Sci.* **308**, 679–726.

Maizels J. (1997) Jökulhlaup deposits in proglacial areas. *Quaternary Sci. Reviews* **16**, 793-819.

Marini L., Vetuschi Zuccolini M., Saldi G. (2003) The bimodal pH distribution of volcanic lake waters. *J. Volcanol. Geothermal Res*. **121**, 83-98.

Marteinsson V.T, Runarsson A., Stefánsson A., Thorsteinsson T., Johannesson T., Magnusson S.H., Reynisson E., Einarsson B., Wade N., Morrison H.G., Gaidos E. (2013) Microbial communities in the subglacial waters of the Vatnajökull ice cap, Iceland. *ISME J*, **7**, 427-437.

Milliman J.D., Syvitski J.P.M. (1992) Geomorphic/tectonic control of sediment discharge to the ocean. The importance of small mountainous rivers. *J. Geology* **100**, 525-544.

Oelkers E.H., Gislason S.R. (2001) The mechanism, rates and consequences of basaltic glass dissolution: I. An experimental study of the dissolution rates of basaltic glass as a function of aqueous Al, Si and oxalic acid concentration at 25 °C and pH = 3 and 11. *Geochim. Cosmochim. Acta* **65**, 3671-3681.

Oelkers E.H., Gislason S.R., Eiriksdottir E.S., Elefsen S.O., Hardardottir J. (2004) The significance of suspended material in the chemical transport in rivers of NE, Iceland. In Water Rock Interactions (Wanty, R.B. and Seal II R.R., eds.), 865-868. Taylor & Francis Group, London.

Oelkers E.H., Gislason S.R., Eiriksdottir E.S., Jones M., Pearce C.R., Jeandel C. (2011) The role of riverine particulate material on the global cycles of the elements. *App. Geochem.* **26**, Supplement, S365-S369.

Oelkers E.H., Jones M.T., Pearce C.R., Jeandel C., Eiriksdottir E.S., Gislason S.R. (2012) Riverine particulate material dissolution in seawater and its implications for the global cycles of the elements. *Comptes Rendus Geosci.* **344**, 646-651.

Óladóttir B.A., Sigmarsson O., Larsen G., Thordarson T. (2008) Katla volcano, Iceland: magmatic composition, dynamics and eruption frequency as recorded by Holocene tephra layers. *Bull. Volcanol.* **70**, 475-493.

Oskarsdottir S.M., Gislason S.R., Snorrason A., Halldorsdottir S.G., Gisladottir G. (2011) Spatial distribution of dissolved constituents in Icelandic river waters. *J. Hydrology* **397**, 175-190.

Óskarsson N. (1980) The interaction between volcanic gases and tephra: fluorine adhering to tephra of the 1970 Hekla eruption. *J. Volcanol. Geothermal Res*. **8**, 251-266.

Pálsson S., Vigfusson G.H. (1996) Results of Suspended Load and Discharge Measurements 1963-1995. Reykjavik, National Energy Authority OS-96032/VOD-05 B.

Pogge von Strandmann P.A.E., Burton K.W., James R.H., van Calsteren P., Gislason S.R., Sigfússon B. (2008) The influence of weathering processes on riverine magnesium isotopes in a basaltic terrain. *Earth and Planetary Sci. Lett.* **276,** 187-197.

Roberts M.J., Russell A.J., Tweed F.S., Knudsen Ó. (2000) Ice fracturing during jökulhlaups: implications for englacial flood water routing and outlet development. *Earth Surface Processes and Landforms* **25**, 1429-1446.

Russell A.J., Roberts M.J., Fay H., Marren P.M., Cassidy N.J., Tweed F.S., Harris T. (2006) Icelandic jökulhlaup impacts: Implications for ice-sheet hydrology, sediment transfer and geomorphology. *Geomorphology* **75,** 33-64.

Russell A.J., Tweed F.S., Roberts M.J., Harris T.D., Gudmundsson M.T., Knudsen Ó., Marren P.M., (2010) An unusual jökulhlaup resulting from subglacial volcanism, Sólheimajökull, Iceland. *Quaternary Sci. Reviews* **29**, 1363-1381.

Sigfússon B. (2009) Reactive transport of arsenic through basaltic porous media. A PhD Thesis submitted for the degree of Doctor of Philosophy at University of Aberdeen, UK.

Sigurdsson F., Ingimarsson J. (1990) The permeability of Icelandic rocks. Lekt íslenskra Jardefna, in Sigbjarnarson, G. editor, The water and the land. A hydrology conference: Reykjavik, National Energy Authority, p. 121-128 (in Icelandic).

Snorrason Á., Jónsson P., Sigurdsson O., Pálsson S., Árnason S., Víkingsson S., Kaldal I. (2002) November 1996 jökulhlaup on Skeidarársandur outwash plan. Iceland. In: Martin P., Baker V.R. and Garzón G. eds. Flood and Megaflood Processes and Deposits. Recent and Ancient Examples. Special Publ. 32 of the International Association of Sedimentologists, Blackwell Science, Oxford, 55-67.

Stefánsdóttir M.B., Gislason S.R. (2005) The erosion and suspended matter/seawater interaction during and after the 1996 outburst flood from the Vatnajökull Glacier, Iceland. *Earth and Planetary Sci. Lett.* **237**, 433-452.

Stefánsson A., Gislason S.R. (2001) Chemical Weathering of Basalts, Southwest Iceland: Effect of Rock Crystallinity and Secondary Minerals on Chemical Fluxes to the Ocean. *Am. J. Sci*. **301**, 513-556.

Steinthórsson S., Óskarsson N. (1986) Energetics of hydrothermal systems. In: Extended abstracts of Fifth International symposium on water-rock interaction, Reykjavik, Iceland, August 8-17. Orkustofnun, National Energy Authority.

Stumm W., Morgan J.J. (1996) Aquatic chemistry. Chemical Equilibria and Rates in Natural Waters. 3rd ed. New York, John Wiley & Sons, p. 683.

Taran Y., Rouwet D., Inguaggiato S., Aiuppa, A. (2008) Major and trace element geochemistry of neutral and acidic thermal springs at El Chichón volcano, Mexico: Implications for monitoring of the volcanic activity. *J. Volcanol. Geothermal Res.* **178**, 224-236.

Thordarson T., Larsen G. (2007) Volcanism in Iceland in historical time: Volcano types, eruption styles and eruptive history. *J. Geodynamics* **43**, 118-152.

Thordarson T., Höskuldsson Á. (2008) Postglacial volcanism in Iceland. *Jökull* **58**, 197-228.

Tómasson H. (1996) The jökuhlaup from Katla in 1918. *Annals of Glaciology* **22**, 249-254.

Vigier N., Gislason S.R., Burton K.W., Millot R., Mokadem F. (2009) The relationship between riverine lithium isotope composition and silicate weathering rates in Iceland. *Earth and Planetary Sci. Lett.* **287**, 434-441.

Wada K., Arnolds O., Kakuto Y., Wilding L.P., Hallmark C.T. (1992) Clay minerals of four soils formed in eolian and tephra materials in Iceland. *Geoderma* **52**, 351-365.

Waitt R.B. (2002) Great Holocene floods along Jökulsá á Fjöllum, north Iceland In: Martin P., Baker V.R. and Garzón G. eds. Flood and Megaflood Processes and Deposits. Recent and Ancient Examples. Special Publ. 32 of the International Association of Sedimentologists, Blackwell Science, Oxford, 37-51.

White D. (1999) The physiology & Biogeochemistry of Prokaryotes, 2nd Ed. Oxford: Oxford University Press.

WHO (2008) Guidelines for Drinking-water Quality. Third edition incorporating the first and second agenda. Volume 1, Recommendations. Geneva.

Wolff-Boenisch D., Gislason S.R., Oelkers E.H., Putnis C.V. (2004) The dissolution rates of natural glasses as a function of their composition at pH 4 and 10.6, and temperatures from 25 to 74 °C. *Geochim. Cosmochim. Acta* **68**, 4843-4858.

Wolff-Boenisch D., Wenau S., Gislason S.R., Oelkers E.H. (2011) Dissolution of basalts and peridotite in seawater, in the presence of ligands, and CO_2: Implications for mineral sequestration of carbon dioxide. *Geochim. Cosmochim. Acta* **75**, 5510-5525.

Zhu C., Lu, P. (2009) Alkali feldspar dissolution and secondary mineral precipitation in batch systems: 3. Saturation states of product minerals and reaction paths. *Geochim. Cosmochim. Acta* **73**, 3171-3200.

Supplementary data for Chapter 5

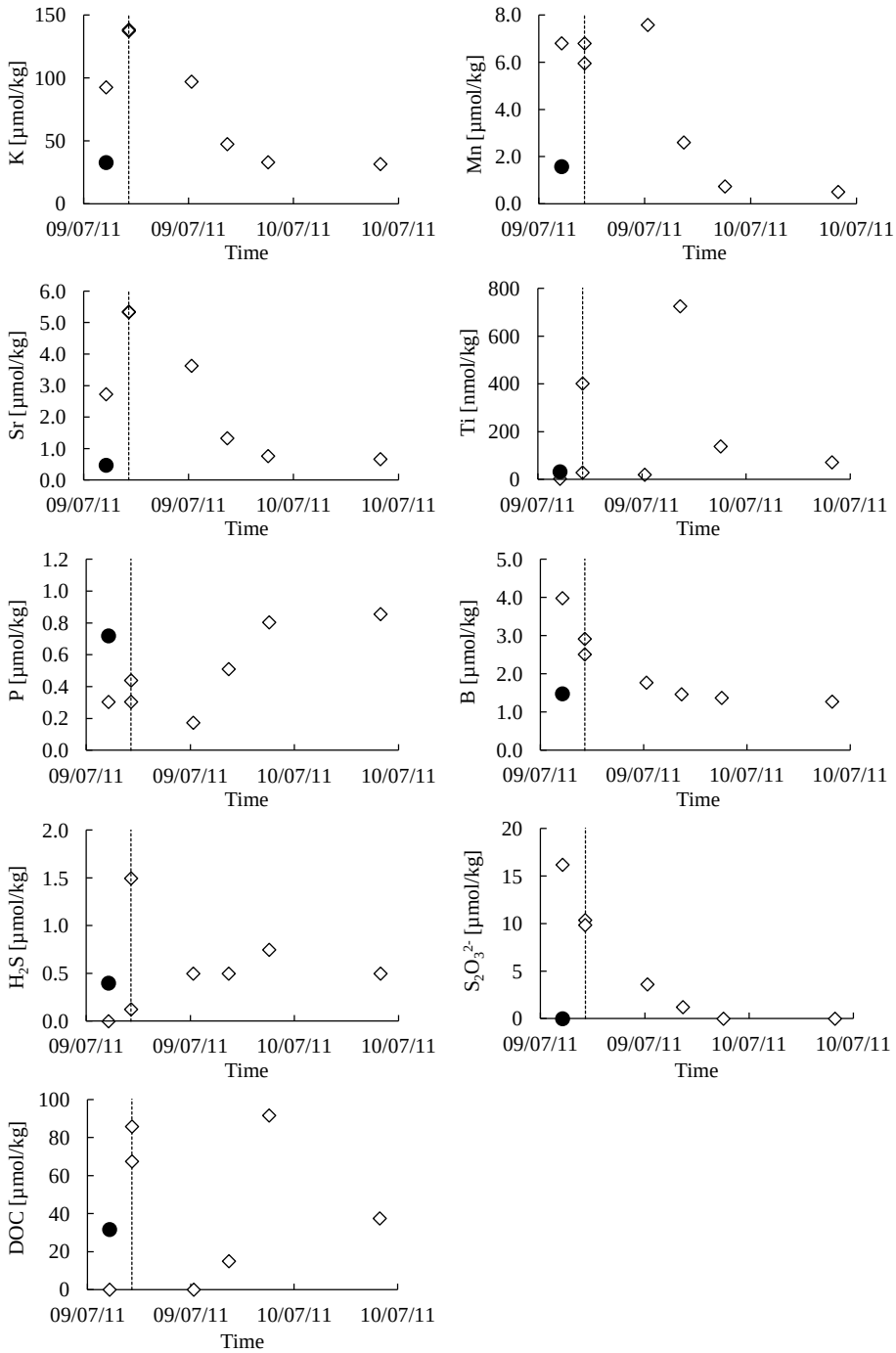

Figure 1. The element concentrations in the sampled waters during the Múlakvísl flood. The filled circles on some of the plots represent the background for the Múlakvísl River. The vertical line represents the peak of the flood.

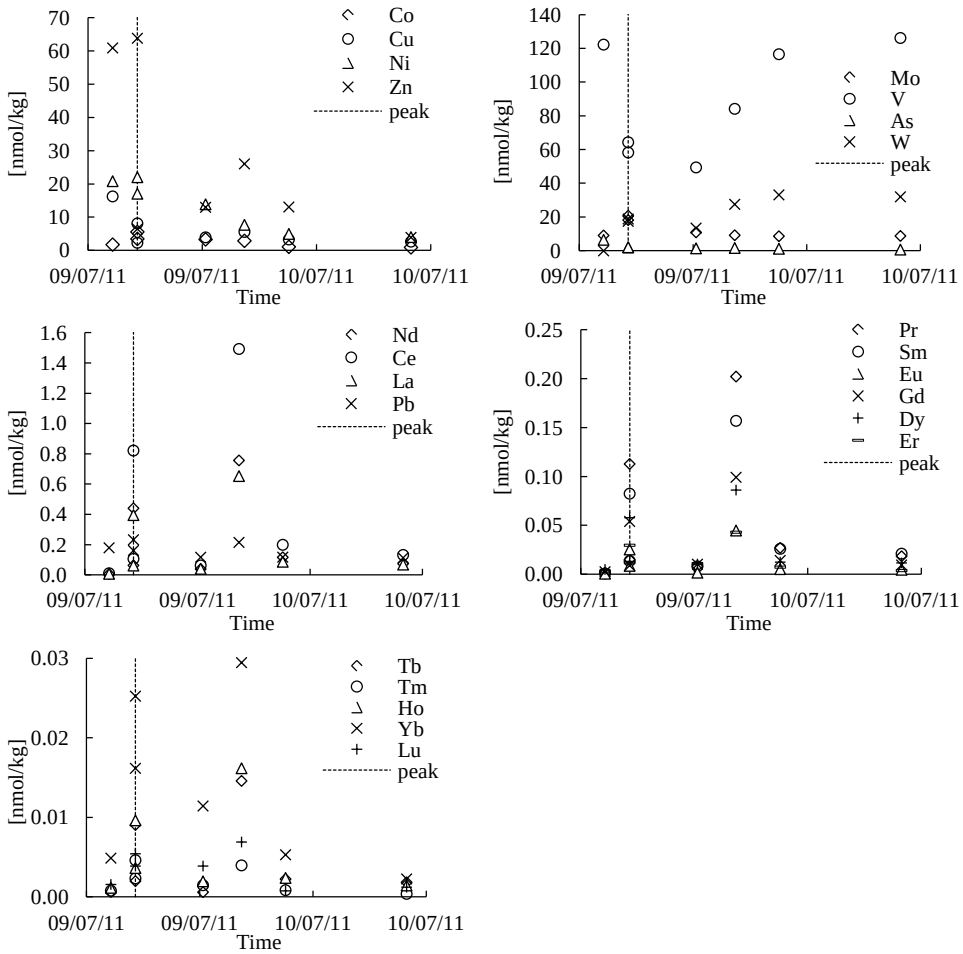

Figure 1. Continuation.

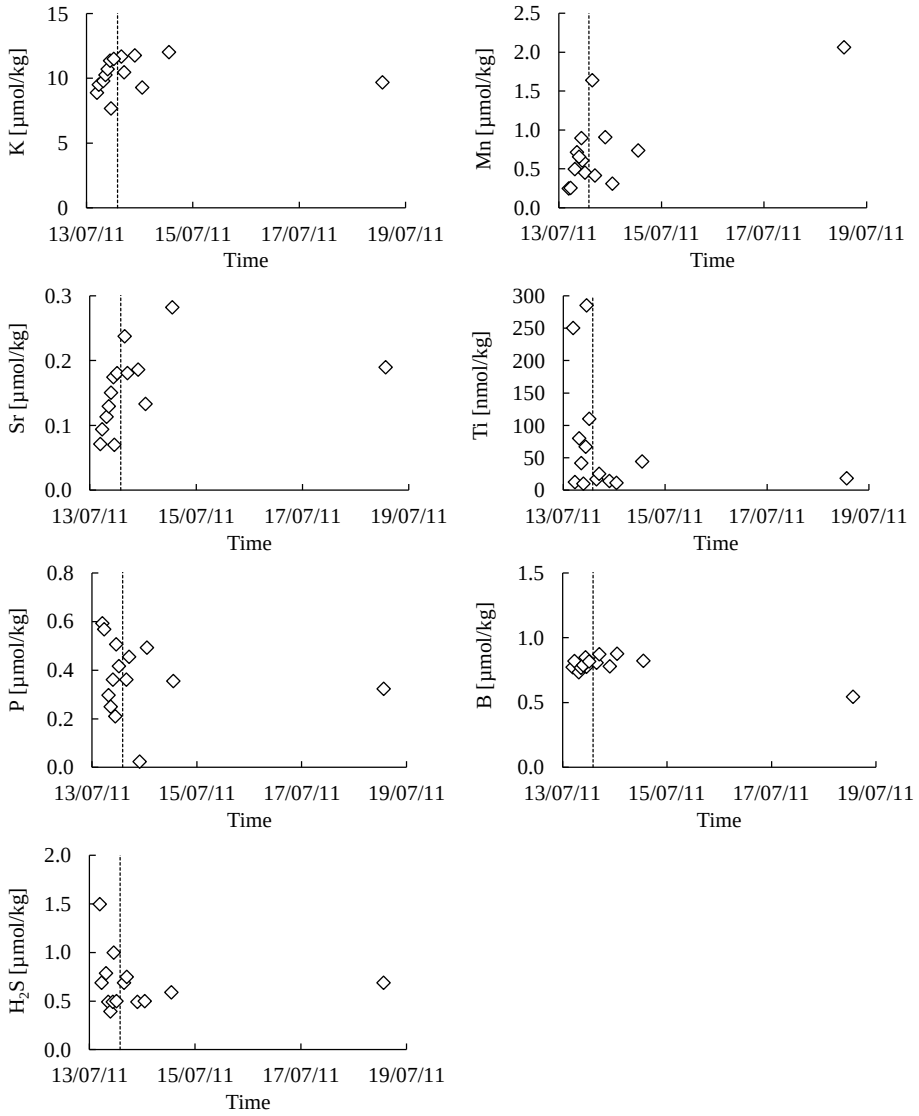

Figure 2. The element concentrations in the sampled waters during the Kaldakvísl flood. The vertical line represents the peak of the flood.

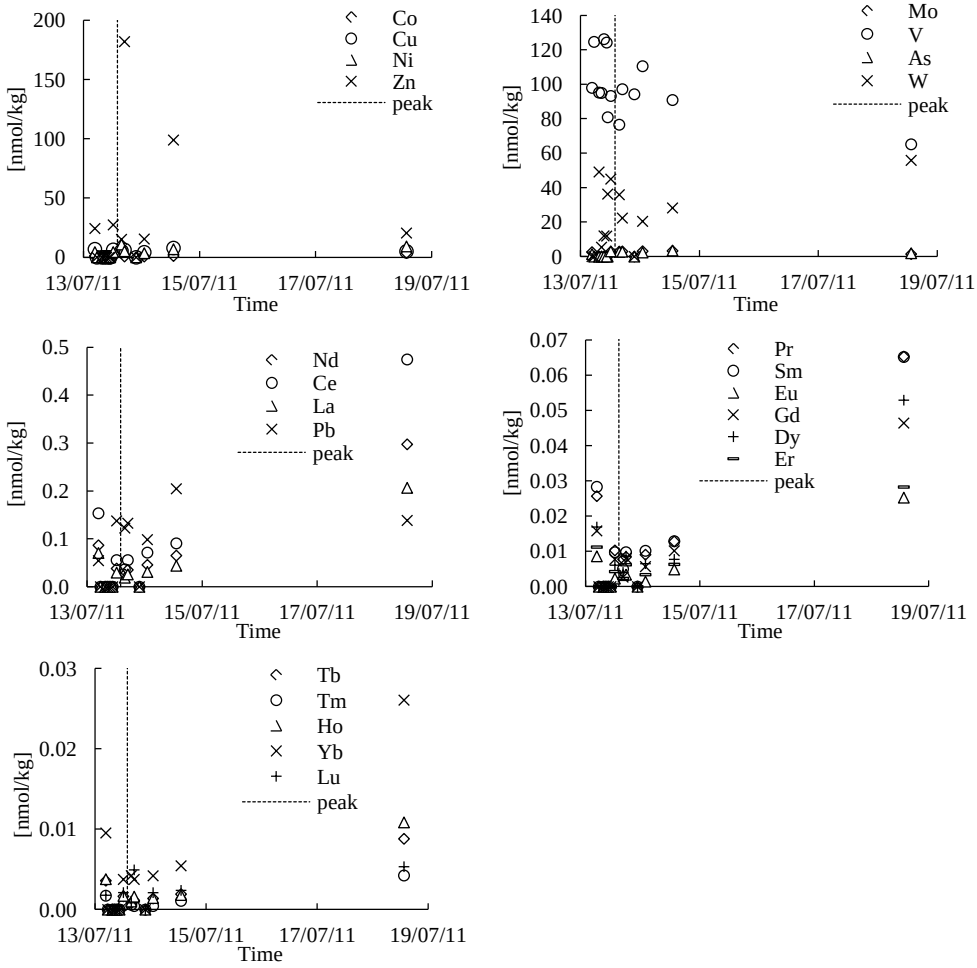

Figure 2. Continuation.

Supplementary data for Chapter 3

An experimental study of basaltic glass-H_2O-CO_2 interaction at 22 and 50 °C: Implications for subsurface storage of CO_2

Table 1. Chemical composition of the basaltic glass measured with X-ray Fluorescence spectrometry (XRF).

Element	Stapafell, Iceland[a]	Stapafell, Iceland[b]
	Weight %	
SiO_2	48.23	48.12
Al_2O_3	14.52	14.62
CaO	11.93	11.84
Fe_2O_3	11.96	1.11
FeO		12.02
K_2O	0.27	0.29
MgO	8.94	9.08
MnO	0.20	0.19
Na_2O	1.80	1.97
P_2O_5	0.19	0.20
TiO_2	1.55	1.56
Total	99.48	99.89

[a] used in this study. Fe_2O_3 represents total iron (Fe^{2+} and Fe^{3+})
[b] used by Gislason and Oelkers 2003

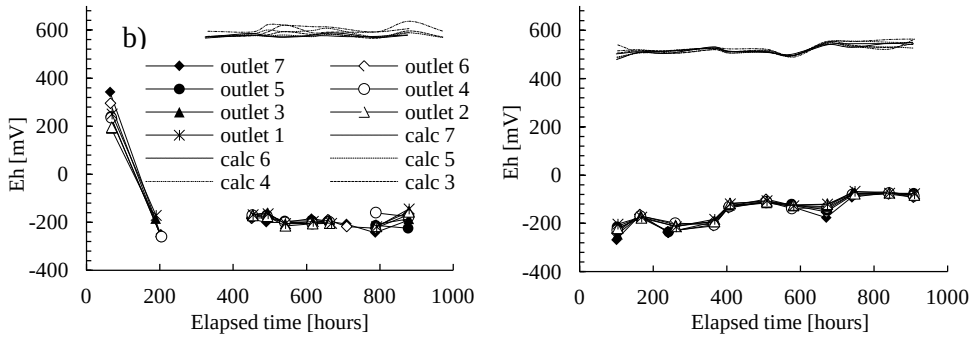

Figure 1. The Eh evolution the flow path within the column during the CO_2-charged water-basaltic glass experiment at 22 °C (a), and the CO_2-charged water-basaltic glass experiment at 50 °C (b). Dotted lines represent Eh calculated with PHREEQC computer code based on the chemical composition of the outlet solution ('calc' in the legend). Lines with symbols represent the Eh measured in-line at sampling outlet ports ('outlet' in the legend).

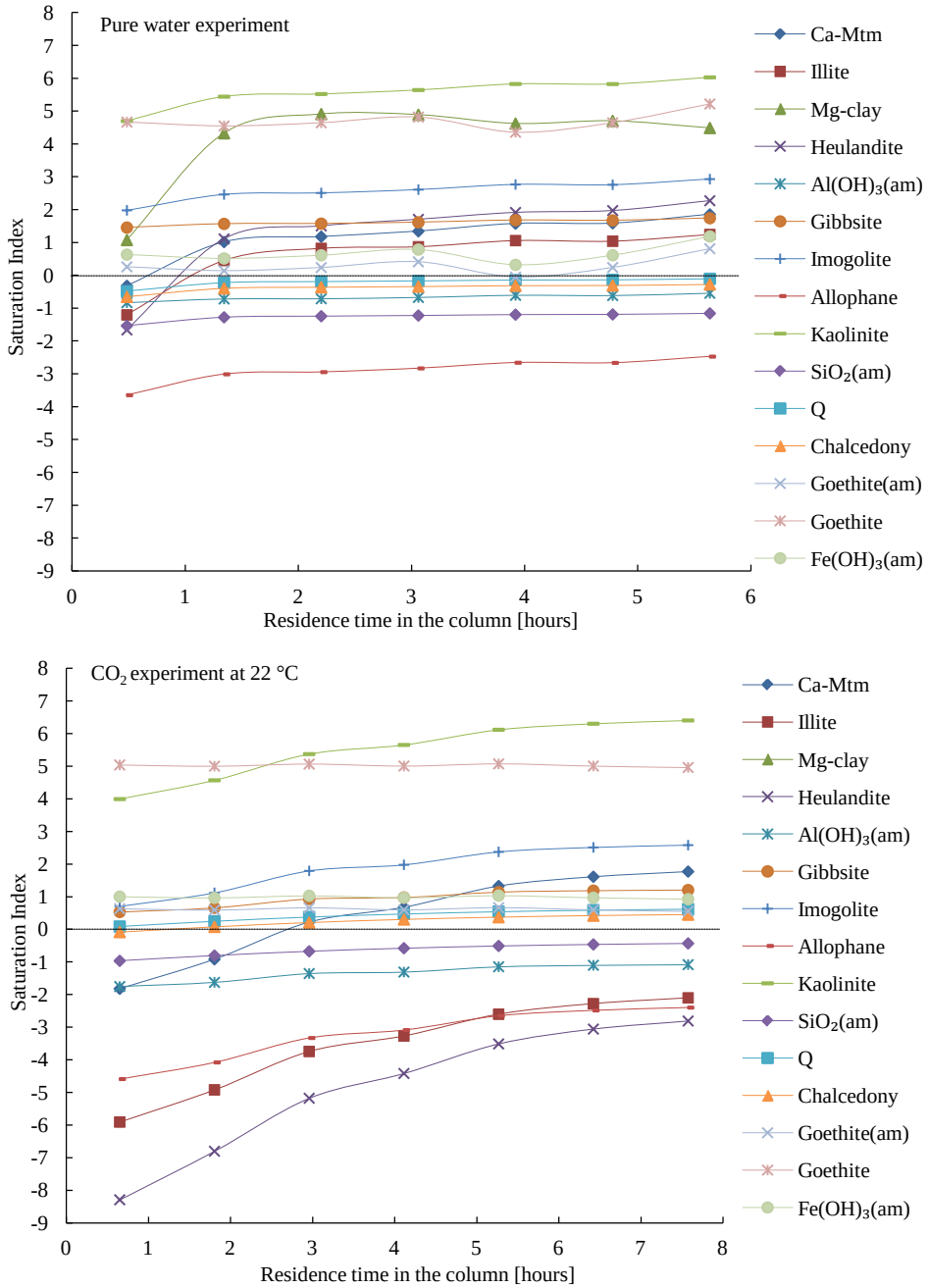

Figure 2. Saturation indexes of selected minerals in fluid samples along the flow path after elapsed times of 2200, 875 and 840 hours for pure water-basaltic glass interaction experiment (a), the CO_2-charged water-basaltic glass interaction experiment at 22 °C (b), and the CO_2-charged water-basaltic glass experiment at 50 °C (c), respectively. The fluid was supersaturated with respect to zeolites (here represented by heulandite) only during the pure water experiment. The supersaturation of the fluid with respect to amorphous $Fe(OH)_3$ happened during the pure water and the CO_2 experiment at 22 °C. The supersaturation with respect to amorphous $Al(OH)_3$ occurred during the CO_2 experiment at 50 °C in the first 2-3 hours of water-rock interaction.

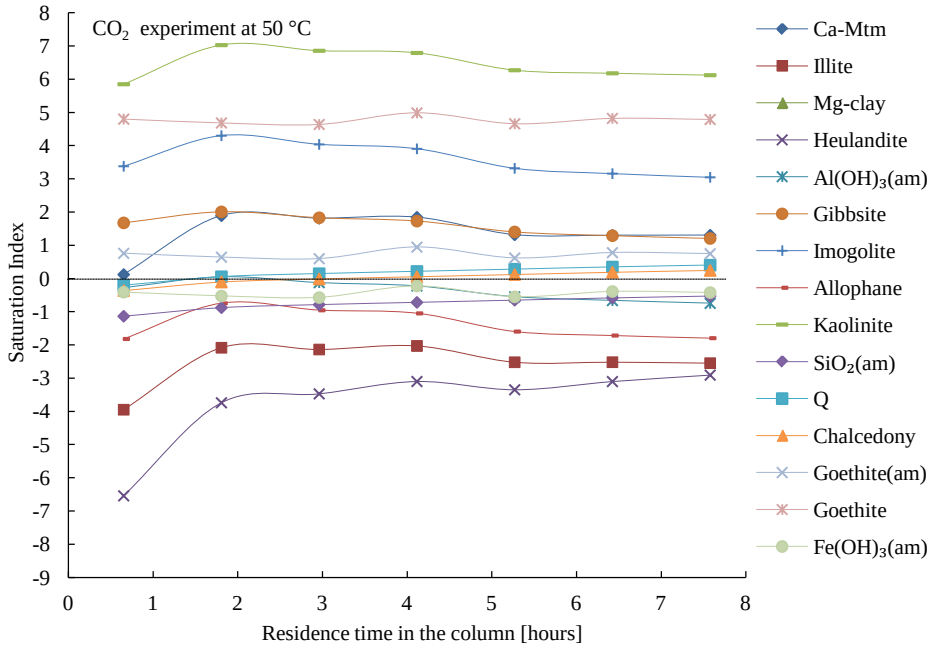

Figure 2. Continuation.

Table 1. Chemical composition of the sampled fluid during the pure water-basaltic glass interaction experiment. DL= Detection limit, n.a. = not analyzed, b.d. = below detection limit.

DL	[µmol/kg]		0.78	0.43	0.03	0.21	0.36	0.37	1.14	0.02	0.11	0.01	0.59	0.12	0.06	0.30	0.27	0.93	0.03	0.06	0.002	0.25	0.24	0.05
Sample	Elapsed time [hours]	pH	Si	Na	Ca	Mg	Fe	Al	K	Sr	Mn	Ti	P	Li	Mo	Cl	Br	B	Cr	W	Ba	Sb	As	V
					[mmol/kg]											[µmol/kg]								
Outlet 7																								
p 7 8	29.0	8.9	0.150	0.016	0.021	0.015	0.000	0.034	2.137	0.019	0.145	0.051	0.407	b.d.	b.d.	1.166	0.449	b.d.	0.060	b.d.	b.d.	b.d.	b.d.	b.d.
p 7 9	97.0	8.9	0.133	0.010	0.023	0.017	0.000	0.042	2.199	0.021	0.128	0.017	0.416	b.d.	b.d.	4.395	0.413	b.d.	0.078	b.d.	b.d.	b.d.	b.d.	b.d.
p 7 10	145.0	8.9	0.132	0.008	0.023	0.017	0.000	0.040	1.415	0.020	0.143	0.023	0.289	b.d.	b.d.	2.082	b.d.	b.d.	0.252	b.d.	b.d.	b.d.	b.d.	b.d.
p 7 11	193.0	9.0	0.135	0.006	0.025	0.018	0.000	0.041	1.877	0.021	0.142	0.017	0.461	b.d.	b.d.	2.273	0.581	b.d.	0.059	b.d.	b.d.	b.d.	b.d.	b.d.
p 7 12	273.0	9.0	0.138	0.007	0.028	0.020	0.000	0.041	1.964	0.024	0.135	0.023	b.d.	b.d.	b.d.	2.037	b.d.	b.d.	0.084	b.d.	b.d.	b.d.	b.d.	b.d.
p 7 13	313.5	9.2	0.139	0.007	0.028	0.020	0.000	0.041	2.124	0.024	0.127	0.010	0.358	b.d.	b.d.	1.151	0.252	b.d.	0.038	b.d.	b.d.	b.d.	b.d.	b.d.
p 7 14	361.5	9.2	0.141	0.007	0.030	0.021	0.000	0.042	2.258	0.025	0.124	0.013	0.392	b.d.	b.d.	0.114	b.d.	b.d.	0.158	b.d.	b.d.	b.d.	b.d.	b.d.
p 7 15	433.5	9.2	0.140	0.008	0.031	0.022	0.000	0.043	2.538	0.027	0.130	0.029	0.424	b.d.	b.d.	0.890	0.267	b.d.	0.234	b.d.	b.d.	b.d.	b.d.	b.d.
p 7 16	505.5	9.3	0.146	0.010	0.033	0.023	0.000	0.044	2.266	0.027	0.125	0.037	0.421	b.d.	b.d.	3.768	0.250	b.d.	b.d.	b.d.	b.d.	b.d.	b.d.	b.d.
p 7 17	623.0	9.1	0.146	0.010	0.033	0.023	0.001	0.043	2.491	0.028	0.125	0.070	0.391	b.d.	b.d.	1.222	0.304	b.d.	b.d.	b.d.	b.d.	b.d.	b.d.	b.d.
p 7 18	672.5	9.3	0.151	0.010	0.035	0.024	0.001	0.044	3.409	0.029	0.133	0.075	0.367	b.d.	b.d.	0.469	b.d.	b.d.	b.d.	b.d.	b.d.	b.d.	b.d.	b.d.
p 7 19	793.0	9.1	0.152	0.010	0.036	0.025	0.000	0.045	2.700	0.030	0.116	0.030	0.414	b.d.	b.d.	b.d.	b.d.	b.d.	b.d.	b.d.	b.d.	b.d.	b.d.	b.d.
p 7 20	939.5	9.2	0.152	0.011	0.037	0.025	0.000	0.045	2.856	0.030	0.110	0.028	0.448	b.d.	b.d.	b.d.	b.d.	b.d.	0.327	b.d.	b.d.	b.d.	b.d.	b.d.
p 7 21	1008.0	9.3	0.148	0.011	0.037	0.026	0.000	0.046	2.391	0.030	0.107	0.040	0.635	b.d.	b.d.	b.d.	b.d.	b.d.	b.d.	b.d.	b.d.	b.d.	b.d.	b.d.
p 7 22	1031.0	9.3	0.151	0.010	0.037	0.026	0.001	0.046	2.514	0.030	0.116	0.065	0.503	b.d.	b.d.	b.d.	b.d.	b.d.	b.d.	b.d.	b.d.	b.d.	b.d.	b.d.
p 7 23	1136.0	9.3	0.149	0.010	0.038	0.026	0.000	0.045	2.629	0.030	0.101	0.028	0.334	b.d.	b.d.	b.d.	b.d.	b.d.	b.d.	b.d.	b.d.	b.d.	b.d.	b.d.
p 7 24	1208.5	n.a.	0.150	0.010	0.038	0.026	0.000	0.045	2.194	0.030	0.101	0.025	0.333	b.d.	b.d.	b.d.	b.d.	b.d.	b.d.	b.d.	b.d.	b.d.	b.d.	b.d.
p 7 25	1303.0	n.a.	0.152	0.011	0.038	0.027	0.000	0.046	1.982	0.031	0.107	0.044	0.415	b.d.	b.d.	b.d.	b.d.	b.d.	b.d.	b.d.	b.d.	b.d.	b.d.	b.d.
p 7 26	1393.5	n.a.	0.151	0.011	0.038	0.028	0.001	0.046	1.854	0.031	0.107	0.061	0.384	b.d.	b.d.	b.d.	b.d.	b.d.	0.027	b.d.	b.d.	b.d.	b.d.	b.d.
p 7 27	1533.0	9.3	0.152	0.011	0.038	0.029	0.000	0.046	2.023	0.030	0.090	0.023	0.473	b.d.	b.d.	b.d.	b.d.	b.d.	0.162	b.d.	b.d.	b.d.	b.d.	b.d.
p 7 28	1659.0	9.2	0.153	0.012	0.037	0.030	0.000	0.047	1.927	0.032	0.091	0.015	0.440	b.d.	b.d.	6.022	b.d.	b.d.	0.112	b.d.	b.d.	b.d.	b.d.	b.d.
p 7 29	1704.5	n.a.	0.153	0.011	0.037	0.030	0.000	0.047	2.278	0.031	0.089	0.016	0.508	b.d.	b.d.	6.299	b.d.	b.d.	b.d.	b.d.	b.d.	b.d.	b.d.	b.d.
p 7 30	1802.5	n.a.	0.154	0.011	0.037	0.030	0.000	0.047	1.391	0.030	0.093	0.024	0.606	b.d.	b.d.	5.319	b.d.	b.d.	0.021	b.d.	b.d.	b.d.	b.d.	b.d.
p 7 31	1873.5	n.a.	0.152	0.011	0.037	0.031	0.000	0.047	1.093	0.029	0.094	0.018	0.523	b.d.	b.d.	2.929	b.d.	b.d.	b.d.	b.d.	b.d.	b.d.	b.d.	b.d.
p 7 32	1965.0	9.3	0.151	0.011	0.036	0.031	0.000	0.046	0.840	0.029	0.077	0.006	0.538	b.d.	b.d.	5.209	b.d.	b.d.	b.d.	b.d.	b.d.	b.d.	b.d.	b.d.
p 7 33	2038.5	n.a.	0.153	0.011	0.037	0.032	0.000	0.047	1.621	0.029	0.081	0.003	0.505	b.d.	b.d.	0.330	b.d.	b.d.	b.d.	b.d.	b.d.	b.d.	b.d.	b.d.
p 7 34	2212.5	9.3	0.156	0.012	0.037	0.032	0.000	0.047	0.900	0.030	0.081	0.009	0.627	b.d.	b.d.	2.551	b.d.	b.d.	b.d.	b.d.	b.d.	b.d.	b.d.	b.d.
p 7 35	2445.5	9.3	0.148	0.012	0.037	0.033	0.000	0.047	1.138	0.029	0.070	0.006	0.305	b.d.	b.d.	b.d.	b.d.	b.d.	b.d.	b.d.	b.d.	b.d.	b.d.	b.d.
Outlet 6																								
p 6 8	29.5	9.0	0.137	0.014	0.022	0.016	0.000	0.040	1.904	0.020	0.201	0.022	0.373	b.d.	b.d.	0.916	0.372	b.d.	0.198	b.d.	b.d.	b.d.	b.d.	b.d.
p 6 9	98.0	9.1	0.129	0.008	0.023	0.017	0.000	0.042	1.977	0.020	0.213	0.038	0.376	b.d.	b.d.	b.d.	b.d.	b.d.	0.041	b.d.	b.d.	b.d.	b.d.	b.d.
p 6 10	145.5	8.9	0.130	0.006	0.025	0.018	0.000	0.041	1.784	0.022	0.208	0.026	0.408	b.d.	b.d.	b.d.	0.317	b.d.	0.029	b.d.	b.d.	b.d.	b.d.	b.d.
p 6 11	194.0	9.2	0.131	0.005	0.027	0.020	0.000	0.041	1.417	0.023	0.204	0.008	0.402	b.d.	b.d.	b.d.	b.d.	b.d.	0.048	b.d.	b.d.	b.d.	b.d.	b.d.
p 6 12	274.0	9.2	0.135	0.007	0.029	0.021	0.000	0.041	1.646	0.025	0.211	0.012	0.379	b.d.	b.d.	b.d.	0.491	b.d.	0.077	b.d.	b.d.	b.d.	b.d.	b.d.
p 6 13	315.0	9.3	0.136	0.007	0.030	0.021	0.000	0.042	1.942	0.025	0.204	0.036	0.351	b.d.	b.d.	b.d.	0.445	b.d.	0.185	b.d.	b.d.	b.d.	b.d.	b.d.
p 6 14	366.0	9.3	0.139	0.007	0.031	0.022	0.000	0.042	2.149	0.026	0.193	0.008	0.392	b.d.	b.d.	b.d.	0.414	b.d.	0.022	b.d.	b.d.	b.d.	b.d.	b.d.
p 6 15	436.5	9.3	0.137	0.007	0.032	0.023	0.000	0.043	2.516	0.027	0.194	0.017	0.385	b.d.	b.d.	b.d.	0.298	b.d.	0.084	b.d.	b.d.	b.d.	b.d.	b.d.
p 6 16	509.0	9.3	0.143	0.009	0.033	0.023	0.000	0.043	2.930	0.028	0.189	0.015	0.427	b.d.	b.d.	0.319	b.d.	b.d.	b.d.	b.d.	b.d.	b.d.	b.d.	b.d.
p 6 17	626.5	9.2	0.145	0.009	0.034	0.024	0.000	0.043	2.582	0.029	0.175	0.010	0.550	b.d.	b.d.	4.430	b.d.	b.d.	b.d.	b.d.	b.d.	b.d.	b.d.	b.d.
p 6 18	677.0	9.2	0.146	0.010	0.035	0.025	0.000	0.044	2.299	0.030	0.179	0.025	0.403	b.d.	b.d.	1.521	b.d.	b.d.	b.d.	b.d.	b.d.	b.d.	b.d.	b.d.
p 6 19	796.5	9.3	0.150	0.011	0.037	0.025	0.000	0.045	2.172	0.030	0.169	0.014	0.296	b.d.	b.d.	1.562	b.d.	b.d.	0.194	b.d.	b.d.	b.d.	b.d.	b.d.
p 6 20	943.0	9.3	0.151	0.011	0.037	0.026	0.000	0.046	2.283	0.031	0.164	0.036	0.808	b.d.	b.d.	b.d.	b.d.	b.d.	0.037	b.d.	b.d.	b.d.	b.d.	b.d.
p 6 21	1011.5	9.3	0.147	0.010	0.037	0.026	0.000	0.046	1.947	0.030	0.161	0.041	0.593	b.d.	b.d.	b.d.	b.d.	b.d.	b.d.	b.d.	b.d.	b.d.	b.d.	b.d.
p 6 22	1035.0	9.4	0.149	0.010	0.038	0.026	0.000	0.046	2.208	0.030	0.155	0.017	0.709	b.d.	b.d.	b.d.	b.d.	b.d.	b.d.	b.d.	b.d.	b.d.	b.d.	b.d.
p 6 23	1140.0	n.a.	0.146	0.010	0.038	0.027	0.000	0.045	2.136	0.030	0.142	0.018	b.d.	b.d.	b.d.	b.d.	b.d.	b.d.	b.d.	b.d.	b.d.	b.d.	b.d.	b.d.
p 6 24	1212.5	n.a.	0.148	0.010	0.038	0.027	0.000	0.046	1.989	0.030	0.143	0.024	0.379	b.d.	b.d.	0.717	b.d.	b.d.	b.d.	b.d.	b.d.	b.d.	b.d.	b.d.
p 6 25	1307.0	n.a.	0.150	0.011	0.038	0.028	0.000	0.046	1.394	0.030	0.139	0.026	0.431	b.d.	b.d.	b.d.	b.d.	b.d.	b.d.	b.d.	b.d.	b.d.	b.d.	b.d.

Table 1. Continuation.

Sample	Elapsed time [hours]	pH	Si	Na	Ca	Mg	Fe	Al	K	Sr	Mn	Ti	P	Li	Mo	Cl	Br	B	Cr	W	Ba	Sb	As	V
			[mmol/kg]													[μmol/kg]								
p 6 26	1397.5	n.a.	0.148	0.011	0.037	0.029	0.000	0.046	1.865	0.029	0.131	0.008	0.550	b.d.	b.d.	b.d.	b.d.	b.d.	0.278	b.d.	b.d.	b.d.	b.d.	b.d.
p 6 27	1537.5	9.3	0.151	0.011	0.036	0.030	0.000	0.046	1.636	0.029	0.124	0.011	0.548	b.d.	b.d.	b.d.	b.d.	b.d.	0.025	b.d.	b.d.	b.d.	b.d.	b.d.
p 6 28	1663.0	9.4	0.152	0.011	0.036	0.031	0.000	0.048	1.491	0.029	0.117	b.d.	0.630	b.d.	b.d.	3.495	b.d.	b.d.	b.d.	b.d.	b.d.	b.d.	b.d.	b.d.
p 6 29	1709.0	n.a.	0.152	0.011	0.036	0.031	0.000	0.047	1.231	0.029	0.117	0.007	0.547	b.d.	b.d.	4.871	b.d.	b.d.	b.d.	b.d.	b.d.	b.d.	b.d.	b.d.
p 6 30	1806.5	n.a.	0.150	0.011	0.036	0.031	0.000	0.047	1.317	0.029	0.111	b.d.	0.555	b.d.	b.d.	2.864	b.d.	b.d.	0.054	b.d.	b.d.	b.d.	b.d.	b.d.
p 6 31	1877.5	n.a.	0.151	0.011	0.036	0.032	0.000	0.047	0.928	0.029	0.110	0.005	0.480	b.d.	b.d.	3.647	b.d.	b.d.	b.d.	b.d.	b.d.	b.d.	b.d.	b.d.
p 6 32	1969.0	n.a.	0.150	0.011	0.036	0.032	0.000	0.047	0.771	0.029	0.107	b.d.	0.502	b.d.	b.d.	4.120	b.d.	b.d.	b.d.	b.d.	b.d.	b.d.	b.d.	b.d.
p 6 33	2042.5	n.a.	0.153	0.011	0.036	0.032	0.000	0.047	1.319	0.030	0.101	b.d.	0.569	b.d.	b.d.	1.743	b.d.	b.d.	b.d.	b.d.	b.d.	b.d.	b.d.	b.d.
p 6 34	2216.5	9.3	0.152	0.011	0.037	0.033	0.000	0.048	0.936	0.030	0.094	0.005	0.611	b.d.	b.d.	2.392	b.d.	b.d.	b.d.	b.d.	b.d.	b.d.	b.d.	b.d.
p 6 35	2448.5	9.3	0.151	0.010	0.037	0.034	0.001	0.049	0.840	0.030	0.111	0.093	0.416	b.d.	b.d.	3.371	b.d.	b.d.	b.d.	b.d.	b.d.	b.d.	b.d.	b.d.
Outlet 5																								
p 5 8	30.5	9.0	0.130	0.013	0.023	0.017	0.000	0.046	2.708	0.020	0.195	0.029	b.d.	b.d.	b.d.	4.041	b.d.	b.d.	0.054	b.d.	b.d.	b.d.	b.d.	b.d.
p 5 9	100.0	9.2	0.124	0.008	0.026	0.018	0.000	0.042	2.194	0.022	0.197	0.026	b.d.	b.d.	b.d.	4.247	0.356	b.d.	0.133	b.d.	b.d.	b.d.	b.d.	b.d.
p 5 10	148.0	9.2	0.125	0.006	0.028	0.019	0.000	0.040	2.420	0.023	0.189	0.013	b.d.	b.d.	b.d.	3.036	0.425	b.d.	0.222	b.d.	b.d.	b.d.	b.d.	b.d.
p 5 11	196.0	9.3	0.127	0.007	0.028	0.020	0.000	0.040	2.638	0.024	0.185	0.010	b.d.	b.d.	b.d.	4.142	0.590	b.d.	0.174	b.d.	b.d.	b.d.	b.d.	b.d.
p 5 12	275.5	9.3	0.131	0.008	0.030	0.021	0.000	0.041	3.061	0.026	0.187	0.012	b.d.	0.001	b.d.	0.697	b.d.	b.d.	0.120	b.d.	b.d.	b.d.	b.d.	b.d.
p 5 14	367.5	9.3	0.137	0.007	0.031	0.022	0.000	0.042	2.477	0.027	0.176	0.006	0.477	b.d.	b.d.	b.d.	b.d.	b.d.	b.d.	b.d.	b.d.	b.d.	b.d.	b.d.
p 5 15	438.5	9.4	0.133	0.007	0.033	0.023	0.000	0.042	2.393	0.028	0.169	0.007	0.382	b.d.	b.d.	b.d.	b.d.	b.d.	0.100	b.d.	b.d.	b.d.	b.d.	b.d.
p 5 16	511.0	9.4	0.139	0.009	0.033	0.023	0.000	0.043	2.293	0.028	0.160	0.013	0.467	b.d.	b.d.	2.197	b.d.	b.d.	b.d.	b.d.	b.d.	b.d.	b.d.	b.d.
p 5 17	628.0	9.3	0.143	0.009	0.035	0.024	0.000	0.042	2.151	0.029	0.152	0.006	0.467	b.d.	b.d.	0.455	0.266	b.d.	b.d.	b.d.	b.d.	b.d.	b.d.	b.d.
p 5 18	678.5	9.3	0.141	0.010	0.036	0.025	0.000	0.044	2.181	0.029	0.151	b.d.	0.221	b.d.	b.d.	0.154	0.308	b.d.	b.d.	b.d.	b.d.	b.d.	b.d.	b.d.
p 5 19	798.5	9.3	0.147	0.010	0.037	0.026	0.000	0.045	1.834	0.030	0.143	b.d.	0.373	b.d.	b.d.	2.198	b.d.	b.d.	b.d.	b.d.	b.d.	b.d.	b.d.	b.d.
p 5 20	944.5	9.3	0.146	0.010	0.037	0.027	0.000	0.045	1.865	0.030	0.139	0.008	b.d.	b.d.	b.d.	b.d.	b.d.	b.d.	b.d.	b.d.	b.d.	b.d.	b.d.	b.d.
p 5 21	1013.0	9.4	0.144	0.010	0.036	0.027	0.000	0.045	1.707	0.030	0.131	0.011	0.558	b.d.	b.d.	0.682	b.d.	b.d.	b.d.	b.d.	b.d.	b.d.	b.d.	b.d.
p 5 22	1035.5	9.4	0.145	0.010	0.036	0.028	0.000	0.045	1.736	0.030	0.128	0.010	0.627	b.d.	b.d.	b.d.	b.d.	b.d.	b.d.	b.d.	b.d.	b.d.	b.d.	b.d.
p 5 23	1140.5	n.a.	0.142	0.010	0.036	0.028	0.000	0.044	1.912	0.030	0.128	0.014	0.358	b.d.	b.d.	b.d.	b.d.	b.d.	b.d.	b.d.	b.d.	b.d.	b.d.	b.d.
p 5 24	1213.0	n.a.	0.144	0.010	0.036	0.029	0.000	0.044	1.318	0.029	0.125	0.007	b.d.	b.d.	b.d.	0.365	b.d.	b.d.	b.d.	b.d.	b.d.	b.d.	b.d.	b.d.
p 5 25	1307.5	n.a.	0.145	0.011	0.035	0.030	0.000	0.045	1.480	0.029	0.123	0.008	0.466	b.d.	b.d.	b.d.	b.d.	b.d.	0.193	b.d.	b.d.	b.d.	b.d.	b.d.
p 5 26	1398.0	n.a.	0.146	0.010	0.035	0.030	0.000	0.045	1.606	0.029	0.122	0.010	0.446	b.d.	b.d.	b.d.	b.d.	b.d.	0.052	b.d.	b.d.	b.d.	b.d.	b.d.
p 5 27	1539.0	9.4	0.148	0.011	0.035	0.032	0.000	0.045	1.102	0.028	0.106	b.d.	0.516	b.d.	b.d.	b.d.	b.d.	b.d.	b.d.	b.d.	b.d.	b.d.	b.d.	b.d.
p 5 28	1664.5	9.4	0.147	0.011	0.035	0.032	0.000	0.047	1.454	0.029	0.101	b.d.	0.467	b.d.	b.d.	0.626	b.d.	b.d.	0.076	b.d.	b.d.	b.d.	b.d.	b.d.
p 5 29	1710.0	n.a.	0.147	0.011	0.036	0.032	0.000	0.047	1.123	0.029	0.097	b.d.	0.507	b.d.	b.d.	4.639	b.d.	b.d.	b.d.	b.d.	b.d.	b.d.	b.d.	b.d.
p 5 30	1807.5	n.a.	0.146	0.011	0.036	0.032	0.000	0.046	1.200	0.029	0.094	b.d.	0.442	b.d.	b.d.	2.137	b.d.	b.d.	0.114	b.d.	b.d.	b.d.	b.d.	b.d.
p 5 31	1878.5	n.a.	0.145	0.011	0.035	0.032	0.000	0.046	1.403	0.028	0.095	b.d.	0.515	b.d.	b.d.	2.176	b.d.	b.d.	b.d.	b.d.	b.d.	b.d.	b.d.	b.d.
p 5 32	1970.5	n.a.	0.148	0.011	0.036	0.033	0.000	0.047	1.250	0.030	0.089	b.d.	0.526	b.d.	b.d.	4.351	b.d.	b.d.	b.d.	b.d.	b.d.	b.d.	b.d.	b.d.
p 5 33	2043.5	n.a.	0.149	0.011	0.036	0.033	0.000	0.047	1.351	0.029	0.086	b.d.	0.457	b.d.	b.d.	0.998	b.d.	b.d.	b.d.	b.d.	b.d.	b.d.	b.d.	b.d.
p 5 34	2217.5	9.3	0.149	0.011	0.036	0.033	0.000	0.047	1.068	0.029	0.085	0.005	0.662	b.d.	b.d.	b.d.	b.d.	b.d.	b.d.	b.d.	b.d.	b.d.	b.d.	b.d.
p 5 35	2449.5	9.3	0.143	0.010	0.036	0.034	0.000	0.047	1.515	0.029	0.067	0.015	0.413	b.d.	b.d.	1.742	b.d.	b.d.	b.d.	b.d.	b.d.	b.d.	b.d.	b.d.
Outlet 4																								
p 4 8	31.5	9.1	0.123	0.011	0.025	0.018	0.000	0.049	2.733	0.021	0.197	0.010	b.d.	b.d.	b.d.	3.266	b.d.	b.d.	b.d.	b.d.	b.d.	b.d.	b.d.	b.d.
p 4 9	100.0	9.3	0.116	0.006	0.028	0.020	0.000	0.040	2.670	0.023	0.183	0.013	b.d.	b.d.	b.d.	3.919	b.d.	b.d.	0.129	b.d.	b.d.	b.d.	b.d.	b.d.
p 4 10	148.0	9.3	0.119	0.006	0.028	0.020	0.000	0.039	2.901	0.024	0.176	0.017	b.d.	b.d.	b.d.	4.398	0.338	b.d.	0.093	b.d.	b.d.	b.d.	b.d.	b.d.
p 4 11	196.0	9.3	0.121	0.007	0.029	0.020	0.000	0.040	2.949	0.025	0.170	b.d.	b.d.	b.d.	b.d.	4.320	b.d.	b.d.	0.101	b.d.	b.d.	b.d.	b.d.	b.d.
p 4 12	275.5	9.3	0.126	0.008	0.031	0.021	0.000	0.040	2.838	0.026	0.171	0.015	b.d.	b.d.	b.d.	4.934	b.d.	b.d.	0.269	b.d.	b.d.	b.d.	b.d.	b.d.
p 4 14	367.5	9.4	0.132	0.008	0.032	0.022	0.000	0.041	3.164	0.027	0.160	0.007	0.365	b.d.	b.d.	1.006	b.d.	b.d.	0.029	b.d.	b.d.	b.d.	b.d.	b.d.
p 4 15	438.5	9.4	0.128	0.008	0.033	0.023	0.000	0.041	2.458	0.027	0.156	0.005	0.442	b.d.	b.d.	2.364	b.d.	b.d.	0.182	b.d.	b.d.	b.d.	b.d.	b.d.
p 4 16	511.0	9.4	0.134	0.009	0.034	0.024	0.000	0.042	2.772	0.028	0.148	0.006	b.d.	b.d.	b.d.	2.495	0.261	b.d.	b.d.	b.d.	b.d.	b.d.	b.d.	b.d.
p 4 17	628.0	9.3	0.139	0.009	0.035	0.025	0.000	0.042	1.504	0.028	0.140	b.d.	0.370	b.d.	b.d.	1.205	b.d.	b.d.	b.d.	b.d.	b.d.	b.d.	b.d.	b.d.
p 4 18	679.0	9.4	0.137	0.010	0.036	0.026	0.000	0.044	1.487	0.029	0.138	0.009	0.540	b.d.	b.d.	2.047	b.d.	b.d.	b.d.	b.d.	b.d.	b.d.	b.d.	b.d.
p 4 19	799.5	9.3	0.143	0.010	0.036	0.027	0.000	0.045	1.460	0.029	0.134	0.006	b.d.	b.d.	b.d.	1.163	b.d.	b.d.	b.d.	b.d.	b.d.	b.d.	b.d.	b.d.
p 4 20	944.5	9.3	0.141	0.010	0.035	0.029	0.000	0.044	1.355	0.028	0.128	0.006	0.614	b.d.	b.d.	b.d.	0.412	b.d.	b.d.	b.d.	b.d.	b.d.	b.d.	b.d.

Table 1. Continuation.

Sample	Elapsed time [hours]	pH	Si	Na	Ca	Mg	Fe	Al	K	Sr	Mn	Ti	P	Li	Mo	Cl	Br	B	Cr	W	Ba	Sb	As	V
			[mmol/kg]													[µmol/kg]								
p 4 21	1014.0	9.4	0.139	0.010	0.034	0.030	0.000	0.044	1.470	0.028	0.122	0.014	0.565	b.d.	b.d.	b.d.	b.d.	b.d.	b.d.	b.d.	b.d.	b.d.	b.d.	b.d.
p 4 22	1037.0	9.4	0.143	0.010	0.035	0.030	0.001	0.045	1.506	0.029	0.136	0.069	0.633	b.d.	b.d.	b.d.	b.d.	b.d.	b.d.	b.d.	b.d.	b.d.	b.d.	b.d.
p 4 23	1142.0	n.a.	0.138	0.010	0.034	0.030	0.000	0.044	1.461	0.028	0.112	0.021	0.483	b.d.	b.d.	b.d.	b.d.	b.d.	b.d.	b.d.	b.d.	b.d.	b.d.	b.d.
p 4 24	1214.5	n.a.	0.140	0.010	0.034	0.031	0.000	0.044	1.264	0.027	0.110	0.018	0.406	b.d.	b.d.	0.205	b.d.	b.d.	0.144	b.d.	b.d.	b.d.	b.d.	b.d.
p 4 25	1309.0	n.a.	0.142	0.010	0.034	0.031	0.000	0.044	1.285	0.027	0.103	0.005	0.454	b.d.	b.d.	b.d.	b.d.	b.d.	0.115	b.d.	b.d.	b.d.	b.d.	b.d.
p 4 26	1399.5	n.a.	0.141	0.010	0.034	0.031	0.000	0.044	1.297	0.027	0.100	0.009	0.481	b.d.	b.d.	b.d.	b.d.	b.d.	b.d.	b.d.	b.d.	b.d.	b.d.	b.d.
p 4 27	1541.5	9.4	0.145	0.010	0.034	0.032	0.000	0.045	1.321	0.028	0.096	0.007	0.381	b.d.	b.d.	b.d.	b.d.	b.d.	b.d.	b.d.	b.d.	b.d.	b.d.	b.d.
p 4 28	1666.0	9.4	0.143	0.010	0.035	0.032	0.000	0.046	1.151	0.028	0.092	b.d.	0.450	b.d.	b.d.	3.292	b.d.	b.d.	b.d.	b.d.	b.d.	b.d.	b.d.	b.d.
p 4 29	1711.0	n.a.	0.144	0.011	0.035	0.032	0.000	0.046	1.171	0.028	0.091	b.d.	0.384	b.d.	b.d.	9.324	b.d.	b.d.	b.d.	b.d.	b.d.	b.d.	b.d.	b.d.
p 4 30	1808.5	n.a.	0.142	0.011	0.035	0.032	0.000	0.045	0.601	0.028	0.088	b.d.	0.492	b.d.	b.d.	0.473	b.d.	b.d.	b.d.	b.d.	b.d.	b.d.	b.d.	b.d.
p 4 31	1879.5	n.a.	0.142	0.011	0.035	0.032	0.000	0.045	0.866	0.028	0.084	b.d.	0.436	b.d.	b.d.	3.703	b.d.	b.d.	b.d.	b.d.	b.d.	b.d.	b.d.	b.d.
p 4 32	1972.5	n.a.	0.143	0.011	0.035	0.033	0.000	0.046	0.652	0.028	0.080	b.d.	b.d.	b.d.	b.d.	0.934	b.d.	b.d.	b.d.	b.d.	b.d.	b.d.	b.d.	b.d.
p 4 33	2045.0	n.a.	0.145	0.011	0.035	0.033	0.000	0.046	0.608	0.029	0.080	b.d.	0.452	b.d.	b.d.	0.546	b.d.	b.d.	b.d.	b.d.	b.d.	b.d.	b.d.	b.d.
p 4 34	2218.5	9.4	0.145	0.011	0.035	0.034	0.000	0.047	1.031	0.029	0.077	b.d.	0.543	b.d.	b.d.	0.943	b.d.	b.d.	0.080	b.d.	b.d.	b.d.	b.d.	b.d.
p 4 35	2450.5	9.4	0.138	0.010	0.035	0.033	0.000	0.046	1.002	0.028	0.061	0.005	0.453	b.d.	b.d.	b.d.	b.d.	b.d.	b.d.	b.d.	b.d.	b.d.	b.d.	b.d.
Outlet 3																								
p 3 8	32.0	9.3	0.113	0.008	0.029	0.020	0.000	0.045	3.215	0.024	0.205	0.014	b.d.	b.d.	b.d.	b.d.	b.d.	b.d.	0.036	b.d.	b.d.	b.d.	b.d.	b.d.
p 3 9	100.5	9.3	0.108	0.005	0.028	0.019	0.000	0.037	2.373	0.023	0.186	0.008	b.d.	b.d.	b.d.	3.488	b.d.	b.d.	0.082	b.d.	b.d.	b.d.	b.d.	b.d.
p 3 10	148.0	9.4	0.112	0.006	0.028	0.020	0.000	0.037	2.400	0.023	0.179	0.004	b.d.	b.d.	b.d.	4.079	b.d.	b.d.	0.056	b.d.	b.d.	b.d.	b.d.	b.d.
p 3 11	195.5	9.4	0.114	0.007	0.029	0.020	0.000	0.038	2.499	0.025	0.177	0.006	b.d.	b.d.	b.d.	5.277	0.299	b.d.	0.073	b.d.	b.d.	b.d.	b.d.	b.d.
p 3 12	275.0	9.4	0.120	0.007	0.031	0.022	0.000	0.038	2.316	0.026	0.174	b.d.	b.d.	b.d.	b.d.	1.480	b.d.	b.d.	0.183	b.d.	b.d.	b.d.	b.d.	b.d.
p 3 14	368.0	9.4	0.125	0.008	0.032	0.022	0.000	0.040	1.704	0.026	0.165	b.d.	b.d.	b.d.	b.d.	2.690	b.d.	b.d.	0.112	b.d.	b.d.	b.d.	b.d.	b.d.
p 3 15	438.5	9.4	0.121	0.008	0.032	0.023	0.000	0.039	1.980	0.026	0.158	0.005	b.d.	b.d.	b.d.	1.363	b.d.	b.d.	0.034	b.d.	b.d.	b.d.	b.d.	b.d.
p 3 16	511.0	9.4	0.127	0.008	0.032	0.025	0.000	0.041	1.206	0.026	0.147	0.002	b.d.	b.d.	b.d.	2.325	b.d.	b.d.	b.d.	b.d.	b.d.	b.d.	b.d.	b.d.
p 3 17	629.5	9.4	0.132	0.009	0.032	0.027	0.000	0.041	1.029	0.026	0.143	0.008	b.d.	b.d.	b.d.	2.934	0.254	b.d.	b.d.	b.d.	b.d.	b.d.	b.d.	b.d.
p 3 18	678.5	9.4	0.130	0.009	0.032	0.028	0.000	0.042	1.176	0.026	0.137	b.d.	0.459	b.d.	b.d.	1.887	b.d.	b.d.	b.d.	b.d.	b.d.	b.d.	b.d.	b.d.
p 3 19	800.0	9.3	0.136	0.009	0.033	0.029	0.000	0.043	1.042	0.027	0.132	0.006	0.325	b.d.	b.d.	0.050	0.392	b.d.	0.023	b.d.	b.d.	b.d.	b.d.	b.d.
p 3 20	944.0	9.3	0.137	0.010	0.033	0.031	0.000	0.043	0.815	0.027	0.134	0.050	0.562	b.d.	b.d.	1.603	b.d.	b.d.	b.d.	b.d.	b.d.	b.d.	b.d.	b.d.
p 3 21	1014.0	9.4	0.134	0.009	0.032	0.030	0.000	0.043	1.215	0.026	0.114	0.009	0.507	b.d.	b.d.	b.d.	b.d.	b.d.	b.d.	b.d.	b.d.	b.d.	b.d.	b.d.
p 3 22	1036.5	9.4	0.134	0.009	0.032	0.030	0.000	0.043	1.126	0.026	0.114	0.012	0.646	b.d.	b.d.	b.d.	b.d.	b.d.	b.d.	b.d.	b.d.	b.d.	b.d.	b.d.
p 3 23	1141.5	n.a.	0.133	0.009	0.032	0.030	0.000	0.042	1.240	0.026	0.110	0.013	0.346	b.d.	b.d.	b.d.	b.d.	b.d.	0.158	b.d.	b.d.	b.d.	b.d.	b.d.
p 3 24	1214.0	n.a.	0.134	0.009	0.032	0.031	0.000	0.042	0.980	0.026	0.105	0.009	b.d.	b.d.	b.d.	b.d.	b.d.	b.d.	b.d.	b.d.	b.d.	b.d.	b.d.	b.d.
p 3 25	1308.5	n.a.	0.136	0.010	0.032	0.031	0.000	0.043	1.256	0.026	0.100	0.009	0.456	b.d.	b.d.	b.d.	b.d.	b.d.	b.d.	b.d.	b.d.	b.d.	b.d.	b.d.
p 3 26	1399.0	n.a.	0.134	0.009	0.032	0.031	0.000	0.043	1.242	0.026	0.095	0.007	0.357	b.d.	b.d.	b.d.	0.295	b.d.	b.d.	b.d.	b.d.	b.d.	b.d.	b.d.
p 3 27	1542.0	9.4	0.138	0.010	0.033	0.032	0.000	0.044	1.536	0.027	0.094	b.d.	0.522	b.d.	b.d.	b.d.	0.348	b.d.	b.d.	b.d.	b.d.	b.d.	b.d.	b.d.
p 3 28	1665.5	9.4	0.137	0.010	0.034	0.032	0.000	0.044					0.000	b.d.	b.d.	0.000	0.000	b.d.	0.000		b.d.	b.d.	b.d.	b.d.
p 3 29	1710.5	n.a.	0.136	0.010	0.033	0.032	0.000	0.044	0.570	0.027	0.088	b.d.	0.394	b.d.	b.d.	4.857	b.d.	b.d.	b.d.	b.d.	b.d.	b.d.	b.d.	b.d.
p 3 30	1808.0	n.a.	0.137	0.010	0.033	0.032	0.000	0.044	0.811	0.027	0.080	b.d.	0.374	b.d.	b.d.	4.030	b.d.	b.d.	b.d.	b.d.	b.d.	b.d.	b.d.	b.d.
p 3 31	1879.0	n.a.	0.137	0.010	0.033	0.032	0.000	0.044	1.124	0.027	0.081	b.d.	0.383	b.d.	b.d.	4.573	b.d.	b.d.	b.d.	b.d.	b.d.	b.d.	b.d.	b.d.
p 3 32	1972.0	n.a.	0.137	0.011	0.033	0.032	0.000	0.044	0.955	0.028	0.077	b.d.	b.d.	b.d.	b.d.	2.182	b.d.	b.d.	b.d.	b.d.	b.d.	b.d.	b.d.	b.d.
p 3 33	2044.5	n.a.	0.139	0.010	0.034	0.032	0.000	0.044	0.567	0.028	0.076	b.d.	b.d.	b.d.	b.d.	5.490	b.d.	b.d.	0.074	b.d.	b.d.	b.d.	b.d.	b.d.
p 3 34	2218.0	9.4	0.140	0.011	0.034	0.033	0.000	0.045	1.481	0.028	0.071	b.d.	0.514	b.d.	b.d.	1.534	b.d.	b.d.	0.042	b.d.	b.d.	b.d.	b.d.	b.d.
p 3 35	2450.0	9.4	0.132	0.009	0.033	0.032	0.000	0.043	0.791	0.026	0.048	b.d.	b.d.	b.d.	b.d.	3.140	b.d.	b.d.	b.d.	b.d.	b.d.	b.d.	b.d.	b.d.
Outlet 2																								
p 2 8	32.5	9.3	0.098	0.005	0.029	0.020	0.000	0.035	2.462	0.023	0.140	0.006	b.d.	b.d.	b.d.	3.790	b.d.	b.d.	0.155	b.d.	b.d.	b.d.	b.d.	b.d.
p 2 9	101.5	9.4	0.098	0.005	0.027	0.018	0.000	0.033	1.881	0.021	0.128	0.005	b.d.	b.d.	b.d.	4.210	b.d.	b.d.	b.d.	b.d.	b.d.	b.d.	b.d.	b.d.
p 2 10	148.5	9.4	0.103	0.006	0.028	0.019	0.000	0.034	2.001	0.022	0.130	b.d.	b.d.	b.d.	b.d.	3.233	b.d.	b.d.	0.260	b.d.	b.d.	b.d.	b.d.	b.d.
p 2 11	196.0	9.4	0.105	0.006	0.028	0.020	0.000	0.034	1.441	0.023	0.127	0.008	b.d.	b.d.	b.d.	3.949	b.d.	b.d.	0.128	b.d.	b.d.	b.d.	b.d.	b.d.
p 2 12	275.5	9.4	0.111	0.007	0.028	0.022	0.000	0.035	1.607	0.023	0.127	b.d.	b.d.	b.d.	b.d.	4.123	0.359	b.d.	0.125	b.d.	b.d.	b.d.	b.d.	b.d.
p 2 14	368.5	9.4	0.116	0.007	0.029	0.024	0.000	0.037	1.553	0.023	0.123	0.007	b.d.	b.d.	b.d.	3.655	0.386	b.d.	b.d.	b.d.	b.d.	b.d.	b.d.	b.d.
p 2 15	439.0	9.4	0.111	0.007	0.028	0.025	0.000	0.036	1.175	0.022	0.115	b.d.	b.d.	b.d.	b.d.	5.463	0.344	b.d.	b.d.	b.d.	b.d.	b.d.	b.d.	b.d.

Table 1. Continuation.

Sample	Elapsed time [hours]	pH	Si	Na	Ca	Mg	Fe	Al	K	Sr	Mn	Ti	P	Li	Mo	Cl	Br	B	Cr	W	Ba	Sb	As	V
			[mmol/kg]													[µmol/kg]								
p 2 16	512.0	9.4	0.115	0.008	0.028	0.026	0.000	0.037	0.974	0.023	0.107	0.003	b.d.	b.d.	b.d.	1.875	b.d.	b.d.	b.d.	b.d.	b.d.	b.d.	b.d.	b.d.
p 2 17	630.5	9.3	0.118	0.009	0.029	0.027	0.000	0.038	0.768	0.024	0.100	0.006	0.431	b.d.	b.d.	5.006	0.671	b.d.	b.d.	b.d.	b.d.	b.d.	b.d.	b.d.
p 2 18	679.5	9.3	0.118	0.008	0.029	0.027	0.000	0.038	0.980	0.024	0.098	0.010	b.d.	b.d.	b.d.	b.d.	b.d.	b.d.	b.d.	b.d.	b.d.	b.d.	b.d.	b.d.
p 2 19	800.5	9.3	0.123	0.009	0.030	0.028	0.000	0.039	1.142	0.025	0.095	b.d.	b.d.	b.d.	b.d.	4.514	b.d.	b.d.	b.d.	b.d.	b.d.	b.d.	b.d.	b.d.
p 2 20	945.0	9.4	0.123	0.008	0.030	0.029	0.000	0.039	1.118	0.025	0.083	0.006	0.484	b.d.	b.d.	b.d.	b.d.	b.d.	b.d.	b.d.	b.d.	b.d.	b.d.	b.d.
p 2 21	1015.0	9.4	0.122	0.008	0.029	0.029	0.000	0.038	0.840	0.025	0.083	0.022	0.393	b.d.	b.d.	b.d.	b.d.	b.d.	b.d.	b.d.	b.d.	b.d.	b.d.	b.d.
p 2 22	1037.0	9.4	0.122	0.009	0.029	0.029	0.000	0.039	0.767	0.025	0.079	0.014	0.495	b.d.	b.d.	b.d.	0.280	b.d.	0.189	b.d.	b.d.	b.d.	b.d.	b.d.
p 2 23	1142.0	n.a.	0.119	0.008	0.029	0.028	0.000	0.038	1.020	0.024	0.074	b.d.	b.d.	b.d.	b.d.	b.d.	b.d.	b.d.	0.227	b.d.	b.d.	b.d.	b.d.	b.d.
p 2 24	1214.5	n.a.	0.122	0.008	0.029	0.029	0.000	0.039	0.924	0.025	0.074	0.009	b.d.	b.d.	b.d.	b.d.	b.d.	b.d.	b.d.	b.d.	b.d.	b.d.	b.d.	b.d.
p 2 25	1309.0	n.a.	0.123	0.008	0.029	0.029	0.000	0.039	0.950	0.024	0.069	0.011	b.d.	b.d.	b.d.	b.d.	b.d.	b.d.	b.d.	b.d.	b.d.	b.d.	b.d.	b.d.
p 2 26	1399.5	n.a.	0.121	0.008	0.029	0.029	0.000	0.039	0.679	0.024	0.070	0.008	0.360	b.d.	b.d.	b.d.	b.d.	b.d.	b.d.	b.d.	b.d.	b.d.	b.d.	b.d.
p 2 27	1544.5	9.4	0.129	0.009	0.030	0.030	0.000	0.040	1.227	0.026	0.059	0.008	0.475	b.d.	b.d.	b.d.	b.d.	b.d.	0.106	b.d.	b.d.	b.d.	b.d.	b.d.
p 2 28	1666.0	9.4	0.125	0.009	0.030	0.029	0.000	0.039	0.591	0.025	0.061	0.009	b.d.	b.d.	b.d.	3.374	b.d.	b.d.	0.056	b.d.	b.d.	b.d.	b.d.	b.d.
p 2 29	1711.0	n.a.	0.123	0.009	0.030	0.029	0.000	0.039	0.215	0.025	0.053	b.d.	b.d.	b.d.	b.d.	4.529	b.d.	b.d.	b.d.	b.d.	b.d.	b.d.	b.d.	b.d.
p 2 30	1809.0	n.a.	0.123	0.009	0.030	0.029	0.000	0.038	0.326	0.026	0.052	b.d.	b.d.	b.d.	b.d.	3.825	b.d.	b.d.	b.d.	b.d.	b.d.	b.d.	b.d.	b.d.
p 2 31	1879.5	n.a.	0.122	0.009	0.030	0.029	0.000	0.039	1.047	0.025	0.054	b.d.	b.d.	b.d.	b.d.	4.079	b.d.	b.d.	0.070	b.d.	b.d.	b.d.	b.d.	b.d.
p 2 32	1973.0	n.a.	0.123	0.009	0.030	0.029	0.000	0.039	0.314	0.026	0.049	b.d.	0.498	b.d.	b.d.	3.490	b.d.	b.d.	b.d.	b.d.	b.d.	b.d.	b.d.	b.d.
p 2 33	2045.5	n.a.	0.125	0.009	0.030	0.029	0.000	0.039	0.650	0.028	0.051	b.d.	b.d.	b.d.	b.d.	2.560	b.d.	b.d.	0.084	b.d.	b.d.	b.d.	b.d.	b.d.
p 2 34	2218.5	9.3	0.126	0.009	0.030	0.030	0.000	0.039	0.775	0.026	0.046	b.d.	0.464	b.d.	b.d.	b.d.	b.d.	b.d.	b.d.	b.d.	b.d.	b.d.	b.d.	b.d.
p 2 35	2450.5	9.3	0.116	0.009	0.029	0.029	0.000	0.038	1.128	0.025	0.029	0.008	0.598	b.d.	b.d.	0.317	b.d.	b.d.	b.d.	b.d.	b.d.	b.d.	b.d.	b.d.
Outlet 1																								
p 1 8	33.0	9.2	0.071	0.004	0.019	0.016	0.000	0.023	1.273	0.016	0.080	b.d.	b.d.	b.d.	b.d.	2.832	b.d.	b.d.	0.050	b.d.	b.d.	b.d.	b.d.	b.d.
p 1 9	102.0	9.3	0.071	0.004	0.018	0.016	0.000	0.022	1.486	0.015	0.078	b.d.	b.d.	b.d.	b.d.	0.482	b.d.	b.d.	0.101	b.d.	b.d.	b.d.	b.d.	b.d.
p 1 10	149.5	9.3	0.071	0.004	0.017	0.016	0.000	0.022	1.112	0.014	0.076	b.d.	b.d.	b.d.	b.d.	1.880	b.d.	b.d.	0.056	b.d.	b.d.	b.d.	b.d.	b.d.
p 1 11	196.5	9.3	0.071	0.004	0.017	0.016	0.000	0.022	1.074	0.015	0.077	b.d.	b.d.	b.d.	b.d.	1.046	b.d.	b.d.	0.031	b.d.	b.d.	b.d.	b.d.	b.d.
p 1 12	276.0	9.3	0.073	0.004	0.017	0.015	0.000	0.023	0.685	0.015	0.075	b.d.	b.d.	b.d.	b.d.	1.061	0.258	b.d.	0.176	b.d.	b.d.	b.d.	b.d.	b.d.
p 1 14	369.0	9.3	0.076	0.005	0.018	0.016	0.000	0.023	0.632	0.015	0.074	b.d.	b.d.	b.d.	b.d.	2.027	b.d.	b.d.	0.110	b.d.	b.d.	b.d.	b.d.	b.d.
p 1 15	439.5	9.3	0.069	0.004	0.017	0.016	0.000	0.021	1.173	0.015	0.070	b.d.	b.d.	b.d.	b.d.	3.122	b.d.	b.d.	0.044	b.d.	b.d.	b.d.	b.d.	b.d.
p 1 16	512.5	9.3	0.071	0.004	0.017	0.016	0.000	0.021	0.424	0.015	0.069	0.007	b.d.	b.d.	b.d.	1.849	0.404	b.d.	b.d.	b.d.	b.d.	b.d.	b.d.	b.d.
p 1 17	631.0	9.2	0.070	0.004	0.017	0.016	0.000	0.022	0.372	0.016	0.065	b.d.	b.d.	b.d.	b.d.	b.d.	b.d.	b.d.	b.d.	b.d.	b.d.	b.d.	b.d.	b.d.
p 1 18	680.0	9.2	0.070	0.005	0.018	0.016	0.000	0.022	0.171	0.016	0.063	b.d.	b.d.	b.d.	b.d.	2.301	b.d.	b.d.	b.d.	b.d.	b.d.	b.d.	b.d.	b.d.
p 1 19	801.0	9.2	0.073	0.005	0.018	0.017	0.000	0.022	0.282	0.016	0.062	0.013	b.d.	b.d.	b.d.	4.085	b.d.	b.d.	b.d.	b.d.	b.d.	b.d.	b.d.	b.d.
p 1 20	947.0	9.2	0.073	0.004	0.017	0.017	0.000	0.022	0.701	0.016	0.056	b.d.	b.d.	b.d.	b.d.	b.d.	b.d.	b.d.	b.d.	b.d.	b.d.	b.d.	b.d.	b.d.
p 1 21	1015.5	9.2	0.070	0.005	0.016	0.016	0.000	0.020	0.650	0.015	0.056	0.013	b.d.	b.d.	b.d.	b.d.	b.d.	b.d.	0.351	b.d.	b.d.	b.d.	b.d.	b.d.
p 1 22	1038.0	9.1	0.071	0.004	0.016	0.016	0.000	0.020	0.533	0.015	0.053	0.009	b.d.	b.d.	b.d.	b.d.	b.d.	b.d.	0.093	b.d.	b.d.	b.d.	b.d.	b.d.
p 1 23	1143.0	n.a.	0.064	0.004	0.016	0.016	0.000	0.020	0.432	0.015	0.054	0.011	b.d.	b.d.	b.d.	b.d.	0.366	b.d.	0.031	b.d.	b.d.	b.d.	b.d.	b.d.
p 1 24	1215.5	n.a.	0.065	0.004	0.016	0.016	0.000	0.020	0.123	0.015	0.051	0.009	b.d.	b.d.	b.d.	b.d.	b.d.	b.d.	b.d.	b.d.	b.d.	b.d.	b.d.	b.d.
p 1 25	1310.0	n.a.	0.066	0.004	0.016	0.016	0.000	0.020	0.632	0.015	0.053	0.018	b.d.	b.d.	b.d.	b.d.	b.d.	b.d.	b.d.	b.d.	b.d.	b.d.	b.d.	b.d.
p 1 26	1400.5	n.a.	0.064	0.004	0.015	0.015	0.000	0.019	0.412	0.014	0.047	0.013	b.d.	b.d.	b.d.	b.d.	b.d.	b.d.	b.d.	b.d.	b.d.	b.d.	b.d.	b.d.
p 1 27	1546.5	9.2	0.070	0.004	0.016	0.015	0.000	0.020	0.599	0.016	0.045	0.008	b.d.	b.d.	b.d.	b.d.	b.d.	b.d.	b.d.	b.d.	b.d.	b.d.	b.d.	b.d.
p 1 28	1667.0	9.2	0.065	0.007	0.015	0.015	0.000	0.019	0.358	0.018	0.046	0.009	b.d.	b.d.	b.d.	2.148	b.d.	b.d.	b.d.	b.d.	b.d.	b.d.	b.d.	b.d.
p 1 29	1712.0	n.a.	0.064	0.005	0.016	0.015	0.000	0.019	0.276	0.016	0.046	b.d.	b.d.	b.d.	b.d.	2.823	b.d.	b.d.	b.d.	b.d.	b.d.	b.d.	b.d.	b.d.
p 1 30	1809.5	n.a.	0.063	0.004	0.015	0.015	0.000	0.018	0.478	0.016	0.041	b.d.	b.d.	b.d.	b.d.	4.788	b.d.	b.d.	b.d.	b.d.	b.d.	b.d.	b.d.	b.d.
p 1 31	1880.0	n.a.	0.064	0.004	0.015	0.014	0.000	0.018	0.126	0.016	0.043	b.d.	b.d.	b.d.	b.d.	3.868	b.d.	b.d.	b.d.	b.d.	b.d.	b.d.	b.d.	b.d.
p 1 32	1973.5	n.a.	0.064	0.004	0.015	0.014	0.000	0.018	0.449	0.016	0.040	b.d.	b.d.	b.d.	b.d.	4.392	b.d.	b.d.	b.d.	b.d.	b.d.	b.d.	b.d.	b.d.
p 1 33	2046.0	n.a.	0.063	0.004	0.015	0.015	0.000	0.018	0.823	0.016	0.040	b.d.	b.d.	b.d.	b.d.	3.691	b.d.	b.d.	b.d.	b.d.	b.d.	b.d.	b.d.	b.d.
p 1 34	2219.0	9.1	0.063	0.005	0.015	0.015	0.000	0.018	0.392	0.017	0.039	b.d.	b.d.	b.d.	b.d.	b.d.	b.d.	b.d.	0.062	b.d.	b.d.	b.d.	b.d.	b.d.
p 1 35	2451.0	9.1	0.057	0.004	0.014	0.014	0.000	0.017	0.122	0.014	0.041	b.d.	b.d.	b.d.	b.d.	0.389	b.d.	b.d.	b.d.	b.d.	b.d.	b.d.	b.d.	b.d.

Table 2. Chemical composition of the sampled fluid during the CO_2-charged water-basaltic glass interaction experiment at 22 °C. n.a. = not analyzed, b.d. = below detection limit.

Sample	Elapsed time [hours]	pH 22 °C	Eh [mV]	DIC	Si	Na	Ca	Mg	Al	Fe	Fe^{3+}	Fe^{2+}	K	Sr	Mn	Ti	P	Li	Mo	Cl	Br	B	W	Cr	Ba	Sb	As	V
					[mmol/kg]								[μmol/kg]															
Column outlet																												
p CO_2 outlet 50	10.3	6.7	272	n.a.	0.137	0.002	0.002	0.005	0.000	0.000	n.a.	n.a.	1.65	0.005	0.23	b.d.	b.d.	b.d.	b.d.	6.250	b.d.	b.d.	b.d.	b.d.	b.d.	b.d.	b.d.	b.d.
p CO_2 outlet 51	17.5	6.4	292	n.a.	0.501	0.031	0.689	1.332	0.010	0.035	n.a.	n.a.	5.51	1.782	70.11	b.d.	4.282	b.d.	b.d.	b.d.	b.d.	1.394	b.d.	0.204	0.128	b.d.	b.d.	b.d.
p CO_2 outlet 52	18.0	6.4	280	n.a.	0.656	0.039	1.091	2.235	0.017	0.056	n.a.	n.a.	6.82	2.748	107.18	0.006	2.861	b.d.	b.d.	b.d.	b.d.	1.654	b.d.	0.342	0.212	b.d.	b.d.	b.d.
p CO_2 outlet 53	18.5	6.4	254	n.a.	0.720	0.041	1.242	2.595	0.023	0.062	n.a.	n.a.	7.38	3.094	115.42	0.013	2.328	b.d.	b.d.	b.d.	b.d.	1.600	b.d.	0.361	0.235	b.d.	b.d.	b.d.
p CO_2 outlet 54	19.5	6.2	291	n.a.	0.850	0.050	1.564	1.560	0.045	0.096	n.a.	n.a.	9.27	3.710	102.27	0.013	1.610	b.d.	b.d.	b.d.	b.d.	1.459	b.d.	0.341	0.328	b.d.	0.146	b.d.
p CO_2 outlet 55	20.0	6.1	300	n.a.	0.865	0.049	1.512	1.255	0.061	0.112	n.a.	n.a.	9.52	3.682	94.49	0.019	1.430	b.d.	b.d.	b.d.	b.d.	1.612	b.d.	0.398	0.353	b.d.	0.157	b.d.
p CO_2 outlet 56	20.5	5.9	290	n.a.	0.900	0.049	1.450	1.114	0.081	0.127	n.a.	n.a.	9.93	3.693	90.43	0.012	1.471	b.d.	b.d.	b.d.	b.d.	1.671	b.d.	0.431	0.392	b.d.	b.d.	b.d.
p CO_2 outlet 57	21.0	5.8	290	n.a.	0.915	0.047	1.339	0.951	0.115	0.140	n.a.	n.a.	11.58	3.580	83.67	0.013	1.461	b.d.	b.d.	b.d.	b.d.	1.896	b.d.	0.516	0.431	b.d.	0.155	b.d.
p CO_2 outlet 58	21.5	5.7	292	n.a.	0.909	0.045	1.203	0.837	0.140	0.143	n.a.	n.a.	11.51	3.363	76.03	0.009	1.436	b.d.	b.d.	b.d.	b.d.	1.825	b.d.	0.532	0.450	b.d.	b.d.	b.d.
p CO_2 outlet 59	22.3	5.6	294	n.a.	0.892	0.040	1.029	0.693	0.192	0.142	n.a.	n.a.	12.45	3.003	65.38	0.008	1.559	b.d.	b.d.	0.848	b.d.	1.815	b.d.	0.613	0.472	b.d.	b.d.	b.d.
p CO_2 outlet 60	23.0	5.5	280	n.a.	0.882	0.037	0.912	0.614	0.226	0.139	n.a.	n.a.	12.81	2.802	58.26	0.006	1.663	b.d.	b.d.	b.d.	b.d.	1.705	b.d.	0.690	0.489	b.d.	0.186	b.d.
p CO_2 outlet 61	24.0	5.4	295	n.a.	0.860	0.033	0.778	0.517	0.268	0.133	n.a.	n.a.	13.18	2.509	50.29	b.d.	1.628	b.d.	b.d.	b.d.	b.d.	1.571	b.d.	0.718	0.505	b.d.	b.d.	b.d.
p CO_2 outlet 62	24.5	5.4	290	n.a.	0.815	0.027	0.571	0.374	0.328	0.119	n.a.	n.a.	13.96	2.006	38.02	0.009	1.729	b.d.	b.d.	1.598	b.d.	1.436	b.d.	0.793	0.509	b.d.	b.d.	b.d.
p CO_2 outlet 63	25.3	5.3	296	n.a.	0.787	0.025	0.420	0.277	0.397	0.108	n.a.	n.a.	14.32	1.675	28.52	0.006	2.053	b.d.	b.d.	0.289	b.d.	1.319	b.d.	0.922	0.527	b.d.	b.d.	b.d.
p CO_2 outlet 64	36.0	5.0	364	n.a.	0.615	0.026	0.170	0.150	0.501	0.070	n.a.	n.a.	12.50	0.764	9.70	0.007	1.868	b.d.	b.d.	0.146	b.d.	0.832	b.d.	0.935	0.578	b.d.	b.d.	b.d.
p CO_2 outlet 65	38.0	4.9	415	n.a.	0.593	0.027	0.161	0.150	0.506	0.070	n.a.	n.a.	12.56	0.669	8.48	0.011	1.818	b.d.	b.d.	1.253	b.d.	0.792	b.d.	0.914	0.622	b.d.	b.d.	b.d.
p CO_2 outlet 66	38.5	4.9	408	n.a.	0.596	0.027	0.162	0.151	0.514	0.071	n.a.	n.a.	12.62	0.673	8.50	0.005	1.771	b.d.	b.d.	0.611	b.d.	0.868	b.d.	0.927	0.623	b.d.	b.d.	b.d.
p CO_2 outlet 67	40.5	4.9	375	n.a.	0.589	0.028	0.160	0.150	0.511	0.071	n.a.	n.a.	12.26	0.645	8.21	0.009	1.864	b.d.	b.d.	b.d.	b.d.	0.868	b.d.	0.908	0.637	b.d.	b.d.	b.d.
p CO_2 outlet 68	45.0	4.9	400	n.a.	0.572	0.029	0.157	0.150	0.507	0.072	n.a.	n.a.	11.07	0.574	7.46	b.d.	1.993	b.d.	b.d.	1.106	b.d.	0.789	b.d.	0.919	0.658	b.d.	b.d.	b.d.
p CO_2 outlet 69	46.5	4.8	440	n.a.	0.554	0.031	0.153	0.152	0.515	0.073	n.a.	n.a.	10.99	0.513	6.82	0.010	1.756	b.d.	b.d.	1.096	b.d.	0.864	b.d.	0.894	0.670	b.d.	b.d.	b.d.
p CO_2 outlet 70	60.0	4.8	417	n.a.	0.525	0.037	0.159	0.164	0.523	0.082	n.a.	n.a.	8.62	0.393	5.78	0.009	1.526	b.d.	b.d.	1.307	b.d.	0.999	b.d.	0.834	0.695	b.d.	b.d.	b.d.
p CO_2 outlet 71	102.5	4.6	-308	n.a.	0.507	0.039	0.150	0.163	0.545	0.087	n.a.	n.a.	6.88	0.248	4.39	0.015	1.380	b.d.	b.d.	2.088	b.d.	1.006	b.d.	0.689	0.535	b.d.	b.d.	b.d.
p CO_2 outlet 72	115.0	4.5	-311	n.a.	0.546	0.039	0.148	0.161	0.614	0.087	n.a.	n.a.	6.44	0.239	4.26	0.041	1.542	b.d.	b.d.	1.264	b.d.	1.030	b.d.	0.733	0.492	b.d.	b.d.	b.d.
p CO_2 outlet 73	132.0	n.a.	n.a.	n.a.	0.527	0.041	0.155	0.171	0.476	0.089	n.a.	n.a.	7.60	0.246	4.50	0.011	1.319	b.d.	b.d.	2.095	b.d.	1.076	b.d.	0.625	0.463	b.d.	b.d.	b.d.
p CO_2 outlet 74	136.5	4.5	-375	n.a.	0.539	0.041	0.156	0.170	0.453	0.092	n.a.	n.a.	6.43	0.246	4.50	0.010	1.467	b.d.	b.d.	1.575	b.d.	1.050	b.d.	0.629	0.460	b.d.	0.192	b.d.
p CO_2 outlet 75	156.3	4.5	-296	n.a.	0.571	0.044	0.164	0.180	0.545	0.097	n.a.	n.a.	7.36	0.256	4.70	0.017	1.577	b.d.	b.d.	1.651	b.d.	1.171	b.d.	0.760	0.454	b.d.	0.148	b.d.
p CO_2 outlet 76	188.0	4.5	-180	n.a.	0.581	0.045	0.168	0.189	0.467	0.098	n.a.	n.a.	6.95	0.252	4.71	0.018	1.478	b.d.	b.d.	3.853	b.d.	1.153	b.d.	0.619	0.391	b.d.	b.d.	b.d.
p CO_2 outlet 77	202.0	4.5	-250	n.a.	0.589	0.044	0.166	0.180	0.479	0.101	n.a.	n.a.	6.91	0.243	4.55	0.015	1.455	b.d.	b.d.	2.380	b.d.	1.202	b.d.	0.640	0.365	b.d.	0.201	b.d.
p CO_2 outlet 78	254.3	4.5	30	n.a.	0.525	0.038	0.142	0.155	0.469	0.086	n.a.	n.a.	5.57	0.199	3.71	0.016	1.521	b.d.	b.d.	b.d.	b.d.	0.945	b.d.	0.564	0.283	b.d.	0.239	b.d.
p CO_2 outlet 79	275.5	4.5	-30	n.a.	0.562	0.043	0.159	0.176	0.504	0.094	28.73	69.35	6.42	0.219	4.15	0.022	1.730	b.d.	b.d.	b.d.	b.d.	1.018	b.d.	0.597	0.296	b.d.	0.259	b.d.
p CO_2 outlet 80	305.5	n.a.	n.a.	n.a.	0.606	0.046	0.182	0.202	0.442	0.108	26.96	76.41	5.03	0.246	4.43	0.028	0.539	b.d.	b.d.	b.d.	b.d.	1.100	b.d.	0.506	0.302	b.d.	0.250	b.d.
p CO_2 outlet 81	322.5	n.a.	n.a.	n.a.	0.601	0.042	0.169	0.194	0.485	0.099	29.10	72.84	5.01	0.232	4.13	0.036	0.547	b.d.	b.d.	b.d.	b.d.	1.053	b.d.	0.585	0.286	b.d.	0.266	b.d.
p CO_2 outlet 82	350.0	n.a.	n.a.	n.a.	0.614	0.044	0.184	0.195	0.332	0.110	24.73	63.50	4.84	0.249	4.31	0.015	0.167	b.d.	b.d.	b.d.	b.d.	1.133	b.d.	0.538	0.280	b.d.	b.d.	b.d.
p CO_2 outlet 83	370.0	n.a.	n.a.	n.a.	0.598	0.040	0.167	0.190	0.370	0.097	32.37	71.59	4.25	0.229	4.08	0.011	0.486	b.d.	b.d.	b.d.	b.d.	0.948	b.d.	0.521	0.264	b.d.	b.d.	b.d.
p CO_2 outlet 84	422.0	4.5	-160	n.a.	0.585	0.038	0.156	0.175	0.446	0.093	35.25	69.81	5.94	0.208	3.93	0.030	1.547	b.d.	b.d.	b.d.	b.d.	0.980	b.d.	0.585	0.225	b.d.	0.146	b.d.
p CO_2 outlet 85	471.5	4.5	-180	n.a.	0.640	0.043	0.176	0.198	0.411	0.104	29.11	70.39	4.81	0.229	4.07	0.023	0.599	b.d.	b.d.	b.d.	b.d.	1.014	b.d.	0.509	0.214	b.d.	0.261	b.d.
p CO_2 outlet 86	514.5	4.5	-200	n.a.	0.576	0.038	0.154	0.181	0.368	0.091	n.a.	n.a.	4.28	0.201	3.76	0.023	0.679	b.d.	b.d.	b.d.	b.d.	0.949	b.d.	0.362	0.191	b.d.	0.168	b.d.
p CO_2 outlet 87	537.5	4.5	-196	n.a.	0.593	0.040	0.145	0.169	0.327	0.086	n.a.	n.a.	4.40	0.189	3.41	0.019	b.d.	b.d.	b.d.	b.d.	b.d.	0.876	b.d.	0.385	0.175	b.d.	b.d.	b.d.
p CO_2 outlet 88	572.8	4.5	-220	n.a.	0.597	0.037	0.135	0.154	0.376	0.085	n.a.	n.a.	4.58	0.182	3.12	0.032	b.d.	b.d.	b.d.	b.d.	b.d.	0.798	b.d.	0.428	0.173	b.d.	b.d.	b.d.
p CO_2 outlet 89	612.0	4.5	-237	n.a.	0.590	0.038	0.141	0.163	0.332	0.084	n.a.	n.a.	3.88	0.180	3.24	0.021	b.d.	b.d.	b.d.	b.d.	b.d.	0.845	b.d.	0.390	0.159	b.d.	b.d.	b.d.
p CO_2 outlet 90	638.0	4.5	-200	n.a.	0.581	0.038	0.137	0.159	0.305	0.081	28.60	56.67	3.88	0.175	3.12	0.028	b.d.	b.d.	b.d.	b.d.	b.d.	0.748	b.d.	0.353	0.152	b.d.	b.d.	b.d.
p CO_2 outlet 91	735.0	4.5	-218	n.a.	0.643	0.045	0.169	0.189	0.426	0.103	n.a.	n.a.	4.21	0.208	3.68	0.026	b.d.	b.d.	b.d.	b.d.	b.d.	1.017	b.d.	0.456	0.163	b.d.	b.d.	b.d.
p CO_2 outlet 92	808.5	4.5	-253	n.a.	0.694	0.051	0.172	0.194	0.369	0.103	n.a.	n.a.	5.17	0.207	3.90	0.032	0.458	0.121	b.d.	b.d.	b.d.	0.960	b.d.	0.428	0.151	b.d.	b.d.	b.d.
p CO_2 outlet 93	834.0	4.5	-254	n.a.	0.672	0.047	0.162	0.181	0.388	0.099	37.72	65.26	4.85	0.198	3.57	0.034	0.377	b.d.	b.d.	1.967	b.d.	0.890	b.d.	0.430	0.147	b.d.	b.d.	b.d.
p CO_2 outlet 94	859.5	4.5	-256	n.a.	0.677	0.047	0.163	0.183	0.411	0.101	42.62	60.61	4.77	0.200	3.59	0.039	b.d.	b.d.	b.d.	b.d.	b.d.	0.870	b.d.	0.428	0.143	b.d.	b.d.	b.d.
p CO_2 outlet 95	874.5	4.5	-257	n.a.	0.686	0.050	0.171	0.192	0.421	0.103	n.a.	n.a.	4.91	0.205	3.76	0.032	0.418	b.d.	b.d.	0.356	b.d.	0.949	b.d.	0.462	0.142	b.d.	b.d.	b.d.

Table 2. Continuation.

Sample	Elapsed time [hours]	pH 22 °C	Eh [mV]	DIC	Si	Na	Ca	Mg	Al	Fe	Fe^{3+}	Fe^{2+}	K	Sr	Mn	Ti	P	Li	Mo	Cl	Br	B	W	Cr	Ba	Sb	As	V
							[mmol/kg]											[µmol/kg]										
$p CO_2$ outlet 96	932.5	4.5	-260	n.a.	0.683	0.050	0.169	0.188	0.437	0.105	46.33	65.02	4.92	0.205	3.62	0.035	0.326	b.d.	b.d.	b.d.	b.d.	0.985	b.d.	0.465	0.138	b.d.	b.d.	b.d.
$p CO_2$ outlet 97	970.0	4.4	-252	n.a.	0.687	0.052	0.176	0.199	0.408	0.106	32.01	77.50	5.28	0.208	3.80	0.027	0.499	b.d.	b.d.	0.567	b.d.	0.947	b.d.	0.442	0.132	b.d.	b.d.	b.d.
Outlet 7																												
$p CO_2$ 7 3	64.0	4.7	342	0.228	0.516	0.037	0.159	0.164	0.531	0.083	n.a.	n.a.	6.70	0.367	5.28	0.007	0.387	b.d.	b.d.	0.415	b.d.	0.935	b.d.	0.745	0.708	b.d.	b.d.	b.d.
$p CO_2$ 7 5	202.3	4.5	-250	0.232	0.595	0.045	0.169	0.181	0.485	0.102	n.a.	n.a.	4.95	0.249	4.32	0.011	0.368	b.d.	b.d.	b.d.	b.d.	1.166	b.d.	0.559	0.368	b.d.	0.260	b.d.
$p CO_2$ 7 6	323.8	n.a.	n.a.	0.266	0.603	0.042	0.167	0.193	0.496	0.101	30.39	73.91	4.67	0.231	4.04	0.029	0.495	b.d.	b.d.	b.d.	b.d.	1.113	b.d.	0.573	0.296	b.d.	0.291	b.d.
$p CO_2$ 7 7	449.5	4.5	-186	0.273	0.600	0.038	0.158	0.175	0.454	0.096	45.02	60.38	4.57	0.212	3.65	0.017	b.d.	b.d.	b.d.	b.d.	b.d.	0.916	b.d.	0.516	0.222	b.d.	0.185	b.d.
$p CO_2$ 7 8	489.8	4.5	-200	0.280	0.601	0.039	0.160	0.197	0.429	0.094	33.81	69.15	4.51	0.210	3.78	0.022	b.d.	b.d.	b.d.	b.d.	b.d.	0.901	b.d.	0.501	0.205	b.d.	0.247	b.d.
$p CO_2$ 7 9	538.5	4.5	-200	0.192	0.587	0.041	0.144	0.168	0.323	0.085	27.55	64.12	4.08	0.188	3.29	0.023	b.d.	b.d.	b.d.	b.d.	b.d.	0.851	b.d.	0.359	0.173	b.d.	b.d.	b.d.
$p CO_2$ 7 10	613.0	4.5	-185	0.220	0.592	0.038	0.141	0.162	0.333	0.084	33.00	58.52	4.06	0.179	3.13	0.031	b.d.	b.d.	b.d.	b.d.	b.d.	0.878	b.d.	0.366	0.160	b.d.	b.d.	b.d.
$p CO_2$ 7 11	657.5	4.5	-195	0.228	0.612	0.039	0.147	0.169	0.374	0.087	43.73	49.32	3.77	0.184	3.24	0.018	b.d.	b.d.	b.d.	b.d.	b.d.	0.866	b.d.	0.396	0.156	b.d.	b.d.	b.d.
$p CO_2$ 7 12	708.5	4.5	-207	0.276	0.613	0.040	0.153	0.175	0.405	0.092	37.79	60.83	4.14	0.189	3.31	0.031	b.d.	b.d.	b.d.	b.d.	b.d.	0.919	b.d.	0.446	0.155	b.d.	b.d.	b.d.
$p CO_2$ 7 13	787.0	4.5	-243	0.297	0.640	0.043	0.162	0.178	0.394	0.099	27.96	72.84	4.38	0.199	3.38	0.024	b.d.	b.d.	b.d.	b.d.	b.d.	0.997	b.d.	0.439	0.145	b.d.	b.d.	b.d.
$p CO_2$ 7 14	875.5	4.5	-193	0.426	0.682	0.051	0.170	0.192	0.417	0.102	33.97	73.46	5.41	0.202	3.65	0.038	b.d.	0.111	b.d.	b.d.	b.d.	0.930	b.d.	0.449	0.142	b.d.	0.166	b.d.
Outlet 6																												
$p CO_2$ 6 3	65.0	4.7	295	0.221	0.489	0.038	0.156	0.162	0.539	0.084	n.a.	n.a.	5.62	0.320	4.94	0.018	0.465	b.d.	b.d.	b.d.	b.d.	0.904	b.d.	0.706	0.685	b.d.	b.d.	b.d.
$p CO_2$ 6 5	202.8	4.5	-260	0.270	0.561	0.041	0.159	0.165	0.522	0.097	n.a.	n.a.	4.99	0.231	3.82	0.023	0.559	b.d.	b.d.	b.d.	b.d.	1.054	b.d.	0.545	0.323	b.d.	0.189	b.d.
$p CO_2$ 6 6	324.5	n.a.	n.a.	0.274	0.574	0.041	0.161	0.179	0.484	0.100	26.50	75.88	5.34	0.221	3.80	0.030	0.496	b.d.	b.d.	b.d.	b.d.	1.097	0.075	0.554	0.263	b.d.	0.252	b.d.
$p CO_2$ 6 7	450.3	4.5	-183	0.270	0.566	0.036	0.150	0.173	0.413	0.090	34.75	64.32	4.09	0.199	3.35	0.030	0.281	b.d.	b.d.	b.d.	b.d.	0.926	b.d.	0.475	0.185	b.d.	0.178	b.d.
$p CO_2$ 6 8	490.5	4.5	-180	0.260	0.580	0.038	0.158	0.176	0.389	0.096	28.83	65.55	4.30	0.204	3.50	0.019	0.406	b.d.	b.d.	b.d.	b.d.	0.970	b.d.	0.427	0.180	b.d.	0.192	b.d.
$p CO_2$ 6 9	539.0	4.5	-199	0.192	0.547	0.039	0.142	0.162	0.292	0.084	25.42	65.47	4.08	0.177	3.11	0.020	b.d.	b.d.	b.d.	b.d.	b.d.	0.793	b.d.	0.320	0.149	b.d.	b.d.	b.d.
$p CO_2$ 6 10	613.5	4.5	-204	0.191	0.536	0.036	0.128	0.147	0.291	0.078	28.65	58.15	3.89	0.162	2.78	0.032	b.d.	b.d.	b.d.	b.d.	b.d.	0.741	b.d.	0.302	0.133	b.d.	b.d.	b.d.
$p CO_2$ 6 11	658.0	4.5	-190	0.234	0.568	0.038	0.138	0.156	0.375	0.086	31.82	56.17	3.95	0.175	2.94	0.031	b.d.	b.d.	b.d.	b.d.	b.d.	0.896	b.d.	0.394	0.140	b.d.	b.d.	b.d.
$p CO_2$ 6 12	709.3	4.5	-218	0.258	0.577	0.041	0.148	0.169	0.386	0.089	27.03	67.72	4.01	0.185	3.13	0.039	b.d.	b.d.	b.d.	b.d.	b.d.	0.918	b.d.	0.378	0.140	b.d.	b.d.	b.d.
$p CO_2$ 6 13	787.5	4.5	-225	0.272	0.594	0.042	0.153	0.171	0.361	0.093	30.07	67.97	4.38	0.188	3.22	0.035	b.d.	b.d.	b.d.	b.d.	b.d.	0.819	b.d.	0.368	0.128	b.d.	0.159	b.d.
$p CO_2$ 6 14	876.0	4.5	-170	0.311	0.636	0.048	0.165	0.184	0.378	0.101	37.18	69.42	4.93	0.194	3.37	0.034	b.d.	b.d.	b.d.	b.d.	b.d.	0.938	b.d.	0.402	0.122	b.d.	b.d.	b.d.
Outlet 5																												
$p CO_2$ 5 3	66.0	4.7	240	0.226	0.441	0.033	0.145	0.155	0.538	0.081	n.a.	n.a.	4.57	0.259	4.21	0.019	b.d.	b.d.	b.d.	b.d.	b.d.	0.844	b.d.	0.629	0.583	b.d.	b.d.	b.d.
$p CO_2$ 5 5	203.5	4.5	-260	0.244	0.478	0.032	0.129	0.146	0.472	0.083	n.a.	n.a.	4.65	0.185	3.08	0.024	b.d.	b.d.	b.d.	b.d.	b.d.	0.942	b.d.	0.508	0.254	b.d.	0.176	b.d.
$p CO_2$ 5 6	325.0	n.a.	n.a.	0.245	0.511	0.038	0.146	0.167	0.406	0.091	28.43	67.32	4.46	0.194	3.30	0.032	0.430	b.d.	b.d.	b.d.	b.d.	1.017	b.d.	0.422	0.195	b.d.	0.316	b.d.
$p CO_2$ 5 7	451.0	4.5	-179	0.265	0.531	0.036	0.148	0.167	0.368	0.090	33.02	63.61	3.85	0.189	3.19	0.025	0.350	b.d.	b.d.	b.d.	b.d.	0.883	b.d.	0.360	0.148	b.d.	0.171	b.d.
$p CO_2$ 5 8	491.0	4.5	-170	0.255	0.524	0.036	0.148	0.169	0.343	0.090	28.81	66.16	3.68	0.186	3.16	0.019	0.399	b.d.	b.d.	b.d.	b.d.	0.853	b.d.	0.358	0.140	b.d.	0.186	b.d.
$p CO_2$ 5 9	540.0	4.4	-195	0.203	0.503	0.036	0.132	0.149	0.274	0.084	29.84	58.02	4.15	0.164	2.76	0.030	b.d.	b.d.	b.d.	b.d.	b.d.	0.796	b.d.	0.287	0.117	b.d.	b.d.	b.d.
$p CO_2$ 5 10	614.5	4.5	-194	0.195	0.502	0.035	0.125	0.141	0.267	0.077	23.77	56.20	3.32	0.153	2.55	0.030	b.d.	b.d.	b.d.	b.d.	b.d.	0.675	b.d.	0.260	0.102	b.d.	b.d.	b.d.
$p CO_2$ 5 11	659.0	4.5	-194	0.245	0.510	0.035	0.128	0.144	0.348	0.081	34.87	50.15	3.53	0.159	2.60	0.037	b.d.	b.d.	b.d.	b.d.	b.d.	0.806	b.d.	0.347	0.107	b.d.	b.d.	b.d.
$p CO_2$ 5 12	735.5	n.a.	n.a.	0.269	0.530	0.041	0.145	0.158	0.324	0.089	n.a.	n.a.	4.05	0.174	2.90	0.033	b.d.	b.d.	b.d.	b.d.	b.d.	0.867	b.d.	0.320	0.103	b.d.	b.d.	b.d.
$p CO_2$ 5 13	788.0	4.5	-213	0.277	0.520	0.041	0.142	0.171	0.304	0.086	27.56	66.79	4.23	0.170	2.95	0.039	b.d.	b.d.	b.d.	b.d.	b.d.	0.894	b.d.	0.313	0.098	b.d.	b.d.	b.d.
$p CO_2$ 5 14	876.5	4.5	-225	0.318	0.569	0.045	0.153	0.171	0.337	0.095	43.24	55.73	4.08	0.178	3.00	0.034	b.d.	b.d.	b.d.	b.d.	b.d.	0.856	b.d.	0.353	0.095	b.d.	b.d.	b.d.
$p CO_2$ 5 15	971.0	n.a.	n.a.	0.337	0.574	0.048	0.163	0.179	0.321	0.101	27.56	76.34	4.77	0.184	3.08	0.037	b.d.	b.d.	b.d.	b.d.	b.d.	0.882	b.d.	0.333	0.086	b.d.	b.d.	b.d.
Outlet 4																												
$p CO_2$ 4 3	67.0	4.7	235	0.233	0.396	0.034	0.141	0.153	0.509	0.079	n.a.	n.a.	4.24	0.219	3.70	0.016	b.d.	b.d.	b.d.	b.d.	b.d.	0.840	b.d.	0.550	0.406	b.d.	b.d.	b.d.
$p CO_2$ 4 5	204.0	4.5	-260	0.227	0.408	0.032	0.124	0.143	0.373	0.075	n.a.	n.a.	4.17	0.161	2.70	0.029	b.d.	b.d.	b.d.	b.d.	b.d.	0.796	b.d.	0.408	0.171	b.d.	0.217	b.d.
$p CO_2$ 4 6	326.0	n.a.	n.a.	0.272	0.450	0.037	0.142	0.160	0.346	0.087	29.43	65.26	4.42	0.175	3.08	0.036	b.d.	b.d.	b.d.	b.d.	b.d.	1.012	b.d.	0.376	0.140	b.d.	0.244	b.d.
$p CO_2$ 4 7	451.8	4.5	-171	0.254	0.443	0.034	0.136	0.159	0.276	0.081	37.76	54.97	3.65	0.161	2.77	0.023	b.d.	b.d.	b.d.	b.d.	b.d.	0.761	b.d.	0.283	0.098	b.d.	0.179	b.d.
$p CO_2$ 4 8	491.8	4.6	-175	0.246	0.450	0.033	0.133	0.152	0.274	0.083	60.21	26.61	3.52	0.161	2.65	0.026	b.d.	b.d.	b.d.	b.d.	b.d.	0.858	b.d.	0.270	0.094	b.d.	0.173	b.d.
$p CO_2$ 4 9	540.5	4.4	-201	0.166	0.412	0.032	0.108	0.128	0.196	0.068	31.05	40.77	3.14	0.131	2.16	0.026	b.d.	b.d.	b.d.	b.d.	b.d.	0.611	b.d.	0.185	0.073	b.d.	b.d.	b.d.
$p CO_2$ 4 10	615.3	4.5	-206	0.197	0.435	0.032	0.115	0.132	0.236	0.072	29.42	49.28	3.51	0.136	2.28	0.028	b.d.	b.d.	b.d.	b.d.	b.d.	0.658	b.d.	0.230	0.073	b.d.	b.d.	b.d.

Table 2. Continuation.

Sample	Elapsed time [hours]	pH 22 °C	Eh [mV]	DIC	Si	Na	Ca	Mg	Al	Fe	Fe^{3+}	Fe^{2+}	K	Sr	Mn	Ti	P	Li	Mo	Cl	Br	B	W	Cr	Ba	Sb	As	V
				[mmol/kg]									[μmol/kg]															
p CO_2 4 11	661.8	4.5	-199	0.205	0.413	0.032	0.109	0.126	0.255	0.068	44.96	26.56	3.16	0.129	2.12	0.034	b.d.	b.d.	b.d.	b.d.	b.d.	0.653	b.d.	0.251	0.069	b.d.	b.d.	b.d.
p CO_2 4 12	736.0	n.a.	n.a.	0.260	0.450	0.036	0.131	0.150	0.261	0.082	n.a.	n.a.	3.42	0.150	2.44	0.032	b.d.	b.d.	b.d.	b.d.	b.d.	0.721	b.d.	0.245	0.067	b.d.	0.137	b.d.
p CO_2 4 13	788.5	4.5	-160	0.276	0.450	0.039	0.137	0.160	0.247	0.083	25.36	64.25	3.81	0.152	2.58	0.037	b.d.	b.d.	b.d.	b.d.	b.d.	0.780	b.d.	0.245	0.064	b.d.	b.d.	b.d.
p CO_2 4 14	878.0	4.5	-177	0.311	0.483	0.043	0.139	0.154	0.272	0.086	40.04	55.40	4.03	0.156	2.57	0.042	b.d.	b.d.	b.d.	b.d.	b.d.	0.795	b.d.	0.259	0.065	b.d.	b.d.	b.d.
Outlet 3																												
p CO_2 3 3	67.5	4.7	190	0.232	0.336	0.034	0.138	0.149	0.432	0.079	n.a.	n.a.	4.13	0.190	3.32	0.007	0.483	b.d.	b.d.	b.d.	b.d.	0.822	b.d.	0.461	0.230	b.d.	b.d.	b.d.
p CO_2 3 4	188.3	4.5	-185	0.267	0.372	0.034	0.130	0.145	0.318	0.088	n.a.	n.a.	3.92	0.170	2.71	0.013	b.d.	b.d.	b.d.	b.d.	b.d.	0.968	b.d.	0.323	0.118	b.d.	0.156	b.d.
p CO_2 3 6	330.5	n.a.	n.a.	0.264	0.399	0.040	0.144	0.167	0.254	0.085	29.14	60.96	3.79	0.162	2.91	0.024	b.d.	b.d.	b.d.	b.d.	b.d.	0.870	b.d.	0.266	0.082	b.d.	0.311	b.d.
p CO_2 3 7	452.5	4.5	-167	0.240	0.363	0.032	0.129	0.145	0.208	0.079	31.14	55.35	3.23	0.141	2.38	0.015	0.322	b.d.	b.d.	b.d.	b.d.	0.770	0.054	0.204	0.059	b.d.	0.165	b.d.
p CO_2 3 8	492.8	4.6	-160	0.246	0.360	0.029	0.121	0.136	0.213	0.076	42.04	43.02	2.91	0.135	2.22	0.015	b.d.	b.d.	b.d.	b.d.	b.d.	0.734	b.d.	0.211	0.058	b.d.	0.200	b.d.
p CO_2 3 9	541.5	4.4	-206	0.172	0.330	0.029	0.101	0.115	0.152	0.062	29.55	39.63	2.59	0.113	1.83	0.025	b.d.	b.d.	b.d.	b.d.	b.d.	0.642	b.d.	0.143	0.045	b.d.	0.055	b.d.
p CO_2 3 10	616.0	4.5	-205	0.197	0.333	0.029	0.098	0.113	0.172	0.061	26.27	43.52	2.73	0.112	1.82	0.023	b.d.	b.d.	b.d.	b.d.	b.d.	0.654	b.d.	0.161	0.044	b.d.	b.d.	b.d.
p CO_2 3 11	662.5	4.5	-190	0.185	0.322	0.028	0.099	0.113	0.168	0.060	28.56	37.39	2.67	0.105	1.75	0.021	b.d.	b.d.	b.d.	b.d.	b.d.	0.552	b.d.	0.155	0.040	b.d.	b.d.	b.d.
p CO_2 3 12	736.5	n.a.	n.a.	0.241	0.352	0.033	0.115	0.132	0.187	0.071	n.a.	n.a.	2.97	0.128	2.06	0.024	b.d.	b.d.	b.d.	b.d.	b.d.	0.617	b.d.	0.173	0.042	b.d.	b.d.	b.d.
p CO_2 3 13	789.0	4.5	-209	0.276	0.374	0.035	0.129	0.137	0.197	0.080	21.29	64.00	3.09	0.137	2.21	0.028	b.d.	b.d.	b.d.	b.d.	b.d.	0.792	b.d.	0.191	0.044	b.d.	0.197	b.d.
p CO_2 3 14	878.5	4.5	-186	0.314	0.387	0.038	0.125	0.138	0.211	0.078	43.45	41.29	3.27	0.135	2.16	0.027	b.d.	b.d.	b.d.	b.d.	b.d.	0.680	b.d.	0.202	0.046	b.d.	b.d.	b.d.
p CO_2 3 15	971.5	n.a.	n.a.	0.346	0.390	0.039	0.129	0.142	0.214	0.082	25.35	64.27	3.68	0.141	2.18	0.032	b.d.	b.d.	b.d.	b.d.	b.d.	0.746	b.d.	0.212	0.045	b.d.	b.d.	b.d.
Outlet 2																												
p CO_2 2 3	68.5	4.7	195	0.207	0.241	0.032	0.124	0.134	0.267	0.073	n.a.	n.a.	3.84	0.152	2.54	0.016	b.d.	b.d.	b.d.	b.d.	b.d.	0.775	b.d.	0.256	0.101	b.d.	b.d.	b.d.
p CO_2 2 6	331.0	n.a.	n.a.	0.261	0.275	0.038	0.130	0.146	0.157	0.080	27.03	56.55	3.45	0.139	2.32	0.026	0.331	b.d.	b.d.	b.d.	b.d.	0.860	0.078	0.152	0.049	b.d.	0.231	b.d.
p CO_2 2 7	453.0	4.5	-172	0.247	0.248	0.025	0.105	0.112	0.140	0.067	26.90	50.14	2.61	0.114	1.70	0.020	b.d.	b.d.	b.d.	b.d.	b.d.	0.614	b.d.	0.135	0.038	b.d.	0.188	b.d.
p CO_2 2 8	493.5	4.6	-175	0.245	0.248	0.025	0.098	0.108	0.144	0.062	41.36	27.08	2.23	0.106	1.62	0.022	b.d.	b.d.	b.d.	b.d.	b.d.	0.523	b.d.	0.128	0.036	b.d.	0.232	b.d.
p CO_2 2 9	542.0	4.4	-215	0.192	0.236	0.024	0.083	0.095	0.118	0.053	38.88	18.62	2.32	0.092	1.35	0.036	b.d.	b.d.	b.d.	b.d.	b.d.	0.598	b.d.	0.104	0.031	b.d.	0.095	b.d.
p CO_2 2 10	616.5	4.4	-206	0.202	0.235	0.025	0.084	0.094	0.121	0.052	25.27	35.80	1.98	0.090	1.34	0.031	b.d.	b.d.	b.d.	b.d.	b.d.	0.524	b.d.	0.096	0.029	b.d.	b.d.	b.d.
p CO_2 2 11	663.0	4.4	-204	0.181	0.228	0.024	0.083	0.092	0.113	0.052	24.61	27.72	2.40	0.090	1.31	0.032	b.d.	b.d.	b.d.	b.d.	b.d.	0.511	b.d.	0.103	0.028	b.d.	b.d.	b.d.
p CO_2 2 12	737.0	n.a.	n.a.	0.267	0.256	0.029	0.099	0.110	0.140	0.062	n.a.	n.a.	2.38	0.109	1.53	0.041	b.d.	b.d.	b.d.	b.d.	b.d.	0.549	b.d.	0.135	0.032	b.d.	0.135	b.d.
p CO_2 2 13	790.0	4.5	-217	0.275	0.268	0.029	0.105	0.115	0.141	0.065	34.32	33.52	2.50	0.111	1.56	0.034	b.d.	b.d.	b.d.	b.d.	b.d.	0.607	b.d.	0.135	0.032	b.d.	b.d.	b.d.
p CO_2 2 14	879.0	4.4	-157	0.312	0.285	0.033	0.105	0.115	0.151	0.065	42.45	33.25	2.99	0.110	1.64	0.037	b.d.	b.d.	b.d.	b.d.	b.d.	0.581	b.d.	0.145	0.034	b.d.	b.d.	b.d.
Outlet 1																												
p CO_2 1 3	69.5	4.6	250	0.201	0.116	0.023	0.084	0.085	0.115	0.051	n.a.	n.a.	2.63	0.107	1.73	0.021	b.d.	b.d.	b.d.	b.d.	b.d.	0.610	b.d.	0.119	0.046	b.d.	b.d.	b.d.
p CO_2 1 4	189.8	4.4	-172	0.226	0.121	0.018	0.069	0.073	0.110	0.044	n.a.	n.a.	2.08	0.083	1.26	0.022	b.d.	b.d.	b.d.	b.d.	b.d.	0.557	b.d.	0.127	0.045	b.d.	0.226	b.d.
p CO_2 1 6	331.5	n.a.	n.a.	0.283	0.137	0.020	0.072	0.076	0.110	0.048	31.19	28.73	2.48	0.077	1.04	0.034	b.d.	b.d.	b.d.	b.d.	b.d.	0.454	b.d.	0.136	0.028	b.d.	0.240	b.d.
p CO_2 1 7	454.0	4.5	-169	0.248	0.148	0.017	0.070	0.073	0.091	0.045	27.23	26.67	1.75	0.077	0.98	0.023	b.d.	b.d.	b.d.	b.d.	b.d.	0.393	b.d.	0.115	0.025	b.d.	0.248	b.d.
p CO_2 1 8	495.0	4.6	-165	0.241	0.156	0.016	0.072	0.070	0.090	0.046	40.91	9.42	1.93	0.077	1.01	0.027	b.d.	b.d.	b.d.	b.d.	b.d.	0.387	b.d.	0.116	0.024	b.d.	0.276	b.d.
p CO_2 1 9	542.5	4.4	-206	0.208	0.149	0.018	0.058	0.063	0.086	0.038	28.52	13.53	1.60	0.064	0.81	0.045	b.d.	b.d.	b.d.	b.d.	b.d.	0.413	b.d.	0.103	0.021	b.d.	b.d.	b.d.
p CO_2 1 10	618.0	4.5	-197	0.200	0.149	0.017	0.058	0.062	0.080	0.037	28.59	13.33	1.39	0.062	0.79	0.040	b.d.	b.d.	b.d.	b.d.	b.d.	0.318	b.d.	0.104	0.018	b.d.	b.d.	b.d.
p CO_2 1 11	668.0	4.5	-205	0.248	0.157	0.018	0.062	0.068	0.101	0.040	30.87	16.32	1.37	0.068	0.86	0.032	b.d.	b.d.	b.d.	b.d.	b.d.	0.378	b.d.	0.126	0.021	b.d.	b.d.	b.d.
p CO_2 1 12	737.5	n.a.	n.a.	0.242	0.170	0.020	0.070	0.076	0.091	0.045	n.a.	n.a.	1.69	0.073	0.95	0.038	b.d.	b.d.	b.d.	b.d.	b.d.	0.377	b.d.	0.118	0.021	b.d.	0.163	b.d.
p CO_2 1 13	791.0	4.4	-219	0.273	0.178	0.021	0.074	0.079	0.096	0.047	24.50	29.60	1.94	0.078	0.98	0.039	b.d.	b.d.	b.d.	b.d.	b.d.	0.491	0.102	0.128	0.021	b.d.	b.d.	b.d.
p CO_2 1 14	879.5	4.4	-145	0.310	0.197	0.024	0.077	0.081	0.102	0.050	44.84	10.33	1.99	0.082	1.06	0.041	b.d.	b.d.	b.d.	b.d.	b.d.	0.391	b.d.	0.163	0.022	b.d.	b.d.	b.d.
p CO_2 1 15	972.0	n.a.	n.a.	0.342	0.200	0.024	0.077	0.082	0.107	0.050	26.20	31.21	2.30	0.080	1.07	0.040	b.d.	b.d.	b.d.	b.d.	b.d.	0.409	b.d.	0.184	0.022	b.d.	b.d.	b.d.

Table 3. Chemical composition of the sampled fluid during the CO_2-charged water-basaltic glass interaction experiment at 50 °C. n.a. = not analyzed, b.d. = below detection limit.

Sample	Elapsed time [hours]	pH 22 °C	Eh [mV]	DIC	Si	Na	K	Ca	Mg	Al	Fe	Fe^{3+}	Fe^{2+}	Sr	Mn	Ti	P	Li	Mo	Cl	Br	B	W	Cr	Ba	Sb	As	V
							[mmol/kg]												[µmol/kg]									
Column outlet																												
p CO_2 outlet 125	43.0	5.8	-275	n.a.	2.193	0.533	56.66	8.644	4.102	0.002	0.005	n.a.	n.a.	3.807	23.79	0.250	2.316	0.307	b.d.	1.389	b.d.	b.d.	b.d.	0.037	0.112	b.d.	b.d.	0.331
p CO_2 outlet 126	44.3	5.7	-276	n.a.	2.187	0.526	57.09	8.571	4.042	0.002	0.005	n.a.	n.a.	3.772	23.68	0.240	2.200	0.419	b.d.	b.d.	b.d.	b.d.	b.d.	0.046	0.111	b.d.	b.d.	0.353
p CO_2 outlet 127	45.8	5.7	-275	n.a.	2.453	0.493	56.78	7.453	3.882	0.003	0.008	n.a.	n.a.	3.415	23.96	0.185	2.063	0.500	b.d.	b.d.	b.d.	0.226	b.d.	0.052	0.103	b.d.	b.d.	0.324
p CO_2 outlet 128	50.5	5.5	-277	n.a.	2.831	0.432	56.89	5.616	3.503	0.003	0.012	n.a.	n.a.	2.814	27.45	0.118	1.787	0.432	b.d.	b.d.	b.d.	0.263	b.d.	0.053	0.092	b.d.	b.d.	0.285
p CO_2 outlet 129	54.3	5.5	-277	n.a.	3.004	0.378	55.98	4.423	2.933	0.003	0.031	n.a.	n.a.	2.401	27.94	0.106	1.556	0.429	0.133	0.731	b.d.	0.471	b.d.	0.295	0.081	b.d.	b.d.	0.267
p CO_2 outlet 130	67.0	5.3	-265	n.a.	3.500	0.277	65.36	3.026	1.912	0.004	0.083	35.86	47.33	2.167	39.16	0.051	1.083	0.421	b.d.	b.d.	b.d.	1.027	b.d.	0.106	0.079	b.d.	b.d.	0.235
p CO_2 outlet 131	99.5	4.9	-279	n.a.	3.741	0.189	50.85	1.628	1.061	0.007	0.219	n.a.	n.a.	2.168	118.77	0.023	1.830	0.962	b.d.	b.d.	b.d.	2.745	b.d.	0.154	0.085	b.d.	b.d.	0.194
p CO_2 outlet 132	161.5	4.6	-168	n.a.	2.943	0.117	16.78	0.588	0.547	0.009	0.208	57.40	133.68	3.926	15.60	0.011	1.024	0.647	b.d.	b.d.	b.d.	2.627	b.d.	0.063	0.105	b.d.	b.d.	b.d.
p CO_2 outlet 133	219.8	4.5	-208	n.a.	2.551	0.114	12.73	0.433	0.438	0.022	0.212	45.20	142.05	0.937	9.06	0.018	1.361	0.522	b.d.	b.d.	b.d.	2.707	b.d.	0.091	0.199	b.d.	b.d.	b.d.
p CO_2 outlet 134	238.2	4.5	-224	n.a.	2.323	0.100	9.72	0.318	0.335	0.013	0.145	34.47	94.50	0.578	6.59	0.015	1.253	0.392	b.d.	b.d.	b.d.	1.868	b.d.	0.073	0.151	b.d.	b.d.	b.d.
p CO_2 outlet 135	258.8	4.6	-200	n.a.	2.089	0.083	7.29	0.237	0.257	0.007	0.093	n.a.	n.a.	0.370	4.93	0.013	1.329	0.366	b.d.	b.d.	b.d.	1.205	b.d.	0.049	0.108	b.d.	b.d.	b.d.
p CO_2 outlet 136	341.8	4.1	-224	n.a.	1.482	0.074	6.39	0.250	0.267	0.087	0.154	32.76	101.36	0.295	4.14	0.034	1.661	0.284	b.d.	b.d.	b.d.	1.947	b.d.	0.121	0.609	b.d.	b.d.	b.d.
p CO_2 outlet 137	362.0	4.4	-216	n.a.	1.262	0.057	4.82	0.165	0.187	0.033	0.090	23.18	58.47	0.186	2.80	0.023	1.878	0.219	b.d.	b.d.	b.d.	1.098	b.d.	0.067	0.261	b.d.	0.123	b.d.
p CO_2 outlet 138	403.3	4.4	-143	n.a.	1.173	0.048	4.31	0.165	0.187	0.020	0.098	19.71	67.05	0.192	2.90	0.016	1.892	0.264	b.d.	b.d.	b.d.	1.181	b.d.	0.044	0.165	b.d.	0.130	b.d.
p CO_2 outlet 139	505.0	4.2	-105	n.a.	1.188	0.073	6.65	0.240	0.269	0.066	0.154	19.75	108.35	0.275	3.82	0.023	0.488	0.156	b.d.	b.d.	b.d.	1.933	b.d.	0.111	0.167	b.d.	b.d.	b.d.
p CO_2 outlet 140	573.8	4.2	-130	n.a.	1.106	0.073	6.54	0.241	0.270	0.086	0.158	15.81	124.86	0.274	3.73	0.026	0.812	0.160	b.d.	b.d.	b.d.	2.065	b.d.	0.114	0.136	b.d.	b.d.	b.d.
p CO_2 outlet 141	669.5	4.2	-218	n.a.	0.981	0.069	5.86	0.228	0.260	0.078	0.149	n.a.	n.a.	0.255	3.49	0.027	0.853	0.170	b.d.	b.d.	b.d.	1.775	b.d.	0.113	0.091	b.d.	b.d.	b.d.
p CO_2 outlet 142	738.8	4.2	-82	n.a.	0.944	0.071	6.42	0.233	0.267	0.080	0.152	n.a.	n.a.	0.260	3.53	0.021	1.228	b.d.	b.d.	b.d.	b.d.	1.885	b.d.	0.128	0.085	b.d.	b.d.	b.d.
p CO_2 outlet 143	837.8	4.2	-77	n.a.	0.880	0.068	5.73	0.226	0.260	0.085	0.148	n.a.	n.a.	0.251	3.36	0.023	1.743	b.d.	b.d.	b.d.	b.d.	1.869	b.d.	0.125	0.075	b.d.	b.d.	b.d.
p CO_2 outlet 144	905.6	4.2	-93	n.a.	0.845	0.069	5.80	0.229	0.270	0.098	0.147	n.a.	n.a.	0.251	3.34	0.027	2.043	b.d.	b.d.	b.d.	b.d.	1.824	b.d.	0.135	0.073	b.d.	0.160	b.d.
Outlet 7																												
p 7 16	99.7	4.9	-268	0.309	3.756	0.187	46.61	1.582	1.040	0.007	0.221	104.51	120.19	2.149	111.32	0.017	0.423	0.928	b.d.	b.d.	b.d.	2.930	b.d.	0.031	0.085	b.d.	b.d.	b.d.
p 7 17	162.0	4.6	-170	0.223	2.956	0.118	16.78	0.587	0.561	0.008	0.212	62.94	130.26	3.906	15.53	0.010	0.899	0.563	b.d.	b.d.	b.d.	2.771	b.d.	0.013	0.109	b.d.	b.d.	b.d.
p 7 18	239.0	4.7	-232	0.175	2.319	0.099	9.50	0.317	0.335	0.014	0.143	44.10	89.28	0.582	6.40	0.013	1.044	0.390	b.d.	b.d.	b.d.	1.833	b.d.	0.024	0.150	b.d.	b.d.	b.d.
p 7 19	362.5	4.4	-211	0.166	1.252	0.057	4.55	0.163	0.183	0.031	0.086	23.72	55.85	0.182	2.76	0.019	1.837	0.232	b.d.	b.d.	b.d.	1.100	b.d.	0.032	0.250	b.d.	b.d.	b.d.
p 7 20	403.8	4.5	-137	0.136	1.185	0.048	4.46	0.175	0.195	0.022	0.104	29.14	69.77	0.203	3.03	0.019	1.895	0.200	b.d.	b.d.	b.d.	1.306	b.d.	0.040	0.175	b.d.	b.d.	b.d.
p 7 21	505.5	4.4	-110	0.300	1.193	0.073	6.84	0.241	0.267	0.065	0.154	23.88	110.29	0.274	3.76	0.020	0.652	0.075	b.d.	b.d.	b.d.	1.992	b.d.	0.097	0.168	b.d.	b.d.	b.d.
p 7 22	574.0	4.3	-130	0.345	1.112	0.072	6.62	0.242	0.270	0.087	0.159	12.55	129.69	0.274	3.69	0.025	0.611	0.111	b.d.	b.d.	b.d.	2.026	b.d.	0.121	0.136	b.d.	b.d.	b.d.
p 7 23	669.8	4.3	-176	0.290	0.987	0.069	6.00	0.229	0.257	0.077	0.149	38.00	102.93	0.254	3.43	0.021	0.892	0.128	b.d.	b.d.	b.d.	1.927	b.d.	0.094	0.091	b.d.	b.d.	b.d.
p 7 24	739.3	4.3	-92	0.306	0.953	0.069	6.11	0.230	0.263	0.079	0.150	30.96	108.68	0.255	3.43	0.021	1.162	b.d.	b.d.	b.d.	b.d.	1.897	b.d.	0.106	0.085	b.d.	b.d.	b.d.
p 7 25	838.3	4.3	-73	0.292	0.897	0.068	5.99	0.226	0.255	0.083	0.150	43.98	92.89	0.251	3.34	0.022	1.455	b.d.	b.d.	b.d.	b.d.	1.856	b.d.	0.110	0.076	b.d.	b.d.	b.d.
p 7 26	906.0	4.3	-92	0.335	0.854	0.069	5.74	0.228	0.267	0.097	0.147	34.59	100.48	0.248	3.36	0.018	1.840	b.d.	b.d.	b.d.	b.d.	1.880	b.d.	0.131	0.074	b.d.	0.138	b.d.
Outlet 6																												
p 6 16	100.5	4.9	-240	0.379	3.548	0.156	29.57	1.028	0.791	0.008	0.283	63.13	186.84	2.558	40.67	0.025	0.360	0.790	0.193	b.d.	b.d.	3.369	b.d.	0.006	0.126	b.d.	b.d.	b.d.
p 6 17	163.0	4.6	-163	0.204	2.714	0.101	12.82	0.452	0.442	0.008	0.175	48.34	111.50	1.558	11.29	0.017	0.573	0.437	0.073	b.d.	b.d.	2.159	b.d.	0.018	0.097	b.d.	b.d.	b.d.
p 6 18	240.0	4.6	-237	0.125	2.041	0.084	7.71	0.259	0.290	0.007	0.111	37.48	64.23	0.373	5.02	0.017	0.861	0.272	b.d.	b.d.	b.d.	1.421	b.d.	n.a.	0.140	b.d.	b.d.	b.d.
p 6 19	363.0	4.4	-195	0.136	1.084	0.050	4.09	0.166	0.183	0.014	0.092	27.97	60.83	0.177	2.87	0.026	1.497	0.127	b.d.	b.d.	b.d.	1.079	b.d.	0.023	0.142	b.d.	b.d.	b.d.
p 6 20	404.5	4.5	-130	0.247	1.170	0.049	5.47	0.185	0.199	0.040	0.148	33.23	96.66	0.247	3.01	0.037	1.681	0.170	b.d.	b.d.	b.d.	1.874	b.d.	0.049	0.181	b.d.	0.148	b.d.
p 6 21	506.0	4.4	-100	0.286	1.030	0.071	6.34	0.233	0.260	0.051	0.147	23.78	104.74	0.260	3.56	0.029	0.372	0.114	b.d.	b.d.	b.d.	1.884	b.d.	0.085	0.128	b.d.	b.d.	b.d.
p 6 22	574.8	4.4	-124	0.371	0.995	0.072	7.19	0.239	0.270	0.091	0.159	11.07	126.89	0.271	3.56	0.032	0.658	b.d.	b.d.	b.d.	b.d.	1.999	b.d.	0.114	0.121	b.d.	b.d.	b.d.
p 6 23	670.3	4.3	-153	0.288	0.865	0.066	5.81	0.217	0.247	0.070	0.141	33.74	98.05	0.240	3.22	0.033	0.897	b.d.	b.d.	b.d.	b.d.	1.824	b.d.	0.084	0.083	b.d.	b.d.	b.d.
p 6 24	739.8	4.4	-85	0.297	0.832	0.063	5.60	0.210	0.240	0.079	0.143	48.36	88.65	0.236	3.06	0.027	1.143	b.d.	b.d.	b.d.	b.d.	1.814	b.d.	0.100	0.078	b.d.	b.d.	b.d.

Table 3. Continuation.

Sample	Elapsed time [hours]	pH 22 °C	Eh [mV]	DIC	Si	Na	K	Ca	Mg	Al	Fe	Fe^{3+}	Fe^{2+}	Sr	Mn	Ti	P	Li	Mo	Cl	Br	B	W	Cr	Ba	Sb	As	V
				[mmol/kg]															[µmol/kg]									
p 6 25	839.0	4.3	-78	0.301	0.793	0.063	6.12	0.209	0.241	0.084	0.140	43.97	86.50	0.232	3.03	0.032	1.589	b.d.	b.d.	b.d.	b.d.	1.781	b.d.	0.104	0.070	b.d.	b.d.	b.d.
p 6 26	906.6	4.3	-91	0.317	0.766	0.064	5.52	0.214	0.248	0.095	0.142	45.29	86.37	0.234	3.04	0.033	1.740	b.d.	b.d.	b.d.	b.d.	1.746	b.d.	0.123	0.067	b.d.	b.d.	b.d.
Outlet 5																												
p 5 16	101.2	4.9	-214	0.283	3.136	0.120	17.07	0.634	0.601	0.012	0.250	74.46	152.97	0.498	19.05	0.018	0.378	0.549	b.d.	b.d.	b.d.	3.052	b.d.	0.032	0.144	b.d.	b.d.	b.d.
p 5 17	163.7	4.6	-175	0.203	2.377	0.092	9.78	0.349	0.389	0.010	0.173	44.01	109.33	0.722	7.73	0.018	0.684	0.359	b.d.	b.d.	b.d.	2.150	b.d.	0.019	0.111	b.d.	b.d.	b.d.
p 5 18	241.0	4.6	-235	0.134	1.733	0.074	7.09	0.252	0.283	0.008	0.110	32.93	66.11	0.301	4.72	0.017	0.961	0.177	b.d.	b.d.	b.d.	1.353	b.d.	0.005	0.387	b.d.	b.d.	b.d.
p 5 19	363.7	4.4	-205	0.149	0.883	0.047	4.39	0.157	0.175	0.016	0.101	30.28	63.11	0.180	2.58	0.029	1.633	0.137	b.d.	b.d.	b.d.	1.163	b.d.	0.021	0.104	b.d.	0.141	b.d.
p 5 20	405.8	4.5	-131	0.245	0.941	0.048	4.20	0.172	0.190	0.043	0.113	24.24	76.17	0.196	2.64	0.037	1.957	0.153	b.d.	b.d.	b.d.	1.293	b.d.	0.067	0.121	b.d.	b.d.	b.d.
p 5 21	506.5	4.5	-115	0.291	0.850	0.067	5.96	0.220	0.246	0.054	0.142	27.04	101.85	0.243	3.27	0.034	0.400	b.d.	b.d.	b.d.	b.d.	1.904	b.d.	0.072	0.099	b.d.	b.d.	b.d.
p 5 22	575.3	4.4	-120	0.382	0.819	0.068	6.22	0.226	0.254	0.096	0.146	10.30	115.22	0.247	3.25	0.037	0.427	b.d.	b.d.	b.d.	b.d.	1.898	b.d.	0.121	0.092	b.d.	b.d.	b.d.
p 5 23	671.0	4.3	-145	0.289	0.716	0.061	5.53	0.199	0.229	0.073	0.129	46.74	77.16	0.217	2.88	0.036	0.855	b.d.	b.d.	b.d.	b.d.	1.734	b.d.	0.086	0.067	b.d.	b.d.	b.d.
p 5 24	740.3	4.4	-80	0.290	0.697	0.057	5.20	0.188	0.219	0.089	0.126	31.77	85.16	0.206	2.66	0.038	1.128	b.d.	b.d.	b.d.	b.d.	1.545	b.d.	0.098	0.064	b.d.	b.d.	b.d.
p 5 25	839.5	4.4	-76	0.296	0.679	0.057	5.24	0.190	0.220	0.095	0.126	28.91	84.86	0.207	2.65	0.041	1.615	b.d.	b.d.	b.d.	b.d.	1.544	b.d.	0.130	0.058	b.d.	b.d.	b.d.
p 5 26	907.2	4.4	-75	0.352	0.667	0.057	5.22	0.191	0.229	0.125	0.132	27.08	95.14	0.213	2.68	0.038	2.117	b.d.	b.d.	b.d.	b.d.	1.739	b.d.	0.143	0.061	b.d.	b.d.	b.d.
Outlet 4																												
p 4 16	101.7	4.8	-227	0.255	2.440	0.098	11.19	0.405	0.449	0.016	0.199	50.60	123.26	0.950	12.10	0.026	0.526	0.349	b.d.	b.d.	b.d.	2.561	b.d.	0.052	0.160	b.d.	b.d.	b.d.
p 4 17	164.5	4.6	-170	0.347	1.978	0.085	8.31	0.347	0.381	0.023	0.205	43.95	137.35	0.498	7.05	0.027	0.550	0.333	b.d.	b.d.	b.d.	2.554	b.d.	0.042	0.896	b.d.	b.d.	b.d.
p 4 18	259.0	4.7	-199	n.a.	1.751	0.096	10.55	0.364	0.409	0.060	0.246	48.96	167.21	0.467	6.04	0.041	0.807	0.274	b.d.	b.d.	b.d.	2.921	b.d.	0.108	0.581	b.d.	b.d.	b.d.
p 4 19	364.5	4.4	-206	0.160	0.634	0.041	3.67	0.138	0.156	0.029	0.094	22.87	61.88	0.155	2.15	0.042	1.642	b.d.	b.d.	b.d.	b.d.	1.179	b.d.	0.041	0.075	b.d.	0.132	b.d.
p 4 20	406.3	4.6	-130	0.255	0.683	0.042	3.41	0.151	0.172	0.067	0.099	21.87	67.98	0.165	2.19	0.044	1.863	b.d.	b.d.	b.d.	b.d.	1.144	b.d.	0.076	0.078	b.d.	0.147	b.d.
p 4 21	507.0	4.5	-110	0.289	0.634	0.050	4.39	0.188	0.206	0.083	0.123	21.75	88.54	0.202	2.66	0.047	0.490	b.d.	b.d.	b.d.	b.d.	1.419	b.d.	0.090	0.069	b.d.	b.d.	b.d.
p 4 22	576.0	4.4	-138	0.376	0.627	0.053	4.85	0.197	0.219	0.140	0.127	10.68	101.80	0.211	2.69	0.051	0.547	0.156	b.d.	b.d.	b.d.	1.432	b.d.	0.153	0.066	b.d.	b.d.	b.d.
p 4 23	671.5	4.4	-135	0.291	0.587	0.048	5.85	0.173	0.194	0.121	0.116	52.81	66.99	0.188	2.37	0.045	0.938	b.d.	b.d.	b.d.	b.d.	1.291	b.d.	0.125	0.055	b.d.	b.d.	b.d.
p 4 24	741.0	4.4	-80	0.293	0.577	0.043	3.83	0.163	0.187	0.136	0.110	52.40	61.71	0.177	2.19	0.051	1.312	b.d.	b.d.	b.d.	b.d.	1.254	b.d.	0.139	0.051	b.d.	0.148	b.d.
p 4 25	840.1	4.4	-74	0.304	0.588	0.046	3.88	0.171	0.198	0.145	0.113	53.52	61.82	0.183	2.29	0.052	1.704	0.156	b.d.	b.d.	b.d.	1.317	b.d.	0.160	0.050	b.d.	0.135	b.d.
p 4 26	907.8	4.4	-86	0.414	0.623	0.046	4.16	0.175	0.202	0.225	0.120	42.27	72.91	0.190	2.23	0.054	2.065	b.d.	b.d.	b.d.	b.d.	1.353	b.d.	0.220	0.054	b.d.	0.194	b.d.
Outlet 3																												
p 3 16	102.3	4.7	-245	0.194	1.546	0.069	7.28	0.262	0.284	0.016	0.129	45.09	69.66	0.372	8.10	0.019	2.006	0.303	b.d.	b.d.	b.d.	1.669	b.d.	0.078	0.548	b.d.	b.d.	b.d.
p 3 17	165.3	4.6	-168	0.410	1.298	0.072	6.84	0.254	0.290	0.042	0.160	43.71	95.32	0.304	4.61	0.028	0.917	0.158	b.d.	b.d.	b.d.	1.994	b.d.	0.072	0.367	b.d.	b.d.	b.d.
p 3 18	260.0	4.7	-205	n.a.	1.179	0.092	7.13	0.328	0.370	0.117	0.199	51.48	125.74	0.354	5.06	0.039	1.082	0.187	b.d.	b.d.	b.d.	2.489	b.d.	0.162	0.205	b.d.	b.d.	b.d.
p 3 19	365.2	4.4	-194	0.152	0.432	0.033	2.87	0.110	0.127	0.066	0.076	20.58	48.01	0.121	1.65	0.033	1.799	b.d.	b.d.	b.d.	b.d.	0.855	b.d.	0.074	0.045	b.d.	0.130	b.d.
p 3 20	407.0	4.5	-125	0.259	0.469	0.036	2.78	0.126	0.148	0.147	0.081	19.53	54.33	0.134	1.73	0.034	1.820	0.117	b.d.	b.d.	b.d.	1.001	b.d.	0.120	0.050	b.d.	0.124	b.d.
p 3 21	507.7	4.5	-115	0.279	0.476	0.040	3.36	0.150	0.172	0.171	0.101	19.80	71.72	0.162	2.02	0.039	0.610	b.d.	b.d.	b.d.	b.d.	1.160	b.d.	0.152	0.046	b.d.	b.d.	b.d.
p 3 22	580.2	4.4	-128	0.379	0.512	0.042	3.77	0.160	0.179	0.238	0.113	8.88	87.25	0.177	2.02	0.043	0.919	b.d.	b.d.	b.d.	b.d.	1.266	b.d.	0.197	0.052	b.d.	b.d.	b.d.
p 3 23	672.2	4.4	-130	0.306	0.499	0.039	3.20	0.149	0.173	0.211	0.101	55.34	57.38	0.159	1.92	0.037	1.449	b.d.	b.d.	b.d.	b.d.	1.116	b.d.	0.188	0.044	b.d.	0.132	b.d.
p 3 24	741.5	4.4	-70	0.301	0.495	0.037	3.31	0.143	0.170	0.212	0.095	35.32	66.28	0.152	1.85	0.036	1.274	0.151	b.d.	b.d.	b.d.	1.053	b.d.	0.178	0.042	b.d.	b.d.	b.d.
p 3 25	840.7	4.4	-70	0.296	0.511	0.039	3.05	0.149	0.176	0.203	0.100	25.34	71.42	0.159	1.91	0.039	1.709	0.157	b.d.	b.d.	b.d.	1.170	b.d.	0.176	0.041	b.d.	0.120	b.d.
p 3 26	908.5	4.4	-85	0.393	0.535	0.039	3.45	0.154	0.180	0.280	0.104	41.75	65.89	0.164	1.88	0.042	2.251	b.d.	b.d.	b.d.	b.d.	1.162	b.d.	0.226	0.044	b.d.	0.248	b.d.
Outlet 2																												
p 2 16	103.0	4.7	-220	0.195	0.789	0.051	5.96	0.197	0.199	0.026	0.106	40.02	56.36	0.256	6.11	0.024	0.802	0.245	b.d.	b.d.	b.d.	1.388	b.d.	0.072	0.140	b.d.	b.d.	b.d.
p 2 17	167.3	4.7	-177	0.351	0.666	0.057	5.03	0.197	0.220	0.090	0.123	49.06	65.39	0.234	3.11	0.033	0.686	b.d.	b.d.	b.d.	b.d.	1.502	b.d.	0.121	0.101	b.d.	b.d.	b.d.
p 2 18	261.0	4.7	-212	n.a.	0.653	0.074	6.54	0.255	0.287	0.246	0.163	34.36	106.41	0.272	3.49	0.067	1.017	0.151	b.d.	b.d.	b.d.	1.935	b.d.	0.205	0.086	b.d.	b.d.	b.d.
p 2 19	366.0	4.6	-192	0.212	0.333	0.026	2.37	0.090	0.107	0.171	0.068	22.64	41.06	0.101	1.12	0.038	1.683	b.d.	b.d.	b.d.	b.d.	0.784	b.d.	0.110	0.033	b.d.	0.190	b.d.
p 2 20	408.2	4.6	-117	0.217	0.313	0.030	2.40	0.101	0.120	0.158	0.068	18.58	42.81	0.106	1.27	0.041	1.818	b.d.	b.d.	b.d.	b.d.	0.877	b.d.	0.121	0.032	b.d.	0.153	b.d.

Table 3. Continuation.

Sample	Elapsed time [hours]	pH 22 °C	Eh [mV]	DIC	Si	Na	K	Ca	Mg	Al	Fe	Fe^{3+}	Fe^{2+}	Sr	Mn	Ti	P	Li	Mo	Cl	Br	B	W	Cr	Ba	Sb	As	V
				[mmol/kg]										[µmol/kg]														
p 2 21	508.3	4.5	-110	0.274	0.363	0.032	2.96	0.123	0.145	0.215	0.085	20.08	61.75	0.133	1.49	0.042	0.659	b.d.	b.d.	b.d.	b.d.	0.965	b.d.	0.156	0.034	b.d.	b.d.	b.d.
p 2 22	580.8	4.4	-124	0.337	0.389	0.035	3.13	0.136	0.160	0.243	0.093	7.76	75.15	0.146	1.63	0.047	0.598	0.174	b.d.	b.d.	b.d.	1.009	b.d.	0.176	0.037	b.d.	b.d.	b.d.
p 2 23	672.7	4.4	-120	0.307	0.397	0.031	2.33	0.119	0.145	0.212	0.084	37.60	50.65	0.129	1.46	0.041	0.967	b.d.	b.d.	b.d.	b.d.	0.930	b.d.	0.175	0.035	b.d.	b.d.	b.d.
p 2 24	747.3	4.4	-77	0.297	0.398	0.031	2.47	0.121	0.148	0.183	0.083	29.64	56.70	0.131	1.52	0.045	1.403	b.d.	b.d.	b.d.	b.d.	0.917	b.d.	0.159	0.033	b.d.	0.164	b.d.
p 2 25	841.3	4.5	-73	0.301	0.415	0.029	2.20	0.115	0.142	0.203	0.083	23.68	63.60	0.125	1.38	0.047	1.648	0.114	b.d.	b.d.	b.d.	0.982	b.d.	0.154	0.032	b.d.	0.137	b.d.
p 2 26	909.2	4.4	-82	0.358	0.404	0.031	2.49	0.120	0.149	0.227	0.083	46.67	44.28	0.129	1.44	0.050	2.155	b.d.	b.d.	b.d.	b.d.	0.883	b.d.	0.167	0.034	b.d.	0.162	b.d.
Outlet 1																												
p 1 16	103.7	4.6	-203	0.187	0.347	0.033	3.92	0.130	0.127	0.086	0.068	38.69	28.16	0.159	4.24	0.031	0.785	0.131	0.276	b.d.	b.d.	0.979	b.d.	0.114	0.047	b.d.	b.d.	b.d.
p 1 17	168.2	4.7	-174	0.251	0.281	0.034	3.02	0.114	0.132	0.162	0.079	28.93	43.43	0.132	1.45	0.031	0.753	b.d.	0.072	b.d.	b.d.	1.010	b.d.	0.129	0.033	b.d.	b.d.	b.d.
p 1 18	262.3	4.7	-214	n.a.	0.339	0.049	4.18	0.164	0.194	0.240	0.111	36.11	64.68	0.174	2.01	0.047	0.948	b.d.	b.d.	b.d.	b.d.	1.378	b.d.	0.200	0.041	b.d.	b.d.	b.d.
p 1 19	366.8	4.5	-183	0.142	0.150	0.016	1.30	0.054	0.070	0.083	0.041	17.42	26.39	0.059	0.68	0.038	1.600	b.d.	b.d.	b.d.	b.d.	0.564	b.d.	0.065	0.017	b.d.	0.139	b.d.
p 1 20	409.0	4.5	-119	0.133	0.156	0.018	1.44	0.059	0.077	0.067	0.040	14.74	25.79	0.060	0.77	0.034	1.868	b.d.	b.d.	b.d.	b.d.	0.478	b.d.	0.051	0.013	b.d.	0.207	b.d.
p 1 21	508.8	4.4	-106	0.271	0.190	0.019	1.41	0.072	0.093	0.124	0.053	12.16	39.20	0.078	0.88	0.046	0.642	0.118	b.d.	b.d.	b.d.	0.610	b.d.	0.094	0.021	b.d.	b.d.	b.d.
p 1 22	581.5	4.4	-127	0.338	0.206	0.021	1.78	0.081	0.103	0.135	0.059	5.44	54.49	0.087	0.98	0.050	0.775	b.d.	b.d.	b.d.	b.d.	0.703	b.d.	0.136	0.023	b.d.	b.d.	b.d.
p 1 23	673.2	4.4	-120	0.288	0.213	0.018	1.52	0.072	0.096	0.115	0.052	26.28	37.87	0.076	0.88	0.051	1.026	b.d.	b.d.	b.d.	b.d.	0.544	b.d.	0.117	0.019	b.d.	b.d.	b.d.
p 1 24	747.3	4.4	-67	0.277	0.230	0.018	1.44	0.074	0.099	0.112	0.055	31.77	32.58	0.079	0.91	0.048	1.270	b.d.	b.d.	b.d.	b.d.	0.588	b.d.	0.124	0.019	b.d.	b.d.	b.d.
p 1 25	841.3	4.4	-75	0.292	0.225	0.016	1.51	0.066	0.093	0.119	0.049	35.18	28.03	0.071	0.81	0.051	1.728	b.d.	b.d.	b.d.	b.d.	0.553	0.078	0.119	0.019	b.d.	0.150	b.d.
p 1 26	909.2	4.3	-77	0.289	0.237	0.018	1.55	0.074	0.103	0.101	0.054	29.93	34.53	0.079	0.95	0.049	2.163	b.d.	b.d.	b.d.	b.d.	0.590	0.024	0.106	0.017	b.d.	0.158	b.d.

Table 1. Saturation indices of sampled fluids with respect to secondary minerals during the pure water-basaltic glass interaction experiment. (am) = amorphous

Sample	Elapsed time [hours]	Aragonite	Calcite	Ca-mont-morillonite	Chalcedony	Dolomite	$Fe(OH)_3$ (am)	Gibbsite	Goethite	Goethite (am)	Hematite	Illite	Kaolinite	Quartz	Siderite	SiO_2 (am)	$Al(OH)_3$ (am)	$Ca_{0.25}Mg_{0.25}Fe_{0.5}$ carbonate	Ca-Mg-Fe smectite	$Ca_{0.25}Mg_{0.5}Fe_{0.25}$ carbonate	Ferrihydrite $Fe(OH)_3$	Imogolite
Outlet 7																						
p 7 8	29.0	-4.52	-4.37	2.16	-0.25	-8.78	1.95	1.91	5.99	1.58	17.47	1.43	6.41	-0.08	-7.76	-1.13	-0.38	-5.79	4.97	-5.10	2.54	3.29
p 7 9	97.0	-4.50	-4.36	2.18	-0.31	-8.69	1.54	2.01	5.57	1.17	16.64	1.50	6.49	-0.14	-8.22	-1.19	-0.27	-5.99	4.64	-5.17	2.13	3.43
p 7 10	145.0	-4.46	-4.32	2.09	-0.32	-8.61	1.50	1.97	5.54	1.13	16.56	1.32	6.41	-0.15	-8.33	-1.20	-0.31	-6.03	4.54	-5.17	2.09	3.35
p 7 11	193.0	-4.37	-4.22	1.85	-0.33	-8.40	1.58	1.87	5.62	1.21	16.73	1.25	6.19	-0.16	-8.46	-1.21	-0.41	-6.04	4.43	-5.12	2.17	3.14
p 7 12	273.0	-4.20	-4.06	2.02	-0.29	-8.20	1.42	1.88	5.45	1.04	16.39	1.40	6.27	-0.12	-8.60	-1.18	-0.40	-6.06	4.48	-5.10	2.01	3.20
p 7 13	313.5	-4.04	-3.89	1.56	-0.32	-7.86	0.94	1.71	4.98	0.57	15.45	1.10	5.86	-0.15	-9.45	-1.20	-0.58	-6.40	3.83	-5.19	1.53	2.81
p 7 14	361.5	-4.01	-3.86	1.48	-0.33	-7.79	1.21	1.68	5.25	0.84	15.99	1.08	5.79	-0.16	-9.24	-1.21	-0.61	-6.28	3.96	-5.10	1.80	2.75
p 7 15	433.5	-4.05	-3.91	1.61	-0.32	-7.86	1.44	1.73	5.47	1.07	16.44	1.19	5.91	-0.15	-8.91	-1.20	-0.56	-6.13	4.21	-5.04	2.03	2.86
p 7 16	505.5	-3.97	-3.83	1.48	-0.31	-7.68	1.35	1.64	5.39	0.98	16.26	1.12	5.76	-0.13	-9.19	-1.19	-0.65	-6.22	4.08	-5.04	1.94	2.69
p 7 17	623.0	-4.15	-4.00	1.98	-0.27	-8.03	1.84	1.82	5.87	1.46	17.23	1.48	6.20	-0.10	-8.31	-1.15	-0.46	-5.87	4.77	-4.95	2.43	3.10
p 7 18	672.5	-4.00	-3.85	1.56	-0.30	-7.71	1.68	1.67	5.72	1.31	16.92	1.28	5.83	-0.13	-8.79	-1.18	-0.62	-6.04	4.37	-4.95	2.27	2.76
p 7 19	793.0	-3.99	-3.84	2.12	-0.28	-7.80	1.50	1.88	5.53	1.12	16.55	1.66	6.30	-0.11	-8.73	-1.16	-0.41	-6.03	4.66	-4.98	2.09	3.21
p 7 20	939.5	-3.90	-3.75	1.86	-0.30	-7.61	1.40	1.78	5.43	1.03	16.36	1.50	6.07	-0.12	-9.03	-1.18	-0.50	-6.13	4.40	-4.99	1.99	2.99
p 7 21	1008.0	-3.87	-3.72	1.78	-0.30	-7.54	1.37	1.75	5.41	1.00	16.30	1.40	6.00	-0.13	-9.13	-1.18	-0.53	-6.16	4.32	-4.99	1.96	2.93
p 7 22	1031.0	-3.88	-3.73	1.81	-0.30	-7.56	1.68	1.76	5.72	1.31	16.92	1.43	6.02	-0.13	-8.80	-1.18	-0.52	-6.00	4.55	-4.91	2.27	2.95
p 7 23	1136.0	-3.83	-3.69	1.67	-0.31	-7.47	1.16	1.71	5.19	0.78	15.87	1.34	5.90	-0.14	-9.43	-1.19	-0.57	-6.29	4.09	-5.03	1.74	2.84
p 7 24	1208.5	-3.83	-3.69	1.67	-0.31	-7.47	1.16	1.71	5.19	0.78	15.87	1.30	5.90	-0.14	-9.43	-1.19	-0.57	-6.29	4.09	-5.03	1.74	2.84
p 7 25	1303.0	-3.83	-3.69	1.67	-0.31	-7.45	1.46	1.71	5.49	1.08	16.47	1.28	5.90	-0.14	-9.12	-1.19	-0.57	-6.14	4.29	-4.95	2.05	2.84
p 7 26	1393.5	-3.83	-3.69	1.67	-0.31	-7.44	1.55	1.71	5.59	1.18	16.67	1.27	5.90	-0.14	-9.03	-1.19	-0.57	-6.09	4.36	-4.92	2.14	2.84
p 7 27	1533.0	-3.84	-3.70	1.70	-0.31	-7.44	1.17	1.72	5.20	0.79	15.89	1.31	5.93	-0.14	-9.39	-1.19	-0.56	-6.27	4.12	-5.01	1.75	2.86
p 7 28	1659.0	-3.89	-3.74	1.84	-0.30	-7.52	1.21	1.77	5.25	0.84	15.99	1.39	6.04	-0.13	-9.24	-1.18	-0.51	-6.21	4.26	-5.00	1.80	2.97
p 7 29	1704.5	-3.88	-3.73	1.81	-0.30	-7.50	1.20	1.76	5.24	0.83	15.97	1.42	6.02	-0.13	-9.27	-1.18	-0.52	-6.22	4.23	-5.00	1.79	2.95
p 7 30	1802.5	-3.88	-3.73	1.81	-0.30	-7.50	1.38	1.76	5.41	1.01	16.32	1.29	6.02	-0.13	-9.10	-1.18	-0.52	-6.14	4.34	-4.95	1.97	2.95
p 7 31	1873.5	-3.83	-3.69	1.67	-0.31	-7.40	1.33	1.71	5.37	0.96	16.22	1.14	5.90	-0.14	-9.25	-1.19	-0.57	-6.19	4.21	-4.95	1.92	2.84
p 7 32	1965.0	-3.84	-3.70	1.70	-0.31	-7.41	0.86	1.72	4.90	0.49	15.29	1.07	5.93	-0.14	-9.70	-1.19	-0.56	-6.41	3.91	-5.07	1.45	2.86
p 7 33	2038.5	-3.83	-3.69	1.67	-0.31	-7.38	0.85	1.71	4.89	0.48	15.27	1.24	5.90	-0.14	-9.73	-1.19	-0.57	-6.42	3.89	-5.06	1.44	2.84
p 7 34	2212.5	-3.86	-3.72	1.86	-0.28	-7.44	1.18	1.74	5.22	0.81	15.93	1.24	6.03	-0.10	-9.33	-1.16	-0.54	-6.24	4.27	-4.99	1.77	2.93
p 7 35	2445.5	-3.83	-3.69	1.67	-0.31	-7.37	0.85	1.71	4.89	0.48	15.27	1.14	5.90	-0.14	-9.73	-1.19	-0.57	-6.42	3.89	-5.06	1.44	2.84
Outlet 6																						
p 6 8	29.5	-4.33	-4.18	1.94	-0.30	-8.42	1.45	1.87	5.48	1.08	16.46	1.31	6.23	-0.13	-8.59	-1.19	-0.41	-6.11	4.42	-5.17	2.04	3.16
p 6 9	98.0	-4.28	-4.13	1.86	-0.33	-8.31	1.62	1.88	5.65	1.25	16.80	1.26	6.19	-0.16	-8.46	-1.21	-0.41	-6.02	4.45	-5.10	2.21	3.15
p 6 10	145.5	-4.37	-4.22	2.13	-0.32	-8.49	1.58	1.98	5.61	1.21	16.72	1.41	6.43	-0.15	-8.26	-1.20	-0.30	-5.96	4.63	-5.12	2.17	3.38
p 6 11	194.0	-4.10	-3.95	1.53	-0.35	-7.95	0.96	1.73	5.00	0.59	15.48	0.96	5.87	-0.17	-9.39	-1.23	-0.55	-6.39	3.78	-5.20	1.55	2.85
p 6 12	274.0	-4.03	-3.88	1.49	-0.34	-7.82	1.07	1.70	5.10	0.70	15.70	0.99	5.82	-0.17	-9.36	-1.22	-0.59	-6.35	3.84	-5.14	1.66	2.78
p 6 13	315.0	-3.95	-3.80	1.30	-0.35	-7.66	1.41	1.63	5.45	1.04	16.39	0.91	5.64	-0.18	-9.19	-1.23	-0.66	-6.22	3.93	-5.04	2.00	2.62
p 6 14	366.0	-3.95	-3.80	1.36	-0.34	-7.66	0.86	1.64	4.89	0.48	15.27	0.99	5.69	-0.17	-9.72	-1.22	-0.65	-6.49	3.62	-5.17	1.44	2.66
p 6 15	436.5	-3.92	-3.77	1.32	-0.35	-7.61	1.12	1.63	5.16	0.75	15.81	1.00	5.66	-0.18	-9.48	-1.23	-0.65	-6.35	3.76	-5.09	1.71	2.64
p 6 16	509.0	-3.89	-3.74	1.36	-0.34	-7.55	0.94	1.62	4.97	0.57	15.44	1.09	5.67	-0.16	-9.70	-1.22	-0.66	-6.45	3.69	-5.13	1.53	2.63
p 6 17	626.5	-3.99	-3.84	1.72	-0.31	-7.75	0.91	1.74	4.94	0.53	15.37	1.31	5.97	-0.13	-9.47	-1.19	-0.54	-6.38	3.95	-5.14	1.50	2.90
p 6 18	677.0	-3.95	-3.80	1.69	-0.31	-7.67	1.27	1.73	5.30	0.89	16.09	1.28	5.94	-0.13	-9.17	-1.19	-0.56	-6.21	4.17	-5.04	1.85	2.87
p 6 19	796.5	-3.89	-3.74	1.62	-0.31	-7.55	0.83	1.69	4.86	0.46	15.22	1.23	5.86	-0.13	-9.71	-1.19	-0.60	-6.46	3.83	-5.13	1.42	2.80
p 6 20	943.0	-3.89	-3.74	1.67	-0.30	-7.55	1.18	1.70	5.22	0.81	15.93	1.29	5.90	-0.13	-9.33	-1.18	-0.58	-6.27	4.11	-5.03	1.77	2.83
p 6 21	1011.5	-3.88	-3.73	1.61	-0.31	-7.52	1.42	1.70	5.45	1.05	16.40	1.20	5.86	-0.14	-9.12	-1.20	-0.59	-6.15	4.21	-4.97	2.01	2.81
p 6 22	1035.0	-3.80	-3.65	1.37	-0.33	-7.36	1.09	1.60	5.12	0.71	15.73	1.06	5.65	-0.16	-9.64	-1.21	-0.68	-6.37	3.82	-5.04	1.68	2.60
p 6 23	1140.0	-3.81	-3.66	1.39	-0.33	-7.39	0.95	1.62	4.99	0.58	15.46	1.06	5.67	-0.16	-9.73	-1.21	-0.67	-6.43	3.73	-5.08	1.54	2.63
p 6 24	1212.5	-3.81	-3.67	1.41	-0.33	-7.39	1.11	1.62	5.14	0.73	15.77	1.06	5.69	-0.16	-9.58	-1.21	-0.66	-6.35	3.86	-5.03	1.70	2.64
p 6 25	1307.0	-3.81	-3.67	1.45	-0.32	-7.37	1.11	1.63	5.14	0.73	15.77	1.01	5.71	-0.15	-9.58	-1.20	-0.66	-6.34	3.89	-5.03	1.70	2.66
p 6 26	1397.5	-3.83	-3.68	1.41	-0.33	-7.37	0.65	1.62	4.69	0.28	14.86	1.06	5.69	-0.16	-10.03	-1.21	-0.66	-6.57	3.56	-5.14	1.24	2.64

Table 1. Continuation.

Sample	Elapsed time [hours]	Imogolite (synth.gel)	Magnesite	Mesolite	$Mg_{0.25}Fe_{0.75}$ carbonate	$Mg_{0.50}Fe_{0.50}$ carbonate	Silica (am)	Moganite	Ca-Mg-Fe clay	Ca-Fe clay	$Mg_{0.75}Fe_{0.25}$ carbonate	Gibbsite (microcr)	Stapafell_ glass	Chrysotile	Allophane	Mg-nontronite	Mg-saponite	Mg-beidellite	Mg-clay	Heulandite	Analcime
Outlet 7																					
p 7 8	29.0	2.92	-4.96	1.53	-6.82	-6.08	-1.10	-0.96	-0.83	11.99	-5.45	1.09	-1.34	-1.56	-2.10	12.05	3.07	6.40	1.25	1.72	-1.17
p 7 9	97.0	3.07	-4.89	1.39	-7.15	-6.27	-1.16	-1.03	-1.56	11.09	-5.51	1.20	-1.36	-1.41	-1.99	11.04	3.17	6.42	1.30	1.52	-1.47
p 7 10	145.0	2.98	-4.85	1.38	-7.23	-6.31	-1.17	-1.03	-1.63	11.01	-5.51	1.16	-1.38	-1.18	-2.08	10.95	3.39	6.33	1.52	1.49	-1.47
p 7 11	193.0	2.78	-4.73	1.35	-7.29	-6.31	-1.18	-1.04	-1.43	11.14	-5.45	1.06	-1.43	-0.53	-2.29	11.08	4.02	6.10	2.15	1.41	-1.50
p 7 12	273.0	2.83	-4.70	1.56	-7.39	-6.37	-1.14	-1.01	-1.53	10.98	-5.46	1.07	-1.39	-0.39	-2.22	10.87	4.23	6.24	2.36	1.82	-1.43
p 7 13	313.5	2.44	-4.53	1.48	-7.98	-6.70	-1.17	-1.04	-2.38	9.95	-5.55	0.89	-1.48	0.63	-2.62	9.82	5.20	5.79	3.33	1.63	-1.48
p 7 14	361.5	2.38	-4.48	1.47	-7.81	-6.58	-1.18	-1.04	-1.86	10.48	-5.46	0.86	-1.50	0.86	-2.69	10.35	5.43	5.71	3.55	1.60	-1.49
p 7 15	433.5	2.49	-4.51	1.49	-7.57	-6.42	-1.17	-1.03	-1.43	10.96	-5.40	0.91	-1.47	0.64	-2.57	10.84	5.23	5.85	3.35	1.66	-1.48
p 7 16	505.5	2.32	-4.40	1.53	-7.75	-6.51	-1.15	-1.02	-1.48	10.83	-5.39	0.82	-1.49	1.26	-2.73	10.71	5.87	5.72	3.99	1.75	-1.45
p 7 17	623.0	2.73	-4.58	1.63	-7.14	-6.16	-1.12	-0.99	-0.60	11.89	-5.30	1.01	-1.39	0.19	-2.30	11.80	4.86	6.22	2.99	1.98	-1.38
p 7 18	672.5	2.39	-4.41	1.55	-7.46	-6.32	-1.15	-1.02	-0.85	11.51	-5.30	0.85	-1.47	1.15	-2.66	11.40	5.77	5.80	3.89	1.79	-1.44
p 7 19	793.0	2.84	-4.51	1.88	-7.44	-6.34	-1.13	-1.00	-1.04	11.34	-5.35	1.07	-1.38	0.52	-2.20	11.14	5.21	6.34	3.32	2.25	-1.30
p 7 20	939.5	2.62	-4.42	1.84	-7.64	-6.44	-1.15	-1.01	-1.21	11.10	-5.36	0.97	-1.43	1.08	-2.42	10.88	5.75	6.08	3.85	2.13	-1.34
p 7 21	1008.0	2.56	-4.37	1.82	-7.70	-6.47	-1.15	-1.02	-1.25	11.03	-5.35	0.94	-1.44	1.30	-2.49	10.80	5.96	6.01	4.06	2.09	-1.35
p 7 22	1031.0	2.58	-4.38	1.82	-7.45	-6.30	-1.15	-1.02	-0.69	11.65	-5.27	0.95	-1.44	1.25	-2.47	11.43	5.91	6.03	4.01	2.11	-1.35
p 7 23	1136.0	2.47	-4.34	1.79	-7.92	-6.60	-1.16	-1.03	-1.64	10.57	-5.40	0.90	-1.47	1.53	-2.59	10.34	6.17	5.90	4.26	2.04	-1.37
p 7 24	1208.5	2.47	-4.34	1.79	-7.92	-6.60	-1.16	-1.03	-1.64	10.57	-5.40	0.90	-1.47	1.53	-2.59	10.34	6.17	5.90	4.26	2.04	-1.37
p 7 25	1303.0	2.47	-4.32	1.79	-7.69	-6.44	-1.16	-1.03	-1.08	11.17	-5.31	0.90	-1.47	1.57	-2.59	10.95	6.22	5.90	4.31	2.04	-1.37
p 7 26	1393.5	2.47	-4.30	1.79	-7.61	-6.38	-1.16	-1.03	-0.89	11.37	-5.27	0.90	-1.47	1.62	-2.59	11.15	6.27	5.90	4.36	2.04	-1.37
p 7 27	1533.0	2.49	-4.30	1.80	-7.88	-6.56	-1.16	-1.02	-1.56	10.60	-5.36	0.91	-1.46	1.61	-2.56	10.38	6.27	5.93	4.35	2.05	-1.36
p 7 28	1659.0	2.60	-4.33	1.83	-7.78	-6.50	-1.15	-1.01	-1.44	10.73	-5.35	0.96	-1.43	1.38	-2.45	10.52	6.05	6.07	4.14	2.12	-1.34
p 7 29	1704.5	2.58	-4.32	1.82	-7.80	-6.51	-1.15	-1.02	-1.46	10.70	-5.35	0.95	-1.44	1.43	-2.47	10.49	6.10	6.04	4.19	2.11	-1.35
p 7 30	1802.5	2.58	-4.32	1.82	-7.67	-6.42	-1.15	-1.02	-1.16	11.06	-5.30	0.95	-1.44	1.43	-2.47	10.84	6.10	6.04	4.19	2.11	-1.35
p 7 31	1873.5	2.47	-4.26	1.79	-7.77	-6.47	-1.16	-1.03	-1.24	10.93	-5.30	0.90	-1.47	1.75	-2.59	10.71	6.41	5.91	4.49	2.03	-1.37
p 7 32	1965.0	2.49	-4.27	1.80	-8.10	-6.70	-1.16	-1.02	-2.07	10.00	-5.42	0.91	-1.46	1.70	-2.56	9.78	6.36	5.94	4.44	2.05	-1.36
p 7 33	2038.5	2.47	-4.25	1.79	-8.12	-6.70	-1.16	-1.03	-2.06	9.98	-5.41	0.90	-1.47	1.79	-2.59	9.76	6.45	5.91	4.53	2.03	-1.37
p 7 34	2212.5	2.56	-4.27	1.90	-7.83	-6.52	-1.12	-0.99	-1.39	10.74	-5.33	0.93	-1.42	1.68	-2.47	10.54	6.40	6.10	4.49	2.27	-1.30
p 7 35	2445.5	2.47	-4.23	1.79	-8.12	-6.70	-1.16	-1.03	-2.05	9.98	-5.40	0.90	-1.47	1.83	-2.59	9.76	6.49	5.91	4.57	2.03	-1.37
Outlet 6																					
p 6 8	29.5	2.80	-4.78	1.54	-7.40	-6.40	-1.15	-1.02	-1.66	10.96	-5.53	1.06	-1.40	-0.65	-2.26	10.88	3.94	6.17	2.08	1.62	-1.31
p 6 9	98.0	2.78	-4.73	1.36	-7.29	-6.31	-1.18	-1.05	-1.37	11.24	-5.46	1.07	-1.43	-0.49	-2.29	11.13	4.06	6.09	2.18	1.49	-1.57
p 6 10	145.5	3.01	-4.82	1.31	-7.16	-6.25	-1.17	-1.03	-1.42	11.21	-5.47	1.17	-1.38	-1.09	-2.05	11.11	3.48	6.36	1.61	1.61	-1.68
p 6 11	194.0	2.48	-4.55	1.22	-7.94	-6.69	-1.19	-1.06	-2.45	9.91	-5.55	0.92	-1.49	0.44	-2.60	9.78	4.97	5.76	3.09	1.44	-1.78
p 6 12	274.0	2.42	-4.49	1.34	-7.91	-6.64	-1.19	-1.06	-2.17	10.16	-5.50	0.89	-1.50	0.77	-2.66	10.02	5.32	5.72	3.43	1.53	-1.67
p 6 13	315.0	2.26	-4.41	1.32	-7.76	-6.52	-1.20	-1.07	-1.54	10.82	-5.40	0.81	-1.54	1.24	-2.83	10.66	5.77	5.53	3.89	1.45	-1.68
p 6 14	366.0	2.29	-4.41	1.37	-8.16	-6.78	-1.19	-1.06	-2.49	9.74	-5.53	0.83	-1.52	1.23	-2.79	9.59	5.78	5.59	3.89	1.54	-1.65
p 6 15	436.5	2.27	-4.39	1.37	-7.97	-6.65	-1.20	-1.07	-2.00	10.26	-5.45	0.82	-1.54	1.32	-2.81	10.09	5.86	5.55	3.97	1.50	-1.66
p 6 16	509.0	2.26	-4.36	1.50	-8.13	-6.75	-1.19	-1.05	-2.24	9.96	-5.49	0.81	-1.52	1.50	-2.81	9.79	6.07	5.59	4.18	1.65	-1.53
p 6 17	626.5	2.53	-4.46	1.61	-7.98	-6.68	-1.15	-1.02	-2.24	9.99	-5.50	0.93	-1.45	0.85	-2.52	9.84	5.47	5.95	3.58	1.86	-1.45
p 6 18	677.0	2.50	-4.42	1.65	-7.75	-6.51	-1.16	-1.02	-1.56	10.72	-5.40	0.92	-1.46	1.05	-2.55	10.56	5.67	5.92	3.78	1.90	-1.42
p 6 19	796.5	2.43	-4.36	1.71	-8.14	-6.75	-1.16	-1.02	-2.28	9.87	-5.49	0.88	-1.47	1.38	-2.63	9.69	6.02	5.85	4.13	1.94	-1.38
p 6 20	943.0	2.46	-4.36	1.74	-7.85	-6.56	-1.15	-1.02	-1.61	10.60	-5.39	0.89	-1.46	1.37	-2.59	10.42	6.02	5.90	4.12	1.99	-1.36
p 6 21	1011.5	2.44	-4.35	1.70	-7.69	-6.45	-1.16	-1.03	-1.23	11.04	-5.33	0.89	-1.47	1.42	-2.62	10.84	6.05	5.84	4.15	1.91	-1.40
p 6 22	1035.0	2.23	-4.27	1.65	-8.06	-6.67	-1.18	-1.04	-1.82	10.33	-5.40	0.79	-1.52	1.93	-2.83	10.13	6.53	5.60	4.63	1.80	-1.44
p 6 23	1140.0	2.26	-4.28	1.63	-8.13	-6.72	-1.18	-1.05	-2.08	10.04	-5.43	0.81	-1.52	1.82	-2.81	9.84	6.41	5.62	4.51	1.77	-1.45
p 6 24	1212.5	2.27	-4.27	1.65	-8.02	-6.64	-1.18	-1.04	-1.78	10.37	-5.39	0.81	-1.51	1.84	-2.79	10.17	6.45	5.64	4.54	1.80	-1.43
p 6 25	1307.0	2.29	-4.26	1.69	-8.01	-6.64	-1.17	-1.04	-1.75	10.40	-5.38	0.82	-1.51	1.89	-2.77	10.20	6.51	5.68	4.61	1.86	-1.40
p 6 26	1397.5	2.28	-4.24	1.66	-8.35	-6.85	-1.18	-1.04	-2.55	9.46	-5.48	0.81	-1.51	1.94	-2.79	9.27	6.55	5.65	4.64	1.80	-1.41

Table 1. Continuation.

Sample	Elapsed time [hours]	Aragonite	Calcite	Ca-mont-morillonite	Chalcedony	Dolomite	$Fe(OH)_3$ (am)	Gibbsite	Goethite	Goethite (am)	Hematite	Illite	Kaolinite	Quartz	Siderite	SiO_2 (am)	$Al(OH)_3$ (am)	$Ca_{0.25}Mg_{0.25}Fe_{0.5}$ carbonate	Ca-Mg-Fe smectite	$Ca_{0.25}Mg_{0.5}Fe_{0.25}$ carbonate	Ferrihydrite $Fe(OH)_3$	Imogolite
Outlet 6																						
p 6 27	1537.5	-3.87	-3.73	1.60	-0.31	-7.44	0.76	1.68	4.79	0.38	15.08	1.17	5.84	-0.13	-9.82	-1.19	-0.61	-6.48	3.77	-5.11	1.35	2.77
p 6 28	1663.0	-3.80	-3.66	1.41	-0.32	-7.29	0.68	1.61	4.71	0.31	14.92	1.03	5.68	-0.15	-10.07	-1.20	-0.67	-6.57	3.58	-5.11	1.27	2.63
p 6 29	1709.0	-3.83	-3.68	1.49	-0.32	-7.34	0.71	1.64	4.74	0.34	14.98	1.04	5.75	-0.14	-9.98	-1.20	-0.65	-6.54	3.66	-5.11	1.30	2.69
p 6 30	1806.5	-3.83	-3.68	1.46	-0.32	-7.34	0.58	1.64	4.62	0.21	14.73	1.03	5.73	-0.15	-10.10	-1.20	-0.65	-6.60	3.55	-5.14	1.17	2.68
p 6 31	1877.5	-3.83	-3.68	1.46	-0.32	-7.33	0.58	1.63	4.62	0.21	14.73	0.94	5.73	-0.15	-10.10	-1.20	-0.65	-6.60	3.55	-5.13	1.17	2.67
p 6 32	1969.0	-3.83	-3.68	1.48	-0.32	-7.33	0.50	1.64	4.54	0.13	14.57	0.90	5.74	-0.15	-10.18	-1.20	-0.65	-6.64	3.50	-5.15	1.09	2.68
p 6 33	2042.5	-3.83	-3.68	1.49	-0.31	-7.32	0.71	1.64	4.74	0.34	14.98	1.06	5.74	-0.14	-9.98	-1.19	-0.65	-6.53	3.67	-5.10	1.30	2.68
p 6 34	2216.5	-3.85	-3.71	1.59	-0.31	-7.37	0.61	1.67	4.65	0.24	14.79	1.04	5.83	-0.14	-10.01	-1.19	-0.61	-6.56	3.67	-5.12	1.20	2.76
p 6 35	2448.5	-3.85	-3.70	1.60	-0.31	-7.35	1.77	1.68	5.80	1.40	17.10	1.03	5.84	-0.14	-8.85	-1.19	-0.60	-5.98	4.45	-4.83	2.36	2.78
Outlet 5																						
p 5 8	30.5	-4.32	-4.17	2.04	-0.33	-8.41	1.51	1.95	5.54	1.13	16.57	1.49	6.35	-0.15	-8.49	-1.21	-0.33	-6.06	4.52	-5.15	2.09	3.30
p 5 9	100.0	-4.14	-3.99	1.50	-0.37	-8.05	1.41	1.76	5.45	1.04	16.39	1.03	5.89	-0.20	-8.90	-1.25	-0.52	-6.17	4.05	-5.11	2.00	2.88
p 5 10	148.0	-4.04	-3.90	1.31	-0.38	-7.86	1.06	1.68	5.09	0.69	15.68	0.92	5.70	-0.21	-9.39	-1.26	-0.61	-6.37	3.67	-5.17	1.65	2.71
p 5 11	196.0	-4.02	-3.88	1.31	-0.37	-7.82	0.90	1.67	4.94	0.53	15.37	0.96	5.70	-0.20	-9.57	-1.25	-0.62	-6.45	3.58	-5.20	1.49	2.69
p 5 12	275.5	-3.95	-3.80	1.24	-0.37	-7.67	0.93	1.63	4.97	0.56	15.43	0.96	5.61	-0.20	-9.65	-1.25	-0.66	-6.45	3.56	-5.16	1.52	2.61
p 5 14	367.5	-3.91	-3.76	1.25	-0.36	-7.59	0.87	1.61	4.90	0.49	15.29	0.94	5.60	-0.18	-9.78	-1.24	-0.68	-6.50	3.54	-5.16	1.46	2.58
p 5 15	438.5	-3.85	-3.71	1.11	-0.38	-7.49	0.83	1.57	4.86	0.46	15.22	0.83	5.48	-0.20	-9.90	-1.26	-0.72	-6.53	3.39	-5.15	1.42	2.49
p 5 16	511.0	-3.86	-3.71	1.21	-0.36	-7.48	0.75	1.59	4.79	0.38	15.06	0.91	5.55	-0.19	-9.96	-1.24	-0.70	-6.56	3.44	-5.17	1.34	2.54
p 5 17	628.0	-3.88	-3.74	1.37	-0.33	-7.54	0.69	1.63	4.72	0.32	14.94	1.01	5.68	-0.16	-9.91	-1.21	-0.66	-6.55	3.54	-5.18	1.28	2.64
p 5 18	678.5	-3.85	-3.70	1.33	-0.34	-7.47	0.51	1.62	4.55	0.14	14.59	1.00	5.64	-0.17	-10.15	-1.23	-0.67	-6.65	3.38	-5.21	1.10	2.61
p 5 19	798.5	-3.89	-3.74	1.58	-0.32	-7.55	0.99	1.69	5.02	0.62	15.54	1.15	5.84	-0.14	-9.55	-1.20	-0.60	-6.37	3.90	-5.09	1.58	2.78
p 5 20	944.5	-3.86	-3.72	1.53	-0.32	-7.49	0.70	1.67	4.73	0.33	14.96	1.12	5.79	-0.15	-9.88	-1.20	-0.62	-6.52	3.67	-5.15	1.29	2.74
p 5 21	1013.0	-3.79	-3.64	1.25	-0.35	-7.33	0.81	1.58	4.84	0.44	15.18	0.90	5.56	-0.18	-9.96	-1.23	-0.71	-6.52	3.52	-5.11	1.40	2.54
p 5 22	1035.5	-3.76	-3.61	1.13	-0.35	-7.25	0.57	1.54	4.61	0.20	14.70	0.83	5.46	-0.18	-10.28	-1.24	-0.75	-6.67	3.28	-5.16	1.16	2.44
p 5 23	1140.5	-3.79	-3.64	1.18	-0.36	-7.30	0.71	1.56	4.75	0.34	14.98	0.88	5.51	-0.18	-10.08	-1.24	-0.72	-6.58	3.40	-5.12	1.30	2.49
p 5 24	1213.0	-3.79	-3.65	1.20	-0.35	-7.30	0.53	1.56	4.57	0.16	14.63	0.80	5.52	-0.18	-10.26	-1.23	-0.72	-6.66	3.30	-5.16	1.12	2.50
p 5 25	1307.5	-3.80	-3.65	1.23	-0.35	-7.28	0.60	1.57	4.64	0.23	14.76	0.86	5.54	-0.18	-10.19	-1.23	-0.72	-6.63	3.37	-5.14	1.19	2.51
p 5 26	1398.0	-3.80	-3.65	1.24	-0.35	-7.28	0.60	1.57	4.64	0.23	14.76	0.90	5.55	-0.17	-10.19	-1.23	-0.71	-6.63	3.38	-5.14	1.19	2.52
p 5 27	1539.0	-3.82	-3.67	1.31	-0.34	-7.30	0.55	1.59	4.59	0.18	14.67	0.86	5.61	-0.16	-10.19	-1.22	-0.70	-6.63	3.41	-5.14	1.14	2.57
p 5 28	1664.5	-3.80	-3.65	1.29	-0.34	-7.26	0.60	1.59	4.64	0.23	14.76	0.93	5.59	-0.17	-10.19	-1.22	-0.70	-6.62	3.42	-5.13	1.19	2.56
p 5 29	1710.0	-3.79	-3.65	1.28	-0.34	-7.25	0.60	1.58	4.64	0.23	14.76	0.85	5.58	-0.17	-10.19	-1.22	-0.70	-6.62	3.41	-5.12	1.19	2.55
p 5 30	1807.5	-3.79	-3.65	1.26	-0.35	-7.25	0.46	1.58	4.49	0.08	14.47	0.85	5.57	-0.17	-10.34	-1.23	-0.70	-6.69	3.30	-5.16	1.04	2.54
p 5 31	1878.5	-3.80	-3.65	1.25	-0.35	-7.25	0.53	1.58	4.57	0.16	14.63	0.88	5.56	-0.18	-10.26	-1.23	-0.70	-6.65	3.35	-5.14	1.12	2.54
p 5 32	1970.5	-3.79	-3.65	1.29	-0.34	-7.24	0.60	1.58	4.64	0.23	14.76	0.89	5.58	-0.17	-10.19	-1.22	-0.70	-6.62	3.42	-5.12	1.19	2.55
p 5 33	2043.5	-3.84	-3.69	1.45	-0.32	-7.33	0.28	1.64	4.32	-0.09	14.13	1.03	5.72	-0.15	-10.40	-1.21	-0.65	-6.75	3.34	-5.21	0.87	2.67
p 5 34	2217.5	-3.87	-3.72	1.58	-0.31	-7.39	0.32	1.68	4.36	-0.05	14.20	1.06	5.83	-0.14	-10.28	-1.19	-0.61	-6.70	3.46	-5.20	0.91	2.77
p 5 35	2449.5	-3.88	-3.74	1.53	-0.33	-7.41	0.97	1.69	5.00	0.60	15.50	1.10	5.81	-0.16	-9.61	-1.21	-0.60	-6.37	3.85	-5.04	1.56	2.77
Outlet 4																						
p 4 8	31.5	-4.23	-4.08	1.85	-0.36	-8.22	1.17	1.91	5.21	0.80	15.91	1.37	6.20	-0.19	-8.97	-1.24	-0.38	-6.25	4.13	-5.19	1.76	3.18
p 4 9	100.0	-4.00	-3.85	1.07	-0.42	-7.77	1.02	1.63	5.06	0.65	15.60	0.75	5.53	-0.24	-9.52	-1.30	-0.65	-6.41	3.44	-5.16	1.61	2.57
p 4 10	148.0	-3.99	-3.85	1.06	-0.41	-7.76	1.04	1.62	5.08	0.67	15.64	0.77	5.51	-0.24	-9.52	-1.29	-0.67	-6.41	3.45	-5.16	1.63	2.55
p 4 11	196.0	-3.97	-3.82	1.08	-0.40	-7.72	0.81	1.61	4.84	0.44	15.18	0.79	5.52	-0.23	-9.77	-1.28	-0.67	-6.53	3.32	-5.21	1.40	2.54
p 4 12	275.5	-3.91	-3.76	1.04	-0.39	-7.59	0.82	1.58	4.85	0.44	15.19	0.78	5.46	-0.22	-9.85	-1.28	-0.71	-6.53	3.32	-5.18	1.41	2.48
p 4 14	367.5	-3.86	-3.71	1.07	-0.38	-7.50	0.69	1.56	4.72	0.32	14.94	0.86	5.46	-0.21	-10.04	-1.26	-0.73	-6.61	3.27	-5.19	1.28	2.46
p 4 15	438.5	-3.82	-3.67	0.93	-0.40	-7.42	0.93	1.53	4.97	0.56	15.43	0.69	5.35	-0.23	-9.86	-1.28	-0.76	-6.50	3.32	-5.12	1.52	2.38
p 4 16	511.0	-3.82	-3.67	1.06	-0.38	-7.41	0.67	1.55	4.70	0.30	14.90	0.84	5.44	-0.21	-10.10	-1.26	-0.73	-6.61	3.26	-5.18	1.26	2.45
p 4 17	628.0	-3.89	-3.75	1.38	-0.34	-7.56	0.56	1.64	4.60	0.19	14.69	0.91	5.70	-0.17	-10.00	-1.22	-0.64	-6.60	3.44	-5.20	1.15	2.67
p 4 18	679.0	-3.84	-3.69	1.25	-0.36	-7.43	0.65	1.60	4.69	0.28	14.86	0.83	5.59	-0.19	-10.03	-1.24	-0.68	-6.59	3.39	-5.17	1.24	2.57
p 4 19	799.5	-3.87	-3.73	1.44	-0.33	-7.48	0.84	1.65	4.88	0.47	15.25	0.99	5.74	-0.16	-9.76	-1.21	-0.63	-6.46	3.69	-5.11	1.43	2.70

Table 1. Continuation.

Sample	Elapsed time [hours]	Imogolite (synth.gel)	Magnesite	Mesolite	$Mg_{0.25}Fe_{0.75}$ carbonate	$Mg_{0.50}Fe_{0.50}$ carbonate	Silica (am)	Moganite	Ca-Mg-Fe clay	Ca-Fe clay	$Mg_{0.75}Fe_{0.25}$ carbonate	Gibbsite (microcr)	Stapafell_ glass	Chrysotile	Allophane	Mg-nontronite	Mg-saponite	Mg-beidellite	Mg-clay	Heulandite	Analcime
Outlet 6																					
p 6 27	1537.5	2.40	-4.27	1.73	-8.20	-6.76	-1.16	-1.02	-2.29	9.74	-5.45	0.86	-1.47	1.74	-2.65	9.56	6.39	5.84	4.48	1.95	-1.36
p 6 28	1663.0	2.26	-4.19	1.71	-8.36	-6.85	-1.17	-1.04	-2.42	9.55	-5.45	0.80	-1.51	2.20	-2.81	9.35	6.83	5.66	4.91	1.86	-1.38
p 6 29	1709.0	2.32	-4.21	1.74	-8.30	-6.81	-1.16	-1.03	-2.36	9.63	-5.44	0.83	-1.50	2.05	-2.74	9.44	6.69	5.74	4.77	1.91	-1.35
p 6 30	1806.5	2.31	-4.21	1.71	-8.39	-6.87	-1.17	-1.04	-2.60	9.36	-5.47	0.82	-1.50	2.05	-2.76	9.16	6.68	5.71	4.76	1.86	-1.38
p 6 31	1877.5	2.30	-4.20	1.71	-8.39	-6.87	-1.17	-1.04	-2.59	9.36	-5.47	0.82	-1.50	2.07	-2.76	9.17	6.70	5.71	4.79	1.87	-1.38
p 6 32	1969.0	2.32	-4.20	1.72	-8.45	-6.91	-1.17	-1.04	-2.73	9.21	-5.49	0.83	-1.50	2.08	-2.75	9.01	6.71	5.72	4.80	1.88	-1.36
p 6 33	2042.5	2.32	-4.20	1.74	-8.29	-6.80	-1.16	-1.03	-2.33	9.64	-5.43	0.83	-1.49	2.10	-2.74	9.45	6.75	5.74	4.83	1.92	-1.34
p 6 34	2216.5	2.39	-4.22	1.77	-8.32	-6.83	-1.16	-1.02	-2.49	9.47	-5.45	0.86	-1.48	1.96	-2.66	9.28	6.62	5.83	4.70	1.97	-1.33
p 6 35	2448.5	2.41	-4.20	1.76	-7.45	-6.24	-1.16	-1.03	-0.42	11.78	-5.16	0.87	-1.48	1.99	-2.65	11.58	6.65	5.85	4.72	1.97	-1.36
Outlet 5																					
p 5 8	30.5	2.93	-4.79	1.59	-7.33	-6.36	-1.17	-1.04	-1.54	11.08	-5.50	1.14	-1.40	-0.76	-2.13	10.94	3.81	6.27	1.93	1.62	-1.33
p 5 9	100.0	2.51	-4.61	1.26	-7.59	-6.47	-1.22	-1.08	-1.75	10.74	-5.47	0.95	-1.51	0.17	-2.58	10.60	4.67	5.73	2.78	1.28	-1.67
p 5 10	148.0	2.34	-4.51	1.17	-7.94	-6.67	-1.23	-1.09	-2.34	10.01	-5.52	0.87	-1.54	0.66	-2.76	9.86	5.14	5.54	3.25	1.22	-1.78
p 5 11	196.0	2.33	-4.50	1.23	-8.06	-6.75	-1.22	-1.09	-2.58	9.72	-5.55	0.86	-1.54	0.76	-2.77	9.57	5.25	5.54	3.37	1.28	-1.72
p 5 12	275.5	2.24	-4.42	1.30	-8.10	-6.75	-1.22	-1.09	-2.44	9.81	-5.52	0.82	-1.55	1.14	-2.85	9.64	5.65	5.47	3.76	1.33	-1.66
p 5 14	367.5	2.21	-4.38	1.32	-8.19	-6.79	-1.21	-1.07	-2.48	9.73	-5.52	0.80	-1.55	1.40	-2.87	9.56	5.93	5.48	4.04	1.46	-1.69
p 5 15	438.5	2.12	-4.33	1.30	-8.27	-6.83	-1.23	-1.09	-2.57	9.60	-5.51	0.76	-1.58	1.64	-2.98	9.41	6.14	5.34	4.24	1.34	-1.71
p 5 16	511.0	2.17	-4.33	1.43	-8.31	-6.86	-1.21	-1.07	-2.63	9.51	-5.52	0.77	-1.56	1.65	-2.91	9.33	6.18	5.44	4.29	1.49	-1.58
p 5 17	628.0	2.27	-4.35	1.50	-8.28	-6.85	-1.18	-1.05	-2.67	9.46	-5.53	0.81	-1.52	1.46	-2.80	9.30	6.03	5.60	4.14	1.65	-1.52
p 5 18	678.5	2.25	-4.32	1.53	-8.45	-6.95	-1.19	-1.06	-2.96	9.11	-5.57	0.81	-1.53	1.64	-2.83	8.92	6.20	5.56	4.30	1.63	-1.51
p 5 19	798.5	2.41	-4.36	1.66	-8.02	-6.67	-1.16	-1.03	-2.03	10.16	-5.45	0.87	-1.48	1.38	-2.65	9.97	5.99	5.81	4.10	1.87	-1.42
p 5 20	944.5	2.37	-4.33	1.66	-8.26	-6.82	-1.17	-1.04	-2.52	9.57	-5.50	0.86	-1.49	1.53	-2.69	9.38	6.14	5.76	4.25	1.84	-1.42
p 5 21	1013.0	2.17	-4.24	1.57	-8.29	-6.81	-1.20	-1.06	-2.36	9.70	-5.46	0.77	-1.55	2.05	-2.91	9.50	6.62	5.48	4.71	1.64	-1.48
p 5 22	1035.5	2.07	-4.19	1.54	-8.52	-6.95	-1.20	-1.07	-2.78	9.21	-5.51	0.72	-1.57	2.29	-3.01	9.00	6.85	5.37	4.94	1.59	-1.50
p 5 23	1140.5	2.12	-4.21	1.52	-8.37	-6.86	-1.20	-1.07	-2.53	9.48	-5.47	0.75	-1.56	2.15	-2.96	9.28	6.70	5.42	4.79	1.57	-1.51
p 5 24	1213.0	2.13	-4.20	1.54	-8.51	-6.94	-1.20	-1.07	-2.83	9.14	-5.50	0.75	-1.56	2.18	-2.95	8.94	6.74	5.44	4.83	1.59	-1.50
p 5 25	1307.5	2.15	-4.19	1.58	-8.45	-6.90	-1.20	-1.06	-2.67	9.29	-5.48	0.76	-1.55	2.23	-2.93	9.10	6.81	5.47	4.90	1.64	-1.46
p 5 26	1398.0	2.15	-4.18	1.58	-8.45	-6.90	-1.19	-1.06	-2.65	9.30	-5.47	0.76	-1.55	2.25	-2.92	9.10	6.83	5.48	4.92	1.65	-1.46
p 5 27	1539.0	2.20	-4.18	1.62	-8.45	-6.90	-1.18	-1.05	-2.70	9.24	-5.47	0.78	-1.53	2.21	-2.87	9.05	6.81	5.56	4.90	1.72	-1.43
p 5 28	1664.5	2.19	-4.16	1.64	-8.44	-6.89	-1.19	-1.06	-2.60	9.33	-5.46	0.78	-1.54	2.32	-2.89	9.13	6.92	5.54	5.00	1.71	-1.42
p 5 29	1710.0	2.18	-4.16	1.64	-8.44	-6.89	-1.19	-1.06	-2.60	9.33	-5.45	0.77	-1.54	2.33	-2.89	9.12	6.93	5.53	5.01	1.70	-1.41
p 5 30	1807.5	2.17	-4.16	1.62	-8.55	-6.96	-1.19	-1.06	-2.88	9.02	-5.49	0.77	-1.55	2.31	-2.90	8.82	6.90	5.51	4.98	1.68	-1.42
p 5 31	1878.5	2.17	-4.15	1.61	-8.49	-6.92	-1.20	-1.06	-2.73	9.17	-5.47	0.77	-1.55	2.33	-2.91	8.97	6.92	5.50	5.00	1.66	-1.43
p 5 32	1970.5	2.18	-4.15	1.64	-8.44	-6.88	-1.19	-1.06	-2.58	9.33	-5.45	0.77	-1.54	2.36	-2.89	9.14	6.96	5.54	5.04	1.72	-1.41
p 5 33	2043.5	2.31	-4.19	1.70	-8.61	-7.01	-1.17	-1.04	-3.12	8.74	-5.53	0.83	-1.51	2.10	-2.76	8.55	6.72	5.70	4.80	1.83	-1.37
p 5 34	2217.5	2.40	-4.22	1.74	-8.53	-6.97	-1.16	-1.03	-3.03	8.86	-5.53	0.87	-1.48	1.89	-2.66	8.67	6.54	5.83	4.62	1.92	-1.35
p 5 35	2449.5	2.40	-4.23	1.65	-8.03	-6.63	-1.18	-1.05	-1.92	10.10	-5.36	0.87	-1.49	1.82	-2.67	9.91	6.44	5.78	4.52	1.80	-1.42
Outlet 4																					
p 4 8	31.5	2.81	-4.69	1.50	-7.66	-6.55	-1.21	-1.07	-2.13	10.35	-5.55	1.10	-1.45	-0.31	-2.27	10.17	4.22	6.08	2.32	1.46	-1.45
p 4 9	100.0	2.21	-4.47	1.02	-8.02	-6.71	-1.27	-1.13	-2.50	9.81	-5.52	0.82	-1.60	0.85	-2.91	9.63	5.26	5.30	3.37	0.94	-1.90
p 4 10	148.0	2.18	-4.47	1.04	-8.02	-6.71	-1.26	-1.12	-2.45	9.86	-5.52	0.80	-1.60	0.90	-2.93	9.70	5.33	5.29	3.44	0.98	-1.87
p 4 11	196.0	2.18	-4.45	1.13	-8.20	-6.82	-1.25	-1.12	-2.82	9.43	-5.57	0.80	-1.59	1.01	-2.93	9.26	5.45	5.30	3.56	1.05	-1.78
p 4 12	275.5	2.12	-4.39	1.20	-8.24	-6.83	-1.24	-1.11	-2.72	9.49	-5.54	0.77	-1.60	1.33	-2.99	9.31	5.79	5.27	3.89	1.14	-1.74
p 4 14	367.5	2.10	-4.34	1.30	-8.38	-6.91	-1.23	-1.10	-2.85	9.30	-5.56	0.75	-1.59	1.59	-3.00	9.11	6.08	5.29	4.19	1.28	-1.68
p 4 15	438.5	2.01	-4.30	1.25	-8.23	-6.79	-1.25	-1.12	-2.44	9.73	-5.48	0.72	-1.62	1.78	-3.10	9.53	6.23	5.16	4.33	1.15	-1.71
p 4 16	511.0	2.08	-4.29	1.37	-8.41	-6.91	-1.23	-1.10	-2.81	9.29	-5.53	0.74	-1.59	1.81	-3.02	9.09	6.31	5.29	4.41	1.34	-1.61
p 4 17	628.0	2.30	-4.36	1.47	-8.35	-6.89	-1.19	-1.06	-2.92	9.19	-5.56	0.83	-1.52	1.35	-2.78	9.01	5.91	5.61	4.02	1.60	-1.55
p 4 18	679.0	2.21	-4.30	1.50	-8.36	-6.88	-1.21	-1.08	-2.75	9.33	-5.52	0.79	-1.55	1.71	-2.88	9.13	6.25	5.48	4.34	1.52	-1.52
p 4 19	799.5	2.33	-4.31	1.59	-8.16	-6.75	-1.18	-1.05	-2.30	9.81	-5.46	0.84	-1.51	1.60	-2.74	9.62	6.19	5.68	4.29	1.72	-1.46

Table 1. Continuation.

Sample	Elapsed time [hours]	Aragonite	Calcite	Ca-mont-morillonite	Chalcedony	Dolomite	$Fe(OH)_3$ (am)	Gibbsite	Goethite	Goethite (am)	Hematite	Illite	Kaolinite	Quartz	Siderite	SiO_2 (am)	$Al(OH)_3$ (am)	$Ca_{0.25}Mg_{0.25}Fe_{0.5}$ carbonate	Ca-Mg-Fe smectite	$Ca_{0.25}Mg_{0.5}Fe_{0.25}$ carbonate	Ferrihydrite $Fe(OH)_3$	Imogolite
Outlet 4																						
p 4 20	944.5	-3.89	-3.74	1.42	-0.34	-7.46	0.80	1.65	4.83	0.43	15.16	0.96	5.72	-0.17	-9.80	-1.22	-0.63	-6.48	3.64	-5.11	1.39	2.69
p 4 21	1014.0	-3.78	-3.64	1.05	-0.37	-7.25	0.84	1.53	4.88	0.47	15.24	0.71	5.41	-0.20	-10.01	-1.25	-0.75	-6.53	3.38	-5.08	1.43	2.41
p 4 22	1037.0	-3.78	-3.63	1.11	-0.36	-7.23	1.51	1.54	5.54	1.13	16.57	0.78	5.45	-0.19	-9.35	-1.24	-0.75	-6.19	3.88	-4.91	2.09	2.44
p 4 23	1142.0	-3.81	-3.67	1.11	-0.37	-7.30	0.84	1.55	4.87	0.46	15.23	0.75	5.47	-0.20	-9.95	-1.25	-0.73	-6.51	3.42	-5.08	1.42	2.46
p 4 24	1214.5	-3.82	-3.67	1.14	-0.36	-7.29	0.71	1.56	4.75	0.34	14.98	0.74	5.48	-0.19	-10.08	-1.24	-0.73	-6.57	3.36	-5.11	1.30	2.47
p 4 25	1309.0	-3.81	-3.67	1.17	-0.36	-7.28	0.60	1.56	4.64	0.23	14.76	0.77	5.50	-0.19	-10.19	-1.24	-0.73	-6.63	3.32	-5.13	1.19	2.49
p 4 26	1399.5	-3.82	-3.67	1.16	-0.36	-7.28	0.60	1.56	4.64	0.23	14.76	0.77	5.50	-0.19	-10.19	-1.24	-0.72	-6.63	3.30	-5.13	1.19	2.49
p 4 27	1541.5	-3.82	-3.67	1.24	-0.35	-7.28	0.47	1.58	4.50	0.09	14.49	0.85	5.56	-0.18	-10.30	-1.23	-0.71	-6.68	3.29	-5.16	1.05	2.53
p 4 28	1666.0	-3.81	-3.66	1.21	-0.36	-7.26	0.71	1.57	4.75	0.34	14.98	0.79	5.54	-0.18	-10.08	-1.24	-0.71	-6.57	3.42	-5.10	1.30	2.52
p 4 29	1711.0	-3.80	-3.66	1.23	-0.35	-7.25	0.71	1.58	4.75	0.34	14.98	0.81	5.55	-0.18	-10.08	-1.23	-0.71	-6.57	3.44	-5.10	1.30	2.53
p 4 30	1808.5	-3.80	-3.66	1.20	-0.36	-7.26	0.46	1.57	4.49	0.08	14.47	0.61	5.53	-0.18	-10.34	-1.24	-0.71	-6.69	3.23	-5.16	1.04	2.51
p 4 31	1879.5	-3.80	-3.66	1.19	-0.36	-7.25	0.60	1.57	4.64	0.23	14.76	0.70	5.53	-0.19	-10.19	-1.24	-0.71	-6.62	3.33	-5.12	1.19	2.51
p 4 32	1972.5	-3.80	-3.65	1.22	-0.35	-7.25	0.46	1.58	4.49	0.08	14.47	0.66	5.55	-0.18	-10.34	-1.23	-0.71	-6.69	3.26	-5.16	1.04	2.53
p 4 33	2045.0	-3.80	-3.65	1.24	-0.35	-7.24	0.53	1.58	4.57	0.16	14.63	0.65	5.55	-0.18	-10.26	-1.23	-0.71	-6.65	3.32	-5.14	1.12	2.53
p 4 34	2218.5	-3.82	-3.68	1.34	-0.34	-7.29	0.79	1.61	4.82	0.41	15.13	0.87	5.64	-0.17	-9.94	-1.22	-0.67	-6.50	3.58	-5.07	1.37	2.61
p 4 35	2450.5	-3.83	-3.69	1.26	-0.36	-7.31	0.56	1.61	4.60	0.19	14.69	0.78	5.59	-0.19	-10.16	-1.24	-0.68	-6.62	3.35	-5.14	1.15	2.58
Outlet 3																						
p 3 8	32.0	-3.98	-3.83	1.12	-0.43	-7.72	0.91	1.67	4.94	0.53	15.37	0.86	5.59	-0.26	-9.65	-1.31	-0.61	-6.47	3.39	-5.18	1.50	2.64
p 3 9	100.5	-3.95	-3.80	0.72	-0.46	-7.67	0.77	1.55	4.81	0.40	15.10	0.43	5.27	-0.29	-9.89	-1.34	-0.74	-6.58	2.98	-5.22	1.36	2.36
p 3 10	148.0	-3.91	-3.76	0.66	-0.46	-7.59	0.56	1.51	4.59	0.18	14.67	0.40	5.20	-0.28	-10.19	-1.34	-0.78	-6.71	2.80	-5.27	1.14	2.28
p 3 11	195.5	-3.92	-3.77	0.80	-0.44	-7.61	0.81	1.54	4.84	0.43	15.17	0.52	5.31	-0.27	-9.88	-1.32	-0.74	-6.55	3.09	-5.20	1.40	2.37
p 3 12	275.0	-3.86	-3.72	0.80	-0.43	-7.51	0.48	1.52	4.51	0.10	14.51	0.53	5.28	-0.25	-10.27	-1.31	-0.77	-6.72	2.89	-5.26	1.06	2.34
p 3 14	368.0	-3.81	-3.67	0.80	-0.42	-7.41	0.44	1.50	4.47	0.06	14.43	0.48	5.26	-0.24	-10.40	-1.30	-0.79	-6.76	2.87	-5.25	1.03	2.30
p 3 15	438.5	-3.80	-3.66	0.70	-0.43	-7.37	0.63	1.48	4.67	0.26	14.82	0.44	5.19	-0.26	-10.22	-1.32	-0.80	-6.67	2.92	-5.19	1.22	2.25
p 3 16	511.0	-3.85	-3.70	0.97	-0.40	-7.43	0.38	1.55	4.41	0.01	14.32	0.53	5.39	-0.23	-10.37	-1.28	-0.74	-6.75	2.97	-5.25	0.97	2.42
p 3 17	629.5	-3.86	-3.71	1.05	-0.38	-7.41	0.49	1.56	4.52	0.11	14.53	0.58	5.45	-0.21	-10.24	-1.26	-0.73	-6.69	3.12	-5.20	1.07	2.45
p 3 18	678.5	-3.86	-3.71	1.07	-0.39	-7.40	0.39	1.57	4.42	0.02	14.34	0.62	5.46	-0.22	-10.34	-1.27	-0.72	-6.73	3.06	-5.22	0.98	2.48
p 3 19	800.0	-3.90	-3.75	1.30	-0.36	-7.46	0.61	1.63	4.65	0.24	14.79	0.79	5.64	-0.18	-10.01	-1.24	-0.66	-6.58	3.41	-5.16	1.20	2.63
p 3 20	944.0	-3.93	-3.78	1.41	-0.35	-7.50	1.53	1.66	5.56	1.15	16.61	0.81	5.73	-0.17	-9.03	-1.23	-0.62	-6.10	4.10	-4.92	2.12	2.70
p 3 21	1014.0	-3.82	-3.67	0.97	-0.39	-7.28	0.64	1.52	4.67	0.27	14.84	0.59	5.37	-0.22	-10.19	-1.27	-0.76	-6.63	3.17	-5.13	1.23	2.38
p 3 22	1036.5	-3.85	-3.71	1.09	-0.38	-7.35	0.73	1.57	4.77	0.36	15.02	0.66	5.47	-0.21	-10.02	-1.26	-0.72	-6.56	3.32	-5.12	1.32	2.48
p 3 23	1141.5	-3.86	-3.71	1.06	-0.38	-7.35	0.68	1.56	4.71	0.31	14.92	0.65	5.45	-0.21	-10.07	-1.26	-0.73	-6.58	3.26	-5.13	1.27	2.45
p 3 24	1214.0	-3.86	-3.71	1.07	-0.38	-7.35	0.68	1.56	4.71	0.31	14.92	0.60	5.46	-0.21	-10.07	-1.26	-0.73	-6.58	3.27	-5.13	1.27	2.46
p 3 25	1308.5	-3.85	-3.71	1.11	-0.37	-7.34	0.68	1.56	4.71	0.31	14.92	0.71	5.48	-0.20	-10.07	-1.25	-0.72	-6.58	3.31	-5.12	1.27	2.48
p 3 26	1399.0	-3.85	-3.71	1.09	-0.38	-7.34	0.62	1.57	4.66	0.25	14.80	0.68	5.47	-0.21	-10.13	-1.26	-0.72	-6.61	3.25	-5.14	1.21	2.48
p 3 27	1542.0	-3.85	-3.71	1.20	-0.36	-7.33	0.63	1.58	4.67	0.26	14.82	0.83	5.54	-0.19	-10.10	-1.24	-0.70	-6.59	3.35	-5.13	1.22	2.53
p 3 28	1665.5	-3.84	-3.69	1.17	-0.37	-7.31	0.95	1.58	4.99	0.58	15.46	–	5.52	-0.19	-9.80	-1.25	-0.71	-6.44	–	-5.04	1.54	2.51
p 3 29	1710.5	-3.84	-3.69	1.15	-0.37	-7.32	0.48	1.58	4.51	0.10	14.51	0.54	5.51	-0.20	-10.27	-1.25	-0.71	-6.68	3.19	-5.17	1.06	2.51
p 3 30	1808.0	-3.84	-3.70	1.15	-0.37	-7.32	0.48	1.57	4.51	0.10	14.51	0.62	5.51	-0.20	-10.27	-1.25	-0.71	-6.68	3.19	-5.17	1.06	2.50
p 3 31	1879.0	-3.84	-3.69	1.16	-0.37	-7.31	0.68	1.57	4.71	0.31	14.92	0.72	5.51	-0.19	-10.07	-1.25	-0.71	-6.57	3.35	-5.11	1.27	2.50
p 3 32	1972.0	-3.84	-3.69	1.16	-0.37	-7.31	0.68	1.58	4.71	0.31	14.92	0.68	5.52	-0.20	-10.07	-1.25	-0.71	-6.57	3.34	-5.11	1.27	2.51
p 3 33	2044.5	-3.84	-3.69	1.18	-0.36	-7.31	0.62	1.58	4.66	0.25	14.80	0.57	5.53	-0.19	-10.13	-1.24	-0.71	-6.60	3.32	-5.13	1.21	2.52
p 3 34	2218.0	-3.82	-3.67	1.18	-0.36	-7.27	0.61	1.57	4.65	0.24	14.78	0.82	5.52	-0.19	-10.16	-1.24	-0.71	-6.61	3.33	-5.12	1.20	2.51
p 3 35	2450.0	-3.84	-3.69	1.06	-0.39	-7.31	0.47	1.56	4.50	0.09	14.49	0.54	5.45	-0.21	-10.30	-1.27	-0.72	-6.69	3.11	-5.17	1.05	2.46
Outlet 2																						
p 2 8	32.5	-3.95	-3.81	0.57	-0.50	-7.69	0.79	1.54	4.82	0.42	15.14	0.27	5.19	-0.33	-9.83	-1.38	-0.74	-6.55	2.84	-5.21	1.38	2.31
p 2 9	101.5	-3.92	-3.77	0.29	-0.51	-7.62	0.47	1.44	4.50	0.09	14.49	-0.02	4.95	-0.34	-10.30	-1.39	-0.85	-6.77	2.41	-5.31	1.06	2.09
p 2 10	148.5	-3.88	-3.74	0.31	-0.50	-7.54	0.52	1.43	4.55	0.14	14.59	0.04	4.94	-0.33	-10.31	-1.38	-0.86	-6.75	2.48	-5.28	1.11	2.07
p 2 11	196.0	-3.91	-3.76	0.47	-0.48	-7.58	0.56	1.47	4.59	0.18	14.67	0.09	5.07	-0.31	-10.19	-1.36	-0.81	-6.70	2.63	-5.26	1.14	2.18

Table 1. Continuation.

Sample	Elapsed time [hours]	Imogolite (synth.gel)	Magnesite	Mesolite	$Mg_{0.25}Fe_{0.75}$ carbonate	$Mg_{0.50}Fe_{0.50}$ carbonate	Silica (am)	Moganite	Ca-Mg-Fe clay	Ca-Fe clay	$Mg_{0.75}Fe_{0.25}$ carbonate	Gibbsite (microcr)	Stapafell_ glass	Chrysotile	Allophane	Mg-nontronite	Mg-saponite	Mg-beidellite	Mg-clay	Heulandite	Analcime
Outlet 4																					
p 4 20	944.5	2.32	-4.28	1.56	-8.18	-6.76	-1.19	-1.05	-2.36	9.70	-5.45	0.84	-1.52	1.68	-2.75	9.52	6.27	5.66	4.36	1.67	-1.47
p 4 21	1014.0	2.04	-4.16	1.45	-8.31	-6.80	-1.22	-1.09	-2.33	9.68	-5.41	0.72	-1.59	2.35	-3.05	9.48	6.88	5.30	4.96	1.42	-1.56
p 4 22	1037.0	2.07	-4.15	1.50	-7.81	-6.47	-1.21	-1.08	-1.08	11.05	-5.24	0.73	-1.58	2.41	-3.02	10.85	6.96	5.36	5.04	1.52	-1.52
p 4 23	1142.0	2.09	-4.18	1.44	-8.27	-6.78	-1.22	-1.09	-2.33	9.67	-5.41	0.74	-1.58	2.20	-3.00	9.48	6.74	5.35	4.82	1.43	-1.56
p 4 24	1214.5	2.11	-4.18	1.48	-8.37	-6.84	-1.21	-1.08	-2.53	9.44	-5.44	0.74	-1.57	2.23	-2.98	9.25	6.77	5.38	4.86	1.48	-1.52
p 4 25	1309.0	2.12	-4.17	1.50	-8.45	-6.89	-1.21	-1.07	-2.69	9.25	-5.46	0.75	-1.57	2.27	-2.97	9.06	6.83	5.42	4.91	1.53	-1.51
p 4 26	1399.5	2.12	-4.17	1.49	-8.45	-6.89	-1.21	-1.08	-2.70	9.24	-5.46	0.75	-1.57	2.26	-2.97	9.05	6.82	5.41	4.90	1.51	-1.51
p 4 27	1541.5	2.16	-4.16	1.56	-8.53	-6.95	-1.20	-1.06	-2.88	9.02	-5.49	0.77	-1.55	2.27	-2.91	8.83	6.85	5.49	4.93	1.62	-1.47
p 4 28	1666.0	2.15	-4.16	1.55	-8.36	-6.83	-1.20	-1.07	-2.46	9.49	-5.43	0.76	-1.56	2.31	-2.93	9.29	6.88	5.46	4.96	1.58	-1.47
p 4 29	1711.0	2.16	-4.15	1.58	-8.36	-6.83	-1.20	-1.07	-2.44	9.51	-5.42	0.77	-1.55	2.32	-2.92	9.31	6.90	5.48	4.98	1.62	-1.46
p 4 30	1808.5	2.14	-4.15	1.55	-8.55	-6.96	-1.21	-1.07	-2.93	8.98	-5.49	0.76	-1.56	2.31	-2.94	8.78	6.88	5.45	4.96	1.57	-1.48
p 4 31	1879.5	2.14	-4.15	1.56	-8.44	-6.89	-1.21	-1.07	-2.66	9.27	-5.45	0.76	-1.56	2.32	-2.94	9.07	6.88	5.44	4.96	1.56	-1.46
p 4 32	1972.5	2.16	-4.14	1.58	-8.55	-6.96	-1.20	-1.07	-2.90	8.99	-5.48	0.77	-1.56	2.35	-2.92	8.79	6.92	5.47	5.00	1.61	-1.45
p 4 33	2045.0	2.16	-4.14	1.59	-8.49	-6.92	-1.20	-1.07	-2.74	9.16	-5.46	0.77	-1.55	2.36	-2.92	8.96	6.94	5.49	5.02	1.63	-1.45
p 4 34	2218.5	2.24	-4.16	1.64	-8.26	-6.77	-1.19	-1.06	-2.26	9.70	-5.40	0.80	-1.53	2.22	-2.83	9.50	6.81	5.60	4.89	1.71	-1.41
p 4 35	2450.5	2.21	-4.17	1.54	-8.43	-6.88	-1.21	-1.08	-2.74	9.19	-5.46	0.80	-1.55	2.15	-2.88	8.98	6.71	5.51	4.78	1.55	-1.50
Outlet 3																					
p 3 8	32.0	2.27	-4.45	1.19	-8.11	-6.77	-1.28	-1.14	-2.66	9.60	-5.54	0.86	-1.60	0.92	-2.85	9.38	5.33	5.35	3.42	0.97	-1.74
p 3 9	100.5	1.99	-4.42	0.81	-8.29	-6.87	-1.31	-1.18	-3.10	9.15	-5.58	0.73	-1.67	1.10	-3.16	8.96	5.43	4.95	3.53	0.58	-2.05
p 3 10	148.0	1.91	-4.38	0.87	-8.50	-7.00	-1.30	-1.17	-3.44	8.73	-5.62	0.70	-1.68	1.35	-3.23	8.55	5.69	4.89	3.80	0.62	-1.98
p 3 11	195.5	2.00	-4.39	0.96	-8.27	-6.85	-1.29	-1.16	-2.93	9.30	-5.55	0.73	-1.65	1.25	-3.13	9.12	5.62	5.03	3.73	0.76	-1.91
p 3 12	275.0	1.97	-4.34	1.06	-8.55	-7.02	-1.28	-1.14	-3.42	8.70	-5.61	0.71	-1.65	1.53	-3.16	8.51	5.93	5.03	4.03	0.89	-1.83
p 3 14	368.0	1.93	-4.29	1.16	-8.63	-7.06	-1.26	-1.13	-3.40	8.67	-5.61	0.68	-1.65	1.84	-3.19	8.48	6.27	5.03	4.37	1.01	-1.77
p 3 15	438.5	1.88	-4.26	1.09	-8.50	-6.96	-1.28	-1.15	-3.08	9.00	-5.54	0.67	-1.67	1.92	-3.25	8.80	6.31	4.94	4.41	0.87	-1.81
p 3 16	511.0	2.05	-4.28	1.24	-8.61	-7.04	-1.25	-1.12	-3.40	8.62	-5.59	0.73	-1.61	1.77	-3.06	8.43	6.24	5.20	4.33	1.15	-1.70
p 3 17	629.5	2.09	-4.25	1.31	-8.51	-6.96	-1.23	-1.10	-3.11	8.89	-5.54	0.74	-1.59	1.86	-3.01	8.72	6.36	5.30	4.46	1.27	-1.65
p 3 18	678.5	2.11	-4.24	1.33	-8.58	-7.01	-1.24	-1.10	-3.27	8.70	-5.55	0.76	-1.59	1.89	-2.99	8.51	6.38	5.31	4.47	1.26	-1.63
p 3 19	800.0	2.26	-4.27	1.46	-8.34	-6.85	-1.21	-1.07	-2.76	9.26	-5.49	0.82	-1.54	1.71	-2.82	9.08	6.26	5.55	4.35	1.50	-1.54
p 3 20	944.0	2.33	-4.27	1.50	-7.60	-6.37	-1.19	-1.06	-1.09	11.12	-5.25	0.85	-1.52	1.62	-2.74	10.95	6.19	5.66	4.28	1.58	-1.52
p 3 21	1014.0	2.02	-4.16	1.34	-8.45	-6.89	-1.24	-1.10	-2.75	9.21	-5.46	0.71	-1.61	2.29	-3.09	9.02	6.79	5.22	4.87	1.26	-1.63
p 3 22	1036.5	2.11	-4.20	1.37	-8.32	-6.82	-1.23	-1.09	-2.57	9.42	-5.44	0.75	-1.58	2.08	-2.99	9.24	6.60	5.34	4.68	1.34	-1.60
p 3 23	1141.5	2.09	-4.20	1.34	-8.36	-6.85	-1.23	-1.10	-2.68	9.30	-5.45	0.74	-1.59	2.06	-3.01	9.12	6.57	5.31	4.66	1.29	-1.61
p 3 24	1214.0	2.09	-4.19	1.36	-8.36	-6.85	-1.23	-1.09	-2.67	9.31	-5.45	0.75	-1.59	2.09	-3.00	9.13	6.60	5.33	4.68	1.31	-1.60
p 3 25	1308.5	2.11	-4.19	1.40	-8.36	-6.84	-1.22	-1.09	-2.63	9.34	-5.45	0.75	-1.58	2.11	-2.98	9.16	6.65	5.37	4.73	1.38	-1.58
p 3 26	1399.0	2.11	-4.19	1.38	-8.40	-6.87	-1.23	-1.09	-2.75	9.20	-5.46	0.76	-1.58	2.10	-2.99	9.02	6.62	5.35	4.70	1.33	-1.60
p 3 27	1542.0	2.16	-4.18	1.46	-8.38	-6.85	-1.21	-1.08	-2.65	9.29	-5.45	0.77	-1.56	2.12	-2.92	9.11	6.67	5.45	4.75	1.48	-1.53
p 3 28	1665.5	2.15	-4.17	1.48	-8.15	-6.70	-1.21	-1.08	–	9.92	-5.37	0.77	-1.57	2.17	-2.94	9.73	6.71	5.42	4.79	1.46	-1.52
p 3 29	1710.5	2.14	-4.18	1.45	-8.51	-6.94	-1.22	-1.09	-2.97	8.95	-5.49	0.77	-1.57	2.15	-2.95	8.76	6.69	5.40	4.77	1.43	-1.54
p 3 30	1808.0	2.13	-4.18	1.44	-8.51	-6.94	-1.22	-1.08	-2.97	8.95	-5.49	0.76	-1.57	2.15	-2.96	8.76	6.69	5.40	4.77	1.42	-1.55
p 3 31	1879.0	2.14	-4.17	1.45	-8.36	-6.84	-1.22	-1.08	-2.58	9.37	-5.44	0.76	-1.57	2.17	-2.95	9.18	6.71	5.41	4.79	1.45	-1.54
p 3 32	1972.0	2.15	-4.17	1.47	-8.36	-6.84	-1.22	-1.09	-2.59	9.37	-5.44	0.77	-1.57	2.16	-2.95	9.17	6.70	5.41	4.78	1.44	-1.52
p 3 33	2044.5	2.15	-4.17	1.48	-8.40	-6.86	-1.21	-1.08	-2.68	9.27	-5.45	0.76	-1.56	2.19	-2.94	9.09	6.74	5.44	4.82	1.49	-1.52
p 3 34	2218.0	2.14	-4.15	1.51	-8.42	-6.87	-1.21	-1.08	-2.65	9.26	-5.44	0.76	-1.57	2.28	-2.95	9.07	6.83	5.43	4.91	1.51	-1.50
p 3 35	2450.0	2.09	-4.17	1.37	-8.53	-6.95	-1.23	-1.10	-3.04	8.87	-5.49	0.75	-1.59	2.18	-3.01	8.68	6.69	5.31	4.76	1.30	-1.60
Outlet 2																					
p 2 8	32.5	1.94	-4.44	0.65	-8.25	-6.85	-1.35	-1.22	-3.21	9.05	-5.58	0.73	-1.71	0.90	-3.22	8.85	5.16	4.79	3.26	0.26	-2.15
p 2 9	101.5	1.72	-4.40	0.52	-8.59	-7.07	-1.36	-1.23	-3.89	8.31	-5.67	0.63	-1.77	1.21	-3.46	8.13	5.42	4.51	3.53	0.07	-2.21
p 2 10	148.5	1.70	-4.36	0.63	-8.59	-7.05	-1.35	-1.22	-3.70	8.47	-5.64	0.61	-1.76	1.47	-3.47	8.28	5.71	4.54	3.82	0.20	-2.13
p 2 11	196.0	1.82	-4.37	0.72	-8.50	-7.00	-1.33	-1.20	-3.56	8.61	-5.62	0.66	-1.72	1.33	-3.34	8.43	5.61	4.71	3.71	0.34	-2.06

Table 1. Continuation.

Sample	Elapsed time [hours]	Aragonite	Calcite	Ca-mont-morillonite	Chalcedony	Dolomite	$Fe(OH)_3$ (am)	Gibbsite	Goethite	Goethite (am)	Hematite	Illite	Kaolinite	Quartz	Siderite	SiO_2 (am)	$Al(OH)_3$ (am)	$Ca_{0.25}Mg_{0.25}Fe_{0.5}$ carbonate	Ca-Mg-Fe smectite	$Ca_{0.25}Mg_{0.5}Fe_{0.25}$ carbonate	Ferrihydrite $Fe(OH)_3$	Imogolite
Outlet 2																						
p 2 12	275.5	-3.89	-3.74	0.50	-0.47	-7.50	0.53	1.45	4.56	0.15	14.61	0.17	5.07	-0.30	-10.28	-1.35	-0.83	-6.73	2.66	-5.25	1.11	2.16
p 2 14	368.5	-3.86	-3.71	0.58	-0.45	-7.42	0.78	1.46	4.81	0.41	15.12	0.25	5.11	-0.28	-10.05	-1.33	-0.83	-6.59	2.90	-5.16	1.37	2.19
p 2 15	439.0	-3.89	-3.74	0.52	-0.47	-7.44	0.65	1.46	4.69	0.28	14.86	0.12	5.08	-0.29	-10.16	-1.35	-0.83	-6.65	2.75	-5.19	1.24	2.17
p 2 16	512.0	-3.89	-3.74	0.61	-0.45	-7.43	0.22	1.48	4.26	-0.15	14.01	0.17	5.14	-0.28	-10.59	-1.33	-0.81	-6.86	2.55	-5.29	0.81	2.22
p 2 17	630.5	-3.94	-3.80	0.91	-0.42	-7.53	0.60	1.57	4.64	0.23	14.77	0.34	5.39	-0.25	-10.04	-1.30	-0.72	-6.61	3.04	-5.19	1.19	2.44
p 2 18	679.5	-3.94	-3.80	0.92	-0.42	-7.53	0.43	1.57	4.46	0.06	14.42	0.41	5.39	-0.25	-10.21	-1.30	-0.72	-6.70	2.93	-5.23	1.02	2.44
p 2 19	800.5	-3.95	-3.80	1.07	-0.40	-7.53	0.92	1.60	4.96	0.55	15.41	0.58	5.50	-0.23	-9.68	-1.28	-0.69	-6.43	3.40	-5.10	1.51	2.53
p 2 20	945.0	-3.90	-3.75	0.89	-0.41	-7.42	0.49	1.54	4.52	0.11	14.53	0.46	5.35	-0.24	-10.24	-1.29	-0.75	-6.69	2.97	-5.20	1.07	2.39
p 2 21	1015.0	-3.88	-3.74	0.80	-0.42	-7.39	1.05	1.51	5.08	0.67	15.65	0.30	5.27	-0.25	-9.72	-1.30	-0.78	-6.42	3.27	-5.06	1.63	2.32
p 2 22	1037.0	-3.88	-3.73	0.79	-0.42	-7.38	0.60	1.51	4.64	0.23	14.76	0.28	5.26	-0.25	-10.19	-1.30	-0.78	-6.65	2.96	-5.17	1.19	2.31
p 2 23	1142.0	-3.91	-3.76	0.81	-0.43	-7.44	0.49	1.53	4.52	0.11	14.53	0.35	5.30	-0.25	-10.24	-1.31	-0.76	-6.69	2.90	-5.20	1.07	2.35
p 2 24	1214.5	-3.90	-3.75	0.87	-0.42	-7.43	0.74	1.53	4.78	0.37	15.04	0.38	5.33	-0.24	-9.99	-1.30	-0.75	-6.56	3.12	-5.13	1.33	2.38
p 2 25	1309.0	-3.90	-3.75	0.88	-0.41	-7.43	0.56	1.53	4.60	0.19	14.69	0.40	5.34	-0.24	-10.16	-1.29	-0.75	-6.65	3.01	-5.18	1.15	2.38
p 2 26	1399.5	-3.90	-3.76	0.86	-0.42	-7.43	0.63	1.53	4.67	0.26	14.82	0.29	5.33	-0.25	-10.09	-1.30	-0.75	-6.62	3.03	-5.16	1.22	2.37
p 2 27	1544.5	-3.89	-3.75	1.01	-0.39	-7.41	0.50	1.55	4.53	0.12	14.55	0.58	5.42	-0.22	-10.21	-1.27	-0.73	-6.67	3.09	-5.18	1.08	2.44
p 2 28	1666.0	-3.88	-3.73	0.85	-0.41	-7.38	0.54	1.51	4.58	0.17	14.65	0.26	5.31	-0.24	-10.22	-1.29	-0.77	-6.67	2.98	-5.18	1.13	2.34
p 2 29	1711.0	-3.87	-3.73	0.84	-0.41	-7.38	0.61	1.52	4.65	0.24	14.78	-0.02	5.30	-0.24	-10.16	-1.30	-0.77	-6.63	3.00	-5.16	1.20	2.34
p 2 30	1809.0	-3.88	-3.73	0.82	-0.42	-7.38	0.54	1.51	4.58	0.17	14.65	0.08	5.28	-0.24	-10.22	-1.30	-0.78	-6.67	2.94	-5.18	1.13	2.33
p 2 31	1879.5	-3.88	-3.73	0.81	-0.42	-7.38	0.47	1.51	4.50	0.09	14.49	0.38	5.28	-0.25	-10.30	-1.30	-0.77	-6.71	2.89	-5.20	1.05	2.33
p 2 32	1973.0	-3.88	-3.73	0.83	-0.42	-7.38	0.47	1.52	4.50	0.09	14.49	0.08	5.29	-0.24	-10.30	-1.30	-0.77	-6.71	2.90	-5.20	1.05	2.34
p 2 33	2045.5	-3.87	-3.73	0.86	-0.41	-7.38	0.47	1.52	4.50	0.09	14.49	0.29	5.31	-0.24	-10.30	-1.29	-0.77	-6.71	2.93	-5.19	1.05	2.35
p 2 34	2218.5	-3.91	-3.77	1.02	-0.40	-7.45	0.51	1.57	4.55	0.14	14.59	0.45	5.44	-0.22	-10.15	-1.28	-0.72	-6.65	3.09	-5.19	1.10	2.46
p 2 35	2450.5	-3.93	-3.79	0.87	-0.43	-7.49	0.82	1.56	4.85	0.44	15.19	0.41	5.35	-0.26	-9.85	-1.31	-0.73	-6.51	3.15	-5.12	1.40	2.41
Outlet 1																						
p 1 8	33.0	-4.20	-4.05	-0.19	-0.62	-8.09	0.76	1.44	4.79	0.39	15.08	-0.69	4.73	-0.45	-9.69	-1.50	-0.85	-6.58	2.12	-5.32	1.35	1.98
p 1 9	102.0	-4.15	-4.00	-0.48	-0.64	-7.96	0.13	1.33	4.16	-0.24	13.82	-0.86	4.47	-0.47	-10.51	-1.52	-0.96	-6.96	1.48	-5.47	0.72	1.74
p 1 10	149.5	-4.16	-4.01	-0.48	-0.64	-7.97	0.13	1.33	4.16	-0.24	13.82	-0.93	4.48	-0.47	-10.51	-1.52	-0.95	-6.96	1.47	-5.48	0.72	1.75
p 1 11	196.5	-4.23	-4.08	-0.27	-0.63	-8.12	0.21	1.41	4.24	-0.17	13.97	-0.80	4.66	-0.45	-10.27	-1.51	-0.88	-6.87	1.68	-5.47	0.80	1.91
p 1 12	276.0	-4.19	-4.04	-0.36	-0.63	-8.03	0.32	1.36	4.36	-0.05	14.21	-0.96	4.57	-0.45	-10.27	-1.51	-0.93	-6.86	1.69	-5.44	0.91	1.82
p 1 14	369.0	-4.20	-4.05	-0.21	-0.60	-8.04	0.18	1.39	4.21	-0.20	13.91	-0.86	4.67	-0.43	-10.36	-1.48	-0.90	-6.90	1.72	-5.46	0.77	1.90
p 1 15	439.5	-4.21	-4.06	-0.45	-0.64	-8.07	0.48	1.35	4.51	0.11	14.52	-0.92	4.52	-0.47	-10.06	-1.52	-0.94	-6.76	1.73	-5.40	1.07	1.79
p 1 16	512.5	-4.24	-4.10	-0.30	-0.63	-8.13	0.75	1.40	4.78	0.38	15.06	-1.07	4.64	-0.45	-9.72	-1.51	-0.89	-6.61	2.01	-5.33	1.34	1.89
p 1 17	631.0	-4.29	-4.15	-0.12	-0.62	-8.23	0.27	1.47	4.31	-0.10	14.11	-0.98	4.80	-0.45	-10.05	-1.50	-0.81	-6.80	1.82	-5.45	0.86	2.05
p 1 18	680.0	-4.26	-4.11	-0.18	-0.62	-8.17	0.55	1.44	4.58	0.17	14.65	-1.22	4.74	-0.45	-9.84	-1.50	-0.84	-6.68	1.95	-5.38	1.13	1.99
p 1 19	801.0	-4.27	-4.12	-0.04	-0.60	-8.19	0.87	1.47	4.90	0.49	15.29	-0.96	4.84	-0.43	-9.48	-1.48	-0.81	-6.50	2.30	-5.30	1.46	2.07
p 1 20	947.0	-4.31	-4.16	-0.02	-0.60	-8.24	0.46	1.48	4.49	0.09	14.48	-0.72	4.87	-0.43	-9.85	-1.48	-0.80	-6.70	2.05	-5.41	1.05	2.09
p 1 21	1015.5	-4.28	-4.13	-0.30	-0.63	-8.19	0.71	1.41	4.75	0.34	14.99	-0.97	4.65	-0.46	-9.70	-1.51	-0.88	-6.61	1.99	-5.35	1.30	1.91
p 1 22	1038.0	-4.37	-4.23	-0.01	-0.60	-8.38	0.93	1.51	4.97	0.56	15.43	-0.83	4.90	-0.43	-9.27	-1.49	-0.78	-6.44	2.35	-5.31	1.52	2.13
p 1 23	1143.0	-4.36	-4.21	-0.24	-0.65	-8.35	0.79	1.48	4.82	0.42	15.14	-1.08	4.75	-0.48	-9.46	-1.53	-0.81	-6.53	2.05	-5.35	1.38	2.03
p 1 24	1215.5	-4.36	-4.22	-0.19	-0.64	-8.35	0.71	1.49	4.75	0.34	14.98	-1.37	4.79	-0.47	-9.53	-1.52	-0.80	-6.57	2.02	-5.37	1.30	2.05
p 1 25	1310.0	-4.36	-4.22	-0.18	-0.64	-8.35	1.13	1.48	5.16	0.75	15.81	-0.93	4.79	-0.47	-9.12	-1.52	-0.80	-6.36	2.33	-5.26	1.71	2.05
p 1 26	1400.5	-4.38	-4.24	-0.27	-0.65	-8.39	0.71	1.46	4.75	0.34	14.98	-1.13	4.73	-0.48	-9.53	-1.53	-0.82	-6.58	1.96	-5.38	1.30	2.00
p 1 27	1546.5	-4.36	-4.21	-0.18	-0.61	-8.34	0.47	1.45	4.50	0.10	14.50	-0.93	4.76	-0.44	-9.82	-1.49	-0.84	-6.70	1.91	-5.43	1.06	2.00
p 1 28	1667.0	-4.33	-4.19	-0.38	-0.65	-8.30	1.11	1.41	5.14	0.74	15.78	-1.24	4.61	-0.48	-9.24	-1.53	-0.88	-6.41	2.16	-5.28	1.70	1.89
p 1 29	1712.0	-4.33	-4.18	-0.42	-0.66	-8.29	0.57	1.41	4.60	0.19	14.69	-1.33	4.60	-0.49	-9.78	-1.54	-0.88	-6.68	1.76	-5.41	1.15	1.88
p 1 30	1809.5	-4.35	-4.20	-0.49	-0.66	-8.32	0.44	1.39	4.48	0.07	14.44	-1.26	4.54	-0.49	-9.91	-1.54	-0.90	-6.75	1.62	-5.45	1.03	1.83
p 1 31	1880.0	-4.35	-4.20	-0.47	-0.66	-8.33	0.44	1.38	4.48	0.07	14.44	-1.59	4.55	-0.49	-9.91	-1.54	-0.90	-6.75	1.62	-5.45	1.03	1.83
p 1 32	1973.5	-4.34	-4.20	-0.49	-0.66	-8.32	0.44	1.38	4.48	0.07	14.44	-1.28	4.54	-0.49	-9.91	-1.54	-0.90	-6.75	1.62	-5.45	1.03	1.83
p 1 33	2046.0	-4.34	-4.20	-0.49	-0.66	-8.32	0.57	1.39	4.60	0.19	14.69	-1.13	4.54	-0.49	-9.78	-1.55	-0.90	-6.68	1.71	-5.42	1.15	1.83
p 1 34	2219.0	-4.41	-4.26	-0.32	-0.65	-8.44	0.63	1.46	4.67	0.26	14.83	-1.20	4.70	-0.48	-9.57	-1.54	-0.83	-6.61	1.87	-5.41	1.22	1.98
p 1 35	2451.0	-4.43	-4.29	-0.55	-0.70	-8.49	1.56	1.43	5.60	1.19	16.69	-1.73	4.56	-0.53	-8.64	-1.58	-0.86	-6.16	2.26	-5.20	2.15	1.88

Table 1. Continuation.

Sample	Elapsed time [hours]	Imogolite (synth.gel)	Magnesite	Mesolite	$Mg_{0.25}Fe_{0.75}$ carbonate	$Mg_{0.50}Fe_{0.50}$ carbonate	Silica (am)	Moganite	Ca-Mg-Fe clay	Ca-Fe clay	$Mg_{0.75}Fe_{0.25}$ carbonate	Gibbsite (microcr)	Stapafell_ glass	Chrysotile	Allophane	Mg-nontronite	Mg-saponite	Mg-beidellite	Mg-clay	Heulandite	Analcime
Outlet 2																					
p 2 12	275.5	1.79	-4.31	0.82	-8.55	-7.02	-1.32	-1.18	-3.49	8.62	-5.60	0.64	-1.71	1.64	-3.36	8.45	5.95	4.74	4.06	0.48	-1.98
p 2 14	368.5	1.82	-4.26	0.92	-8.37	-6.87	-1.30	-1.17	-2.90	9.20	-5.50	0.65	-1.70	1.87	-3.32	9.02	6.23	4.82	4.32	0.64	-1.91
p 2 15	439.0	1.80	-4.26	0.84	-8.45	-6.92	-1.31	-1.18	-3.18	8.88	-5.52	0.64	-1.71	1.81	-3.35	8.71	6.15	4.76	4.24	0.50	-1.95
p 2 16	512.0	1.85	-4.24	0.93	-8.76	-7.13	-1.30	-1.17	-3.86	8.09	-5.62	0.66	-1.69	1.89	-3.29	7.92	6.25	4.86	4.34	0.64	-1.89
p 2 17	630.5	2.07	-4.29	1.09	-8.36	-6.88	-1.27	-1.14	-3.09	8.96	-5.51	0.76	-1.63	1.54	-3.05	8.80	5.96	5.16	4.05	0.89	-1.77
p 2 18	679.5	2.07	-4.28	1.08	-8.49	-6.97	-1.27	-1.14	-3.39	8.61	-5.56	0.76	-1.63	1.55	-3.05	8.45	5.97	5.17	4.06	0.89	-1.78
p 2 19	800.5	2.16	-4.29	1.20	-8.09	-6.70	-1.25	-1.11	-2.40	9.69	-5.42	0.79	-1.59	1.52	-2.95	9.53	5.99	5.32	4.08	1.09	-1.71
p 2 20	945.0	2.02	-4.23	1.14	-8.50	-6.95	-1.26	-1.13	-3.19	8.77	-5.52	0.73	-1.63	1.88	-3.10	8.60	6.32	5.15	4.41	0.99	-1.75
p 2 21	1015.0	1.95	-4.21	1.09	-8.11	-6.68	-1.27	-1.14	-2.23	9.85	-5.38	0.70	-1.65	1.97	-3.17	9.69	6.40	5.05	4.48	0.90	-1.78
p 2 22	1037.0	1.94	-4.20	1.11	-8.45	-6.91	-1.27	-1.14	-3.02	8.97	-5.49	0.69	-1.65	2.03	-3.18	8.80	6.45	5.04	4.54	0.90	-1.76
p 2 23	1142.0	1.98	-4.23	1.06	-8.50	-6.95	-1.27	-1.14	-3.26	8.71	-5.52	0.71	-1.65	1.83	-3.14	8.55	6.25	5.07	4.34	0.85	-1.80
p 2 24	1214.5	2.01	-4.23	1.12	-8.31	-6.82	-1.26	-1.13	-2.76	9.27	-5.46	0.72	-1.63	1.87	-3.11	9.10	6.31	5.12	4.39	0.95	-1.76
p 2 25	1309.0	2.01	-4.23	1.13	-8.44	-6.91	-1.26	-1.13	-3.06	8.92	-5.50	0.72	-1.63	1.88	-3.11	8.75	6.32	5.13	4.40	0.96	-1.75
p 2 26	1399.5	2.00	-4.23	1.11	-8.39	-6.88	-1.27	-1.14	-2.97	9.03	-5.48	0.72	-1.64	1.86	-3.12	8.87	6.29	5.11	4.38	0.92	-1.77
p 2 27	1544.5	2.07	-4.22	1.24	-8.47	-6.93	-1.24	-1.11	-3.08	8.87	-5.50	0.74	-1.60	1.92	-3.03	8.71	6.41	5.26	4.50	1.16	-1.67
p 2 28	1666.0	1.97	-4.21	1.16	-8.48	-6.93	-1.26	-1.13	-3.08	8.90	-5.50	0.70	-1.63	2.01	-3.14	8.73	6.46	5.11	4.55	1.00	-1.72
p 2 29	1711.0	1.97	-4.20	1.16	-8.43	-6.90	-1.26	-1.13	-3.00	9.02	-5.48	0.70	-1.64	2.01	-3.15	8.84	6.45	5.09	4.53	0.96	-1.72
p 2 30	1809.0	1.96	-4.20	1.13	-8.48	-6.93	-1.26	-1.13	-3.12	8.87	-5.50	0.70	-1.64	2.01	-3.16	8.71	6.44	5.08	4.53	0.95	-1.75
p 2 31	1879.5	1.96	-4.20	1.13	-8.54	-6.97	-1.27	-1.14	-3.24	8.70	-5.52	0.70	-1.65	1.99	-3.16	8.53	6.42	5.07	4.51	0.92	-1.74
p 2 32	1973.0	1.97	-4.20	1.14	-8.54	-6.97	-1.26	-1.13	-3.25	8.72	-5.52	0.70	-1.64	2.01	-3.15	8.55	6.45	5.09	4.53	0.95	-1.74
p 2 33	2045.5	1.98	-4.20	1.18	-8.54	-6.97	-1.26	-1.13	-3.22	8.74	-5.52	0.71	-1.63	2.02	-3.14	8.57	6.47	5.11	4.55	1.00	-1.70
p 2 34	2218.5	2.10	-4.24	1.22	-8.43	-6.91	-1.24	-1.11	-3.09	8.89	-5.51	0.76	-1.60	1.77	-3.01	8.72	6.24	5.27	4.33	1.11	-1.68
p 2 35	2450.5	2.04	-4.26	1.07	-8.21	-6.77	-1.28	-1.15	-2.69	9.37	-5.44	0.75	-1.64	1.66	-3.08	9.20	6.07	5.12	4.15	0.83	-1.78
Outlet 1																					
p 1 8	33.0	1.61	-4.59	-0.30	-8.18	-6.86	-1.47	-1.34	-4.03	8.35	-5.65	0.63	-1.87	-0.06	-3.63	8.26	3.92	4.05	2.04	-1.15	-2.72
p 1 9	102.0	1.37	-4.51	-0.39	-8.77	-7.23	-1.49	-1.36	-5.19	7.01	-5.80	0.52	-1.93	0.43	-3.88	6.93	4.37	3.77	2.49	-1.32	-2.74
p 1 10	149.5	1.38	-4.52	-0.39	-8.78	-7.23	-1.49	-1.36	-5.20	7.00	-5.81	0.52	-1.93	0.41	-3.87	6.92	4.35	3.77	2.47	-1.34	-2.74
p 1 11	196.5	1.55	-4.59	-0.35	-8.61	-7.14	-1.48	-1.34	-5.06	7.20	-5.80	0.60	-1.89	-0.03	-3.70	7.13	3.93	3.98	2.06	-1.24	-2.71
p 1 12	276.0	1.45	-4.54	-0.31	-8.60	-7.12	-1.48	-1.34	-4.83	7.44	-5.76	0.55	-1.90	0.30	-3.79	7.37	4.26	3.88	2.39	-1.23	-2.67
p 1 14	369.0	1.53	-4.55	-0.23	-8.67	-7.17	-1.45	-1.32	-5.00	7.23	-5.79	0.58	-1.87	0.23	-3.70	7.17	4.24	4.03	2.37	-1.04	-2.62
p 1 15	439.5	1.42	-4.56	-0.45	-8.45	-7.02	-1.49	-1.36	-4.63	7.67	-5.72	0.54	-1.92	0.12	-3.83	7.62	4.05	3.80	2.18	-1.40	-2.76
p 1 16	512.5	1.52	-4.59	-0.37	-8.20	-6.87	-1.47	-1.34	-4.12	8.27	-5.66	0.58	-1.89	-0.03	-3.72	8.22	3.93	3.95	2.05	-1.27	-2.70
p 1 17	631.0	1.68	-4.64	-0.32	-8.46	-7.06	-1.47	-1.34	-4.95	7.35	-5.78	0.66	-1.86	-0.39	-3.56	7.30	3.58	4.13	1.71	-1.20	-2.68
p 1 18	680.0	1.62	-4.61	-0.32	-8.30	-6.94	-1.47	-1.34	-4.47	7.90	-5.71	0.63	-1.87	-0.21	-3.62	7.84	3.76	4.07	1.89	-1.21	-2.67
p 1 19	801.0	1.70	-4.62	-0.22	-8.03	-6.76	-1.45	-1.31	-3.81	8.62	-5.62	0.66	-1.84	-0.26	-3.52	8.56	3.76	4.21	1.88	-1.02	-2.60
p 1 20	947.0	1.72	-4.63	-0.26	-8.31	-6.96	-1.45	-1.31	-4.53	7.79	-5.73	0.67	-1.83	-0.37	-3.50	7.75	3.65	4.24	1.77	-1.05	-2.63
p 1 21	1015.5	1.54	-4.61	-0.41	-8.19	-6.87	-1.48	-1.34	-4.21	8.17	-5.67	0.59	-1.89	-0.20	-3.70	8.13	3.76	3.96	1.89	-1.34	-2.71
p 1 22	1038.0	1.76	-4.70	-0.35	-7.89	-6.70	-1.45	-1.32	-3.80	8.68	-5.63	0.69	-1.83	-0.75	-3.47	8.66	3.24	4.24	1.37	-1.18	-2.68
p 1 23	1143.0	1.66	-4.69	-0.52	-8.03	-6.79	-1.50	-1.36	-4.20	8.25	-5.67	0.67	-1.89	-0.73	-3.60	8.20	3.18	4.02	1.30	-1.51	-2.81
p 1 24	1215.5	1.68	-4.68	-0.48	-8.08	-6.83	-1.49	-1.36	-4.34	8.12	-5.69	0.67	-1.88	-0.71	-3.57	8.08	3.22	4.07	1.35	-1.44	-2.78
p 1 25	1310.0	1.68	-4.69	-0.48	-7.77	-6.62	-1.49	-1.35	-3.56	8.96	-5.58	0.67	-1.87	-0.71	-3.57	8.92	3.22	4.07	1.35	-1.43	-2.77
p 1 26	1400.5	1.63	-4.71	-0.59	-8.09	-6.84	-1.50	-1.37	-4.39	8.06	-5.70	0.65	-1.89	-0.79	-3.62	8.04	3.11	3.98	1.25	-1.57	-2.84
p 1 27	1546.5	1.63	-4.68	-0.45	-8.30	-6.96	-1.46	-1.33	-4.68	7.69	-5.75	0.63	-1.86	-0.58	-3.61	7.69	3.38	4.07	1.52	-1.31	-2.74
p 1 28	1667.0	1.52	-4.67	-0.43	-7.86	-6.67	-1.50	-1.36	-3.67	8.86	-5.60	0.60	-1.91	-0.51	-3.73	8.83	3.40	3.87	1.53	-1.57	-2.62
p 1 29	1712.0	1.51	-4.66	-0.54	-8.26	-6.94	-1.51	-1.37	-4.66	7.75	-5.73	0.59	-1.92	-0.51	-3.75	7.71	3.38	3.84	1.51	-1.63	-2.76
p 1 30	1809.5	1.47	-4.68	-0.65	-8.36	-7.01	-1.51	-1.38	-4.94	7.45	-5.77	0.57	-1.93	-0.57	-3.80	7.43	3.30	3.76	1.44	-1.73	-2.84
p 1 31	1880.0	1.47	-4.68	-0.64	-8.36	-7.01	-1.51	-1.37	-4.96	7.46	-5.78	0.57	-1.93	-0.56	-3.80	7.45	3.31	3.78	1.45	-1.69	-2.84
p 1 32	1973.5	1.46	-4.68	-0.66	-8.36	-7.01	-1.51	-1.38	-4.94	7.45	-5.78	0.57	-1.93	-0.57	-3.81	7.44	3.30	3.76	1.44	-1.72	-2.86
p 1 33	2046.0	1.46	-4.68	-0.66	-8.27	-6.95	-1.51	-1.38	-4.71	7.70	-5.74	0.58	-1.93	-0.58	-3.80	7.68	3.29	3.76	1.43	-1.73	-2.86
p 1 34	2219.0	1.61	-4.73	-0.60	-8.12	-6.87	-1.50	-1.37	-4.59	7.86	-5.73	0.64	-1.90	-0.95	-3.65	7.85	2.94	3.94	1.08	-1.66	-2.80
p 1 35	2451.0	1.51	-4.76	-0.86	-7.43	-6.42	-1.55	-1.42	-3.18	9.55	-5.52	0.62	-1.95	-1.12	-3.77	9.53	2.68	3.71	0.81	-2.05	-2.99

Table 2. Saturation indices of sampled fluids with respect to secondary minerals during the CO_2-charged water-basaltic glass interaction experiment at 22 °C. (am) = amorphous

Sample	Elapsed time [hours]	Aragonite	Calcite	Ca-mont-morillonite	Chalcedony	Dolomite	$Fe(OH)_3$ (am)	Gibbsite	Goethite	Goethite (am)	Hematite	Illite	Kaolinite	Quartz	Siderite	SiO_2 (am)	$Al(OH)_3$ (am)	$Ca_{0.25}Mg_{0.25}Fe_{0.5}$ carbonate	Ca-Mg-Fe smectite	$Ca_{0.25}Mg_{0.5}Fe_{0.25}$ carbonate	Ferrihydrite $Fe(OH)_3$	Imogolite
Outlet 7																						
p CO_2 7 6	323.8	-3.91	-3.76	1.85	0.39	-7.37	0.89	1.33	4.93	0.52	15.35	-2.04	6.53	0.56	-1.61	-0.49	-0.96	-2.36	3.11	-3.01	1.48	2.77
p CO_2 7 7	449.5	-3.92	-3.77	1.76	0.39	-7.41	1.06	1.29	5.10	0.69	15.69	-2.14	6.46	0.56	-1.69	-0.49	-0.99	-2.41	3.10	-3.05	1.65	2.70
p CO_2 7 8	489.8	-3.92	-3.78	1.64	0.39	-7.37	0.93	1.24	4.96	0.56	15.42	-2.26	6.36	0.56	-1.64	-0.49	-1.05	-2.37	2.96	-3.01	1.51	2.59
p CO_2 7 9	538.5	-4.13	-3.99	1.31	0.38	-7.81	0.83	1.12	4.87	0.46	15.23	-2.62	6.10	0.55	-1.81	-0.50	-1.17	-2.57	2.67	-3.22	1.42	2.34
p CO_2 7 10	613.0	-4.07	-3.92	1.41	0.39	-7.69	0.92	1.15	4.96	0.55	15.41	-2.52	6.17	0.56	-1.78	-0.50	-1.13	-2.53	2.77	-3.17	1.51	2.42
p CO_2 7 11	657.5	-4.00	-3.85	1.70	0.40	-7.55	1.06	1.25	5.10	0.69	15.69	-2.24	6.40	0.57	-1.81	-0.48	-1.04	-2.51	3.05	-3.13	1.65	2.62
p CO_2 7 12	708.5	-3.98	-3.84	1.49	0.40	-7.52	0.95	1.16	4.99	0.58	15.47	-2.46	6.23	0.57	-1.73	-0.48	-1.12	-2.46	2.84	-3.10	1.54	2.45
p CO_2 7 13	787.0	-3.85	-3.71	1.79	0.42	-7.28	0.87	1.26	4.90	0.50	15.30	-2.12	6.45	0.59	-1.56	-0.46	-1.03	-2.31	3.09	-2.97	1.45	2.66
p CO_2 7 14	875.5	-3.73	-3.59	1.77	0.45	-7.03	0.92	1.20	4.96	0.55	15.41	-2.10	6.40	0.62	-1.49	-0.43	-1.08	-2.21	3.11	-2.85	1.51	2.58
Outlet 6																						
p CO_2 6 6	324.5	-3.91	-3.76	1.74	0.37	-7.39	0.83	1.32	4.87	0.46	15.23	-2.11	6.47	0.54	-1.59	-0.51	-0.97	-2.35	2.99	-3.01	1.42	2.73
p CO_2 6 7	450.3	-3.96	-3.82	1.51	0.36	-7.48	0.94	1.23	4.98	0.57	15.44	-2.41	6.28	0.54	-1.68	-0.52	-1.06	-2.42	2.84	-3.07	1.53	2.55
p CO_2 6 8	490.5	-3.97	-3.83	1.44	0.38	-7.51	0.85	1.18	4.88	0.48	15.26	-2.48	6.21	0.55	-1.70	-0.50	-1.11	-2.44	2.76	-3.09	1.44	2.46
p CO_2 6 9	539.0	-4.15	-4.01	1.05	0.35	-7.87	0.79	1.05	4.82	0.41	15.14	-2.89	5.90	0.52	-1.81	-0.53	-1.23	-2.59	2.42	-3.25	1.38	2.18
p CO_2 6 10	613.5	-4.18	-4.04	1.07	0.34	-7.92	0.85	1.08	4.89	0.48	15.26	-2.87	5.94	0.51	-1.85	-0.54	-1.21	-2.62	2.45	-3.28	1.44	2.23
p CO_2 6 11	658.0	-3.99	-3.85	1.64	0.37	-7.55	0.94	1.28	4.97	0.57	15.44	-2.28	6.39	0.54	-1.73	-0.51	-1.01	-2.46	2.94	-3.11	1.53	2.65
p CO_2 6 12	709.3	-4.02	-3.88	1.36	0.37	-7.60	0.81	1.15	4.84	0.44	15.18	-2.59	6.14	0.55	-1.71	-0.51	-1.14	-2.47	2.67	-3.12	1.40	2.40
p CO_2 6 13	787.5	-3.95	-3.80	1.47	0.39	-7.46	0.88	1.17	4.91	0.51	15.32	-2.44	6.22	0.56	-1.65	-0.49	-1.11	-2.40	2.81	-3.06	1.47	2.46
p CO_2 6 14	876.0	-3.86	-3.72	1.61	0.42	-7.30	0.97	1.18	5.00	0.60	15.50	-2.28	6.30	0.59	-1.60	-0.46	-1.10	-2.34	2.99	-2.98	1.56	2.51
Outlet 5																						
p CO_2 5 6	325.0	-3.99	-3.85	1.41	0.32	-7.54	0.86	1.26	4.90	0.49	15.29	-2.47	6.25	0.49	-1.67	-0.56	-1.03	-2.43	2.70	-3.09	1.45	2.56
p CO_2 5 7	451.0	-3.95	-3.81	1.38	0.34	-7.47	0.93	1.21	4.97	0.56	15.42	-2.55	6.20	0.51	-1.67	-0.54	-1.07	-2.41	2.71	-3.06	1.52	2.49
p CO_2 5 8	491.0	-4.03	-3.88	1.10	0.33	-7.61	0.84	1.10	4.87	0.47	15.24	-2.86	5.97	0.50	-1.72	-0.55	-1.18	-2.47	2.45	-3.13	1.43	2.27
p CO_2 5 9	540.0	-4.20	-4.05	0.72	0.32	-7.96	0.83	0.97	4.87	0.46	15.23	-3.22	5.67	0.49	-1.88	-0.56	-1.31	-2.64	2.14	-3.30	1.42	1.98
p CO_2 5 10	614.5	-4.20	-4.05	0.82	0.31	-7.96	0.76	1.02	4.79	0.39	15.08	-3.17	5.76	0.49	-1.87	-0.57	-1.27	-2.64	2.18	-3.30	1.35	2.08
p CO_2 5 11	659.0	-4.01	-3.86	1.40	0.32	-7.58	0.98	1.25	5.01	0.61	15.52	-2.54	6.24	0.49	-1.76	-0.56	-1.04	-2.49	2.72	-3.13	1.57	2.55
p CO_2 5 13	788.0	-3.95	-3.80	1.17	0.33	-7.43	0.85	1.13	4.89	0.48	15.27	-2.73	6.02	0.50	-1.63	-0.55	-1.15	-2.39	2.53	-3.04	1.44	2.32
p CO_2 5 14	876.5	-3.89	-3.74	1.33	0.37	-7.34	1.03	1.14	5.07	0.66	15.63	-2.60	6.12	0.54	-1.69	-0.51	-1.15	-2.39	2.73	-3.02	1.62	2.37
p CO_2 5 15	971.0	-3.82	-3.67	1.36	0.37	-7.21	0.85	1.14	4.89	0.48	15.26	-2.52	6.13	0.55	-1.52	-0.51	-1.14	-2.27	2.72	-2.93	1.44	2.38
Outlet 4																						
p CO_2 4 6	326.0	-3.96	-3.82	1.06	0.27	-7.48	0.88	1.19	4.92	0.51	15.32	-2.82	6.01	0.44	-1.65	-0.61	-1.10	-2.41	2.39	-3.06	1.47	2.37
p CO_2 4 7	451.8	-4.02	-3.87	0.77	0.26	-7.59	0.98	1.07	5.02	0.61	15.52	-3.16	5.77	0.43	-1.76	-0.62	-1.21	-2.49	2.20	-3.13	1.57	2.13
p CO_2 4 8	491.8	-3.76	-3.61	1.77	0.27	-7.07	1.35	1.48	5.38	0.98	16.26	-2.08	6.58	0.44	-1.83	-0.61	-0.81	-2.40	3.11	-2.95	1.94	2.94
p CO_2 4 9	540.5	-4.46	-4.31	-0.23	0.23	-8.46	0.80	0.71	4.83	0.43	15.16	-4.26	4.98	0.40	-2.19	-0.65	-1.58	-2.92	1.28	-3.56	1.39	1.38
p CO_2 4 10	615.3	-4.21	-4.07	0.55	0.25	-7.98	0.86	1.00	4.90	0.49	15.29	-3.40	5.60	0.43	-1.91	-0.63	-1.29	-2.66	1.96	-3.31	1.45	1.97
p CO_2 4 11	661.8	-4.22	-4.07	0.54	0.23	-7.99	1.05	1.03	5.08	0.68	15.66	-3.44	5.62	0.40	-2.16	-0.65	-1.26	-2.79	1.94	-3.38	1.64	2.02
p CO_2 4 13	788.5	-4.00	-3.86	0.62	0.27	-7.55	0.79	1.00	4.83	0.42	15.15	-3.31	5.63	0.44	-1.68	-0.61	-1.29	-2.44	2.02	-3.10	1.38	1.99
p CO_2 4 14	878.0	-3.99	-3.84	0.68	0.30	-7.55	0.97	0.98	5.00	0.60	15.50	-3.27	5.65	0.47	-1.75	-0.58	-1.31	-2.47	2.14	-3.11	1.56	1.98
Outlet 3																						
p CO_2 3 6	330.5	-3.96	-3.81	0.59	0.22	-7.47	0.88	1.07	4.91	0.51	15.32	-3.32	5.66	0.39	-1.69	-0.66	-1.22	-2.42	2.00	-3.07	1.47	2.07
p CO_2 3 7	452.5	-4.06	-3.92	0.20	0.18	-7.69	0.90	0.96	4.93	0.53	15.36	-3.76	5.38	0.35	-1.77	-0.70	-1.32	-2.52	1.66	-3.17	1.49	1.83
p CO_2 3 8	492.8	-3.83	-3.69	1.05	0.17	-7.23	1.17	1.32	5.21	0.80	15.91	-2.85	6.08	0.34	-1.65	-0.71	-0.96	-2.35	2.44	-2.97	1.76	2.54
p CO_2 3 9	541.5	-4.51	-4.36	-0.96	0.14	-8.57	0.75	0.55	4.79	0.38	15.07	-5.04	4.47	0.31	-2.22	-0.75	-1.73	-2.97	0.61	-3.62	1.34	0.97
p CO_2 3 10	616.0	-4.31	-4.17	-0.30	0.14	-8.18	0.79	0.82	4.83	0.42	15.15	-4.32	5.02	0.31	-1.99	-0.74	-1.47	-2.75	1.16	-3.41	1.38	1.50
p CO_2 3 11	662.5	-4.29	-4.15	-0.24	0.12	-8.15	0.85	0.87	4.89	0.48	15.27	-4.24	5.08	0.30	-2.04	-0.76	-1.42	-2.77	1.22	-3.41	1.44	1.58
p CO_2 3 13	789.0	-4.00	-3.86	0.18	0.19	-7.60	0.73	0.94	4.77	0.36	15.03	-3.79	5.35	0.36	-1.66	-0.69	-1.35	-2.44	1.60	-3.11	1.32	1.78

Table 2. Continuation.

Sample	Elapsed time [hours]	Imogolite (synth.gel)	Magnesite	Mesolite	$Mg_{0.25}Fe_{0.75}$ carbonate	$Mg_{0.50}Fe_{0.50}$ carbonate	Silica (am)	Moganite	Ca-Mg-Fe clay	Ca-Fe clay	$Mg_{0.75}Fe_{0.25}$ carbonate	Gibbsite (microcr)	Stapafell_ glass	Chrysotile	Allophane	Mg-nontronite	Mg-saponite	Mg-beidellite	Mg-clay	Heulandite	Analcime
Outlet 7																					
p CO_2 7 6	323.8	2.40	-4.16	-5.74	-2.01	-2.60	-0.46	-0.33	-16.51	7.24	-3.31	0.51	-0.90	-23.60	-2.25	10.80	-19.37	6.11	-20.02	-2.94	-4.34
p CO_2 7 7	449.5	2.33	-4.19	-5.86	-2.08	-2.65	-0.46	-0.33	-16.77	7.54	-3.35	0.48	-0.91	-23.72	-2.31	11.12	-19.51	6.02	-20.15	-3.03	-4.42
p CO_2 7 8	489.8	2.23	-4.15	-5.97	-2.03	-2.61	-0.46	-0.33	-16.71	7.21	-3.31	0.43	-0.93	-23.63	-2.42	10.85	-19.43	5.91	-20.05	-3.14	-4.47
p CO_2 7 9	538.5	1.97	-4.38	-6.26	-2.21	-2.81	-0.47	-0.33	-16.97	6.85	-3.52	0.31	-0.98	-23.84	-2.68	10.57	-19.71	5.58	-20.31	-3.50	-4.59
p CO_2 7 10	613.0	2.05	-4.32	-6.19	-2.18	-2.77	-0.46	-0.33	-16.99	7.08	-3.48	0.34	-0.97	-23.84	-2.60	10.77	-19.69	5.68	-20.29	-3.39	-4.57
p CO_2 7 11	657.5	2.26	-4.25	-5.90	-2.19	-2.75	-0.45	-0.32	-16.84	7.53	-3.43	0.44	-0.92	-23.66	-2.38	11.15	-19.44	5.96	-20.07	-3.05	-4.42
p CO_2 7 12	708.5	2.09	-4.24	-6.13	-2.12	-2.70	-0.45	-0.32	-17.05	7.19	-3.40	0.35	-0.95	-23.87	-2.55	10.89	-19.69	5.75	-20.29	-3.28	-4.52
p CO_2 7 13	787.0	2.29	-4.13	-5.78	-1.97	-2.56	-0.43	-0.30	-16.51	7.21	-3.27	0.44	-0.90	-23.59	-2.34	10.83	-19.34	6.05	-19.96	-2.87	-4.33
p CO_2 7 14	875.5	2.21	-3.99	-5.79	-1.88	-2.46	-0.40	-0.27	-16.66	7.35	-3.16	0.39	-0.89	-23.60	-2.40	11.03	-19.32	6.03	-19.93	-2.81	-4.28
Outlet 6																					
p CO_2 6 6	324.5	2.36	-4.18	-5.85	-2.00	-2.60	-0.48	-0.35	-16.62	7.04	-3.32	0.50	-0.92	-23.74	-2.30	10.60	-19.56	6.01	-20.20	-3.12	-4.41
p CO_2 6 7	450.3	2.18	-4.21	-6.10	-2.08	-2.66	-0.48	-0.35	-16.93	7.13	-3.37	0.42	-0.96	-23.84	-2.48	10.76	-19.69	5.78	-20.32	-3.37	-4.56
p CO_2 6 8	490.5	2.09	-4.24	-6.15	-2.10	-2.69	-0.47	-0.34	-16.96	6.94	-3.39	0.37	-0.97	-23.84	-2.56	10.60	-19.70	5.71	-20.31	-3.38	-4.57
p CO_2 6 9	539.0	1.81	-4.41	-6.51	-2.23	-2.83	-0.50	-0.36	-17.20	6.59	-3.55	0.24	-1.04	-24.01	-2.86	10.34	-19.95	5.31	-20.53	-3.86	-4.74
p CO_2 6 10	613.5	1.86	-4.43	-6.52	-2.26	-2.86	-0.51	-0.37	-17.29	6.71	-3.58	0.27	-1.03	-24.09	-2.81	10.44	-20.05	5.34	-20.63	-3.89	-4.76
p CO_2 6 11	658.0	2.28	-4.25	-5.95	-2.12	-2.71	-0.48	-0.35	-16.81	7.20	-3.41	0.47	-0.94	-23.77	-2.38	10.79	-19.60	5.91	-20.24	-3.23	-4.46
p CO_2 6 12	709.3	2.03	-4.28	-6.24	-2.11	-2.71	-0.48	-0.34	-17.06	6.80	-3.42	0.34	-0.98	-23.95	-2.63	10.50	-19.83	5.62	-20.43	-3.51	-4.58
p CO_2 6 13	787.5	2.09	-4.21	-6.10	-2.05	-2.65	-0.46	-0.33	-16.87	7.03	-3.36	0.36	-0.96	-23.80	-2.55	10.70	-19.64	5.74	-20.25	-3.31	-4.51
p CO_2 6 14	876.0	2.14	-4.13	-5.93	-2.00	-2.58	-0.43	-0.30	-16.74	7.32	-3.29	0.37	-0.92	-23.67	-2.49	11.00	-19.45	5.87	-20.05	-3.06	-4.38
Outlet 5																					
p CO_2 5 6	325.0	2.19	-4.25	-6.16	-2.08	-2.68	-0.53	-0.40	-16.93	6.88	-3.39	0.44	-1.00	-23.90	-2.50	10.46	-19.82	5.68	-20.46	-3.62	-4.60
p CO_2 5 7	451.0	2.12	-4.22	-6.20	-2.07	-2.66	-0.51	-0.38	-16.98	7.03	-3.37	0.40	-0.99	-23.87	-2.56	10.64	-19.78	5.64	-20.40	-3.58	-4.62
p CO_2 5 8	491.0	1.90	-4.28	-6.49	-2.12	-2.72	-0.52	-0.38	-17.24	6.69	-3.43	0.29	-1.04	-24.03	-2.78	10.39	-19.99	5.37	-20.59	-3.88	-4.77
p CO_2 5 9	540.0	1.62	-4.46	-6.86	-2.29	-2.89	-0.53	-0.40	-17.67	6.46	-3.61	0.16	-1.10	-24.31	-3.07	10.27	-20.35	4.98	-20.91	-4.34	-4.94
p CO_2 5 10	614.5	1.71	-4.46	-6.76	-2.28	-2.88	-0.53	-0.40	-17.56	6.36	-3.60	0.21	-1.08	-24.26	-2.98	10.13	-20.29	5.09	-20.86	-4.24	-4.89
p CO_2 5 11	659.0	2.18	-4.27	-6.18	-2.15	-2.73	-0.53	-0.40	-17.13	7.10	-3.43	0.44	-1.00	-23.96	-2.51	10.68	-19.89	5.67	-20.53	-3.64	-4.61
p CO_2 5 13	788.0	1.95	-4.18	-6.36	-2.03	-2.62	-0.52	-0.39	-17.03	6.77	-3.34	0.32	-1.03	-23.85	-2.73	10.43	-19.79	5.44	-20.40	-3.80	-4.66
p CO_2 5 14	876.5	2.00	-4.15	-6.20	-2.07	-2.64	-0.48	-0.35	-17.15	7.25	-3.33	0.33	-0.99	-23.85	-2.65	10.94	-19.73	5.59	-20.33	-3.51	-4.55
p CO_2 5 15	971.0	2.01	-4.09	-6.13	-1.92	-2.52	-0.48	-0.34	-16.81	6.92	-3.24	0.33	-0.98	-23.73	-2.64	10.59	-19.60	5.62	-20.20	-3.43	-4.49
Outlet 4																					
p CO_2 4 6	326.0	2.00	-4.22	-6.47	-2.06	-2.65	-0.58	-0.45	-17.23	6.68	-3.37	0.38	-1.07	-24.06	-2.72	10.27	-20.10	5.33	-20.73	-4.14	-4.78
p CO_2 4 7	451.3	1.77	-4.27	-6.76	-2.15	-2.73	-0.59	-0.45	-17.54	6.73	-3.43	0.26	-1.12	-24.12	-2.95	10.41	-20.20	5.04	-20.81	-4.43	-4.94
p CO_2 4 8	491.3	2.57	-4.01	-5.67	-2.14	-2.64	-0.58	-0.45	-16.77	8.03	-3.26	0.66	-0.97	-23.30	-2.14	11.34	-19.20	6.04	-19.93	-3.32	-4.42
p CO_2 4 9	540.5	1.01	-4.70	-7.83	-2.58	-3.16	-0.62	-0.48	-18.84	5.79	-3.86	-0.10	-1.27	-24.92	-3.73	9.77	-21.22	4.04	-21.72	-5.63	-5.47
p CO_2 4 10	615.3	1.61	-4.46	-7.01	-2.31	-2.90	-0.60	-0.46	-17.84	6.36	-3.61	0.19	-1.15	-24.40	-3.12	10.11	-20.53	4.82	-21.12	-4.72	-5.06
p CO_2 4 11	661.8	1.65	-4.47	-7.03	-2.50	-3.03	-0.62	-0.49	-18.40	6.68	-3.68	0.22	-1.16	-24.51	-3.09	10.40	-20.68	4.80	-21.27	-4.84	-5.07
p CO_2 4 13	788.5	1.62	-4.25	-6.87	-2.09	-2.68	-0.58	-0.45	-17.55	6.30	-3.40	0.19	-1.14	-24.16	-3.09	10.04	-20.26	4.89	-20.85	-4.55	-4.95
p CO_2 4 14	878.0	1.61	-4.26	-6.83	-2.14	-2.72	-0.55	-0.42	-17.77	6.70	-3.42	0.16	-1.11	-24.28	-3.09	10.48	-20.35	4.94	-20.92	-4.42	-4.89
Outlet 3																					
p CO_2 3 6	330.5	1.70	-4.21	-6.83	-2.08	-2.66	-0.63	-0.50	-17.51	6.41	-3.37	0.25	-1.17	-24.09	-3.04	10.04	-20.25	4.86	-20.87	-4.73	-4.97
p CO_2 3 7	452.5	1.46	-4.32	-7.26	-2.17	-2.76	-0.67	-0.54	-17.94	6.20	-3.48	0.15	-1.24	-24.39	-3.31	9.89	-20.66	4.46	-21.26	-5.27	-5.24
p CO_2 3 8	492.8	2.17	-4.09	-6.36	-2.03	-2.59	-0.68	-0.55	-17.03	7.20	-3.27	0.51	-1.12	-23.74	-2.60	10.57	-19.86	5.31	-20.57	-4.37	-4.83
p CO_2 3 9	541.5	0.60	-4.77	-8.51	-2.62	-3.21	-0.71	-0.58	-19.52	5.22	-3.92	-0.26	-1.43	-25.37	-4.20	9.27	-21.89	3.30	-22.37	-6.68	-5.86
p CO_2 3 10	616.0	1.14	-4.56	-7.82	-2.40	-2.99	-0.71	-0.58	-18.69	5.65	-3.71	0.01	-1.33	-24.93	-3.66	9.47	-21.33	3.96	-21.89	-5.98	-5.53
p CO_2 3 11	662.5	1.21	-4.55	-7.74	-2.43	-3.01	-0.73	-0.59	-18.66	5.79	-3.71	0.05	-1.33	-24.83	-3.59	9.56	-21.24	4.02	-21.82	-5.95	-5.51
p CO_2 3 13	789.0	1.42	-4.29	-7.26	-2.08	-2.70	-0.66	-0.53	-17.89	5.87	-3.43	0.12	-1.24	-24.46	-3.35	9.59	-20.72	4.44	-21.30	-5.24	-5.21

Table 2. Continuation.

Sample	Elapsed time [hours]	Aragonite	Calcite	Ca-mont-morillonite	Chalcedony	Dolomite	$Fe(OH)_3$ (am)	Gibbsite	Goethite	Goethite (am)	Hematite	Illite	Kaolinite	Quartz	Siderite	SiO_2 (am)	$Al(OH)_3$ (am)	$Ca_{0.25}Mg_{0.25}Fe_{0.5}$ carbonate	Ca-Mg-Fe smectite	$Ca_{0.25}Mg_{0.5}Fe_{0.25}$ carbonate	Ferrihydrite $Fe(OH)_3$	Imogolite
Outlet 3																						
p CO_2 3 14	878.5	-3.99	-3.84	0.22	0.21	-7.55	1.03	0.93	5.06	0.66	15.62	-3.74	5.37	0.38	-1.83	-0.68	-1.36	-2.52	1.72	-3.14	1.62	1.79
p CO_2 3 15	971.5	-3.90	-3.76	0.36	0.21	-7.38	0.81	0.98	4.85	0.44	15.20	-3.56	5.48	0.38	-1.58	-0.67	-1.30	-2.35	1.78	-3.01	1.40	1.90
Outlet 2																						
p CO_2 2 6	331.0	-4.00	-3.86	-0.45	0.06	-7.57	0.85	0.87	4.88	0.48	15.26	-4.35	4.96	0.23	-1.72	-0.82	-1.41	-2.46	1.06	-3.11	1.44	1.53
p CO_2 2 7	453.0	-4.13	-3.99	-0.79	0.01	-7.85	0.84	0.80	4.87	0.46	15.24	-4.78	4.73	0.18	-1.80	-0.87	-1.48	-2.58	0.73	-3.24	1.42	1.35
p CO_2 2 8	493.5	-3.94	-3.79	0.02	0.01	-7.45	1.16	1.14	5.19	0.78	15.88	-3.93	5.40	0.18	-1.87	-0.87	-1.15	-2.51	1.47	-3.11	1.74	2.02
p CO_2 2 9	542.0	-4.54	-4.40	-1.74	-0.01	-8.65	0.87	0.45	4.91	0.50	15.31	-5.83	3.98	0.16	-2.51	-0.89	-1.83	-3.13	-0.14	-3.71	1.46	0.62
p CO_2 2 10	616.5	-4.42	-4.27	-1.40	-0.01	-8.41	0.74	0.59	4.78	0.37	15.05	-5.49	4.27	0.16	-2.12	-0.89	-1.69	-2.87	0.15	-3.53	1.33	0.90
p CO_2 2 11	663.0	-4.43	-4.29	-1.37	-0.02	-8.43	0.76	0.63	4.79	0.39	15.08	-5.40	4.30	0.15	-2.23	-0.91	-1.66	-2.93	0.15	-3.57	1.35	0.95
p CO_2 2 13	790.0	-4.05	-3.91	-0.54	0.05	-7.68	0.96	0.86	5.00	0.59	15.49	-4.53	4.90	0.22	-1.91	-0.84	-1.43	-2.59	0.97	-3.20	1.55	1.49
p CO_2 2 14	879.0	-4.16	-4.01	-0.92	0.07	-7.89	0.96	0.66	5.00	0.59	15.49	-4.92	4.57	0.25	-2.01	-0.81	-1.63	-2.69	0.67	-3.31	1.55	1.12
Outlet 1																						
p CO_2 1 6	331.5	-4.22	-4.08	-1.92	-0.24	-8.04	0.91	0.73	4.95	0.54	15.39	-5.89	4.07	-0.07	-1.98	-1.13	-1.55	-2.71	-0.39	-3.36	1.50	0.95
p CO_2 1 7	454.0	-4.29	-4.14	-1.97	-0.21	-8.17	0.85	0.66	4.89	0.48	15.27	-6.02	4.00	-0.04	-2.05	-1.09	-1.63	-2.78	-0.42	-3.42	1.44	0.83
p CO_2 1 8	495.0	-4.15	-4.01	-1.43	-0.19	-7.93	1.11	0.85	5.15	0.74	15.78	-5.43	4.42	-0.02	-2.39	-1.07	-1.44	-2.89	0.05	-3.42	1.70	1.23
p CO_2 1 9	542.5	-4.64	-4.50	-2.74	-0.21	-8.86	0.75	0.35	4.79	0.38	15.07	-6.89	3.38	-0.04	-2.60	-1.09	-1.94	-3.22	-1.16	-3.82	1.34	0.21
p CO_2 1 10	618.0	-4.53	-4.38	-2.33	-0.21	-8.63	0.83	0.51	4.87	0.46	15.23	-6.48	3.70	-0.04	-2.49	-1.09	-1.78	-3.12	-0.79	-3.71	1.42	0.54
p CO_2 1 11	668.0	-4.41	-4.27	-2.05	-0.19	-8.40	0.86	0.60	4.90	0.49	15.29	-6.20	3.92	-0.01	-2.33	-1.07	-1.69	-2.98	-0.54	-3.58	1.45	0.73
p CO_2 1 13	791.0	-4.32	-4.17	-1.96	-0.13	-8.22	0.75	0.54	4.79	0.38	15.07	-6.04	3.92	0.04	-2.06	-1.01	-1.75	-2.80	-0.40	-3.45	1.34	0.68
p CO_2 1 14	879.5	-4.27	-4.12	-1.82	-0.09	-8.13	1.00	0.53	5.04	0.63	15.57	-5.91	3.99	0.09	-2.50	-0.97	-1.75	-2.99	-0.26	-3.52	1.59	0.70
p CO_2 1 15	972.0	-4.23	-4.08	-1.77	-0.08	-8.05	0.76	0.54	4.80	0.39	15.10	-5.82	4.03	0.09	-1.99	-0.96	-1.74	-2.72	-0.20	-3.36	1.35	0.74

Sample	Elapsed time [hours]	Imogolite (synth.gel)	Magnesite	Mesolite	$Mg_{0.25}Fe_{0.75}$ carbonate	$Mg_{0.50}Fe_{0.50}$ carbonate	Silica (am)	Moganite	Ca-Mg-Fe clay	Ca-Fe clay	$Mg_{0.75}Fe_{0.25}$ carbonate	Gibbsite (microcr)	Stapafell_ glass	Chrysotile	Allophane	Mg-nontronite	Mg-saponite	Mg-beidellite	Mg-clay	Heulandite	Analcime
Outlet 3																					
p CO_2 3 14	878.5	1.42	-4.26	-7.23	-2.20	-2.76	-0.64	-0.51	-18.28	6.49	-3.44	0.12	-1.22	-24.49	-3.33	10.24	-20.73	4.48	-21.31	-5.18	-5.16
p CO_2 3 15	971.5	1.53	-4.17	-7.07	-1.99	-2.59	-0.64	-0.51	-17.77	6.15	-3.31	0.17	-1.20	-24.35	-3.22	9.85	-20.56	4.62	-21.16	-5.01	-5.07
Outlet 2																					
p CO_2 2 6	331.0	1.16	-4.27	-7.73	-2.12	-2.71	-0.79	-0.66	-18.32	5.66	-3.42	0.06	-1.39	-24.57	-3.68	9.33	-21.06	3.82	-21.67	-6.26	-5.49
p CO_2 2 7	453.0	0.98	-4.42	-8.21	-2.22	-2.83	-0.84	-0.70	-18.85	5.37	-3.55	-0.01	-1.46	-25.04	-3.89	9.09	-21.66	3.47	-22.24	-6.82	-5.84
p CO_2 2 8	493.5	1.65	-4.21	-7.33	-2.22	-2.75	-0.84	-0.70	-18.27	6.45	-3.41	0.33	-1.34	-24.40	-3.22	9.88	-20.87	4.28	-21.56	-5.95	-5.41
p CO_2 2 9	542.0	0.25	-4.80	-9.25	-2.84	-3.37	-0.86	-0.73	-20.79	4.88	-4.02	-0.36	-1.61	-25.91	-4.63	8.93	-22.72	2.52	-23.20	-7.98	-6.33
p CO_2 2 10	616.5	0.53	-4.69	-8.87	-2.52	-3.12	-0.86	-0.73	-19.84	4.81	-3.83	-0.22	-1.56	-25.63	-4.35	8.73	-22.39	2.87	-22.91	-7.60	-6.14
p CO_2 2 11	663.0	0.58	-4.70	-8.82	-2.61	-3.18	-0.87	-0.74	-19.90	4.85	-3.87	-0.19	-1.56	-25.55	-4.31	8.72	-22.31	2.89	-22.85	-7.60	-6.14
p CO_2 2 13	790.0	1.12	-4.33	-7.92	-2.28	-2.83	-0.80	-0.67	-18.89	5.80	-3.51	0.05	-1.41	-24.84	-3.73	9.50	-21.37	3.72	-21.97	-6.45	-5.64
p CO_2 2 14	879.0	0.75	-4.43	-8.35	-2.38	-2.94	-0.77	-0.64	-19.54	5.61	-3.62	-0.15	-1.45	-25.26	-4.08	9.51	-21.83	3.34	-22.36	-6.80	-5.79
Outlet 1																					
p CO_2 1 6	331.5	0.58	-4.51	-9.28	-2.38	-2.96	-1.09	-0.96	-20.37	4.61	-3.67	-0.08	-1.74	-26.02	-4.44	8.25	-23.11	2.34	-23.72	-8.91	-6.52
p CO_2 1 7	454.0	0.47	-4.58	-9.38	-2.45	-3.03	-1.06	-0.93	-20.39	4.52	-3.74	-0.15	-1.73	-25.98	-4.53	8.24	-23.04	2.29	-23.62	-8.82	-6.59
p CO_2 1 8	495.0	0.86	-4.48	-8.79	-2.68	-3.15	-1.04	-0.90	-20.51	5.36	-3.74	0.03	-1.65	-25.58	-4.12	8.92	-22.51	2.83	-23.15	-8.14	-6.30
p CO_2 1 9	542.5	-0.16	-4.92	-10.23	-2.94	-3.47	-1.06	-0.92	-21.96	3.87	-4.13	-0.47	-1.84	-26.76	-5.16	7.90	-23.96	1.53	-24.44	-9.71	-6.96
p CO_2 1 10	618.0	0.17	-4.81	-9.77	-2.83	-3.36	-1.06	-0.92	-21.37	4.27	-4.02	-0.30	-1.78	-26.37	-4.83	8.14	-23.49	1.93	-24.03	-9.25	-6.74
p CO_2 1 11	668.0	0.36	-4.69	-9.51	-2.68	-3.23	-1.03	-0.90	-21.06	4.49	-3.89	-0.22	-1.73	-26.25	-4.62	8.31	-23.31	2.21	-23.86	-8.91	-6.60
p CO_2 1 13	791.0	0.31	-4.60	-9.38	-2.46	-3.05	-0.98	-0.85	-20.46	4.40	-3.76	-0.27	-1.70	-26.01	-4.64	8.28	-22.99	2.30	-23.52	-8.57	-6.48
p CO_2 1 14	879.5	0.34	-4.56	-9.25	-2.78	-3.25	-0.94	-0.80	-21.23	5.02	-3.84	-0.28	-1.65	-25.97	-4.59	8.93	-22.87	2.44	-23.39	-8.29	-6.37
p CO_2 1 15	972.0	0.37	-4.52	-9.19	-2.38	-2.97	-0.93	-0.79	-20.36	4.59	-3.67	-0.27	-1.64	-25.94	-4.55	8.50	-22.83	2.49	-23.35	-8.22	-6.33

Table 3. Saturation indices of sampled fluids with respect to secondary minerals during the CO_2-charged water-basaltic glass interaction experiment at 50 °C. (am) = amorphous

Sample	Elapsed time [hours]	Aragonite	Calcite	Ca-mont-morillonite	Chalcedony	Dolomite	$Fe(OH)_3$ (am)	Gibbsite	Goethite	Goethite (am)	Hematite	Illite	Kaolinite	Quartz	Siderite	SiO_2 (am)	$Al(OH)_3$ (am)	$Ca_{0.25}Mg_{0.25}Fe_{0.5}$ carbonate	Ca-Mg-Fe smectite	$Ca_{0.25}Mg_{0.5}Fe_{0.25}$ carbonate	Ferrihydrite $Fe(OH)_3$	Imogolite
Outlet 7																						
p 7 16	99.7	-1.86	-1.74	3.69	0.87	-3.35	0.55	1.10	5.76	1.72	16.65	0.71	7.17	1.03	-0.35	0.10	-0.85	-0.67	6.22	-1.09	2.53	3.47
p 7 17	162.0	-2.90	-2.77	2.31	0.77	-5.26	0.06	0.74	5.27	1.23	15.66	-1.10	6.24	0.93	-0.83	0.00	-1.21	-1.38	4.69	-1.91	2.04	2.64
p 7 18	239.0	-3.17	-3.05	2.75	0.66	-5.76	-0.05	1.11	5.16	1.12	15.45	-0.77	6.77	0.82	-0.99	-0.11	-0.84	-1.59	4.81	-2.13	1.94	3.28
p 7 19	362.5	-4.01	-3.88	1.25	0.39	-7.40	-0.60	0.95	4.61	0.56	14.34	-2.64	5.91	0.55	-1.70	-0.38	-1.00	-2.35	2.92	-2.92	1.38	2.69
p 7 20	403.8	-3.79	-3.66	1.64	0.37	-6.97	-0.37	1.13	4.84	0.80	14.81	-2.15	6.22	0.53	-1.42	-0.40	-0.82	-2.11	3.41	-2.69	1.62	3.02
p 7 21	505.5	-3.48	-3.35	2.27	0.37	-6.36	-0.54	1.40	4.67	0.63	14.47	-1.47	6.77	0.53	-1.09	-0.40	-0.55	-1.79	3.78	-2.38	1.45	3.56
p 7 22	574.0	-3.65	-3.53	1.76	0.34	-6.70	-0.94	1.25	4.27	0.22	13.66	-2.07	6.40	0.50	-1.19	-0.43	-0.70	-1.92	3.13	-2.53	1.04	3.23
p 7 23	669.8	-3.82	-3.69	1.26	0.29	-7.04	-0.50	1.12	4.71	0.66	14.54	-2.62	6.04	0.45	-1.41	-0.49	-0.83	-2.12	2.86	-2.71	1.48	2.92
p 7 24	739.3	-3.72	-3.59	1.46	0.27	-6.83	-0.55	1.23	4.66	0.62	14.44	-2.38	6.22	0.43	-1.30	-0.50	-0.72	-2.01	3.00	-2.61	1.43	3.12
p 7 25	838.3	-3.79	-3.66	1.31	0.25	-6.96	-0.42	1.21	4.79	0.75	14.71	-2.55	6.13	0.40	-1.42	-0.53	-0.75	-2.10	2.89	-2.69	1.56	3.05
p 7 26	906.0	-3.79	-3.66	1.20	0.22	-6.95	-0.56	1.20	4.65	0.61	14.43	-2.68	6.07	0.38	-1.40	-0.55	-0.75	-2.09	2.71	-2.67	1.43	3.01
Outlet 6																						
p 6 16	100.5	-1.97	-1.84	3.82	0.85	-3.49	0.33	1.21	5.54	1.50	16.21	0.73	7.34	1.01	-0.11	0.08	-0.74	-0.58	6.21	-1.08	2.32	3.66
p 6 17	163.0	-3.08	-2.95	2.04	0.73	-5.61	-0.07	0.70	5.14	1.10	15.40	-1.45	6.08	0.89	-0.95	-0.04	-1.25	-1.53	4.36	-2.07	1.91	2.52
p 6 18	240.0	-3.50	-3.37	1.59	0.61	-6.40	-0.17	0.72	5.03	0.99	15.19	-2.01	5.86	0.77	-1.35	-0.17	-1.24	-1.92	3.79	-2.46	1.81	2.43
p 6 19	363.0	-3.97	-3.84	0.57	0.33	-7.35	-0.48	0.75	4.73	0.69	14.59	-3.30	5.38	0.49	-1.64	-0.44	-1.20	-2.31	2.47	-2.89	1.51	2.22
p 6 20	404.5	-3.54	-3.41	2.16	0.36	-6.48	-0.32	1.36	4.89	0.85	14.91	-1.59	6.67	0.52	-1.08	-0.41	-0.59	-1.81	3.81	-2.43	1.67	3.48
p 6 21	506.0	-3.53	-3.41	1.78	0.31	-6.46	-0.55	1.29	4.66	0.62	14.45	-1.97	6.42	0.47	-1.14	-0.47	-0.66	-1.84	3.34	-2.43	1.44	3.28
p 6 22	574.8	-3.57	-3.44	1.81	0.29	-6.53	-0.97	1.35	4.24	0.20	13.61	-1.97	6.49	0.45	-1.12	-0.48	-0.61	-1.85	3.12	-2.45	1.02	3.37
p 6 23	670.3	-3.84	-3.71	0.97	0.23	-7.07	-0.56	1.09	4.66	0.61	14.44	-2.90	5.86	0.39	-1.44	-0.54	-0.86	-2.14	2.56	-2.73	1.43	2.80
p 6 24	739.8	-3.71	-3.59	1.44	0.21	-6.81	-0.33	1.31	4.89	0.84	14.90	-2.40	6.27	0.37	-1.35	-0.56	-0.64	-2.03	3.01	-2.61	1.66	3.22
p 6 25	839.0	-3.75	-3.62	1.30	0.19	-6.88	-0.39	1.29	4.82	0.78	14.77	-2.52	6.18	0.35	-1.39	-0.58	-0.66	-2.07	2.85	-2.65	1.60	3.16
p 6 26	906.6	-3.81	-3.68	1.15	0.18	-6.98	-0.42	1.25	4.79	0.75	14.71	-2.72	6.08	0.34	-1.44	-0.59	-0.70	-2.12	2.69	-2.70	1.57	3.07
Outlet 5																						
p 5 16	101.2	-2.36	-2.23	3.86	0.80	-4.18	0.36	1.34	5.57	1.53	16.27	0.61	7.48	0.95	-0.33	0.02	-0.62	-0.86	6.13	-1.38	2.35	3.86
p 5 17	163.7	-3.21	-3.08	2.09	0.67	-5.81	-0.12	0.82	5.09	1.05	15.30	-1.46	6.20	0.83	-0.98	-0.10	-1.13	-1.59	4.29	-2.15	1.86	2.70
p 5 18	241.0	-3.54	-3.42	1.38	0.54	-6.48	-0.26	0.74	4.95	0.91	15.02	-2.25	5.77	0.69	-1.36	-0.24	-1.21	-1.95	3.51	-2.49	1.72	2.41
p 5 19	363.7	-3.93	-3.80	0.52	0.24	-7.25	-0.42	0.87	4.79	0.75	14.70	-3.30	5.43	0.40	-1.55	-0.53	-1.09	-2.24	2.38	-2.83	1.56	2.36
p 5 20	405.8	-3.51	-3.38	2.10	0.27	-6.41	-0.42	1.49	4.79	0.75	14.70	-1.69	6.73	0.43	-1.14	-0.50	-0.47	-1.82	3.61	-2.41	1.56	3.63
p 5 21	506.5	-3.47	-3.34	1.79	0.22	-6.34	-0.45	1.43	4.76	0.72	14.65	-1.94	6.52	0.38	-1.08	-0.55	-0.53	-1.78	3.33	-2.37	1.53	3.47
p 5 22	575.3	-3.55	-3.42	1.70	0.21	-6.49	-0.98	1.43	4.23	0.19	13.59	-2.09	6.49	0.36	-1.12	-0.57	-0.52	-1.83	2.95	-2.43	1.01	3.46
p 5 23	671.0	-3.77	-3.64	1.10	0.15	-6.91	-0.35	1.27	4.86	0.82	14.85	-2.73	6.05	0.31	-1.43	-0.63	-0.68	-2.10	2.67	-2.67	1.63	3.08
p 5 24	740.3	-3.73	-3.61	1.41	0.13	-6.84	-0.49	1.42	4.72	0.68	14.57	-2.41	6.34	0.29	-1.33	-0.64	-0.53	-2.03	2.85	-2.62	1.50	3.37
p 5 25	839.5	-3.76	-3.63	1.32	0.12	-6.90	-0.55	1.41	4.66	0.62	14.45	-2.52	6.27	0.28	-1.37	-0.65	-0.55	-2.06	2.73	-2.65	1.44	3.32
p 5 26	907.2	-3.67	-3.55	1.60	0.11	-6.71	-0.57	1.54	4.64	0.60	14.41	-2.23	6.52	0.27	-1.25	-0.66	-0.41	-1.95	2.92	-2.55	1.41	3.58
Outlet 4																						
p 4 16	101.7	-2.64	-2.51	3.71	0.69	-4.67	0.17	1.46	5.38	1.34	15.88	0.34	7.51	0.84	-0.48	-0.09	-0.49	-1.06	5.76	-1.60	2.15	4.00
p 4 17	164.5	-3.02	-2.90	2.59	0.60	-5.45	-0.14	1.16	5.07	1.03	15.27	-1.02	6.73	0.75	-0.74	-0.18	-0.80	-1.38	4.55	-1.95	1.84	3.30
p 4 18	259.0	-2.59	-2.46	3.74	0.54	-4.56	-0.02	1.72	5.20	1.16	15.52	0.25	7.76	0.70	-0.35	-0.23	-0.23	-0.97	5.41	-1.52	1.97	4.38
p 4 19	364.5	-3.97	-3.84	0.56	0.09	-7.33	-0.56	1.12	4.65	0.61	14.43	-3.30	5.65	0.25	-1.56	-0.68	-0.83	-2.26	2.18	-2.86	1.43	2.73
p 4 20	406.3	-3.53	-3.41	2.12	0.12	-6.45	-0.46	1.73	4.75	0.71	14.63	-1.70	6.92	0.28	-1.16	-0.65	-0.23	-1.84	3.44	-2.43	1.53	3.96
p 4 21	507.0	-3.60	-3.47	1.60	0.09	-6.60	-0.58	1.57	4.63	0.59	14.39	-2.22	6.53	0.25	-1.20	-0.68	-0.39	-1.90	2.95	-2.50	1.41	3.61
p 4 22	576.0	-3.55	-3.43	1.85	0.09	-6.51	-0.93	1.68	4.28	0.24	13.68	-1.99	6.75	0.25	-1.13	-0.69	-0.27	-1.84	2.94	-2.45	1.05	3.84
p 4 23	671.5	-3.76	-3.63	1.51	0.06	-6.90	-0.26	1.59	4.95	0.91	15.03	-2.27	6.51	0.22	-1.42	-0.71	-0.37	-2.09	2.92	-2.67	1.73	3.62
p 4 24	741.0	-3.82	-3.70	1.47	0.05	-7.02	-0.28	1.59	4.93	0.89	14.98	-2.44	6.50	0.21	-1.49	-0.72	-0.36	-2.15	2.84	-2.73	1.70	3.62

Table 3. Continuation.

Sample	Elapsed time [hours]	Imogolite (synth.gel)	Magnesite	Mesolite	$Mg_{0.25}Fe_{0.75}$ carbonate	$Mg_{0.50}Fe_{0.50}$ carbonate	Silica (am)	Moganite	Ca-Mg-Fe clay	Ca-Fe clay	$Mg_{0.75}Fe_{0.25}$ carbonate	Gibbsite (microcr)	Stapafell_ glass	Chrysotile	Allophane	Mg-nontronite	Mg-saponite	Mg-beidellite	Mg-clay	Heulandite	Analcime
Outlet 7																					
p 7 16	99.7	3.05	-2.06	-1.59	-0.53	-0.90	0.13	0.30	-7.73	11.80	-1.39	0.47	-0.38	-14.94	-1.00	14.50	-9.38	7.98	-10.21	3.20	-1.94
p 7 17	162.0	2.22	-2.94	-3.54	-1.11	-1.58	0.02	0.19	-10.30	9.70	-2.16	0.11	-0.62	-17.39	-1.89	12.89	-12.25	6.62	-12.94	0.83	-2.95
p 7 18	239.0	2.86	-3.16	-3.25	-1.29	-1.77	-0.08	0.09	-10.55	9.46	-2.38	0.48	-0.59	-17.96	-1.32	12.38	-12.90	7.08	-13.69	0.66	-2.84
p 7 19	362.5	2.27	-3.97	-5.26	-2.02	-2.53	-0.35	-0.18	-14.06	6.97	-3.16	0.32	-0.92	-20.87	-2.07	10.10	-16.44	5.58	-17.17	-2.36	-4.04
p 7 20	403.8	2.61	-3.76	-4.72	-1.76	-2.29	-0.38	-0.21	-12.80	7.71	-2.93	0.50	-0.88	-20.01	-1.75	10.59	-15.51	5.97	-16.31	-1.85	-3.84
p 7 21	505.5	3.15	-3.45	-4.14	-1.43	-1.97	-0.37	-0.21	-12.60	7.63	-2.62	0.77	-0.78	-20.12	-1.20	10.35	-15.54	6.60	-16.40	-1.34	-3.49
p 7 22	574.0	2.81	-3.62	-4.78	-1.55	-2.10	-0.41	-0.24	-13.51	6.45	-2.77	0.62	-0.87	-20.89	-1.56	9.33	-16.44	6.09	-17.25	-2.10	-3.81
p 7 23	669.8	2.50	-3.79	-5.29	-1.76	-2.30	-0.46	-0.29	-14.22	7.00	-2.95	0.49	-0.96	-21.26	-1.90	9.96	-16.96	5.58	-17.74	-2.81	-4.10
p 7 24	739.3	2.70	-3.68	-5.04	-1.65	-2.19	-0.47	-0.30	-13.87	7.00	-2.84	0.60	-0.94	-21.04	-1.71	9.86	-16.71	5.79	-17.53	-2.63	-3.99
p 7 25	838.3	2.63	-3.75	-5.21	-1.76	-2.28	-0.50	-0.33	-14.23	7.14	-2.92	0.58	-0.98	-21.24	-1.79	10.01	-16.98	5.64	-17.79	-2.91	-4.09
p 7 26	906.0	2.59	-3.73	-5.35	-1.73	-2.26	-0.52	-0.35	-14.44	6.77	-2.90	0.57	-1.00	-21.42	-1.84	9.64	-17.20	5.53	-18.01	-3.13	-4.17
Outlet 6																					
p 6 16	100.5	3.24	-2.09	-1.63	-0.36	-0.80	0.11	0.27	-7.64	11.31	-1.35	0.58	-0.37	-15.36	-0.82	13.99	-9.83	8.12	-10.68	3.05	-1.96
p 6 17	163.0	2.10	-3.10	-3.89	-1.25	-1.73	-0.01	0.15	-10.82	9.21	-2.32	0.07	-0.67	-17.85	-2.04	12.45	-12.81	6.36	-13.49	0.34	-3.15
p 6 18	240.0	2.01	-3.47	-4.42	-1.63	-2.10	-0.14	0.03	-11.77	8.55	-2.69	0.09	-0.79	-18.56	-2.20	11.76	-13.75	5.92	-14.44	-0.70	-3.46
p 6 19	363.0	1.80	-3.95	-5.78	-1.97	-2.49	-0.42	-0.25	-14.03	6.89	-3.13	0.12	-1.05	-20.68	-2.58	10.07	-16.41	4.90	-17.11	-3.08	-4.37
p 6 20	404.5	3.06	-3.51	-4.29	-1.44	-1.99	-0.38	-0.21	-12.46	8.02	-2.66	0.73	-0.80	-20.07	-1.29	10.75	-15.51	6.48	-16.36	-1.45	-3.63
p 6 21	506.0	2.86	-3.50	-4.58	-1.49	-2.02	-0.44	-0.27	-13.01	7.29	-2.66	0.66	-0.88	-20.33	-1.52	10.05	-15.89	6.11	-16.73	-2.04	-3.74
p 6 22	574.8	2.95	-3.54	-4.68	-1.48	-2.02	-0.46	-0.29	-13.42	6.37	-2.69	0.72	-0.88	-20.82	-1.45	9.14	-16.42	6.14	-17.27	-2.22	-3.80
p 6 23	670.3	2.39	-3.80	-5.54	-1.78	-2.32	-0.52	-0.35	-14.49	6.68	-2.97	0.46	-1.03	-21.42	-2.05	9.63	-17.23	5.30	-18.02	-3.30	-4.27
p 6 24	739.8	2.81	-3.67	-5.05	-1.68	-2.21	-0.53	-0.36	-13.99	7.37	-2.85	0.68	-0.97	-21.09	-1.64	10.12	-16.84	5.77	-17.69	-2.87	-4.04
p 6 25	839.0	2.74	-3.70	-5.20	-1.72	-2.24	-0.55	-0.39	-14.22	7.14	-2.88	0.66	-1.00	-21.25	-1.71	9.90	-17.05	5.63	-17.90	-3.10	-4.13
p 6 26	906.6	2.65	-3.75	-5.39	-1.77	-2.29	-0.57	-0.40	-14.55	6.96	-2.93	0.62	-1.03	-21.48	-1.81	9.77	-17.32	5.49	-18.15	-3.34	-4.22
Outlet 5																					
p 5 16	101.2	3.44	-2.39	-1.82	-0.60	-1.06	0.05	0.22	-8.16	11.20	-1.63	0.71	-0.38	-16.00	-0.66	13.86	-10.55	8.18	-11.42	2.65	-2.10
p 5 17	163.7	2.28	-3.18	-3.94	-1.28	-1.77	-0.07	0.10	-11.04	9.00	-2.38	0.19	-0.68	-18.17	-1.89	12.17	-13.20	6.42	-13.91	0.06	-3.20
p 5 18	241.0	1.99	-3.51	-4.68	-1.65	-2.13	-0.21	-0.04	-12.16	8.15	-2.73	0.11	-0.85	-18.91	-2.26	11.33	-14.22	5.71	-14.92	-1.22	-3.65
p 5 19	363.7	1.94	-3.90	-5.81	-1.89	-2.42	-0.50	-0.34	-14.07	6.86	-3.07	0.24	-1.10	-20.81	-2.48	9.90	-16.64	4.85	-17.39	-3.46	-4.44
p 5 20	405.8	3.21	-3.48	-4.29	-1.48	-2.00	-0.48	-0.31	-12.66	7.66	-2.65	0.86	-0.86	-20.14	-1.20	10.24	-15.69	6.43	-16.61	-1.83	-3.69
p 5 21	506.5	3.05	-3.44	-4.52	-1.42	-1.96	-0.52	-0.35	-12.94	7.40	-2.60	0.80	-0.92	-20.34	-1.39	9.99	-15.98	6.12	-16.89	-2.30	-3.77
p 5 22	575.3	3.04	-3.51	-4.76	-1.47	-2.01	-0.54	-0.37	-13.58	6.19	-2.67	0.80	-0.94	-20.96	-1.41	8.84	-16.66	6.03	-17.55	-2.62	-3.89
p 5 23	671.0	2.66	-3.72	-5.37	-1.76	-2.27	-0.60	-0.43	-14.41	7.07	-2.90	0.64	-1.05	-21.33	-1.82	9.82	-17.21	5.43	-18.06	-3.44	-4.24
p 5 24	740.3	2.95	-3.68	-5.08	-1.68	-2.21	-0.61	-0.44	-14.07	6.92	-2.85	0.79	-1.01	-21.25	-1.54	9.55	-17.09	5.74	-17.99	-3.19	-4.12
p 5 25	839.5	2.90	-3.71	-5.19	-1.71	-2.23	-0.62	-0.45	-14.26	6.73	-2.88	0.77	-1.03	-21.38	-1.59	9.37	-17.25	5.65	-18.14	-3.35	-4.18
p 5 26	907.2	3.16	-3.61	-4.94	-1.59	-2.12	-0.63	-0.46	-14.03	6.80	-2.77	0.91	-0.99	-21.33	-1.34	9.34	-17.17	5.93	-18.09	-3.14	-4.06
Outlet 4																					
p 4 16	101.7	3.58	-2.60	-2.14	-0.77	-1.24	-0.06	0.11	-8.86	10.50	-1.83	0.83	-0.45	-16.72	-0.59	13.08	-11.43	8.04	-12.35	1.90	-2.32
p 4 17	164.5	2.88	-3.00	-3.56	-1.06	-1.57	-0.15	0.02	-11.01	9.05	-2.19	0.53	-0.64	-18.50	-1.34	11.95	-13.56	6.92	-14.36	0.13	-3.08
p 4 18	259.0	3.96	-2.54	-2.43	-0.65	-1.14	-0.20	-0.03	-10.28	9.77	-1.75	1.09	-0.50	-18.24	-0.29	12.22	-13.16	8.08	-14.12	1.00	-2.52
p 4 19	364.5	2.31	-3.94	-5.84	-1.91	-2.44	-0.65	-0.48	-14.43	6.37	-3.10	0.49	-1.16	-21.32	-2.20	9.16	-17.32	4.89	-18.16	-4.05	-4.56
p 4 20	406.3	3.55	-3.49	-4.30	-1.49	-2.02	-0.62	-0.45	-12.97	7.38	-2.66	1.10	-0.92	-20.52	-0.95	9.71	-16.23	6.45	-17.23	-2.40	-3.80
p 4 21	507.0	3.19	-3.58	-4.83	-1.54	-2.08	-0.65	-0.49	-13.63	6.82	-2.74	0.93	-1.01	-21.01	-1.32	9.27	-16.85	5.93	-17.81	-3.08	-4.06
p 4 22	576.0	3.42	-3.53	-4.67	-1.48	-2.03	-0.66	-0.49	-13.72	6.18	-2.68	1.05	-0.97	-21.22	-1.10	8.58	-17.05	6.17	-18.02	-2.95	-3.97
p 4 23	671.5	3.20	-3.72	-5.04	-1.75	-2.27	-0.69	-0.52	-14.35	7.30	-2.90	0.96	-1.03	-21.51	-1.33	9.78	-17.43	5.84	-18.37	-3.42	-4.18
p 4 24	741.0	3.20	-3.77	-5.15	-1.82	-2.33	-0.69	-0.53	-14.61	7.20	-2.96	0.96	-1.04	-21.70	-1.34	9.69	-17.63	5.81	-18.58	-3.54	-4.26

Table 3. Continuation.

Sample	Elapsed time [hours]	Aragonite	Calcite	Ca-mont-morillonite	Chalcedony	Dolomite	$Fe(OH)_3$ (am)	Gibbsite	Goethite	Goethite (am)	Hematite	Illite	Kaolinite	Quartz	Siderite	SiO_2 (am)	$Al(OH)_3$ (am)	$Ca_{0.25}Mg_{0.25}Fe_{0.5}$ carbonate	Ca-Mg-Fe smectite	$Ca_{0.25}Mg_{0.5}Fe_{0.25}$ carbonate	Ferrihydrite $Fe(OH)_3$	Imogolite
Outlet 4																						
p 4 25	840.1	-3.69	-3.56	1.85	0.06	-6.75	-0.22	1.73	4.99	0.95	15.10	-2.03	6.79	0.22	-1.39	-0.72	-0.22	-2.04	3.17	-2.60	1.76	3.91
p 4 26	907.8	-3.66	-3.54	1.95	0.07	-6.72	-0.39	1.76	4.82	0.78	14.76	-1.96	6.88	0.23	-1.34	-0.70	-0.20	-2.00	3.15	-2.58	1.59	3.97
Outlet 3																						
p 3 16	102.3	-3.08	-2.96	2.76	0.49	-5.57	0.03	1.39	5.24	1.20	15.61	-0.76	6.97	0.64	-0.94	-0.29	-0.56	-1.52	4.67	-2.05	2.02	3.66
p 3 17	165.3	-3.04	-2.91	2.77	0.41	-5.47	-0.11	1.53	5.10	1.06	15.32	-0.85	7.11	0.57	-0.80	-0.36	-0.42	-1.42	4.45	-1.97	1.87	3.87
p 3 18	260.0	-2.58	-2.45	3.97	0.37	-4.54	0.02	2.10	5.24	1.20	15.60	0.40	8.16	0.53	-0.44	-0.40	0.15	-1.00	5.37	-1.53	2.01	4.96
p 3 19	365.2	-4.10	-3.97	0.80	-0.07	-7.58	-0.60	1.50	4.61	0.56	14.33	-3.12	6.06	0.08	-1.69	-0.85	-0.46	-2.39	2.10	-2.99	1.38	3.31
p 3 20	407.0	-3.65	-3.52	2.20	-0.05	-6.67	-0.53	2.04	4.68	0.64	14.48	-1.67	7.20	0.11	-1.29	-0.82	0.08	-1.97	3.23	-2.55	1.45	4.41
p 3 21	507.7	-3.70	-3.57	1.91	-0.04	-6.79	-0.61	1.91	4.60	0.56	14.32	-1.97	6.96	0.12	-1.29	-0.81	-0.04	-1.99	2.98	-2.59	1.37	4.17
p 3 22	580.2	-3.65	-3.53	2.00	-0.01	-6.70	-1.02	1.91	4.19	0.15	13.51	-1.89	7.02	0.15	-1.20	-0.78	-0.04	-1.93	2.87	-2.54	0.97	4.20
p 3 23	672.2	-3.73	-3.60	1.98	-0.02	-6.84	-0.20	1.92	5.01	0.97	15.15	-1.94	7.01	0.14	-1.41	-0.80	-0.04	-2.07	3.18	-2.64	1.78	4.20
p 3 24	741.5	-3.77	-3.65	1.92	-0.03	-6.91	-0.40	1.90	4.81	0.76	14.74	-2.00	6.96	0.13	-1.37	-0.80	-0.06	-2.07	3.05	-2.66	1.58	4.16
p 3 25	840.7	-3.80	-3.67	1.82	-0.01	-6.97	-0.57	1.83	4.64	0.60	14.41	-2.13	6.86	0.15	-1.38	-0.78	-0.12	-2.09	2.91	-2.68	1.41	4.04
p 3 26	908.5	-3.64	-3.52	2.26	0.00	-6.66	-0.34	2.00	4.87	0.83	14.87	-1.66	7.22	0.16	-1.30	-0.77	0.04	-1.97	3.34	-2.54	1.65	4.39
Outlet 2																						
p 2 16	103.0	-3.33	-3.20	1.95	0.19	-6.10	-0.09	1.53	5.12	1.08	15.37	-1.64	6.65	0.35	-1.15	-0.58	-0.43	-1.75	3.64	-2.30	1.90	3.63
p 2 17	167.3	-3.06	-2.94	3.03	0.11	-5.52	0.02	2.11	5.23	1.19	15.59	-0.59	7.66	0.27	-0.88	-0.66	0.16	-1.47	4.38	-2.01	2.00	4.72
p 2 18	261.0	-2.77	-2.64	3.81	0.09	-4.92	-0.16	2.47	5.05	1.01	15.23	0.24	8.35	0.25	-0.56	-0.68	0.52	-1.16	4.86	-1.71	1.82	5.43
p 2 19	366.0	-3.84	-3.71	1.93	-0.20	-7.05	-0.45	2.17	4.76	0.72	14.65	-1.96	7.15	-0.04	-1.44	-0.97	0.21	-2.14	2.88	-2.72	1.54	4.52
p 2 20	408.2	-3.74	-3.61	1.88	-0.22	-6.85	-0.51	2.18	4.70	0.66	14.52	-1.98	7.13	-0.07	-1.38	-1.00	0.23	-2.06	2.82	-2.63	1.47	4.53
p 2 21	508.3	-3.78	-3.65	1.75	-0.16	-6.93	-0.60	2.04	4.61	0.57	14.35	-2.14	6.97	0.00	-1.35	-0.94	0.09	-2.06	2.72	-2.66	1.39	4.30
p 2 22	580.8	-3.81	-3.68	1.49	-0.13	-6.99	-1.10	1.89	4.11	0.07	13.35	-2.45	6.73	0.03	-1.34	-0.91	-0.06	-2.07	2.31	-2.68	0.89	4.04
p 2 23	672.7	-3.82	-3.70	1.64	-0.12	-7.01	-0.37	1.93	4.84	0.80	14.81	-2.35	6.84	0.04	-1.46	-0.90	-0.02	-2.14	2.73	-2.71	1.62	4.13
p 2 24	747.3	-3.79	-3.66	1.63	-0.12	-6.93	-0.45	1.92	4.76	0.72	14.65	-2.32	6.82	0.04	-1.39	-0.89	-0.03	-2.08	2.72	-2.67	1.54	4.11
p 2 25	841.3	-3.77	-3.64	1.89	-0.10	-6.89	-0.52	2.01	4.69	0.64	14.50	-2.08	7.03	0.06	-1.30	-0.88	0.06	-2.03	2.91	-2.63	1.46	4.30
p 2 26	909.2	-3.86	-3.73	1.42	-0.12	-7.06	-0.33	1.84	4.88	0.84	14.89	-2.58	6.66	0.04	-1.56	-0.89	-0.12	-2.20	2.55	-2.76	1.66	3.95
Outlet 1																						
p 1 16	103.7	-3.62	-3.49	1.66	-0.17	-6.70	-0.16	2.00	5.05	1.01	15.23	-2.06	6.86	-0.01	-1.55	-0.95	0.04	-2.10	2.88	-2.63	1.83	4.21
p 1 17	168.2	-3.33	-3.21	2.57	-0.27	-6.05	-0.16	2.53	5.05	1.01	15.23	-1.11	7.73	-0.11	-1.07	-1.05	0.58	-1.70	3.54	-2.26	1.83	5.18
p 1 18	262.3	-3.05	-2.93	2.78	-0.20	-5.47	-0.14	2.50	5.07	1.03	15.26	-0.87	7.83	-0.04	-0.83	-0.97	0.55	-1.44	3.76	-1.98	1.84	5.19
p 1 19	366.8	-4.28	-4.15	-0.18	-0.54	-7.89	-0.59	1.82	4.62	0.58	14.36	-4.19	5.77	-0.38	-1.83	-1.31	-0.14	-2.54	0.87	-3.13	1.39	3.48
p 1 20	409.0	-4.26	-4.14	-0.31	-0.52	-7.86	-0.66	1.73	4.55	0.50	14.22	-4.29	5.64	-0.36	-1.86	-1.29	-0.23	-2.55	0.77	-3.13	1.32	3.32
p 1 21	508.8	-4.09	-3.96	-0.04	-0.44	-7.52	-0.86	1.72	4.35	0.31	13.83	-4.11	5.79	-0.28	-1.62	-1.21	-0.23	-2.34	0.93	-2.94	1.13	3.40
p 1 22	581.5	-3.92	-3.80	0.27	-0.40	-7.18	-1.19	1.79	4.02	-0.02	13.17	-3.73	6.01	-0.24	-1.37	-1.17	-0.16	-2.13	1.09	-2.75	0.79	3.58
p 1 23	673.2	-4.18	-4.06	-0.28	-0.38	-7.68	-0.59	1.55	4.62	0.58	14.37	-4.38	5.54	-0.22	-1.72	-1.16	-0.41	-2.43	0.88	-3.02	1.40	3.10
p 1 24	747.3	-4.07	-3.95	0.17	-0.35	-7.46	-0.44	1.68	4.77	0.73	14.66	-3.91	5.87	-0.19	-1.69	-1.12	-0.28	-2.36	1.33	-2.93	1.54	3.39
p 1 25	841.3	-4.12	-3.99	0.12	-0.36	-7.54	-0.41	1.68	4.80	0.76	14.73	-3.95	5.85	-0.20	-1.76	-1.13	-0.28	-2.42	1.27	-2.98	1.58	3.38
p 1 26	909.2	-4.28	-4.15	-0.59	-0.34	-7.86	-0.59	1.35	4.62	0.58	14.36	-4.71	5.24	-0.18	-1.86	-1.11	-0.61	-2.55	0.66	-3.13	1.39	2.74

Table 3. Continuation.

Sample	Elapsed time [hours]	Imogolite (synth.gel)	Magnesite	Mesolite	$Mg_{0.25}Fe_{0.75}$ carbonate	$Mg_{0.50}Fe_{0.50}$ carbonate	Silica (am)	Moganite	Ca-Mg-Fe clay	Ca-Fe clay	$Mg_{0.75}Fe_{0.25}$ carbonate	Gibbsite (microcr)	Stapafell_ glass	Chrysotile	Allophane	Mg-nontronite	Mg-saponite	Mg-beidellite	Mg-clay	Heulandite	Analcime
Outlet 4																					
p 4 25	840.1	3.49	-3.64	-4.72	-1.71	-2.21	-0.69	-0.52	-14.10	7.54	-2.83	1.10	-0.98	-21.33	-1.05	9.90	-17.19	6.18	-18.18	-3.10	-4.03
p 4 26	907.8	3.56	-3.63	-4.74	-1.66	-2.18	-0.67	-0.50	-14.36	7.21	-2.81	1.12	-0.96	-21.68	-0.97	9.61	-17.52	6.28	-18.50	-3.04	-4.04
Outlet 3																					
p 3 16	102.3	3.24	-3.06	-3.25	-1.23	-1.70	-0.26	-0.09	-10.71	9.39	-2.29	0.76	-0.67	-18.14	-1.04	12.00	-13.27	7.09	-14.17	0.03	-3.01
p 3 17	165.3	3.45	-3.00	-3.45	-1.10	-1.60	-0.33	-0.17	-11.55	8.88	-2.20	0.90	-0.70	-19.08	-0.88	11.44	-14.33	7.11	-15.26	-0.50	-3.14
p 3 18	260.0	4.54	-2.53	-2.22	-0.71	-1.18	-0.38	-0.21	-10.67	9.69	-1.76	1.47	-0.54	-18.64	0.19	11.78	-13.74	8.30	-14.83	0.50	-2.52
p 3 19	365.2	2.89	-4.05	-5.73	-2.04	-2.57	-0.82	-0.65	-14.92	6.08	-3.22	0.87	-1.19	-21.93	-1.72	8.56	-18.11	5.13	-19.06	-4.59	-4.64
p 3 20	407.0	4.00	-3.59	-4.34	-1.62	-2.14	-0.79	-0.62	-13.61	6.97	-2.77	1.41	-0.98	-21.19	-0.60	9.02	-17.11	6.53	-18.20	-3.10	-3.94
p 3 21	507.7	3.75	-3.66	-4.65	-1.64	-2.17	-0.78	-0.62	-13.93	6.65	-2.82	1.28	-1.02	-21.47	-0.85	8.83	-17.43	6.24	-18.49	-3.40	-4.08
p 3 22	580.2	3.78	-3.62	-4.64	-1.56	-2.11	-0.76	-0.59	-14.08	5.89	-2.77	1.28	-0.99	-21.71	-0.80	8.10	-17.64	6.33	-18.68	-3.29	-4.05
p 3 23	672.2	3.78	-3.68	-4.66	-1.73	-2.24	-0.77	-0.60	-14.27	7.50	-2.87	1.29	-1.00	-21.63	-0.80	9.71	-17.57	6.31	-18.61	-3.33	-4.08
p 3 24	741.5	3.74	-3.71	-4.75	-1.71	-2.24	-0.77	-0.60	-14.26	7.05	-2.88	1.27	-1.01	-21.71	-0.85	9.27	-17.67	6.25	-18.71	-3.43	-4.14
p 3 25	840.7	3.62	-3.74	-4.85	-1.73	-2.26	-0.76	-0.59	-14.32	6.69	-2.91	1.20	-1.01	-21.75	-0.95	8.97	-17.71	6.15	-18.72	-3.47	-4.16
p 3 26	908.5	3.97	-3.59	-4.44	-1.63	-2.14	-0.74	-0.57	-14.13	7.38	-2.77	1.37	-0.94	-21.63	-0.60	9.55	-17.51	6.59	-18.56	-3.01	-3.96
Outlet 2																					
p 2 16	103.0	3.21	-3.34	-4.16	-1.45	-1.94	-0.55	-0.38	-12.29	8.27	-2.55	0.89	-0.92	-19.57	-1.24	10.68	-15.19	6.28	-16.16	-2.00	-3.68
p 2 17	167.3	4.30	-3.03	-3.18	-1.17	-1.65	-0.63	-0.46	-11.82	8.85	-2.25	1.48	-0.79	-19.56	-0.20	10.81	-15.11	7.36	-16.24	-1.38	-3.21
p 2 18	261.0	5.01	-2.73	-2.43	-0.85	-1.34	-0.65	-0.48	-11.36	8.82	-1.94	1.84	-0.68	-19.51	0.49	10.51	-14.97	8.14	-16.19	-0.77	-2.82
p 2 19	366.0	4.11	-3.78	-4.68	-1.78	-2.31	-0.94	-0.78	-14.22	6.76	-2.95	1.54	-1.08	-21.79	-0.58	8.66	-17.93	6.26	-19.08	-4.00	-4.24
p 2 20	408.2	4.11	-3.68	-4.62	-1.71	-2.23	-0.97	-0.80	-14.05	6.61	-2.86	1.55	-1.10	-21.57	-0.59	8.46	-17.74	6.21	-18.91	-4.07	-4.21
p 2 21	508.3	3.89	-3.73	-4.87	-1.70	-2.23	-0.91	-0.74	-14.36	6.41	-2.89	1.41	-1.09	-21.90	-0.78	8.44	-18.03	6.08	-19.14	-4.07	-4.29
p 2 22	580.8	3.62	-3.76	-5.18	-1.70	-2.24	-0.88	-0.71	-14.76	5.29	-2.91	1.26	-1.12	-22.20	-1.03	7.48	-18.35	5.83	-19.40	-4.28	-4.41
p 2 23	672.7	3.72	-3.75	-5.06	-1.79	-2.31	-0.87	-0.70	-14.78	6.84	-2.94	1.30	-1.09	-22.05	-0.93	9.00	-18.17	5.97	-19.23	-4.09	-4.37
p 2 24	747.3	3.69	-3.72	-5.02	-1.72	-2.25	-0.86	-0.70	-14.54	6.70	-2.89	1.29	-1.09	-21.89	-0.95	8.86	-17.99	5.96	-19.06	-4.04	-4.35
p 2 25	841.3	3.89	-3.69	-4.80	-1.65	-2.19	-0.85	-0.68	-14.23	6.69	-2.85	1.38	-1.04	-21.81	-0.75	8.79	-17.85	6.23	-18.94	-3.74	-4.24
p 2 26	909.2	3.53	-3.78	-5.33	-1.87	-2.37	-0.86	-0.69	-15.30	6.80	-2.98	1.21	-1.12	-22.31	-1.11	9.06	-18.46	5.76	-19.49	-4.33	-4.49
Outlet 1																					
p 1 16	103.7	3.79	-3.65	-4.66	-1.83	-2.30	-0.92	-0.75	-14.08	7.37	-2.88	1.36	-1.12	-21.18	-0.88	9.31	-17.31	5.98	-18.43	-3.89	-4.20
p 1 17	168.2	4.76	-3.29	-3.69	-1.38	-1.87	-1.02	-0.85	-12.83	7.70	-2.49	1.90	-1.03	-20.67	0.03	9.16	-16.74	6.90	-18.04	-3.36	-3.76
p 1 18	262.3	4.77	-2.99	-3.49	-1.13	-1.61	-0.94	-0.77	-12.79	7.92	-2.21	1.87	-0.96	-20.57	0.09	9.46	-16.53	7.11	-17.80	-2.92	-3.56
p 1 19	366.8	3.06	-4.18	-6.73	-2.17	-2.70	-1.28	-1.11	-16.37	4.96	-3.35	1.18	-1.55	-23.16	-1.82	6.97	-20.02	4.16	-21.14	-7.34	-5.49
p 1 20	409.0	2.91	-4.17	-6.80	-2.19	-2.71	-1.26	-1.09	-16.33	4.81	-3.34	1.10	-1.56	-22.98	-1.97	6.88	-19.83	4.03	-20.93	-7.34	-5.50
p 1 21	508.8	2.98	-4.00	-6.71	-1.97	-2.50	-1.18	-1.01	-16.45	4.60	-3.16	1.09	-1.48	-23.24	-1.85	6.76	-19.98	4.30	-21.05	-6.91	-5.42
p 1 22	581.5	3.16	-3.83	-6.36	-1.74	-2.30	-1.14	-0.98	-15.88	4.15	-2.97	1.16	-1.42	-22.96	-1.65	6.27	-19.60	4.61	-20.69	-6.45	-5.21
p 1 23	673.2	2.68	-4.07	-7.04	-2.06	-2.59	-1.13	-0.96	-16.86	5.06	-3.24	0.92	-1.49	-23.45	-2.12	7.42	-20.17	4.06	-21.18	-7.03	-5.56
p 1 24	747.3	2.97	-3.96	-6.56	-2.01	-2.52	-1.09	-0.93	-16.34	5.65	-3.15	1.04	-1.41	-22.99	-1.81	7.90	-19.59	4.51	-20.63	-6.40	-5.32
p 1 25	841.3	2.97	-3.99	-6.67	-2.07	-2.57	-1.10	-0.94	-16.62	5.65	-3.19	1.05	-1.42	-23.17	-1.82	7.92	-19.80	4.47	-20.84	-6.54	-5.39
p 1 26	909.2	2.33	-4.15	-7.40	-2.19	-2.70	-1.08	-0.91	-17.32	4.94	-3.34	0.72	-1.51	-23.60	-2.44	7.51	-20.33	3.76	-21.27	-7.19	-5.71